IDŐJÁRÁS

QUARTERLY JOURNAL
OF THE HUNGARIAN METEOROLOGICAL SERVICE

CONTENTS

****

http://omsz.met.hu/irodalom/firat_ido/ido_hu.html

VOL. 107 * NO. 1 * JANUARY–MARCH 2003

IDŐJÁRÁS

Quarterly Journal of the Hungarian Meteorological Service

Editorial Office: P.O. Box 39, H-1675 Budapest, Hungary or
Gilice tér 39, H-1181 Budapest, Hungary
E-mail: prager.t@met.hu or *antal.e@met.hu*
Fax: (36-1) 346-4809

Subscription by

mail: IDŐJÁRÁS, P.O. Box 39, H-1675 Budapest, Hungary
E-mail: prager.t@met.hu or *antal.e@met.hu*; *Fax: (36-1) 346-4809*

IDŐJÁRÁS

Quarterly Journal of the Hungarian Meteorological Service
Vol. 107, No. 1, January–March 2003, pp. 1–29

High-latitude environmental dynamics in the context of global change

Kirill Ya. Kondratyev

Research Centre for Ecological Safety, St. Petersburg Centre, RAS
Nansen Fund on Environment and Remote Sensing, St. Petersburg
Korpusnaya St., 18, 197110 St. Petersburg, Russia
E-mail: kondratyev@KK10221.spb.edu

(Manuscript received May 8, 2002; in final form November 21, 2002)

Abstract—Key problems of high-latitude environmental dynamics are discussed including present-day and paleo environmental changes. We review a range of international and national programs aimed at informing of knowledge and understanding of these changes through further development of observation systems, multivariate multidisciplinary analysis, and numerical simulation modeling approaches.

Key-words: global change, global climate change, Arctic system, Arctic ocean, thermohaline circulation, sea ice extent, permafrost, stratospheric ozone, Arctic shelf, paleoclimate, atmospheric pollution, Arctic haze, extended cloudiness, Siberian rivers, ice sheets.

1. Introduction

Recent growing attention to the Arctic environmental problems is motivated by a number of circumstances, including (*Arctic Climate System Assessment (ACIA)*, 2000; *Arctic Science...*, 1999; *CAFF...*, 2001; *Everett* and *Fitzharris*, 2001; *Johannessen et al.*, 2000; *Kalabin*, 2000; *Kondratyev et al.*, 1996; *Rapley*, 1999; *Toward an Arctic...*, 1998; *Toward Prediction...*, 1998; *Vörösmarty et al.*, 2001; *Wadhams et al.*, 1997; *Weller* and *Lange*, 1999; *White et al.*, 2000; *Yudakhine*, 2000; *Zakharov* and *Malinin*, 2000): a stronger sensitivity of high latitude environment to various external forcings; increasing understanding of the importance of numerous interactions and feedbacks between components of the Earth's system; growing necessity to use natural resources located at high latitudes (Arctic shelf especially). It is fair to say

(*Vörösmarty et al.,* 2001), that "the Arctic system constitutes a unique and important environment with a central role in the dynamics and evolution of the earth system".

Some of the recent scientific results have been pointed out in the *ACIA* Implementation Plan (2000):

- There has been increased coastal erosion in the Bering Sea from storm surges resulting from reduced sea ice.
- Sea ice extent in the Arctic has decreased Arctic-wide by 0.35% per year since 1979. During summer of 1998, record reduction of sea ice coverage was observed in the Beaufort and Chukchi Seas.
- Sea ice thickness has also been reduced by between 1–2 meters in many parts of the Arctic Ocean and the sub-Arctic seas.
- Streamflow discharge of major Siberian rivers into the Arctic Ocean has increased in recent years and is associated with a warmer climate and enhanced precipitation in the river basins.
- Since 1970, the Arctic Oscillation, which is a measure of the strength of the circumpolar vortex, has strengthened. This has been found to be consistent with temperature and sea ice coverage changes in the Arctic.
- There has been an increased warming of the Arctic Ocean's Atlantic layer and an approximate 20% greater coverage of Atlantic water types.
- Record low levels of ozone were measured in 2000 in the Arctic with increasing evidence that these levels are likely to continue for at least the next 20 years.
- Ongoing studies indicate that the current UV levels can have a significant effect of fish larvae survival rates.
- General warming of soils in regions with permafrost, derived primarily from Alaskan data, has been observed over recent year.

It has been emphasized in *ACIA* (2000), that past assessments indicated that the Arctic is important to global-scale processes in at least four important ways:

- Thermohaline circulation dominated by the Arctic Ocean and Nordic Seas is responsible for a considerable part of the Earth's poleward heat transport, and may also serve as a sink as well as a source for CO_2. Alterations of this circulation, as have been observed during climatic changes of the past, can affect global climate and in particular the climate of Europe and North America.
- Melting of the Arctic land ice sheets can cause sea level rise around the world. A compilation of studies suggests that a global warming of 1°C will lead to ~1 mm per year of sea-level rise from small ice caps and

glaciers. The Arctic will supply over half of this total, with an additional 0.3–0.4 mm per year contributed from Greenland although uncertainties remain about the mass balance of the Greenland ice sheet.

- Arctic soils can act as either sinks or sources of greenhouse gases depending on temperature and moisture changes within the Arctic. Moisture has opposing effects on the concentrations of the two major trace gases: CH flux declines with soil drying, while CO_2 flux initially increases. These changes can influence greenhouse gas warming globally.
- Our current understanding of the Arctic climate system suggests that positive feedbacks in high-latitude systems, including the snow and ice albedo effect, amplify anthropogenically-induced atmospheric changes, and that disturbances in the circumpolar Arctic climate may substantially influence global climate.

In the context of the health of the Arctic marine environment, from the viewpoint of proper functioning of economically important ecosystems, D. Drewry and O. Orheim (*Arctic Science...,* 1999) have formulated a number of key questions:

- How was the polar basin formed, where are the plate boundaries?
- What has been the detailed paleo-climatic history of the high Arctic Ocean during the last 1 million years?
- Do decreases in ice extent and upper stratification of the ocean signal a different sea ice regime?
- What is the stability of the sea ice cover, what are the effects of radiative feedback in the Arctic, and how do they modulate global ocean circulation?
- What is the role of continental shelves in the cycling of C, N, Si, and other chemicals?
- What is the productivity of the Arctic Ocean, and what is the structure and diversity of higher trophic levels?
- What are the effects of environmental change, both of climate and of pollutants and contaminants such as the introduction of POPs (persistent organic pollutants) into the food chain?

High-latitude climate dynamics is of particular interest. According to *Weller* and *Lange* (1999), "While considerable uncertainty still exists about the exact nature of the future impacts of global climate change, there can no longer be any doubt that major changes in the climate have occurred in recent decades in the Arctic, with visible and measurable impacts following the

climatic changes. Greater impacts are likely in the future and while some of them will be positive, others will be detrimental to human activities".

Recent analysis of ice cores from the Arctic (*Everett* and *Fitzharris,* 2001) has revealed large-scale and rapid paleo-climate changes. Rapid warming took place ~11,500 years ago, at the end of the last glacial period. The coldest parts of ice cores had been as much as 21°C colder than the present temperature in Central Greenland; and the temperatures increased by more than 10°C in a few decades. There is evidence of even more rapid change in the precipitation pattern, rapid reorganizations of atmospheric circulation, and periods of rapid warming during the previous 20,000 years. Rapid warmings of ~10°C in a few decades during the last glacial period in Central Greenland had been followed by periods of slower cooling over a few centuries, and then a generally rapid return to glacial conditions. About 20 such intervals, each lasting between 500 and 2,000 years, occurred during the last glacial period.

It has been emphasized *(Everett* and *Fitzharris,* 2001), that the polar systems are extremely sensitive to the variability of temperature, and several aspects of these systems will be affected by any further climate change. Primary impacts will be on the physical environment, including ice, permafrost, and hydrology; on biota and ecosystems, including fisheries and terrestrial systems; and on human activities, including social and economic impacts on settlements, resource extraction and transportation, and existing infrastructure. Scenario predictions of potential future global warming indicate a necessity to particularly take into account various phenomena, such as thermocarst erosion in lowland areas, thawing of permafrost accompanied by hydrological and climatic changes. Climate change will affect terrestrial ecological systems through changes in permafrost as well as direct climatic changes, including changes in precipitation, snow cover, and temperature. Terrestrial ecosystems are likely to change from tundra to boreal forests, although vegetative changes are likely to lag behind climatic change. Major shifts in biomass will be associated with changes in microbiological (bacteria, algae, etc.) and insect communities (some of them may diminish while others prosper).

It has been pointed out (*Everett* and *Fitzharris,* 2001), that in the recent geologic past, tundra was a carbon sink, but recent climatic warming in the Arctic, coupled with the concomitant drying of the active layer and lowering of the water table, has shifted areas of the Arctic from sinks to sources of CO_2 (this problem is, however, far from being solved). An important potential consequence of permafrost thawing is emission of methane – a greenhouse gas. Changes in an other greenhouse gas, the tropospheric ozone, might happen due to warming of the troposphere (*Kondratyev* and *Varotsos,* 2000).

An interesting illustration of potential future surprises due to interactions and feedbacks has been discussed by *Stevenson et al.* (2000), who obtained future estimates of tropospheric ozone radiative forcing and methane turnover in the context of the impact of climate change. (It should be pointed out, that studies of the contribution of tropospheric ozone, O_{3T}, as a greenhouse gas, as well as assessments of potential impact of global warming on permafrost melting and methane emissions are still at the preliminary stage of development.) Interactive simulations of climate dynamics and O_{3T} changes during the time period 1990–2100 for scenarios of "high" (A2) or "central" (B2) cases of CO_2 emissions resulted in tropospheric ozone radiative forcing (RF) equal to +0.27(A2) or +0.09(B2) W/m^2. If climate-ozone coupling was neglected, relevant RF values would be equal to +0.43 (+0.22) W/m^2. When climate change was included, CH_4 lifetime fell by 0–5%. Hence, climate warming exerts a negative feedback on itself by enhancing O_{3T} and CH_4 destruction.

Three principal achievements have stimulated recent progress in studying the Arctic environment (*Dickson,* 1999): (1) further development of observation programs with the use of various observation means (including satellites and submarines); (2) declassification of the military Soviet-American archive of ocean "climatology" data; (3) discovery of the fact that the climatic forcing in the region of Arctic and northern seas in the 1990s has increased in comparison with that observed during the previous century (similar situation also took place with respect to climate dynamics indicators (such as Arctic Oscillation (AO) and North Atlantic Oscillation (NAO)).

Overland and *Adams* (2001) have pointed out that "decadal differences between the 1990s and 1980s in winter (JFM) sea-level pressure and 300 hPa zonal winds have an Arctic-centered character with nearly equal contributions from the Atlantic and Pacific sectors. In contrast, the differences between positive and negative AO composites defined from monthly values of Principal Components from the same period have similar magnitudes in the Pacific and Arctic, but have additional large NAO signature in the Atlantic sector. Thus Arctic changes of decadal scales are more symmetric with the pole than suggested by the standard AO index definition. Change point analysis of the AO shows that a shift in value near 1989 is an alternative hypothesis to a linear trend. Analysis of zonal and meridional winds by longitudinal sectors shows the importance of the standing wave pattern in interpreting the AO, which supplements the view of the AO as a simple zonal average (annular) mode". Thus, the Arctic Oscillation should be considered as a physical phenomenon connected with the enhancement of circumpolar vortex and relevant mass and temperature changes in the troposphere and stratosphere.

By the end of the 1980s – beginning of the 1990s, a very strong NAO enhancement resulted in powerful transport of warmer and fresher Norwegian Atlantic waters to the north of the Fram Strait and the Barents Sea. Entering the Arctic, the sub-layer of Atlantic waters was becoming thinner, warming (by about 2°C) and increasing its horizontal extent (~20%). At smaller depths, the cold haloclyne (which thermally isolates the sea ice cover from the warm Atlantic layer located below) shifted towards the euroasiatic basin, which resulted in substantial changes of mass and energy balances of the ice cover surface. This and other phenomena have been studied within a number of recent programs (*Aagard et al.,* 1998; *Allison et al.,* 2001; *Arctic Science...,* 2000; Barry, 1998; *Climate Change...,* 2001; *Toward an Arctic...,* 1998; *Toward Predictiion...,* 1998; *Wadhams et al.,* 1997). Climatic impact of polynyas is of particular interest (*Holland,* 2001; *Lemke,* 2001).

Alekseev (1998) has emphasized that the Arctic is in many respects a key part of the global climatic system, where the strongest natural fluctuations of climatic characteristics develop. The global impact of the Arctic is primarily accomplished through the Arctic Ocean, which is capable of changing the structure of its circulation regime under the influence of changes in fresh water, salt, and heat exchange with the non-polar parts of the global system. The freshened upper layer and sea ice located above it turn out to be most active components, with fresh water, heat, and salt transport being the major processes responsible for coupling between the high-latitude environment and its lower-latitude parts.

Specific features of the arctic atmosphere, such as phenomena of arctic haze as well as extended cloudiness and radiation, have been studied during the period of the First GARP (Global Atmospheric Research Programme) Global Experiment – FGGE (*Kondratyev et al.,* 1992; *Kondratyev,* 1999).

Important progress has been achieved in the field of arctic climate diagnostics (*Adamenko* and *Kondratyev,* 1999; *Nagurny* and *Maistrova,* 2002). Basic features of arctic climate dynamics have been demonstrated, such as strong space and time variability of various scales. *Nagurny* and *Maistrova* (2002) have shown, for instance, that as far as interannual lower troposphere temperature variations are concerned, before the 1980s negative anomalies had prevailed, while later on, for the whole troposphere, positive temperature anomalies were typical. Total polar atmosphere energy (potential plus internal) during the previous 40 years has not changed, however.

A much more difficult situation exists in the field of numerical modeling of high-latitude climate change. It has been mentioned in the *Report...* (2001), that current estimates of future changes to the Arctic vary significantly. The model results disagree as to both the magnitude of changes and regional aspects of these changes.

2. Climate and cryosphere

An important step forward in studying the Arctic environment is the Climate and Cryosphere (CliC) Project (*Allison et al.,* 2001). The term "cryosphere" describes those portions of the earth's surface, where water is in solid form. This includes all kinds of ice, snow, and frozen ground such as permafrost. The cryosphere is an important part of the global climate system. It is strongly influenced by temperature, solar radiation, and precipitation, and, in turn, influences each of these properties. It also has an effect on the exchange of heat and moisture between the Earth's surface (land or sea) and the atmosphere, clouds, river flow (hydrology), and atmospheric and oceanic circulation. Parts of the cryosphere are strongly influenced by changes in climate. The cryosphere may therefore act as an early indicator of both natural and human-induced climate changes.

As a core project of the World Climate Research Programme, the "Climate and Cryosphere" (CliC) project encourages and promotes research into the cryosphere and its interactions as part of the global climate system. It seeks to focus attention on the most important issues, encourage communication between researchers with common interests in cryospheric and climate science, promote international co-operation, and highlight the importance of this field of science to policy makers, funding agencies, and the general public. CliC also publicizes significant findings regarding the role of the cryosphere in climate, and recommends directions for future study.

CliC aims to improve understanding of the cryosphere and its interactions with the global climate system, and to enhance the ability to use parts of the cryosphere for detection of climate change. To attain scientific goals, CliC seeks to develop and coordinate national and international activities aimed at increasing the understanding of four main scientific themes:

- Interactions between the atmosphere and snow and ice on the land surface.
- Interactions between glaciers and ice sheets and sea level.
- Interactions between sea ice, oceans, and the atmosphere.
- Interactions of the cryosphere with the atmosphere and oceans on a global scale.

CliC encourages the use of observations, process studies, and numerical modeling within each of the above topic areas. In addition, CliC promotes the establishment of new cryospheric monitoring programs.

The cryosphere is also considered as an indicator of climate variability and change. It has been pointed out in (*Allison et al.,* 2001):

"Atmosphere-snow/ice-land interactions are concerned with the role of the terrestrial cryosphere within the climate system and with improved understanding of the processes, and of observational and predictive capabilities

applicable over a range of time and space scales. Better understanding of the interactions and feedback of the land/cryosphere system and their adequate parameterization within climate and hydrological models are still needed. Specific issues include the interactions and feedback of terrestrial snow and ice in the current climate and their variability; in land surface processes; and in the hydrological cycle. Improved knowledge is required of the amount, distribution, and variability of solid precipitation on a regional and global scale, and its response to a changing climate. Seasonally-frozen ground and permafrost modulate water and energy fluxes, and the exchange of carbon, between the land and the atmosphere. How do changes of the seasonal thaw depth alter the land-atmosphere interaction, and what will be the response and feedback of permafrost to changes in the climate system? These issues require improved understanding of the processes and improved observational and modeling capabilities that describe the terrestrial cryosphere in the entire coupled atmosphere-land-ice-ocean climate system.

Over a considerable fraction of the high-latitude global ocean, sea ice forms a boundary between the atmosphere and the ocean, and considerably influences their interaction. The details and consequences of the role of sea ice in the global climate system are still poorly known. Improved knowledge is needed of the broad-scale time-varying distributions of the physical characteristics of sea ice, particularly ice thickness and the overlying snow-cover thickness, in both hemispheres, and the dominant processes of ice formation, modification, decay, and transport which influence and determine ice thickness, composition, and distribution. We do not know how accurate present model predictions of the sea ice responses to climate change are, since the representation of much of the physics is incomplete in many models, and it will be necessary to improve coupled models considerably to provide this predictive capability.

Key issues on the global scale are: understanding the direct interactions between the cryosphere and atmosphere, correctly parameterizing the processes involved in models, and providing improved data sets to support these activities. In particular, improved interactive modeling of the atmosphere-cryosphere surface energy budget and surface hydrology, including fresh-water runoff, is required.

The scientific strategy for a CliC project is similar in each of the areas of interaction: a combination of measurement, observation, monitoring, and analysis, field process studies and modeling at a range of time and space scales. A CliC modeling strategy must address improved parameterization in models of the direct interactions between all components of the cryosphere, atmosphere, and ocean. It will need to do this at a variety of scales from the regional to global; and with a hierarchy of models ranging from those of

individual processes to fully coupled climate models. It will also be essential to provide the improved data sets needed for validation of models and parameterization schemes."

Data presented in *Table 1* characterize major components of the cryosphere (*Allison et al.,* 2001). It has been mentioned (*Allison et al.,* 2001), that the processes operating in the coupled cryosphere-climate system involve three time scales – intraseasonal-interannual, decadal-centennial, and millennial or longer. The longest time scale is addressed through the IGBP PAGES program, although abrupt climate shifts evidenced in ice core and ocean sediment records (Heinrich events, involving extensive deposition of ice-rafted detritus in the North Atlantic) are also highly relevant to CliC. The other two time scales are commensurate with WCRP interests, as it is manifest in ACSYS, GEWEX, and CLIVAR. In the space domain, cryospheric processes and phenomena need to be investigated over a wide range of scales from meters to thousands of kilometers.

Table 1. Areal and volumetric extent of major components of the cryosphere

Component	**Area (10^6 km^2)**	**Ice volume (10^6 km^3)**	**Sea level equivalent (m)** (a)
LAND SNOW COVER (b)			
Northern Hemisphere Late January	46.5	0.002	
Late August	3.9		
Southern Hemisphere Late July	0.85		
Early May	0.07		
SEA ICE			
Northern Hemisphere Late March	14.0 (c)	0.05	
Early September	6.0 (c)	0.02	
Southern Hemisphere Late September	15.0 (d)	0.02	
Late February	2.0 (d)	0.002	
PERMAFROST (underlying the exposed land surface, excluding Antarctica and Southern Hemisphere high mountains)			
Continuous (e)	10.69	0.0097–0.0250	0.024–0.063
Discontinuous and Sporadic	12.10	0.0017–0.0115	0.004–0.028
CONTINENTAL ICE AND ICE SHELVES			
East Antarctica (f)	10.1	22.7	56.8
West Antarctica and Antarctic Peninsula (f)	2.3	3.0	7.5
Greenland	1.8	2.6	6.6
Small ice caps and Mountain glaciers	0.68	0.18	0.5
Ice shelves (f)	1.5	0.66	–

(a) Sea level equivalent does not equate directly with potential sea-level rise, as a correction is required for the volume of the Antarctic and Greenland ice sheets that are presently below sea level. 400,000 km^3 of ice is equivalent to 1 m of global sea level.

(b) Snow cover includes that on land ice, but excludes snow-covered sea ice.

(c) Actual ice areas, excluding open water. Ice extent ranges between approximately 7.0 and 15.4 $\times$ 10^6 km^2.

(d) Actual ice area excluding open water. Ice extent ranges between approximately 3.8 and 18.8 $\times$ 10^6 km^2. Southern Hemisphere sea ice is mostly seasonal and generally much thinner than Arctic sea ice.

(e) Data calculated using the Digital Circum-Arctic Map of Permafrost and Ground-Ice Conditions, and the GLOBE-1 km Elevation Data Set.

(f) Ice sheet data include only grounded ice. Floating ice shelves, which do not affect sea level, are considered separately.

2.1 Cryosphere dynamics

Studying the cryosphere dynamics has a great importance for many applications. Data of *Table 2* illustrate some of the applications (*Allison et al.*, 2001).

Four overarching goals, that address major concerns for the WCRP, can be identified (*Allison et al.*, 2001). These are:

- To improve understanding of the physical processes and feedbacks through which the cryosphere interacts within the climate system.
- To improve the representation of cryospheric processes in models to reduce uncertainties in simulations of climate and predictions of climate change.
- To assess and quantify the impacts of past and future climatic variability and change on components of the cryosphere and their consequences, particularly for global energy and water budgets, frozen ground conditions, sea level change, and the maintenance of polar sea-ice covers.
- To enhance the observation and monitoring of the cryosphere in support of process studies, model evaluation, and change detection.

Table 2. Examples of socio-economic sectors affected by changes in the cryosphere

SOCIO-ECONOMIC COMPONENT	CRYOSPHERE FACTOR
A. Direct effects	
Loss of coastal land and population displacement:	• Land ice melt contribution to sea level
Transportation	
• Shipping	• Iceberg hazard; sea-ice extent, thickness
• Barge traffic	• Fresh-water ice season
• Tundra roads	• Fresh-water ice thaw; frozen ground thaw
• Road/rail traffic	• Freeze events; snowfall
Water Resources	
• Consumption	
• Irrigation	• Snow/glacier melt runoff
• Hydropower	• Glacier melt runoff
• Agriculture	• Moisture recharge extremes
Hydrocarbon and mineral resource development	• Icebergs and sea ice; frozen ground duration and thickness
Wildlife population	• Snow cover; frozen ground and sea ice
Recreation/safety	• Snow cover; avalanches
B. Indirect effects	
Enhanced greenhouse effect	• Thaw of clathrates
Traditional lifestyles (Arctic, sub-arctic and high mountains)	• Changes in sea ice and fresh-water ice, snow cover, and frozen ground
Tourism/local economies	• Loss of glaciers; shorter snow season
Insurance sector	• Changes in risk factor

Specific questions that help define the primary tasks of CliC are:

- How stable is the global cryosphere?
  - How well do we understand and model the key processes involved in each cryospheric component of the climate system?
  - How do we best determine the rates of change in the cryospheric components?
- What is the contribution of glaciers, ice caps, and ice sheets to changes in global sea level on decadal-to-century time scales?
  - How can we reduce the current uncertainties in these estimates?
- What changes in frozen ground regimes can be anticipated on decadal-to-century time scales that would have major socio-economic consequences, either directly or through feedback on the climate system?

- What will be the annual magnitudes, rates of change, and patterns of seasonal redistribution in water supplies from snow- and ice-fed rivers under climate changes?
- What will be the nature of changes in sea-ice mass balance in both polar regions in response to climate change?
- What is the likelihood of abrupt climate changes resulting from regime changes in ice shelf – ocean and sea ice – ocean interactions that impact the ocean thermohaline circulation?
- How do we monitor cryospheric components as indicators of change in the climate system?

Monitoring cryosphere dynamics is a key aspect of high-latitude environmental studies (*Kondratyev et al.,* 1996; *Kondratyev* and *Cracknell,* 1998), especially because of rather controversial information concerning ice cover dynamics. It is true, for instance, for ice thickness observations. *Holloway* and *Sou* (2001) have pointed out that "while submarine records had indicated a stunningly rapid thinning, model results show that the position of submarine observations was exceptionally biased towards regions of thinning. A conclusion is that observations to date, along as with much physics as models represent, imply little or no overall thinning".

2.2 Arctic environmental pollution

The Arctic region exploration strategy in a broad context of biospheric studies has been discussed in details by *Matishov* (1998, 2000) as well as *Matishov* and *Matishov* (2001), where a necessity of an ecosystem approach in studying land and marine biota, as well as conditions of socio-economic development in high-latitude regions have been particularly emphasized. *Aibulatov* (2000) and *Matishov* and *Matishov* (2001) have discussed general problems of high-latitude environmental dynamics with special emphasis on radioactive pollution as an echo of the cold war. *Aibulatov* (2000) has analyzed principal sources of artificial radioisotopes in the Russian Arctic seas such as atomic explosions on Novaya Zemlya, the global radionuclide background as a result of the overall nuclear tests conducted on the planet, Russian chemical and mining plants, Chernobyl accident, West-European radiochemical plants, solid and liquid radioactive waste dumping in the Barents and Kara Seas, the Northern Military Marine and its bases, atomic submarine construction and maintenance facilities, and Atomflot (atomic fleet) of the Murmansk Shipping Company.

Studying of the distribution of ^{137}Cs, ^{90}Sr, and $^{239,240}Pu$ in the water masses of the North, Norwegian, Barents, Kara, White, and Laptev Seas has resulted in the following conclusions (*Aibulatov,* 2000):

- The general level of radioactive contamination of the waters of Arctic seas, except for several local areas, is characterized at the present time by little difference in comparison with background level (~ 6 Bq/kg).
- The radioactive pollution of the waters of the North and Norwegian Seas is entirely due to the emissions from radiochemical plants located in Western Europe.
- The contamination of waters of the Barents, White, Kara, and Laptev Seas is due to both local (Russian) sources and West-European plants.
- The field observations in the Kara Sea in 1992–1995 have resulted in the conclusion, that there have been no substantial radioactive emissions from the burial sites in the area.
- The contribution of the Ob and Yenisei river runoff to the overall radioactive transport is not significant at the present time, except cases of extremely heavy floods which happen very rarely.
- Compared to open waters of the Arctic Ocean, shelf seas of the Russian Arctic are more heavily contaminated.

Aibulatov (2000) has pointed out that judging from the ^{137}Cs-distribution patterns in the Kara Sea, it becomes evident that the Yenisei and Ob rivers (less evident, however, in the latter case) should be considered as transport channels for inputs of technogenic radionuclides to the Arctic Ocean waters. There are radioactive sources in the ocean as well. The ^{137}Cs activity level reached its maximum in 1984 and was equal to 245 Bq/kg in open sea; during the 1990s (1993) this level was found to be equal to 100 Bq/kg in the Yenisei estuary.

Arctic fjords have been classified into categories of comparatively clean, contaminated, heavily contaminated, and potentially contaminated. Contaminated areas include, for instance, Kola Gulf and, probably, all the fjords of the northern Kola Peninsula, west of Murmansk. The content of radionuclides in phytobenthos, in the coastal zone east of Murmansk, is low. Evidently, there has not been recently any serious radionuclide penetration into this area. A rather low gamma-nuclide level (1–3 Bq/kg) is typical for the zoobenthos of the Barents Sea. This is also true for the Kara Sea.

Impact of all the sources of radioactivity in the zone of the Arctic coast on the local population has not been assessed reliably enough. It was particularly difficult to separately identify natural and anthropogenic components of such

an impact. *Aibulatov* (2000) has discussed future research on the Russian Arctic radioactive pollution, including:

- Development of a coordinated Russian Arctic Sea Radioactivity Ecological Monitoring Programme.
- Assessments of impacts of different radioactive sources on the contamination of the Arctic marine environment including water basins, land, and atmosphere.
- Studies of detailed space and time variability of various long-lived technogenic radionuclides in bottom sediments.
- A detailed examination of all Novaya Zemlya fjords in connection with dumping radioactive waste.
- Research of the impact of radioactive pollution on the Arctic marine ecosystem dynamics.
- Studying medical aspects of environmental pollution in the Arctic.

2.3 High-latitude ecodynamics

The fundamental study of radioactivity of the Arctic and sub-Arctic marine ecosystems has been undertaken by *Matishov* and *Matishov* (2001), which resulted in the substantiation of a new branch of science – radiational ecological oceanology. Investigations have been conducted of the level of artificial radionuclide concentration in both environment and biota of the bays and inlets (the Kola, the Chernaya, the West Litsa), where radioactively dangerous objects are located. In this context, a classification has been suggested for coastal areas (bays, gulfs, fjords) in accordance with contamination levels for bottom sediments. Important role of a biofilter of pelagic zone and coastal zone has been discovered during the processes of self-purification of water reservoirs and transport of radionuclides from water to bottom sediments. For the first time, the levels of ^{137}Cs, ^{90}Sr, $^{239,240}Pu$ concentrations for different types and populations of sea organisms were measured. Migrations of radioisotopes along the trophic chains (from macrophytes and plankton to zoobenthos, fish, birds, seals, and whales) were studied as well. The assessments of comparative contributions of global, regional, and local sources of radioactive environmental contamination during the time-period from nuclear tests till recent time have been analyzed and used as a source of information for environmental predictions. An important optimistic conclusion concerning consequences of potential accidents is that for all prescribed scenarios of radioactive emissions, it is highly improbable that large-scale contamination of the Arctic Ocean will take place with ruinous

impacts on marine bioresources. High biological assimilation capacity in combination with specific features of hydrodynamic and other processes is supposed to serve as a barrier against dangerous pollution of the Arctic Ocean.

Kalabin (2000) has accomplished a study of the environmental dynamics and industrial potential of the Murmansk region, the most urbanized and industrially developed trans-polar region of the planet. Under these conditions, specific features of environmental dynamics result in the enhancement of anthropogenic impacts. In this context, *Kalabin* (2000) has analyzed critical environmental loads for some of the northern ecosystems, and emphasized a necessity to investigate their assimilation (buffer) capacity as a principal aspect of sustainably functioning natural systems. The solution of regional problems of sustainable development requires a careful analysis of the interaction between ecodynamics and socio-economic development.

3. Scientific field programs

The progress achieved in studying the Arctic environment variability is due to the accomplishment of a number of international research programs. The Arctic Climate System Study (ACSYS) project is of particular importance, developed in 1991 as the WCRP initiative, and a practicable program for the next decade to assess the role of the Arctic in global climate (*Arctic Climate...*, 1994; *Kondratyev et al.*, 1996). Five areas are emphasized: ocean circulation; sea ice climatology; Arctic atmosphere; hydrological cycle; and modeling. The scientific goals of ACSYS, which started its main observational phase in January 1994 and will continue for a ten-year period, includes the three main objectives (*Arctic Climate...*, 1994):

- understanding the interaction between the Arctic Ocean circulation, ice cover, and hydrological cycle;
- initiating long-term climate research and monitoring programs for the Arctic;
- providing a scientific basis for an accurate representation of Arctic processes in global climate models.

The Arctic Ocean Circulation Programme of ACSYS consists of four components:

- the Arctic Ocean Hydrographic Survey to collect a high-quality hydrographic data-base representative of the Arctic Ocean;
- the Arctic Ocean Shelf Studies, which are aimed at understanding how the shelf processes partition salt- and fresh-water components; at defining the

dynamics and thermodynamics of the shelf waters as well as other processes;

- the Arctic Ocean Variability Project designed to assess the variability of the circulation and density structure of the Arctic Ocean;
- the Historical Arctic Ocean Climate Database Project aimed to establish a universally available digital hydrographic database for the Arctic Ocean for analysis of climate-related processes and variability, and to provide a data set suitable for initialization and verification of arctic climate and circulation models.

The ACSYS sea ice program includes three main components:

- establishing an Arctic basin-wide sea ice climatology database;
- monitoring the export of sea ice through the Fram Strait;
- arctic sea ice processes studies.

One of the main tasks of the ACSYS arctic sea ice program is to establish a climatology of ice thickness and ice velocity. Such data will be supplied by the WCRP Arctic Ice Thickness Project, the International Arctic Buoy Programme, sonar profiling from naval submarines and unmanned vehicles, airborne oceanographic lidars, and polar satellites carrying appropriate instruments.

The arctic atmosphere provides the dynamic and thermodynamic forcing of the Arctic Ocean circulation and sea ice. Key directions of research include problems such as cloud-radiation interaction, air-sea interaction in the presence of ice cover (impacts of polynyas and leads are of special interest), arctic haze, etc.

Primary ACSYS efforts within the project of the Hydrological Cycle in the arctic region are aimed at:

- documentation and intercomparison of solid precipitation measurement procedures used in high latitudes and
- development of methodologies for determining areal (regional) distributions of precipitation from station data.

There are two relevant data-archiving efforts: Arctic Precipitation Data Archive (APDA) and Arctic Run-off Data Base (ARDB).

The principal purpose of the ACSYS modeling program is simulations of climate variations in polar regions, which arise from the interaction between atmosphere, sea ice, and ocean.

Apart from the ACSYS project described above, a number of new research programs have been developed, such as the Study of Environmental Arctic Change (SEARCH), which is an interdisciplinary, multi-scale program dedicated to understanding the complex interrelated changes that have been observed in the Arctic environment in the past few decades (*SEARCH...*, 2000,

2001). SEARCH is envisioned as a long-term effort of observations, modeling, process studies, and applications with emphasis on five major thematic areas:

- human society;
- marine/terrestrial biosphere;
- atmosphere and cryosphere;
- ocean, and
- integrated projects/models/assessment.

The Arctic System Science (ARCSS) Programme (*Toward Prediction...*, 1998) is an interdisciplinary program with the principal goals to (1) understand the physical, geological, chemical, biological, and sociocultural processes of the arctic system that interact with the total Earth's system, and thus contribute to or are influenced by global change, in order to (2) advance the scientific basis for predicting environmental change on a seasonal-to-centuries time scale, and for formulating policy options in response to the anticipated impacts of global change on humans and societal support systems. The following four scientific thrusts include central aims of ARCSS:

- to understand the global and regional impacts of the arctic climate system and its variability;
- to determine the role of the Arctic in global biogeochemical cycling;
- to identify global change impacts on the structure and stability of arctic ecosystems;
- to establish the links between environmental change and human activity.

ARCSS has four linked ongoing components: Ocean/Atmosphere/Ice Interactions (OAII); Land/Atmosphere/Ice Interactions (LAII); Paleoenvironmental Studies (including GISP2, Greenland Ice Sheet Project Two, and PALE, Paleoclimates of Arctic Lakes and Estuaries); Synthesis, Integration, and Modeling Studies (SIMS), and Human Dimensions of the Arctic System (HARC). K. Aagard (*Toward an Arctic...*, 1998) discussed basic problems with a multidisciplinary look at the Arctic Ocean, including: physical and chemical studies; biological studies; contaminant studies; measurements of the properties, and variability of the ice cover and surface radiation budget; studies of atmospheric chemistry; geological observations.

LAII research has three main goals (*Witness...*, 1994):

- to estimate important fluxes in the region, including the amount of carbon dioxide, and methane reaching the atmosphere, the amount of river water reaching the Arctic Ocean, and the radiative flux back to the atmosphere;
- to predict how possible changes in the arctic energy balance, temperature, and precipitation will lead to feedback affecting large areas; this

incorporates changes in water budget, duration of snow cover, extent of permafrost, and soil warming, wetting, and drying; and

- to predict how the land and fresh-water biotic communities of the Arctic will change, and how this change will affect future ecosystem structure and function.

A major LAII research project is the Flux Study; its principal purpose is a regional estimate of the present and future movement of materials between the land, atmosphere, and ocean in the Kuparuk river basin in northern Alaska.

Three of the nineteen LAII projects are part of the International Tundra Experiment (ITEX), which looks at the response of plant communities to climate change. Three others are concerned with atmosphere processes, including weather patterns affecting snowmelt, arctic-wide temperature trends, and water vapor over the Arctic, and its relationship to the atmospheric circulation and surface conditions. One project deals with response of large birds to climate and sea-level change at river deltas, and one studies the balance and recent volume changes of McCall Glacier in the Brooks Range.

Synthesis, integration, and modeling studies are intended to discover linkages and strengthen system-level understanding. Research on the past and contemporary relationship of humans to global climate change is thought to be critical to understanding the consequences of global change in the Arctic.

There are a number of ARCSS data projects, including: LAII Flux Study Alaska North Slope data sampler CD-ROM; OAII Northeast Water (NEW) polynya project CD-ROM; Arctic solar and terrestrial radiation CD-ROM, etc.

The list of the OAII components includes the joint US/Japan cruise, the Western Arctic Mooring project, and the Northeast Water Polynya project. Among other OAII projects, the most notable are the US/Canada Arctic Ocean Section and the Surface Heat Budget of the Arctic Ocean (SHEBA) projects.

An outstanding effort has been accomplished in 1994 within the Canada/US 1994 Arctic Ocean Section, when two icebreakers entered the ice in the northern Chukchi Sea on July 26, 1994, reached the North Pole on August 22, and left the ice northwest of Spitsbergen on August 30, thereby completing the first crossing of the Arctic Ocean by surface vessels. This voyage will greatly alter our understanding of biological productivity, the food web, ocean circulation and thermal structure, and the role of clouds in the summer radiation balance, as well as the extent of contamination and spreading pathways (especially related to radionuclides and chlorinated organics), and the extent and effects of sediment transport by sea ice (*Witness...*, 1994).

In connection with the SHEBA project, the US Department of Energy's Atmosphere Radiation Measurement (ARM) program indicated its intention to develop a Cloud and Radiation Testbed (CART) facility on the North Slope of

Alaska. The principal focus of this program will be on atmospheric radiative transport, especially as modified by clouds (which impacts the growth and decay of sea ice), as well as testing, validation, and comparison of radiation transfer models in both ice pack and arctic coastal environment.

A special place is occupied by the Russian-American Initiative on Shelf-Land Environments in the Arctic (RAISE) with the principal goal of facilitating ship-based research in the Russian Arctic (*RAISE...*, 2001). Earlier relevant land-based research projects under the RAISE umbrella included studies of:

- organic material and nutrient fluxes from Russian rivers;
- seasonal flooding dynamics along rivers, and
- reconstruction of late Pleistocene glacial and sea-level history on Wrangel Island.

New scientific topics in the near-shore waters of the Russian continental shelf will include a broad range of studies: from the biogeochemical fate of organic materials contributed to the Arctic Ocean by shoreline erosion and river runoff to the social and biological impacts of changes in sea-ice distributions.

The Western Arctic Shelf-Basin Interactions (SBI) project, sponsored by ARCSS Programme and the U.S. Office of Naval Research, is investigating the arctic marine ecosystem to improve our capacity to predict environmental change. The SBI Phase II Field Implementation Plan (2002–2006) focuses on three research topics in the core study area:

- northward fluxes of water and bioactive elements through the Bering Strait input region;
- seasonal and spatial variability in the prediction and recycling of biogenic matter on the shelf-slope area; and
- temporal and spatial variability of exchanges across the shelf-slope region into the Canada Basin.

4. Priorities and perspectives

The recent meeting of the International Arctic Science Committee (IASC) has identified the following four science priorities (*Witness...*, 1994):

- arctic processes relevant to global systems;
- effects of global change on the Arctic and its peoples;
- natural processes within the Arctic; and
- sustainable development in the Arctic.

The following areas in arctic global change research have been considered the most significant:

- terrestrial ecosystem;
- mass balance of glaciers and ice sheets;
- regional cumulative impacts; and
- human dimensions.

An important aspect of studying high-latitude environmental dynamics is an assessment of the impact of potential anthropogenic climate warming. In this context *Frederick* (1994) has formulated key issues of integrated assessments of the impact of climate change on natural resources. Specific project objectives include: (1) characterizing the current state of natural science and socioeconomic modeling of the impacts of climate change and current climate variability on forests, grasslands, and water; (2) identifying what can be done currently with impact assessments and how to undertake such assessments; (3) identifying impediments linking biophysical and socioeconomic models into integrated assessments for policy purposes; (4) recommending research activities that will improve the state of the art and remove impediments model integration.

The following questions are supposed to be answered:

- How will the overall system (physical-biological-economic) respond to various imposed stresses?
- How do the uncertainties in the component models add up to give an overall system response uncertainty?
- Is society made more vulnerable to extreme natural events either by changing those events or by reducing human ability to respond with corrective actions?
- How likely is it that the consequences of climate change will be severe or catastrophic?
- What is at risk and when is it a risk?
- What are the likely impacts on the landscape and hydrological system?
- How might the boundary conditions and overall productivity of the forests, grasslands, and other rangelands be affected?
- How might increasing carbon dioxide levels affect crops and food supplies for humans, livestock, and wildlife?
- What are the socioeconomic consequences of these physical and biological changes?
- What are the likely consequences of mitigation actions for ecosystems?

- Can the costs associated with climate change be reduced through natural adaptation of ecosystems or policy-initiated adaptation?

Frederick (1994) has emphasized, that the accumulated results of many regional and local climate impact assessments may help provide informed answers to these questions. Nevertheless, the uncertainties surrounding both the nature and impacts of any future climate change are likely to remain very large, precluding precise estimates of the net benefits associated with alternative policy responses. Even if the range of uncertainty were diminished, it might still be difficult to justify specific measures on narrow economic grounds, because (as noted above) the impacts on natural resource systems are apt to be poorly reflected in standard benefit-cost analysis.

Mendelsohn and *Rosenberg* (1994) have formulated the following questions relevant to global warming effects in the area of ecological and water resources:

- Do changes in ecosystems provide important feedbacks to the natural carbon, nitrogen, and methane cycles? For example, will the natural sinks or emitters be affected by changing precipitation, temperature, and CO_2 levels?
- What are the appropriate output measures of ecosystem component models? What are the ecological effects of climate change that policy analysts should use to determinate the importance of an ecosystem change?
- What climate change-driven shifts in ecosystem boundaries can be predicted?
- Will these effects be subtle and small or large and dramatic, and over what time frame and spatial dimensions?
- Will climate change cause a change in the productivity of valuable market or non-market species? For example, to what extent will some forests grow more quickly or more slowly? Will desired non-market species, such as bear, elk, and bald eagles, be more or less plentiful?
- What species could be lost with rapid climate changes? How do the vulnerable species break down by type and geographic distribution? How should conservation policies adapt to a world requiring change?
- How are ecosystems likely to change as the climate evolves over time: will there be a large increase in early succession species and where?
- How will average flows in rivers change with greenhouse warming? How will these flows change over seasons? Will the probabilities of catastrophic events change?

- What values do people assign to the changes in ecosystems by climate change? Which changes are important and which are minor? Can a value be assigned to non-use?
- How much should the society be willing to pay to reduce the probability of losing specific species? If different scenarios favour different species, how should the society trade between these outcomes?
- What impact do ecosystem changes have upon the economy? For example, how will climate change affect grazing, commercial fishing, timber, or commercial tourism?

It has been suggested (*Proceedings...*, 1999) that priority program areas and relevant projects are as follows:

- Impacts of global changes on the arctic region and its peoples:
  - regional cumulative impacts,
  - effects of increased UV radiation.
- Arctic processes of relevance to global systems:
  - mass balance of glaciers and ice sheets,
  - terrestrial ecosystems and feedback on climate change.
- Natural processes within the Arctic:
  - arctic marine/coastal/riverine systems,
  - disturbance and recovery of terrestrial ecosystems.
- Sustainable development in the Arctic:
  - sustainable use of living resources,
  - dynamics of arctic populations and ecosystems,
  - environmental and social impacts of industrial development.

Future priorities of the ARCSS include the following research questions (*Toward Prediction...*, 1998): How will the arctic climate change over the next 50 to 100 years? How will human activities interact with future global change to affect the sustainability of natural ecosystems and human societies? How will changes in arctic biogeochemical cycles and feedbacks affect arctic and global systems? How will changes in arctic hydrological cycles and feedbacks affect arctic and global systems? Are predicted changes in the Arctic detectable?

Important perspectives are connected with paleoenvironmental studies by the Paleoenvironmental Arctic Sciences (PARCS) community (*PARCS...*, 2000), which have a principal aim of answering the question: how much do recent observations of climate change in the Arctic reflect natural climate cycles? Relevant major topics include:

- the medieval warm period (apparently, AD 1000–1400) and Little Ice Age (approximately AD 1400–1850);
- high-amplitude Holocene climate cycles, and
- the possible connection of the onset of the neoglacial (a mid-Holocene cooling, particularly evident at high northern latitudes) with shifts in the frequency and amplitude of such climate cycles.

According to the PARCS, there are very warm past scenarios, that can serve as analogues for future climate warming:

- the early Holocene, when the Arctic had experienced high summer insolation anomalies, and
- the last interglacial period (marine isotope stage 5), which appears as a very strong warming in the paleorecord approximately 125,000 years ago.

Key topics to investigate in relation to these periods are:

- feedbacks and nonlinear changes (surprises) as consequences of strong warming - particularly the role of sea ice, ice sheets, and land surface cover;
- implications of strong warming for arctic and global carbon budgets.

To summarize what has been mentioned in connection with recent Arctic environmental programs, it must be emphasized, that the relevant information was not at all exhaustive (see also *IASC...*, 2001). An obvious conclusion is that the number of programs is too great. A clear necessity exists of better coordination of all on-going efforts and their "regularization".

Vörösmarty et al. (2001) are right in their conclusion that "understanding the full dimension of arctic change is a fundamental challenge to the scientific community over the coming decades, and will require a major new effort at interdisciplinary synthesis. It also requires an unprecedented degree of international cooperation".

Undoubtedly, the Second International Polar Year is an urgent necessity.

References

Aagard, K. and *Carmack, E.C.*, 1994: The Arctic Ocean and climate: A perspective. *Geophysical Monograph 85. AGU, Washington, D.C.*, 5-20.

Aagard, K. et al. (eds.), 1998: *Proc. of the ACSYS Conference on Polar Processes and Global Climate* (Rosario, USA, 3-6 November 1997). WCRP-106 (WMO/TD No. 908). Geneva.

ACD: Arctic Coastal Dynamics. Science and Implementation Plan, 2001: Int. Arctic Science Committee. Oslo, 20 pp.

ACIA (Arctic Climate Impact Assessment), 2000: Prepared by the Assessment Steering Committee. Fairbanks, Alaska, September 2000, 35 pp.

Adamenko, V.N. and *Kondratyev, K.Ya.*, 1999: Global climate change and its empirical diagnostics. In *Anthropogenic Impact on Northern Nature and Its Consequences* (in Russian). Kola Centre of the Russian Acad. Sci., Apatity, 17-35.

Aibulatov, N.A., 2000: *Cold War Echo in the Russian Arctic Seas* (in Russian). Moscow, GEOS, 307 pp.

Alekseev, G.V., 1998: Arctic climate dynamics in the global environment. *World Clim. Res. Progr./World Meteorol. Org.*, Geneva, No. 908, 11-14.

Alekseev, G.V., Aleksandrov, E.I., Svyaschennikov, P.N., and *Kharlanenkova, N.E.*, 2000: On interaction of climate oscillations in the Arctic and in mid- and low latitudes (in Russian). *Meteorol. and Hydrol.*, No. 6, 5-17.

Allison, I., Barry, R.G., and *Goodison, B.E.* (eds.), 2001: *Climate and Cryosphere (CliC) Project Science and Co-Ordination Plan.* Version 1. WCRP-114 (WMO/TD No. 1053). Geneva, 73 pp, Appendices.

Arctic Climate System Study (ACSYS). Initial Implementation Plan, 1994: WCRP-85 (WMO/TD No. 627), Geneva, Switzerland, 66 pp.

Arctic Pollution, 1997: Arctic Monitoring and Assessment Program. AMAP, Oslo, Norway, 188 pp.

Arctic Science Summit Week. 25-29 April 1999. Tromsø, Norway. *Joint-Science Day: Marine Climate of the Arctic* , 2000. Norsk Polarinstitutt. INTERNRAPPORT. Tromsø, No. 3, 32 pp.

Arfeuille, G., Mysak, L.A., and *Tremblay, L.B.*, 2000: Simulation of the interannual variability of the wind-driven Arctic sea-ice cover during 1958-1998. *Clim. Dynamics 16*, No.2-3, 107-122.

Atkinson, D.E., Alt, B., and *Gajewski, K.*, 2000: A new database of high Arctic climate data from the polar continental shelf project archives. *Bull. Amer. Meteorol. Soc. 81*, 2621-2630.

Baldwin, M.P. and *Dunkerton, T.J.*, 1999: Propagation of the Arctic Oscillation from the stratosphere to the troposphere. *J. Geophys. Res. 104*, ND24, 30,937-30,946.

Barry, R.G. (ed.), 1998: *Organization of Internationally Co-ordinated Research Into Cryosphere and Climate.* WCRP-102 (WMO/TD No. 867). WMO, Geneva, 10 pp. Appendices.

Benner, T.C., Curry, J.A., and *Pinto, J.O.*, 2001: Radiative transfer in the summertime Arctic. *J. Geophys. Res. 106*, N14, 15,173-15,184.

Brebbia, C.A., Villacampa, Y., and *Uso, J.-L.* (eds.), 2001: *Ecosystems and Sustainable Development.* Adv. In Ecol. Sci., 10, 800 pp.

CAFF (Conservation of Arctic Flora and Fauna) 2001. Arctic Flora and Fauna: Status and Conservation. Edita, Helsinki. 272 pp.

Casleden, J., 200: Bridging scientific and traditional knowledge of climate change in the Canadian Arctic. *Global Change Newsletter,* No. 47, 5-8.

Changes in Climate and Environment at High Latitudes, 2001: Abstracts and Proceedings of the Norwegian Geological Society. Tapir Academie Press, Trondheim. 102 pp.

Chao, S.-Y., 1999: Ocean feedback to wind-driven coastal polynyas. *J. Geophys. Res. 104*, NC8, 18,073-18,086.

Chýlek, P. and *Lesins, G.*, 2001: Recent temperature changes in Greenland. In *First Int. Conf. On Global Warming and the Next Ice Age.* Dalhousie Univ., 19-24 Aug. 2001, 71-84.

Climate Change 2001: The Scientific Basis. Contribution of WG1 to the Third Assessment Report of the IPCC (J. T. Houghton et al.), 2001: Cambridge University Press, 881 pp.

Curry, J.A., 2001: Introduction to special section: FIRE Arctic Clouds Experiment. *J. Geophys. Res. 106*, ND14, 14,985-14,989.

Curry, J.A., Schramm, J.L., Perovich, D. K., and *Pinto, J.C.*, 2001: Applications of SHEBA/FIRE data to evaluation of snow/ice albedo parameterizations. *J. Geophys. Res. 106*, N14, 15,345-15,356.

Dare, R.A. and *Atkinson, B.W.*, 1999: Numerical modeling of atmospheric response to polynyas in the Southern Ocean sea ice zone. *J. Geophys. Res. 104*, ND14, 16,691-16,708.

Dickson, R., 1999: All change in the Arctic. *Nature 397*, 389-391.

Doelling, D.R., Minnis, P., Spangenberg, D.A., Chakrapani, V., Mahesh, A., Pope, S.K., and *Valero, P.J.*, 2001: Cloud radiative forcing at the top of the atmosphere during FIRE ACE derived from AVHRR data. *J. Geophys. Res. 106*, N14, 15,279-15,296.

Doiban, V.A., Backich, Yu. M., and *Luzin, G.P.*, 1995: *Northern Sea Route and Market Economics: New Possibilities for Development* (in Russian). Kola Sci. Centre of the Russian Acad. Sci., Apatity, 140 pp.

Dong, X., Mace, G.G., Minnis, P., and *Young, D.F.*, 2001: Arctic stratus cloud properties and their effect on the surface radiation budget: Selected cases from FIRE ACE. *J. Geophys. Res. 106*, N14, 15,297-15,312.

Dorn, W., Dethloff, K., Rinke, A., and *Botzet, M.*, 2000: Distinct circulation states of the Arctic atmosphere induced by natural climate variability. *J. Geophys. Res. 105*, ND24, 29,659-29,668.

Duynkerke, P.G. and *Roode, S.R.*, 2001: Surface energy balance and turbulence characteristics observed at the SHEBA Ice Camp during FIRE III. *J. Geophys. Res. 106*, N14, 15,313-15,322.

Edwards, M., Anderson, R., Chayes, D., Coakley, B., Cochran, J., Jacobsson, M., Kurras, G., Polyak, L., and *Rognstad, M.*, 2001: SCICEX sonars chart new topographies, new theories. *Witness the Arctic 9*, N1, 1-2.

Edwards, M.H., Kurras, G.J., Tolstoy, M., Bohnenstiehl, D.R., Coakley, B.J., and *Cochran, J.R.*, 2001: Evidence of recent volcanic activity on the ultra-slow spreading Gakkel Ridge. *Nature 409*, 808-812.

Ekwurzel, B., Schlosser, P., Mortlock, R. A., Fairbanks, R.G., and *Swift, J.H.*, 2001: River runoff, sea ice meltwater, and Pacific water distribution and mean residence times in the Arctic Ocean. *J. Geophys. Res. 106*, NC5, 9075-9092.

Everett, J.T. and *Fitzharris, B.B.* (eds.), 2001: *The Regional Impacts of Climate Change. Chapter 3: The Arctic and Antarctic.* The IPCC Working Group 2 Report – 2001 (http://www.grida.no/climate/ipcc/regional/042.htm).

First GARP Global Experiment. Vol. 2. Polar aerosols, extended cloudiness and radiation, 1981, (eds.: *K.Ya. Kondratyev* and *V.F. Zhvalev*). Gidrometeoizdat, Leningrad, 150 pp.

Forland, E.J. and *Hanssen-Bauer, I.*, 2000: Increased precipitation in the Norwegian Arctic: True or false? *Clim. Change 46*, N4, 485-509.

Frederick, K.D., 1994: Integrated assessment of the impacts of climate change on natural resources. An Introductory essay. *Clim. Change 28*, N102, 1-14.

French, H.M., 1999: Past and present permafrost as an indicator of climate change. *Polar Research 18*, 269-274.

Garrett, T.J., Hobbs, P.V., and *Gerber, H.*, 2001: Shortwave, single-scattering properties of arctic ice clouds. *J. Geophys. Res. 106*, 15,155-15,172.

Girard, E. and *Curry, J.A.*, 2001: Simulation of arctic low-level clouds observed during the FIRE Arctic Experiment using a new bulk microphysics scheme. *J. Geophys. Res. 106*, 15,139-15,154.

Gloersen, P., Parkinson, C.L., Cavalieri, D.J., Comiso, J.C., and *Zwally, H.J.*, 1999: Spatial distribution of trends and seasonality in the hemispheric sea ice covers: 1978-1996. *J. Geophys. Res. 104*, NC9, 20,827-20,836.

Goldner, D.R., 1999: On the uncertainty of the mass, heat, and salt budgets of the Arctic Ocean. *J. Geophys. Res. 104,* NC12, 29,757-29,770.

Goody, R., 1980: Polar processes and world climate (a brief review). *Mon. Weather Rev. 108*, N12, 1935-1942.

Gordon, C., Cooper, C., Senior, C.A., Banks, H., Gregory, J.M., Johns, T.C., Mitchell, J.F.B., and *Wood, R.A.*, 2000: The simulation of SST, sea ice extents and ocean heat transports in a version of the Hadley Centre coupled model without flux adjustments. *Clim. Dynamics 16*, N2-3, 147-168.

Gramberg, I.S. et al. (eds.) (2000). *Arctic at the Threshold of the Third Millennium* (in Russian). NAUKA, St. Petersburg, 204 pp.

Grassl, H., 1999: The cryosphere: An early indicator and global player. *Polar Research 18*, N2, 119-125.

Grotefendt, K., Lagemann, K., Quadfasel, D., and *Ronski, S.*, 1998: Is the Arctic warming? *J. Geophys. Res. 103*, NC12, 27,679-27,688.

Haas, C. and *Eicken, H.*, 2001: Interannual variability of summer sea ice thickness in the Siberian and central Arctic under different atmospheric circulation regimes. *J. Geophys. Res. 106*, NC3, 4449-4462.

Haggerry, J.A. and *Curry, J.A.*, 2001: Variability of sea ice emissivity estimated from airborne passive microwave measurements during FIRE SHEBA. *J. Geophys. Res. 106*, N14, 15,265-15,278.

Hanesiak, J.M., Barber, D.G., De Abreu, R.A., and *Yackel, J.J.*, 2001: Local and regional albedo observations of arctic first-year sea ice during melt ponding. *J. Geophys. Res. 106*, NC1, 1005-1016.

Hobbs, P.V., Rangno, A.L., Shupe, M., and *Uttal, T.*, 2001: Airborne studies of cloud structures over the Arctic Ocean and comparisons with retrievals from shipbased remote sensing measurements. *J. Geophys. Res. 106*, N14, 15,029-15,044.

Hoerling, M.P., Hurrell, J.W., and *Xu, T.*, 2001: Tropical origins for recent North Atlantic climate change. *Science 292*, No. 5514, 90-92.

Holland, D.M., 2001: Explaining the Weddell Polynya – a large ocean eddy shed at Maud Rise. *Science 292*, 1697-1700.

Holloway, G. and *Sou, T.*, 2001: Is Arctic sea ice rapidly thinning? *Ice and Climate News*, No. 1, 2-5.

Hoskins, B.J. and *Yang, G.-Y.*, 2000: The equatorial response to higher-latitude forcing. *J. Atmos. Sci. 57*, 1197-1213.

Hunke, E.C. and *Ackley, S.F.*, 2001: A numerical investigation of the 1997-1998 Ronne Polynya. *J. Geophys. Res. 106*, N15, 22,373-22,382.

IASC Project Catalogue, 2001: The International Arctic Science Committee. Oslo, Norway, 57 pp.

Impacts of Global Climate Change in the Arctic Region, 1999: IASC, Fairbanks, Alaska, 59 pp.

Interactions Between the Cryosphere, Climate, and Greenhouse Gases, 1999. Eds.: *M. Trauter et al.* IAHS Press, 281 pp.

Iversen, T., 1996: Atmospheric transport pathways for the Arctic. *Chem. Exchange between the Atmos. and Polar Snow: Proc. NATO Adv. Res. Workshop "Process. Chem. Exchange Between Atmos. and Polar Snow"*, Ciocco, March 19-23, 1995. Berlin e.a., 71-92.

Izrael, Y.A., Kalabin, G.V., and *Nikonov, V.V.* (eds.), 1999: *Anthropogenic Impact on Northern Nature and Its Ecological Consequences* (in Russian). Kola Sci. Centre, Russian Acad. Sci., Apatity, 314 pp.

Jaworowski, Z., 1989: *Pollution of the Norwegian Arctic: A review*. Rapportserie Nr. 55. Norsk Polarinstitutt, Oslo. 93 pp.

Jaworowski, Z., Segalstad, T.V., and *Hisdal, V.*, 1990: *Atmospheric CO_2 and global warming: A critical review*. Norsk Polarinstitutt, Rapportserie Nr. 39, 75 pp.

Jiang, H., Feingold, G., Cotton, W.R., and *Duynkerke, P.G.*, 2001: Large-eddy simulations of entrainment of cloud condensation nuclei into the Arctic boundary layer: May 18, 1998, FIRE/SHEBA case study. *J. Geophys. Res. 106*, ND14, 15,113-15,122.

Johannessen, O.M., Muench, R.D., and *Overland, J.E.* (eds.), 2000: *The Polar Oceans and Their Role in Shaping the Global Environment*. Amer. Geophys. Union. Geophys. Monogr. 85. Washington, D.C., 525 pp.

Kalabin, G.V., 2000: *Ecodynamics of Anthropogenic Environment Province of the North* (in Russian). Kola Sci. Centre, Russian Acad. Sci., Apatity, 294 pp.

Khvorostyanov, V.I., Curry, J.A., Pinto, J.O., Shupe, M., Baker, M., and *Sassen, K.*, 2001: Modeling with explicit spectral water and ice microphysics of two-layer cloud system of altostratus and cirrus observed during the FIRE Arctic Clouds Experiment. *J. Geophys. Res. 106*, N14, 15,099-15,112.

Kienast, S.S. and *McKay, J.L.*, 2001: Sea surface temperatures in the subarctic Northeast Pacific reflect millenial scale climate oscillations during the last 16 kyrs. *Geophys. Res. Lett. 28*, N8, 1563-1566.

Kondratyev, K.Ya., Bondarenko, V.G., and *Khvorostyanov, V.I.*, 1992: A three-dimensional numerical model of cloud formation and aerosol transport in the orographically inhomogeneous atmospheric boundary layer. *Boundary-Layer Meteorol. 61*, N3, 265-285.

Kondratyev, K.Ya., Johannessen, O.M., and *Melentyev, V.V.*, 1996: *High-Latitude Climate and Remote Sensing*. Wiley/PRAXIS, Chichester, U. K., 200 pp.

Kondratyev, K.Ya. and *Cracknell, A.P.*, 1998: *Observing Global Climate Change*. London e.a., Taylor & Francis, 761 pp.

Kondratyev, K.Ya., 1999: *Climatic Effects of Aerosols and Clouds*. Springer/PRAXIS, Chichester, U. K., 264 pp.

Kondratyev, K.Ya. and *Varotsos, C.A.*, 2000: *Atmospheric Ozone Variability: Implications for Climate Change, Human Health, and Ecosystems*. Springer/PRAXIS, Chichester, U. K., 614 pp.

Krapivin, V.F. and *Kondratyev, K.Ya.*, 2002: *Global Environmental Change: Ecoinformatics* (in Russian). St. Petersburg State Univ., 721 pp.

Lawson, R.P., Baker, B.A., Schmitt, C.G., and *Jensen, T.L.*, 2001: An overview of microphysical properties of Arctic clouds observed in May and July 1998 during FIRE ACE. *J. Geophys. Res. 106,* N14, 14,989-15,014.

Lemke, P., Harder, M., and *Hilmer, M.*, 2000: The response of Arctic sea ice to global change. *Clim. Change 46,* N3, 277-287.

Lemke, P., 2001: Open windows to the polar oceans. *Science 292*, 1670-1671.

Lohmann, U., Humble, J., Leaitch, W.R., Isaac, G.A., and *Gultepe, I.*, 2001: Simulations of ice clouds during FIRE ACE using the CCCMA single-column model. *J. Geophys. Res. 106,* N14, 15,123-15,138.

Losev, K.S., 2001: *Ecological Issues and Sustainable Development Perspectives of Russia in the XXI Century*. Cosmoinform Publ., Moscow, 400 pp.

Marchand, R.T., Ackerman, T.P., King, M.D., Moroney, C., Davies, R., Muller, J.-P.A.L., and *Gerber, H.*, 2001: Multiangle observations of Arctic clouds from FIRE ACE: June 3, 1998, case study. *J. Geophys. Res. 106,* N14, 15,201-15,214.

Matishov, G.G., 1998: Strategy of Arctic studies (in Russian). *Herald of the Russian Acad. Sci. 68*, N6, 515-520.

Matishov, G.G., 2000: Contemporary problems of oceanology and geography of the World Ocean (in Russian). *Herald of the Russian Acad. Sci. 70,* N8, 682-687.

Matishov, D.G. and *Matishov, G.G.*, 2001: *Radiational Ecological Oceanology* (in Russian). Kola Science Centre, Russian Acad. Sci., Apatity, 419 pp.

May, B.D. and *Lley, D.E.*, 2001: Growth and steady state stages of thermohaline intrusion in the Arctic Ocean. *J. Geophys. Res. 106*, NC8, 16,783-16,794.

Mendelsohn, R. and *Rosenberg, N.J.*, 1994: Framework for integrated assessment of global warming impacts. *Clim. Change 28*, N1-2, 15-44.

Minnis, P., Chakrapani, V., Doelling, D.R., Nguyen, L., Palikonda, R., Spangenberg, D.A., Uttal, T., Arduini, R.F., and *Shupe, M.*, 2001: *J. Geophys. Res. 106*, N14, 15,215-15,232.

Mysak, L.A. and *Venegas, S.A.*, 1998: Decadal climate oscillations in the Arctic: A new feedback loop for atmosphere-ice-ocean interactions. *Geophys. Res. Lett. 25,* N19, 3607-3610.

Nagurny, A. P. and *Maistrova, V.V.*, 2002: Long-term temperature trends for the free atmosphere in the Arctic (in Russian). *Doklady RAS,* (in press).

Newman, P.A., Nash, E.R., and *Rosenfeld, J.E.*, 2001: What controls the temperature of the Arctic stratosphere during the spring? *J. Geophys. Res. 106,* ND17, 19,999-20,010.

Overland, J.E. and *Adams, J.M.*, 2001: On the temporal character and regionality of the Arctic Oscillation. *Geophys. Res. Lett. 28,* N14, 2811-2814.

PARCS develops two updated research goals, 2000: *Witness the Arctic 9*, N1, p.8.

Parkinson, C.L., Cavalieri, D.J., Gloersen, P., Zwally, H.J., and *Comiso, J.C.*, 1999: Arctic sea ice extents, areas, and trends, 1978-1996. *J. Geophys. Res. 104*, NC9, 20,837-20,856.

Polyakov, I.V., Proshutinsky, A.Y., and *Johnson, M.A.,* 1999: Seasonal cycles in two regimes of Arctic climate. *J. Geophys. Res. 104*, NC11, 25,761-25,788.

Proceedings of the International Symposium on Polar Aspects of Global Change, 1999. Tromsø, Norway, 24-28 August 1998. Polar Research, 18, N2, 404 pp.

Proshutinsky, A., 2000: Arctic climate variability during 20th century. *Int. WOCE Newsletter,* N40, 9-12.

Przybylak, R., 2000: Diurnal temperature range in the Arctic and its relation to hemispheric and Arctic circulation patterns. *Int. J. of Climatol. 20*, N3, 231-254.

RAISE Plan focuses on ship-based research in Russia, 2001: *Witness the Arctic 9*, N1, p.7.

Rangno, A.L. and *Hobbs, P.V.,* 2001: Ice particles in stratiform clouds in the Arctic and possible mechanisms for the production of high ice concentrations. *J. Geophys. Res. 106*, N14, 15,065-15,076.

Rapley, C., 1999: Global change and the polar regions. *Polar Research 18,* N2, 117-118.

Report from the Arctic Climate Impact Assessment Modeling and Scenarios Workshop. Stockholm, Sweden, January 29-31, 2001. The ACIA Secretariat, Fairbanks, 28 pp.

Riedlinger, D. and *Berkes, F.,* 2001: Contributions of traditional knowledge to understanding climate change in the Canadian Arctic. *Polar Research 37*, N203, 315-328.

Rimbu, N., Lohmann, G., Felis, T., and *Pätzold, J.,* 2001: Arctic Oscillation signature in a Red Sea coral. *Geophys. Res. Lett. 28*, N15, 2959-2962.

Rind, D., Chandler, M., Lerner, J., Martinson, D.G., and *Yuan, X.,* 2001: Climate response to basin-specific changes in latitudinal temperature gradients and implications for sea ice variability. *J. Geophys. Res. 106*, ND17, 20,161-20,174.

Rinke, A., Lynch, A.H., and *Dethloff, K.,* 2000: Intercomparison of Arctic regional climate simulations: Case studies of January and June 1990. *J. Geophys. Res. 105*, ND24, 29,669-29,684.

Rogachev, K.A. and *Carmack, E.C.,* 2002: Eddies in the western Subarctic Pacific: Their internal structure and linkages to the regime shift phenomena. *Int. WOCE Newsletter,* N42, 25-28.

Rybak, E. and *Rybak, O.,* 2001: Changes of the ice cover in the Barents Sea: Links with the large-scale processes in the atmosphere. In *First Int. Conf. On Global Warming and the Next Ice Age*. Dalhousie Univ., 19-24 Aug., 2001, 155-159.

Sandven, S., Johannessen, O.M., Miles, M.W., Pettersson, L.H., and *Kloster, K.,* 1999: Barents Sea seasonal ice zone features and processes from ERS-1 synthetic aperture radar: Seasonal Ice Zone Experiment 1992. *J. Geophys. Res. 104*, NC7, 15,843-15,857.

SEARCH research opportunities emerging, Winter 2000/2001. *Witness the Arctic 8*, N2, p.8.

SEARCH develops implementation framework, 2001. *Witness the Arctic 9*, N1, p.3.

Semiletov, I.P., 1999: Aquatic sources and sinks of CO_2 and CH_4 in the polar regions. *J. Atmos. Sci. 56*, N2, 286-306.

Serreze, M.C., Walsh, J.E., Chapin, F.S. III, Ostercamp, T., Dyurgerov, M., Romanovsky, V., Oechel, W.C., Morison, J., Zhang, T., and *Barry, R.G.,* 2000: Observational evidence of recent change in the northern high-latitude environment. *Clim. Change 46,* N1-2, 159-307.

Shupe, M.D., Uttal, T., Matronson, S.Y., and *Frisch, A.S.,* 2001: Cloud water contents and hydrometeor sizes during FIRE Arctic Clouds Experiment. *J. Geophys. Res. 106*, N14, 15,015-15,028.

Stevens, T., 2001: Climate change in the Arctic and the 107th Congress. *Witness the Arctic 9*, N1, p. 21.

Stevenson, D.S., Johnson, C.E., Collins, W.J., Derwent, R.G., and *Edwards, J.M.,* 2000: Future estimates of tropospheric ozone radiative forcing and methane turnover – the impact of climate change. *Geophys. Res. Lett. 27*, N14, 2073-2076.

Sumner, A.L. and *Shepson, P.B.,* 1999: Snowpack production of formaldehyde and its effect on the Arctic troposphere. *Nature 398*, N6724, 230-233.

Suortti, T., Karhu, J., Kivi, R., Kyro, E., Rosen, J., Kjome, N., Larsen, N., Neuber, R., Khattatov, V., Rudakov, V., and *Nakane, H.,* 2001: Evolution of the Arctic stratospheric aerosol mixing

ratio measured with balloon-borne aerosol backscatter sounders for years 1988-2000. *J. Geophys. Res. 106*, ND18, 20,759-20,766.

Toward An Arctic System Synthesis: Results and Recommendations, 1998: The Arctic Research Consortium of the United States (ARCUS). Fairbanks, Alaska, 165 pp.

Toward Prediction of the Arctic System: predicting future states of the arctic system on seasonal-to-century time scales by interacting observations, process research, modeling, and assessment, 1998: The Arctic Research Consortium of the United States (ARCUS). Fairbanks, Alaska, 54 pp.

Tschudi, M.A., Curry, J.A., and *Maslanik, J.A.,* 2001: Airborne observations of summertime surface features and their effect on surface albedo during FIRE/SHEBA. *J. Geophys. Res. 106*, N14, 15,335-15,344.

Volkov, V.A., Johannessen, O.M., Borodachev, V.E., Voinov, G.M., Pettersen, L.H., Bobylev, L.P., and *Kouraev, A.V.*, 2002: *Polar Seas Oceanography. An integrated case study of the Kara Sea.* Springer/PRAXIS, Chichester, UK., 450 pp.

Vörösmarty, C.J., Hinzman, L.D., Peterson, B.J., Bromwich, D.H., Hamilton, L.C., Morison, J., Romanovsky, V.E., Sturm, M., and *Webb, R.S.*, 2001: *The Hydrological Cycle and Its Role in Arctic and Global Environmental Change: A Rationale and Strategy for Synthesis Study.* Arctic Research Consortium of the U. S., Fairbanks, Alaska, 84 pp.

Wadhams, P., Dowdeswell, J.A., and *Schofield, A.N.* (eds.), 1997: *The Arctic and Environmental Change.* Gordon & Breach, Newark, NJ, e.a., 208 pp.

Wang, M., 2001: Temperature decadal change over Arctic as seen from TOVS and NCEP analysis. In *First Int. Conf. On Global Warming and the Next Ice Age*, Dalhousie Univ., 19-224 Aug. 2001. p.177.

Wang, S., Wang, Q., Jordan, R.E., and *Persson, P.O.G.,* 2001: Interactions among longwave radiation of clouds, turbulence, and snow surface temperature in the Arctic: A model sensitivity study. *J. Geophys. Res. 106*, N14, 15,323-15,334

Warren, S.G., Rigor, I.G., Untersteiner, N., Radionov, V.F., Bryazgin, N.N., Aleksandrov, Y.I., and *Colony, R.*, 1999: Snow depth on Arctic sea ice. *J. Climate 12*, N6, 1814-1829.

Weatherly, J.W., Briegleb, B.P., Large, W.G., and *Maslanik, J.A.*, 1998: Sea ice and polar climate in the NCAR CSM. *J. Climate 11*, 1472-1486.

Weller, G., 1999: The aim of the symposium. *Polar Research 18*, N2, 115-116.

Weller, G. and *Lange, M.*, (eds.), 1999: *Impacts of Global Climate Change in the Arctic Region.* Intern. Arctic Science Com., Fairbanks, Alaska, 59 pp.

Wetzel, P.J., 2001: Ice house effect: A selective Arctic cooling trend current models are missing. In *First Int. Conf. On Global Warming and the Next Ice Age,* Dalhousie Univ., 19-24 Aug., 2001, 178-181.

White, A., Cannell, M.G.R., and *Friend, A.D.*, 2000: The high-latitude terrestrial carbon sink: a model analysis. *Global Change Biology 6*, 227-245.

Winsor, P. and *Bjork, G.*, 2000: Polynya activity in the Arctic Ocean from 1958 to 1997. *J. Geophys. Res. 105,* NC4, 8789-8804.

Young, O.R., 1999: The interplay of global and polar regimes. *Polar Research 18*, N2, 397-402.

Yudakhine, F.N., (ed.), 2000: *The North: Ecology* (in Russian). Ural Section of the Russian Acad. Sci., Ekaterinburg, 415 pp.

Zakharov, V.F. and *Malinin, V.N.*, 2000: *Sea Ice and Climate* (in Russian). Gidrometeoizdat, St. Petersburg, 92 pp.

Zhang, Y. and *Hunke, E.C.*, 2001: Recent Arctic change simulated with a coupled ice-ocean model. *J. Geophys. Res. 106*, NC3, 4369-4390.

Zhou, X., Seine, H.J., Honrath, R.E., Fuentes, J.D., Simpson, W., Shepson, P.B., and *Bottenheim, J.W.*, 2001: Snowpack photochemical production of HONO: a major source of OH in the Arctic boundary layer in springtime. *Geophys. Res. Lett. 28*, N21, 4087-4090.

IDŐJÁRÁS

Quarterly Journal of the Hungarian Meteorological Service
Vol. 107, No. 1, January–March 2003, pp. 31–48

Homogeneity analysis of climatological time series – experiments and problems

Margarita Syrakova

Department of Meteorology and Geophysics, Faculty of Physics, University of Sofia
5, J. Bourchier blvd., Sofia 1164, Bulgaria; E-mail: marsyr@phys.uni-sofia.bg

(Manuscript received 27 August 2001; in final form 19 February, 2002)

Abstract—Experiments with different tests for homogeneity are performed. Sensitivity of the tests to different modifications of the time series is examined. Experiments were made with artificially generated normally distributed random series, on which different modifications were imposed: trends (constant and changing), simple periodicity (sine wave), jump, and various combinations of jump plus another change. Experiments with the combined models aimed to examine whether the jump can be detected in the presence of other modifications (with a presumption that the most probable form of inhomogeneity is an abrupt change). To obtain reliable results, each experiment was repeated with 100 different random series, and the results for individual series were averaged.

The experiments show that graphical tests can give an indication about the form of the change. Serious problems are the cases when two or more modifications interfere in such a way that the tests fail to indicate the change.

An example with the annual precipitation series of Sofia (Bulgaria) is presented.

Key-words: homogeneity tests, precipitation series.

1. Introduction

In recent years much attention has been directed at climate variability and climate change. Empirical investigations of the problem are based on long-term climate time series. This, in turn, has enhanced the concern about the quality of the series – first of all the homogeneity of the series should be tested. In the first place, the homogeneity tests are aimed at detecting abrupt changes in the series, which cause slippage of the mean. The presumption is that in many cases such changes are "artificial" – a consequence of change of

measuring instrument, location, averaging method, etc. In other cases the series may be "contaminated" by anthropogenic trend, e.g., an increasing trend in temperature series at a station located in an enlarging urban area.

Many tests exist and are used in climate series homogeneity analysis. Results, however, should be interpreted very carefully, because the detected changes may not be "artificial". Natural climate changes may also have effect on the statistics, i.e., one should distinguish between statistical and climatic (in)homogeneity, where climatic inhomogeneity means the influence of the mentioned nonclimatic factors. One way to distinguish between these two possibilities is to take into account metadata, i.e., information about the measurement and station history. This information is very valuable in time series homogeneity analysis, but unfortunately is not always available, or is not of good quality. Another way to overcome the problem is to compare the tested series to reference series placed in very similar climate conditions. Since various forms of natural climate variation (trends, periodicities, abrupt changes, etc.) are almost coherent in tested and reference series, they will not dominate the resultant series (the series of differences or ratios between tested and reference series), and the inhomogeneity will be revealed as a systematic change in the difference/ratio series. This relative approach in homogeneity analysis is very fruitful and widely and successfully used (*Alisov et al.*, 1952; *Potter*, 1981; *Alexandersson*, 1986; *Karl* and *Williams*, 1987; *Rhoades* and *Salinger*, 1993; *Hanssen-Bauer* and *Forland*, 1994; *Peterson* and *Easterling*, 1994; *Easterling* and *Peterson*, 1995; *Alexandersson* and *Moberg*, 1997; *Moberg* and *Alexandersson*, 1997; *Szentimrey*, 1998). Reference series are defined in different ways by different authors.

There are, however, situations when it is not possible to find appropriate reference series. This is valid, for example, for the initial part of a long series – up to certain year one cannot find any series well correlated with it, because the observations in the surrounding stations (with large enough correlation coefficients) have started much later. This problem is especially valid for the precipitation due to its high spatial variability.

The aim of this investigation was to examine the sensitivity of different tests to different modifications of the time series. For this purpose, artificial but realistic time series were generated and tested for inhomogeneity.

2. Series and method

Normally distributed random numbers were generated to form time series reproducing the mean and variance of annual precipitation on the territory of Bulgaria. Each series has a length of $n=100$, i.e., simulated series cover 100-

year periods. Random series were modified in various ways and tested for homogeneity using several statistical techniques. The procedure (modification and testing) was repeated with 100 different random series and the results for the individual series were averaged.

Modifications imposed on the random series can be divided into two groups: simple and combined models. They represent imitations of possible climate variability and abrupt change. The magnitude of a modification is expressed by the standard deviation of the random series (σ). Experiments include the following models (1 to 4 – simple, 5 to 9 – combined):

(1) *Linear trend* from 0 to Δ_t, i.e., with a slope $\Delta_t / n = \Delta_t / 100$, Δ_t is from $\pm 0.25\sigma$ to $\pm 2\sigma$ ("+" means an increase, "–" means a decrease from the beginning to the end of the series).

(2) *Linear trend with changing slope* (*changing trend*). This model may have various modifications. We have chosen the modification with an increase/decrease from 0 to Δ_c at a certain point n_c, followed by a returning to the initial "zero" level at the last point, i.e., the two slopes are Δ_c / n_c and $\Delta_c / (100 - n_c)$. The magnitude of Δ_c is from $\pm 0.25\sigma$ to $\pm 2\sigma$ ("+" means an increasing initial trend, "–" means a decreasing initial trend). This model may roughly be considered as a part of a long-term oscillation.

(3) *Long-term oscillation* (periodicity) in the form of one *sine wave* with amplitude Δ_s. The experiments include amplitudes from $\pm 0.25\sigma$ to $\pm 2\sigma$, the minus sign means opposite phase. Very big amplitudes, however, are not realistic.

(4) *Abrupt change* (*jump*) at point n_j, with a magnitude Δ_j from $\pm 0.25\sigma$ to $\pm 2\sigma$.

(5) *Jump+trend* with different combinations of the magnitudes Δ_j and Δ_t, each one is from $\pm 0.5\sigma$ to $\pm 1.5\sigma$, and two different points of the jump: $n_{j1} = 30$ or $n_{j2} = 60$.

(6) *Jump+sine wave* with Δ_j from $\pm 0.5\sigma$ to $\pm 1.5\sigma$, and Δ_s from $\pm 0.25\sigma$ to $\pm \sigma$. The jump is located at different points of the sine wave.

(7) *Jump+sine+trend* with Δ_j, Δ_t from $\pm 0.5\sigma$ to $\pm 1.5\sigma$, and $\Delta_s = \pm 0.3\sigma$, jump located at $n_j = 30$, i.e., not far from the extremum of the sine wave.

(8) *Jump+changing trend* with Δ_j and Δ_c from $\pm 0.5\sigma$ to $\pm 1.5\sigma$, change of the slope at $n_c = 40$, and jump at $n_{j1} = 30$ or $n_{j2} = 70$ (at different distances from the break of the slope).

(9) *Jump+jump* with different magnitudes and signs from $\pm 0.5\sigma$ to $\pm 1.5\sigma$ at points $n_{j1} = 30$ and $n_{j2} = 60$. This combination (more than one change point) has been examined by many authors (*Lanzante*, 1996; *Mestre*, 1998; *Sneyers et al.*, 1998).

Several statistical techniques for homogeneity analysis were used in the experiments. Critical values of the test statistics for the acceptance of null hypotheses were chosen according to a significance level $\alpha = 5\%$.

First, the series were tested for randomness using several techniques. One of them is the comparison of lag-1 serial correlation coefficient, r_1, with its critical value (*Mitchell*, 1966; *Zhukovskii et al.*, 1976; *Sneyers*, 1990, 1992). The critical value is $|r_1|_c = t_c \sqrt{(1 - r_1^2)/(n-2)}$ with t_c taken from the table of Student (or normal – for long series) probability distribution at the level of significance desired.

Similar techniques include Abbe and von Neumann tests (*Mitchell*, 1966; *Rozhdestvenskii* and *Chebotarev*, 1974; *Brownlee*, 1977) based on the ratio $q = d^2/2\sigma^2$ (Abbe) or $V = d^2/\sigma^2$ (von Neumann), where σ^2 is the variance and d^2 is the mean square successive difference $[\sum_{1}^{n-1}(x_{i+1} - x_i)^2]/(n-1)$. Because of the relationship between q (or V) and r_1 (in fact $q = 1 - r_1$), these three tests give identical results, and only the results for r_1 will be discussed.

As a non-parametric alternative to the lag-1 correlation coefficient, the Spearman rank correlation coefficient, r_s, is recommended (*Mitchell*, 1966; *Sneyers*, 1990; *Lanzante*, 1996),

$$r_s = 1 - \frac{6}{n(n^2-1)} \sum_{i=1}^{n} [r(x_i) - i]^2 , \qquad (1)$$

where $r(x_i)$ are the ranks of the elements x_i of the series, arranged in increasing order. Under the hypothesis of randomness, the test statistic $u_s = u(r_s) = r_s \sqrt{n-1}$ has a standard normal distribution and the critical values are ± 1.96.

Another test of randomness is the run-test (*Thom*, 1966; *Davis*, 1973; *Rozhdestvenskii* and *Chebotarev*, 1974; *Brownlee*, 1977; *Sneyers*, 1990). This is a non-parametric test, which counts the number of the runs U_r above and below the median of the series. The counted number U_r is compared with the tabulated critical values for a certain significance level (*Bol'shev* and *Smirnov*,

1983). Too many runs indicate high frequency oscillations, while too few runs suggest a trend or abrupt changes.

A test used to detect inconstancy of the mean is based on the statistic (*Mitchell*, 1966; *Rozhdestvenskii* and *Chebotarev*, 1974; *Zhukovskii et al.*, 1976; *Kobisheva* and *Narovlianskii*, 1978; *Isaev*, 1988; *Zwiers* and *von Storch*, 1995)

$$t = \frac{\bar{x}_2 - \bar{x}_1}{\sqrt{n_1\sigma_1^2 + n_2\sigma_2^2}} \sqrt{\frac{n_1 n_2 (n_1 + n_2 - 2)}{n_1 + n_2}}, \tag{2}$$

where $n_1 + n_2 = n$, $\bar{x}_1$ and $\bar{x}_2$, ${\sigma_1}^2$ and ${\sigma_2}^2$ are the means and variances over n_1 and n_2 terms of the series, respectively. If the observations, x_i, are independent and normally distributed, the expectations (represented by the sample means) are not significantly different, and the *t*-statistic has a Student's distribution with $(n_1 + n_2 - 2)$ degrees of freedom. When the stability of the mean is tested, the series is divided into two subseries with lengths $n_1 = 3,4,...,n-3$, and $n_2 = n-3,...,3$, and after calculating the values of $|t|$ for each combination of n_1 and n_2, the maximum value $|t|_{\max}$ is found. If $|t|_{\max}$ is less than the critical value, the series may be considered homogeneous with probability $(1-\alpha)$. If $|t|_{\max}$ exceeds the critical value and if the cause is an abrupt change, its location can be identified with the place of $|t|_{\max}$.

A statistic, similar to the Student's *t*-statistic, is (*Kobisheva* and *Narovlianskii*, 1978; *Isaev*, 1988; *Zwiers* and *von Storch*, 1995)

$$z = (\bar{x}_2 - \bar{x}_1) \Big/ \sqrt{\frac{\sigma_1^2}{n_1} + \frac{\sigma_2^2}{n_2}}, \tag{3}$$

which has a standard normal distribution for large *n*.

Both statistics assume independence of the observations. Methods to overcome this restriction are suggested by *Zwiers* and *von Storch* (1995), where one can find tables with critical values of $|z|$, for $|r_1| > |r_1|_c$.

In our experiments, instead of determining one single value $|t|_{\max}$ or $|z|_{\max}$, sequential versions of both tests were realized, and the values of $|t|$ or $|z|$ were represented graphically along the time axis. This representation is more informative on the peculiarities of the analyzed series than only the magnitude

of $|t|_{\max}$ or $|z|_{\max}$. Results from the *t*-test and *z*-test turned out to be almost identical, that is why only results of the *t*-test will be discussed.

Another test, the widely used non-parametric Mann-Kendall test, is applied in a sequential forward and backward way (*Goossens* and *Berger*, 1986; *Sneyers*, 1990, 1992). The method consists of calculating the test statistic $u(d_n) = [d_n - E(d_n)] / \sigma(d_n)$, where $d_n = \sum_{i=1}^{n} m_i$, m_i is the number of inequalities $x_j < x_i$ with $j < i$. For long series, under the hypothesis of randomness, d_n is normally distributed with expected value $E(d_n) = n(n-1)/4$ and variance $\sigma^2(d_n) = n(n-1)(2n+5)/72$, i.e., $u(d_n)$ has a standard normal distribution. The sequential version is based on computation of all $u(d_i)$, $i = 1,...,n$, which form a curve $u(t)$ along the time axis. The same principle is applied to the backward series to calculate the values $u'(d_i)$ and construct the backward curve $u'(t)$. In the absence of any systematic change in the series, the curves $u(t)$ and $u'(t)$ remain within the critical limits (± 1.96 for $\alpha = 5\%$). In case of significant trend or abrupt change, they exceed the critical levels. Intersection of $u(t)$ and $u'(t)$ is expected to localize the point of the change.

Another method for detecting changes in the mean is based on the cumulative sums (cusums) (*Alisov et al.*, 1952; *Craddock*, 1979; *Rubinshtein*, 1979; *Rhoades* and *Salinger*, 1993). These may be the sums of successive terms of the series (*CS*), sums of successive deviations from the general mean (*CS*1), or sums of successive deviations from the current means (*CS*2), i.e., the means, which are calculated over the terms included in the current sum. (It should be noticed that the first value of *CS*2 and the last value of *CS*1 are equal to zero.) In our experiments the cusums were calculated not for the "original" series but for the series of rank expectations $F(x_i) = r(x_i)/(n+1)$ (*Sneyers*, 1997; *Sneyers et al.*, 1998), where $r(x_i)$ are the ranks of the elements x_i of the series, arranged in increasing order. In this way, these tests as well as the Mann-Kendall test take into account only the arrangement of the terms in the series but not their magnitudes.

The method is graphical. When the terms of the series are arranged randomly, i.e., when small (big) values are not concentrated in one or another part of the series, the mean values are statistically stable. In such case, the cusums *CS* will lie along a straight line with a constant slope, and the cumulative deviations *CS*1 and *CS*2 will fluctuate around the zero level (the *x*-axis). In case of a systematic change in the series, the slope of the *CS*-curve is not constant, and the curves *CS*1 and *CS*2 do not fluctuate around the *x*-axis. An abrupt change results in a sharp change of the slope of the curves *CS* and *CS*2. The place of the jump can be identified by a sharp extreme value of *CS*1 plot.

Buishand (1982) has suggested several statistics based on the cusums $(CS1)_i = \sum_{j=1}^{i} (x_j - \bar{x})$, $i = 1,...,n$, and more exactly, on the rescaled cusums $S_i = (CS1)_i / \sigma_x$, where σ_x is the standard deviation of the examined series. These statistics are as follows:

$$Q = \max |S_i| , \tag{4}$$

$$R = (S_i)_{\max} - (S_i)_{\min} , \tag{5}$$

$$U = \frac{1}{n(n+1)} \sum_{i=1}^{n-1} S_i^2 , \tag{6}$$

$$A = \sum_{i=1}^{n-1} \frac{S_i^2}{i(n-i)} . \tag{7}$$

Critical values of these statistics are given in *Buishand* (1982).

Pettitt test (*Pettitt*, 1979) was also used in our experiments. It is a non-parametric technique for detecting a change point. However, we will not discuss it here, because the graphical representation of the Pettitt's test statistic is identical with the graphical representation of the cusums *CS*1 applied to rank expectations.

3. Results and discussion

First, the results for nongraphical tests are discussed. *Table 1* shows the sensitivity of the tests to different systematic changes, i.e., the influence of the magnitude of certain modification on the test statistic. Results of the tests for both the randomness and stability of the mean (the Buishand statistics) are included in the table. These results are valid for the simple modes (models (1)–(4) described in the previous section) with $\Delta > 0$. Two stars (**) indicate that the test statistic exceeds the critical value, empty places mean that the test statistic is below the critical value, and one star (*) corresponds to almost critical value of the test statistic.

The most sensitive one turned out to be the Buishand test, i.e., modifications have greater influence on the mean values than on the randomness. The least sensitive one is the run-test. All tests are most sensitive to an abrupt change, but a jump $\Delta_j < 0.5\sigma$ is not detected by any of the tests. The tests are sensitive to periodicity, but periodicities with rather high

amplitudes are included in the table. (Quasi)periodicities can be visualized in climate time series by means of low-pass filters (see *Fig. 6*). Almost all tests detect the changing trend at higher Δ than in case of other modifications, so such variations may remain undetected unless they are quite big.

Table 1. Influence of the magnitude Δ of certain modification on the test statistics. An empty place shows that the respective statistic is below the critical value, one star (*) shows that it is about the critical value, two stars (**) mean that the critical value is exceeded at 5% significance level. r_1 is lag-1 correlation coefficient, u_s is the Spearman test statistic, U_r is run test statistic, *Q, R, U, A* are Buishand statistics.

Δ	**0.25σ**	**0.5σ**	**0.75σ**	**σ**	**1.25σ**	**1.5σ**	**1.75σ**	**2σ**
				Linear trend				
r_1						*	**	**
u_s			*	**	**	**	**	**
U_r								
Q			*	**	**	**	**	**
R				*	**	**	**	**
U			**	**	**	**	**	**
A			**	**	**	**	**	**
				Linear trend with changing slope (at n_c = 40)				
r_1							**	**
u_s								
U_r								
Q					*	**	**	**
R			*	**	**	**	**	**
U					*	**	**	**
A				*	**	**	**	**
				Sine wave				
r_1						**	**	**
u_s			*	**	**	**	**	**
U_r							**	**
Q			**	**	**	**	**	**
R			**	**	**	**	**	**
U			**	**	**	**	**	**
A			**	**	**	**	**	**
				Jump (at n_j = 30)				
r_1				*	**	**	**	**
u_s			**	**	**	**	**	**
U_r						**	**	**
Q		*	**	**	**	**	**	**
R			**	**	**	**	**	**
U		**	**	**	**	**	**	**
A		**	**	**	**	**	**	**

Experiments with models of changing trends and jump are made for different locations of the change. The results (not included in the table) show that the closer the change of the slope is to the midpoint, the less sensitive the tests are to this modification. On the contrary, when the jump is closer to the midpoint, it can be detected for smaller Δ.

As it was mentioned, these results are averages obtained from 100 experiments for each magnitude Δ of every modification. Dispersion of individual results around the mean value of the respective statistic shows that the probability for the test statistic exceeding the critical level increases with the increase of Δ. For example, in the case of a linear trend, this probability for r_1 is 6% for $\Delta_t = 0.25\sigma$, about 45% for $\Delta_t = 1.5\sigma$, and becomes 100% only for $\Delta_t > 3\sigma$. The results show that tests may fail to detect even a big systematic change. The risk is the least in case of an abrupt change (jump), and "the least risky" ones are the Buishand statistics.

The combined models are more interesting than the "pure" changes. It is not possible to represent results from the numerous combinations of "jump + another change" which were tested, but the main conclusion is that in some cases the effect is enhanced, while in others, due to compensation, the test statistics remain below the critical levels. In the model "jump + trend", one can easily suppose that a positive jump may be compensated by a negative trend and vice versa. This is confirmed even by the most sensitive Buishand statistics (hereafter we will discuss these statistics because of their higher sensitivity). When Δ_j is about 0.5σ, the jump is compensated by a trend with magnitude $|\Delta_t| \geq |\Delta_j|$; however, when $|\Delta_t| >> |\Delta_j|$, the test statistic exceeds the critical value because of the effect of the trend. For larger jumps, some of the Buishand statistics remain below the critical levels for $|\Delta_t| > |\Delta_j|$, but not for $|\Delta_t| \approx |\Delta_j|$.

In the combination "jump + sine", the effect of the jump Δ_j is compensated when Δ_s is of the same sign, i.e., the effect depends on the phase of the oscillation and direction of the jump. The compensation is most probable when the jump is near the point of inflection and with $\Delta_s \approx \Delta_j$.

The model "jump+sine+trend" is more complicated. With the assumed parameters of the model (jump near the extremum of a sine wave with an amplitude 0.3σ), the Buishand test statistics are below the critical levels for the following combinations: Δ_j and Δ_s of the same sign, Δ_t of the opposite sign, with $|\Delta_t| \approx |\Delta_j|$, or opposite signs of Δ_j and Δ_s, compensated by a trend in the direction opposite to the jump with magnitude $|\Delta_t| > |\Delta_j|$. With the chosen amplitude of the oscillation, the compensation is most probable for $\Delta_j < \sigma$.

In the model "jump + changing trend", a compensation is possible when the jump is relatively small ($\approx 0.5\sigma$) and occurs far from the point of change of the slope. Under these conditions, the Buishand statistics are under critical values when positive jump is located in the decreasing branch, or negative jump is located in the increasing branch.

The combination "jump+jump" is a matter of discussion in many works. Compensation may be expected in the case of opposite signs of jumps with almost equal magnitudes. Some tests confirm this, even for $\Delta_j > \sigma$, but for the Buishand statistics this is valid only for $\Delta_j < \sigma$.

Results from the graphical tests were plotted for each model with chosen magnitudes of modifications (each plot was an average over 100 results). In this way we have obtained a set of "ideal" patterns for the models considered here.

In *Figs. 1–3* examples of these results are given for four simple models. These include plots of the Student's *t*-test in the sequential version used here (*Fig. 1*), Mann-Kendall test (*Fig. 2*), and cusums *CS*1 and *CS*2 (*Fig. 3*). Plots of the cusums *CS* are not represented and not discussed, because they give worse visualization of the changes in the series compared to the other tests. Interpretation of the results obtained by the Student's and Mann-Kendall tests is based not only on the form of the curves (which is important for all tests) but on the critical values of the test statistics as well. Examples in *Figs. 1* and *2* include patterns in which test statistics remain within the critical limits, and patterns in which they exceed the critical levels, depending on the magnitude Δ of the respective modification. All curves are quite smooth and easy for interpretation (the slight disturbance around the beginning is common for all curves and will not be taken into account).

We shall notice that the indication given by the magnitudes of the Student's and Mann-Kendall test statistics is identical with the indication given by the Buishand statistics: t, $u(t)$, $u'(t)$, and the Buishand statistics exceed the critical values for almost one and the same magnitude of certain change ($\Delta_t \approx \sigma$, $\Delta_c \approx 1.25\sigma$, $\Delta_s \approx 0.75\sigma$, $\Delta_j \approx 0.75\sigma$).

In *Figs. 1–3*, the differences between the specific patterns of the curves, corresponding to different forms of modifications can be seen quite clearly. The jump can be easily indicated by the sharp peak (*t*-test and *CS*1), or the sharp change of the slope ($u(t)$, $u'(t)$, and *CS*2) at the place of its occurrence. In the case of a linear trend, t and *CS*1 curves are flat (the patterns resemble a plateau, not a peak), and the slopes of $u(t)$, $u'(t)$, and *CS*2 do not change significantly. The curves for the model of a changing trend are more complicated – each curve consists of two parts, indicating the two opposite trends. Patterns for the model of a sine wave can result in a wrong interpretation, either as an indication of a jump, or as an indication of a trend.

For this model, the peak of the curve (t, *CS*1) or the change of the slope ($u(t)$, $u'(t)$, *CS*2) is located at the point of inflection, i.e., at the place of the transition from values above/below the average to values below/above the average, which seems like a jump (trend) from one level to another.

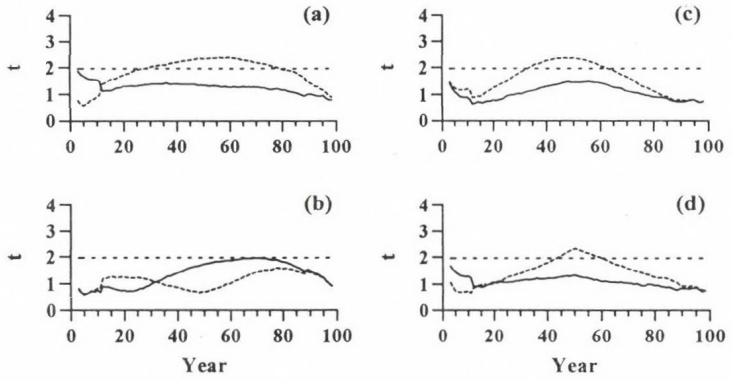

Fig. 1. Plots of the Student's t-test for models of linear trend, changing trend, sine wave, and jump. The 5% significance value is denoted. (*a*) linear trend, $\Delta_t = 0.5\sigma$ (solid line) and $\Delta_t = -\sigma$ (dashed line); (*b*) changing trend, $\Delta_c = -\sigma$, $n_c = 25$ (solid line) and $\Delta_c = -\sigma$, $n_c = 50$ (dashed line); (*c*) sine wave, $\Delta_s = 0.5\sigma$ (solid line) and $\Delta_s = -0.75\sigma$ (dashed line); (*d*) jump, $\Delta_j = 0.25\sigma$, $n_j = 50$ (solid line) and $\Delta_j = 0.5\sigma$, $n_j = 50$ (dashed line).

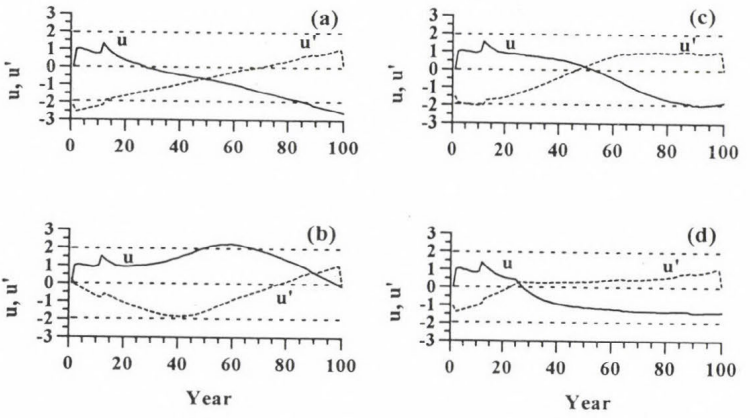

Fig. 2. Plots of the Mann-Kendall test for models of linear trend, changing trend, sine wave, and jump (u is the forward sequential statistic, u' is the backward sequential statistic). The 5% significance values are denoted. (*a*) linear trend, $\Delta_t = -\sigma$; (*b*) changing trend, $\Delta_c = \sigma$, $n_c = 50$; (*c*) sine wave, $\Delta_s = 0.75\sigma$; (*d*) jump, $\Delta_j = -0.5\sigma$ $n_j = 25$.

Graphical tests (except the t-test, which is based on $|t|$) indicate also the direction of the systematic change. A positive trend or jump ($\Delta_t, \Delta_j > 0$) results in negative values of $CS1$ and monotonic increase of $CS2$ and $u(t)$; the effect is the same for negative amplitude of the sine wave ($\Delta_s < 0$ means a decrease followed by an increase). An opposite (negative) direction of the change results in an opposite evolution of the test curves.

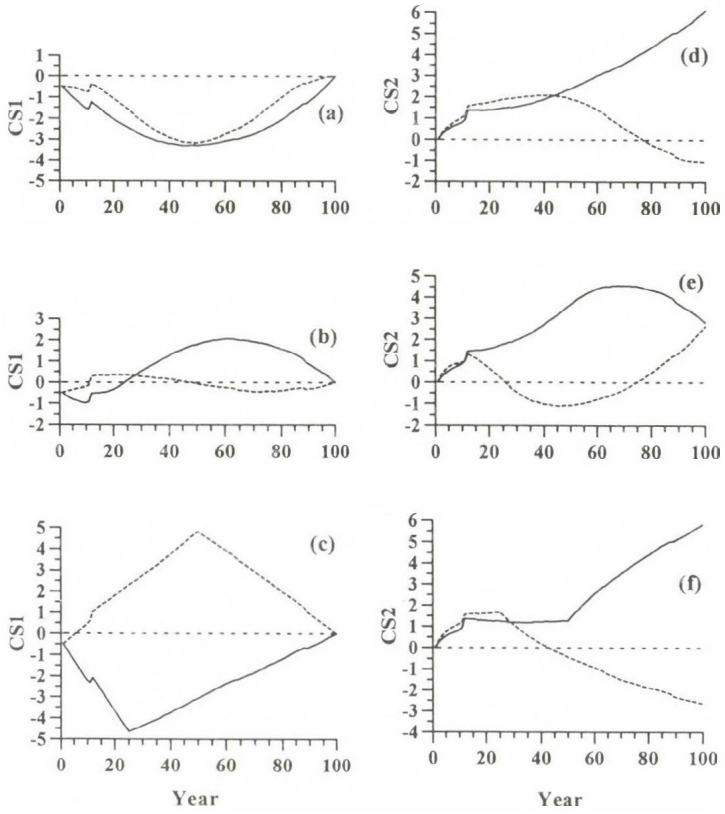

Fig. 3. Plots of cumulative deviations from the general mean ($CS1$) and from the current mean ($CS2$) for models of linear trend, changing trend, sine wave, and jump. (*a*) linear trend, $\Delta_t = \sigma$ (solid line) and sine wave, $\Delta_s = -0.75\sigma$ (dashed line); (*b*) changing trend, $\Delta_c = 0.75\sigma$, $n_c = 25$ (solid line) and $\Delta_c = -0.25\sigma$, $n_c = 50$ (dashed line); (*c*) jump, $\Delta_j = \sigma$, $n_j = 25$ (solid line) and $\Delta_j = -0.75\sigma$, $n_j = 50$ (dashed line); (*d*) linear trend, $\Delta_t = 0.75\sigma$ (solid line) and sine wave, $\Delta_s = 0.25\sigma$ (dashed line); (*e*) changing trend, $\Delta_c = 0.75\sigma$, $n_c = 50$ (solid line) and $\Delta_c = -\sigma$, $n_c = 25$ (dashed line); (*f*) jump, $\Delta_j = 0.5\sigma$, $n_j = 50$ (solid line) and $\Delta_j = -0.5\sigma$, $n_j = 25$ (dashed line).

The graphical tests applied to the combined models confirm the effects of mutual compensation or enhancement of certain systematic changes in the series. In *Fig. 4*, examples of the effect of compensation are given - in spite of the systematic changes, imposed on the series, the tests give indication of randomness. Yet it seems possible to detect the jump in some of these ideal smooth curves, this is not the case with the individual curves.

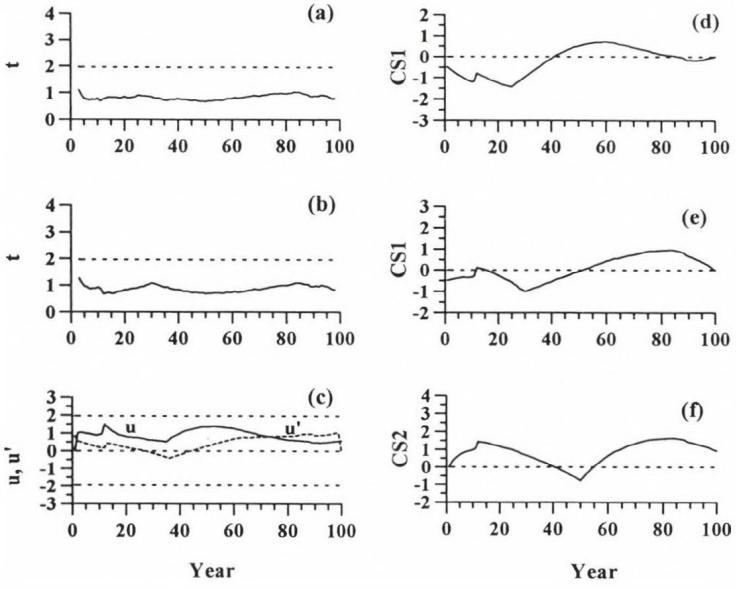

Fig. 4. Examples of the effect of compensation of different systematic changes imposed on the random series. (*a*) Student's *t*-test for the combination "jump+trend" with $\Delta_j = 0.5\sigma$ ($n_j = 50$), $\Delta_t = -\sigma$; (*b*) Student's *t*-test for the combination "jump+sine+trend" with $\Delta_j = 0.5\sigma$ ($n_j = 30$), $\Delta_s = -0.3\sigma$, $\Delta_t = -\sigma$; (*c*) Mann-Kendall test for the combination "jump+sine" with $\Delta_j = 0.5\sigma$ ($n_j = 35$), $\Delta_s = 0.5\sigma$; (*d*) *CS*1 for the combination "jump+sine" with $\Delta_j = 0.5\sigma$ ($n_j = 25$), $\Delta_s = 0.5\sigma$; (*e*) *CS*1 for the combination "jump+sine+trend" with $\Delta_j = 0.5\sigma$ ($n_j = 30$), $\Delta_s = -0.3\sigma$, $\Delta_t = -\sigma$; (*f*) CS2 for the combination "jump+trend" with $\Delta_j = \sigma$ ($n_j = 50$), $\Delta_t = -1.5\sigma$.

Although the results from different tests are similar, they are not completely identical. Here the results for the combination "jump+trend" with $\Delta_j = 0.5\sigma$ and $\Delta_t = -0.5\sigma$ are presented. All Buishand test statistics are below the critical values. Student's and Mann-Kendall test statistics (*Fig. 5*) are also within the critical limits. The curve *CS*1 also may be interpreted as an indication

of randomness (relatively small values around zero level). The plot of *CS*2-curve, however, indicates that the hypothesis of randomness cannot be accepted.

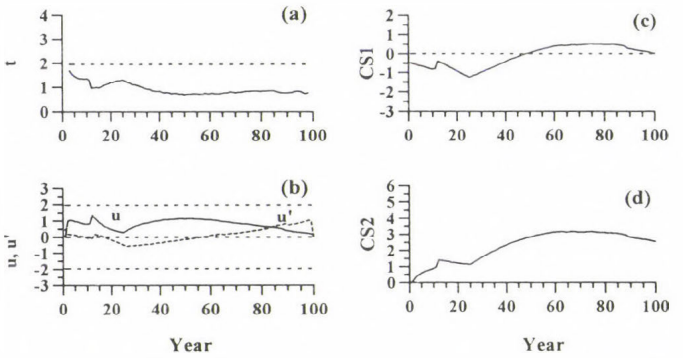

Fig. 5. Plots of the Student's *t*-test (*a*), Mann-Kendall test (*b*) and the cumulative deviations *CS*1 (*c*) and *CS*2 (*d*) for the combined modification "jump+trend" with $\Delta_j = 0.5\sigma$ ($n_j = 25$), $\Delta_t = -0.5\sigma$.

4. Example

As an example, an analysis of the time series of annual precipitation at Sofia (Bulgaria) is presented. Data are shown in *Fig. 6* and a smooth curve is added obtained by a 9-point Gaussian filter applied twice. The horizontal dashed line corresponds to the mean calculated from the reference period 1961–1990.

The selected station has longest regular observations in Bulgaria. It was set up on February 1, 1887 in the centre of the city in an area where a year

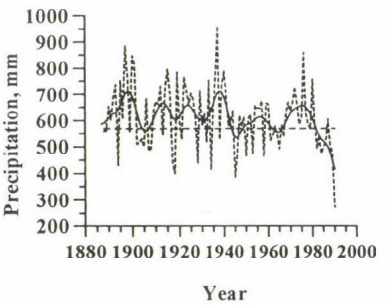

Fig. 6. Time series of annual precipitation at Sofia (Bulgaria). The smooth curve is obtained by 9-point Gaussian filter applied twice, the horizontal line corresponds to the mean value for the reference period 1961–1990.

later the Botanical Garden was established and was closed in 1992. The site and the type of the rain-gauge have not been changed. The period considered here is 1888–1990.

In *Fig. 6*, a definite tendency to a decrease can be noticed and a jump about 1940 may be suspected. The values of the test statistics are: $r_1 = 0.140$, $u_s = -1.76$, $U_r = 48$, $Q = 1.35$, $R = 1.44$, $U = 0.52$, $A = 3.25$. The corresponding critical values are $|r_1|_c = 0.193$, $|u_s|_c = 1.96$, $U_r = [41,62]$, $Q_c = 1.29$, $R_c = 1.62$, $U_c = 0.457$, $A_c = 2.48$, meaning that Buishand statistics Q, U, and A give an indication for some systematic changes.

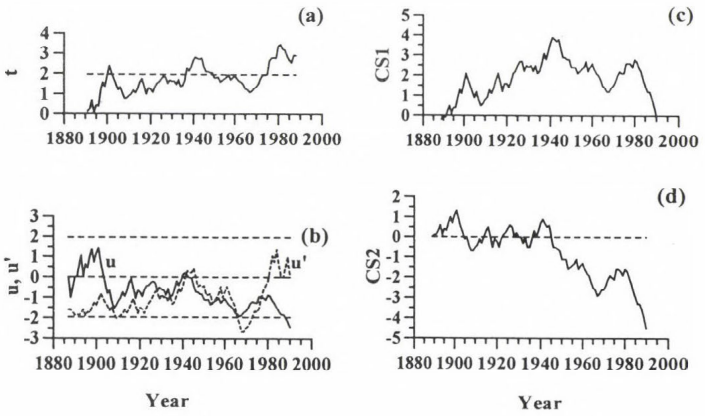

Fig. 7. Plots of the Student's *t*-test (*a*), Mann-Kendall test (*b*), and cumulative deviations *CS*1 (*c*) and *CS*2 (*d*) for the time series of annual precipitation at Sofia.

Graphical tests are presented in *Fig. 7*. The Student's *t*-statistic exceeds the critical value in three periods, maximums occur in 1900, 1940, and 1980. Each of them is localized about the midpoint of a period with sharp decrease in the series. The first and second periods may be regarded as transitions from a maximum to a minimum of a quasi-periodic oscillation. Maximums of the curve *CS*1 are localized at the same points, but the main one in this plot is in 1940. The curve *CS*2 also indicates a sharp change in 1940, after a period of random oscillations. In the plot representing Mann-Kendall test, the two curves intersect in 1940, but without exceeding the critical level as a result of the downward march of $u(t)$ (to the right) and $u'(t)$ (to the left). More "suspicious" is the intersection of the curves about 1980 indicating a new sharp decrease of precipitation. Comparing the results of these tests, one can see that the *t*-test and the Mann-Kendall test give priority to the change occurring in 1980, while the cumulative deviations give priority to the change in 1940.

Analyzing all the results, one may conclude that the series contains abrupt systematic changes. Considering, however, the station history, we may suppose that they are rather manifestations of climate instability than of inhomogeneities of observations. In order to check this assumption we should take into account some other available information. For instance, we can examine seasonal precipitation series and compare the results of different seasons to each other and to the results of the annual series. In case of inhomogeneity, the change of the level should occur at the same moment in all series, while in case of a climatic change, such coincidence may not be excluded but is not likely. Downward shifts around 1940 and 1980 in the annual series are detected in spring and summer series dominating the annual precipitation. The autumn and winter series, however, show different features. Downward shift in the autumn series takes place about 15 years earlier (in 1925), and the decrease after 1980 is followed by an increase after a short period. Winter precipitation exhibits an upward shift after 1925, the higher level is still persisting around and after 1940, and an upward trend can be seen around 1980. Therefore, it is reasonable to conclude that detected changes represent climate variability and are not a manifestation of inhomogeneity.

5. Summary and conclusions

Experiments with different tests for detecting inhomogeneity in climate time series are performed. In these experiments modifications with different forms and magnitudes are imposed on artificial normally distributed random series: trends (constant and changing), simple periodicity (sine wave), jump, and various combinations of jump plus another change. Results from following tests are discussed: the lag-1 serial correlation coefficient r_1, the Spearman rank correlation coefficient r_s, the run test U_r, the Buishand statistics Q, R, U, A, the Student's t-test in a serial version, the serial version of the Mann-Kendall test based on the evolution of the curves $u(t)$ and $u'(t)$, the cumulative deviations from the general mean (*CS*1) and current mean (*CS*2). The last two are applied to the rank expectations of the elements of the series. Conclusions are based on 100 times repeated experiments for each model and each magnitude of respective modifications, and are the following.

Buishand, Student, and Mann-Kendall statistics show almost equal sensitivity. The correlation coefficients and run test are less sensitive, i.e., they reach the critical values for greater magnitudes of the respective modification. This diminishes the risk of failure of the requirement for simple randomness of the series, which has to be satisfied for some tests for stability of the mean. If the magnitude of the change is not big enough, even the most

sensitive test statistics may fail to detect it, remaining within the critical limits (e.g., the "critical magnitude" in the case of a jump is about 0.5σ).

Identification of the form of the change may be obtained by means of the graphical tests. The jump causes a sharp change in the curve evolution – well manifested peak (t, $CS1$) or change of the slope ($u(t)$, $u'(t)$, $CS2$). In the case of a trend, the curve is flat (t, $CS1$) or monotonically increasing/decreasing with a smooth (gradual) change of the slope ($u(t)$, $u'(t)$, $CS2$). A (quasi)-periodicity may obtain a wrong interpretation, mostly as a jump indicated at the place of transition from the period of higher/lower than the average to the period of lower/higher than the average values.

Problems arise also in the cases of realistic combined modifications in the series, e.g., "jump + trend", "jump + periodicity", etc. In these cases, when the effect of the jump is enhanced by other changes, the jump can be easily detected. In such combinations the problem is when the effect of the jump is obscured by other modifications, and the tests give an indication of randomness. The most "promising" in these cases are the plots of the cumulative deviations of the type $CS2$.

When it is not possible to find suitable reference series (the situation considered here), as many tests should be used in the analysis as possible, and all reliable information should be taken into account. This information is also necessary to make a conclusion about the nature of certain modification revealed by the tests and minimize the risk to interpret a natural climate change as an artificial contamination of the series.

As an example, the tests are applied to annual precipitation series in Sofia (Bulgaria), and the results are discussed.

Acknowledgements—This work is supported by the Sofia University Science Foundation, Grant 3300/2000. The author wishes to thank the National Institute of Meteorology and Hydrology, Bulgaria, for providing the precipitation data, and *Prof. D. Syrakov* for the computer programs used in the work.

References

Alexandersson, H., 1986: A homogeneity test applied to precipitation data. *J. Climatol. 6*, 661-675.

Alexandersson, H. and *Moberg, A.*, 1997: Homogenization of Swedish temperature data. Part I: Homogeneity test for linear trends. *Int. J. Climatol. 17*, 25-34.

Alisov, B.P., *Drozdov, O.A.*, and *Rubinshtein, E.S.*, 1952: *Course on Climatology*. Part I, II (in Russian). Gidrometeoizdat, Leningrad, 487 pp.

Bol'shev, L.N. and *Smirnov, N.V.*, 1983: *Tables of Mathematical Statistics* (in Russian). Nauka, Moscow, 416 pp.

Brownlee, K.A., 1977: *Statistical Theory and Methodology in Science and Engineering* (Translated in Russian). Nauka, Moscow, 407 pp.

Buishand, T.A., 1982: Some methods for testing the homogeneity of rainfall records. *J. Hydrology 58*, 11-27.

Craddock, J.M., 1979: Methods of comparing annual rainfall records for climatic purposes. *Weather 34*, 332-346.

Davis, J.C., 1973. *Statistics and Data Analysis in Geology* (Translated in Russian, 1977). Mir, Moscow, 572 pp.

Easterling, D.R. and *Peterson, T.C.*, 1995: A new method for detecting undocumented discontinuities in climatological time series. *Int. J. Climatol. 15*, 369-377.

Goossens, Ch. and *Berger, A.*, 1986: Annual and seasonal climatic variations over the Northern Hemisphere and Europe during the last century. *Ann. Geophys. 4B (4)*, 385-400.

Hanssen-Bauer, I. and *Forland, E.J.*, 1994: Homogenizing long Norwegian precipitation series. *J. Climate 7*, 1001-1013.

Isaev, A.A., 1988: *Statistics in Meteorology and Climatology* (in Russian). Moscow University Press, 245 pp.

Karl, T.R. and *Williams, C.N. Jr.*, 1987: An approach to adjusting climatological time series for discontinuous inhomogeneity. *J. Climate Appl. Meteorol. 26*, 1744-1763.

Kobisheva, N.V. and *Narovlianskii, G.Ya.*, 1978: *Climatological Treatment of Meteorological Information* (in Russian). Gidrometeoizdat, Leningrad, 295 pp.

Lanzante, J.R., 1996: Resistant, robust and non-parametric techniques for the analysis of climate data: Theory and examples, including applications to historical radiosonde station data. *Int. J. Climatol. 16*, 1197-1226.

Mestre, O., 1998: Step-by-step procedures for choosing a model with change-points. *Proc. of the Second Seminar for Homogenization of Surface Climatological Data.* Budapest, Hungary, 9-13 Nov. 1998, 15-25.

Mitchell, J.M., 1966: Climatic Change. *WMO Technical Note 79*, WMO, Geneva, 79 pp.

Moberg, A. and *Alexandersson, H.*, 1997: Homogenization of Swedish temperature data. Part II: Homogenized gridded air temperature compared with a subset of global gridded air temperature since 1861. *Int. J. Climatol. 17*, 35-54.

Peterson, T.C. and *Easterling, D.R.*, 1994: Creating of homogeneous composite climatological reference series. *Int. J. Climatol. 14*, 671-679.

Pettitt, A.N., 1979: A non-parametric approach to the change-point problem. *Appl. Statistics 28*, 126-135.

Potter, K.W., 1981: Illustration of a new test for detecting a shift in mean in precipitation series. *Mon. Wea. Rev. 109*, 2040-2045.

Rhoades, D.A. and *Salinger, M.J.*, 1993: Adjustment of temperature and rainfall records for site changes. *Int. J. Climatol. 13*, 899-913.

Rozhdestvenskii, A.V. and *Chebotarev, A.I.*, 1974: *Statistical Methods in Hydrology* (in Russian). Gidrometeoizdat, Leningrad, 433 pp.

Rubinshtein, E.S., 1979: *Homogeneity of Meteorological Series in Time and Space in Connection with Climate Change Research* (in Russian). Gidrometeoizdat, Leningrad, 80 pp.

Sneyers, R., 1990: On the Statistical Analysis of Series of Observations. *WMO Technical Note 143*, 190 pp.

Sneyers, R., 1992: On the use of statistical analysis for the objective determination of climate change. *Meteorol. Zeitschrift, N.F. 1*, 247-256.

Sneyers, R., 1997: Climate chaotic instability: statistical determination and theoretical background. *Environmetrics 8*, 517-532.

Sneyers, R., Tuomenvirta, H., and *Heino, R.*, 1998: Observations inhomogeneities and detection of climate change. *Geophysica 34(3)*, 159-178.

Szentimrey, T., 1998: Multiple analysis of series for homogenization (MASH). *Proc. of the Second Seminar for Homogenization of Surface Climatological Data.* Budapest, Hungary, 9-13 Nov. 1998, 27-46.

Thom, H.C.S., 1966: Some Methods of Climatological Analysis. *WMO Technical Note 81*, 53 p.

Zhukovskii, E.E., Kiseleva, T.L., and *Mandel'shtam, S.M.*, 1976: *Statistical Analysis of Random Processes* (in Russian). Gidrometeoizdat, Leningrad, 407 pp.

Zwiers, F.W. and *von Storch, H.*, 1995: Taking serial correlation into account in tests of the mean. *J. Climate 8*, 336-351.

IDŐJÁRÁS

Quarterly Journal of the Hungarian Meteorological Service
Vol. 107, No. 1, January–March 2003, pp. 49–65

Preliminary results of high resolution sensitivity studies using the adjoint of the ALADIN mesoscale numerical weather prediction model

Cornel Soci[1], **András Horányi**[2], and **Claude Fischer**[3]

[1]*National Institute of Meteorology and Hidrology,*
97, Sos. Bucuresti-Ploiesti, 71552 Bucharest, Romania
E-mail: cornel.soci@meteo.inmh.ro
[2]*Hungarian Meteorological Service, P.O. Box 38, H-1525 Budapest, Hungary*
E-mail: horanyi.a@met.hu
[3]*Météo France, 42, Av. G. Coriolis, 31057 Toulouse Cedex 1, France*
E-mail: claude.fischer@meteo.fr

(Manuscript received February 6, 2002; in final form October 3, 2002)

Abstract—This paper reviews the theoretical background and practical implementation of adjoint computations in numerical weather prediction. In our study, the limited area model ALADIN has been used. Preliminary results obtained for meso-beta type of resolutions, focusing on a local domain inside Central Europe with an 8 km grid mesh are presented. The purpose is to obtain a closer match of a model forecast with a verifying analysis, as measured by a given cost function. To achieve this goal, gradients with respect to the initial conditions are computed; these gradient fields give the sensitivity of the forecast error cost function with respect to the initial conditions. Additionally, the impact on other features of the forecast, mainly precipitation, is also investigated. Two cases were selected, when the precipitation amounts were overestimated over the Pannonian Plains. Mesoscale sensitivities computed adiabatically or using different parameterization schemes are compared. Results from sensitivity experiments with respect to initial conditions show that the errors in initial data can, at least partially, be made responsible for the misforecast of precipitation quantities.

Key-words: limited area model, adjoint method, sensitivity studies, ALADIN.

1. Introduction

The quality of numerical weather forecasts produced by a limited area model is subject to several possible causes. Besides the weaknesses in the model formulation, the forecast could depend crucially on initial and lateral boundary conditions.

A common problem in numerical weather prediction models is the inaccuracy in the initial data. Experiments with forecast error sensitivity studies have revealed that errors in the initial data are most responsible for the quality of a forecast. As explained in *Le Dimet* and *Talagrand* (1986), the adjoint model allows efficient computation of the gradient of a forecast aspect of a numerical weather prediction model with respect to the initial conditions. Forecast aspect can be any model output. The gradient fields strongly suggest where to look for initial condition errors that may have a big effect in the consecutive forecasts. They also indicate what to expect from any small changes in the initial conditions that might be applied (*Errico*, 1997), provided that a linear type of evolution is sustained. In the last decade, several approaches to diagnose such errors have been proposed (*Errico* and *Vukićević,* 1992; *Rabier et al.*, 1996; *Gustafsson* and *Huang*, 1996). These studies mostly have addressed synoptic scale features predicted by global or large-sized limited area models.

Sensitivity analysis using the adjoint of the high resolution doubly-periodic primitive equation model ALADIN has been initiated by *Horányi* and *Joly* (1996). Using an adiabatic adjoint model, they studied the sensitivity of two idealised frontal waves. They showed that the steady fronts are associated with very strong amplifications of the fastest growing eigenvectors. In this article, features of mesoscale sensitivity for a selected case study are described. Sensitivities of forecast errors with respect to the initial conditions are computed and used as small perturbations added to the model dynamical fields for improving the 6 hours precipitation forecast.

With the present state-of-the-art knowledge, one may consider the adjoint approach not to be so beneficial because small scale meteorology is more dominated by non-linear processes such as saturation or boundary layer fluxes. However, the adjoint framework still remains a candidate for a dynamically consistent assimilation of high-frequency data, even if possibly restricted to time intervals much smaller than those employed for synoptic scale studies. At synoptic scale, 48 hours long windows are usual, in accordance with the typical time scale of baroclinic development. We stress that the developments of the adjoint tools in the ALADIN model give the opportunity to evaluate these ideas.

Although this article only presents preliminary results, for example ignoring moist diabatic processes in the adjoint computation, it shows that the ALADIN adjoint tools can provide answers for the previously raised questions. What is at stake in the long term is the evolution of the benefit of a 4D-VAR data assimilation at small scales.

The paper is organized as follows. Section 2 describes the mathematical basis for using an adjoint operator for sensitivity analysis. Section 3 deals

with the description of the steps needed for performing a sensitivity experiment. Results are presented in section 4 and concluding remarks follow in section 5.

2. *Methodology*

Let **x** define the model state vector. Typically, **x** is a set of three dimensional fields, namely u, v, T, q, which stand for zonal and meridional wind components, temperature, and specific humidity respectively, and a two dimensional field p_s, which is surface pressure. Depending on whether the model is spectral or finite-differences, the components of the state vector are spectral coefficients or values at all model grid points. A non-linear numerical weather prediction model, M, is a set of discretized primitive equations which approximate the processes of the real atmosphere. Hereafter, the non-linear model considered is ALADIN, a limited area spectral model (*Horányi et al.*, 1996). Since the non-linear model is discretized in time, formally, its evolution within a time interval, $[t_0, t]$, can be described by using a discrete equation

$$\mathbf{x}(t_{i+1}) = M\,[\mathbf{x}(t_i)], \tag{1}$$

where $\mathbf{x}(t_i)$ and $\mathbf{x}(t_{i+1})$ are the model vectors at time step i and $i+1$, respectively. Therefore, the final model state, $\mathbf{x}(t)$, is determined from the model initial state, $\mathbf{x}(t_0)$, by n successive steps.

In sensitivity computations, we are concerned about small perturbations, hereafter denoted $\delta\mathbf{x}(t)$. By definition, $\delta\mathbf{x}(t) = \mathbf{x}(t) - \bar{\mathbf{x}}(t)$, where $\bar{\mathbf{x}}(t)$ is an evolving basic state that we will specify as a solution to Eq. (1) given an initial condition $\bar{\mathbf{x}}(t_0)$, while $\mathbf{x}(t)$ is a perturbed non-linear solution that is initially close to $\bar{\mathbf{x}}(t)$. The perturbation of the model state, $\delta\mathbf{x}(t)$, is governed by the tangent linear equation which can be derived from Eq. (1) using first order Taylor expansion. Hence,

$$\delta\mathbf{x}(t_{i+1}) = \mathbf{M}\,\delta\mathbf{x}(t_i), \tag{2}$$

where $\mathbf{M}$ is the derivative of M with respect to $\mathbf{x}$ evaluated at $\bar{\mathbf{x}}(t)$. $\mathbf{M}$ is also called the tangent linear model (a more proper wording would be the propagator, see *Joly,* 1995), and it can be understood as the Jacobian matrix of M evaluated along the non-linear trajectory, $\bar{\mathbf{x}}(t)$. The tangent linear model describes the linearized evolution of errors or perturbations in a forecast model. It is obtained by the differentiation of the code of the direct model, M.

If M includes discontinuous functions, then some values of the Jacobian derivatives will not exist. This is, for instance, the case of some physical parameterization schemes, such as large scale precipitation or deep convection, which involve strong non-linear processes. In such a case, the strategy adopted for the tangent linear model is to simplify the parameterization scheme by neglecting some diabatic terms, while, at the same time remaining as close as possible to the physical parameterization scheme of the non-linear model (*Janisková et al.*, 1999).

Furthermore, we stress that in the ALADIN model, the treatment of lateral boundary conditions is presently done in a very crude way. Consistently, with the full, non-linear model, a Davies-type of coupling is retained (*Davies*, 1983). However, the tangent linear model, and the adjoint model as well, is coupled with zeroed perturbations along the lateral boundaries. This formulation forces to ignore any incoming perturbation (the flow is supposed to coincide with the reference trajectory). It also forces to forget about outgoing sensitivity information. Thus, such a treatment is sub-optimal for sensitivity studies, but it appears as a very convenient framework, especially when the focus is put on narrow time windows, where most of the sensitivity signal is kept inside the model domain, as will be the case here. At the same time, when using a high resolution model, the computational cost often forces to choose a small model domain, therefore the sensitivity study is performed in an experimental framework defined as a compromise between targeted small scale processes technically allowed and the computational cost.

Since $\mathbf{M}$ is a linear operator, it is possible to define its adjoint, denoted $\mathbf{M}^*$. It is defined such as for any two vectors, $\mathbf{y}$ and $\mathbf{z}$, in the phase space of the system, the following equality holds:

$$<\mathbf{y}, \mathbf{M}\,\mathbf{z}> = <\mathbf{M}^*\mathbf{y}, \mathbf{z}>, \tag{3}$$

where $<,>$ stands for the inner product. The adjoint operator is also linear, and for the discretized models it represents the transpose matrix, $\mathbf{M}^T$, of $\mathbf{M}$.

The adjoint model is constructed as the exact adjoint of the tangent linear model with the purpose of computation of phase space gradients. It is developed mainly for data assimilation applications and predictability, but it can be used also as a tool which relates the origin of numerical forecast errors to errors in initial data through sensitivity experiments. If a verifying analysis, denoted $\mathbf{x}^a(t)$, is available at time t, it is possible to compare the forecast with the analysis taken as an estimate of the true state of the atmosphere. The difference between the non-linear model solution, i.e., the forecast, and the verifying analysis is defined as the forecast error. This misfit can be quantified

by a diagnostic function, J, usually called forecast error cost function. Typically, J is a temporally weighted squared function which can be written as

$$J = \frac{1}{2} < \mathbf{x}(t) - \mathbf{x}^a(t), \mathbf{x}(t) - \mathbf{x}^a(t) > . \quad (4)$$

In our study the square norm $<,>$ is the so-called dry total energy. It is defined as

$$< \chi,\chi > = \frac{1}{2} \int_0^1 \int_\Sigma \left(u^2 + v^2 + \frac{C_p}{T_r} T^2 \right) d\Sigma \frac{\partial p}{\partial \eta} d\eta + \frac{1}{2} \int_\Sigma R_d T_r (\ln p_s)^2 d\Sigma . \quad (5)$$

In the definition of the norm, χ is the vector representing a *perturbation* of the atmospheric flow, the inner product being defined in the space of the perturbations. The weights given to its components are functions of the reference temperature, T_r, the specific heat of dry air at constant pressure, C_p, and the gas constant for dry air, R_d. $p(\eta)$ is the pressure at η levels, η being the vertical coordinate, 0 is the surface and 1 is the top of the atmosphere. Σ represents the horizontal integration domain, an area on which the diagnostic function is computed. Hereafter, this is referred as a target area. When using a target area, the input to the forecast error norm is set to zero outside, and only inner values are kept for further computations. This is important for the estimation of the origin of the initial forecast errors, because in such a way the obtained gradients are relevant only to the errors in that target area. The norm is called "dry" since there is no term involving specific humidity, q. Thus, there are no perturbations in the moisture field, which, at the end of the adjoint integration, could be considered as sensitivity of the forecast error cost function to the humidity field. The norm is also called "total" energy, since the first two terms of the right-hand side of Eq. (5) are kinetic energy and the third one is dry static energy. The fourth one is related to the surface pressure with weights chosen such that its dimension becomes energy.

In the adjoint computation, the goal is to determine $\nabla_{\mathbf{x}(t_0)} J$, that is the gradient of J with respect to the initial model state, $\mathbf{x}(t_0)$. To derive $\nabla_{\mathbf{x}(t_0)} J$, we begin by constructing δJ, that is the first order variation of the diagnostic function at the verification time. This is achieved by a given perturbation in the initial conditions, $\delta\mathbf{x}(t_0)$ which will lead to a perturbation $\delta\mathbf{x}(t)$ at the final time. Consequently, a small change, δJ, of the cost function J, can be written

$$\delta J = < \mathbf{M}^* [\mathbf{x}(t) - \mathbf{x}^a(t)], \delta\mathbf{x}(t_0) > . \quad (6)$$

By definition, the gradient of the forecast error cost function at time t_i, $t_0 \leq t_i \leq t$ is such that to first order approximation, $\delta J = < \nabla_{\mathbf{x}(t_i)} J , \delta \mathbf{x}(t_i) >$. Thus, using Eq. (6), the gradient of the forecast error cost function with respect to the initial conditions $\mathbf{x}(t_0)$ reads

$$\nabla_{\mathbf{x}(t_0)} J = \mathbf{M}^* [\mathbf{x}(t) - \mathbf{x}^a(t)], \tag{7}$$

where $\mathbf{M}^*$ is the adjoint of the tangent linear model. This is the basic relation used in sensitivity computations. The right-hand side term is computed by a backward integration of the adjoint model between times t and t_0.

The gradient of the forecast error cost function with respect to the initial conditions is used to generate perturbations to be added to the original initial data. An initial perturbation is a vector of the form $\delta \mathbf{x}_0 = -\alpha \nabla_{\mathbf{x}(t_0)} J$, where α is a scaling factor chosen by experimentation. As explained in *Rabier et al.* (1996), the gradient is dominated by the most unstable components of the analysis errors, because these are the directions along which the forecast error is likely to vary the most. They have shown that for large-scale flows and 48 hours time evolution, these fastest growing components can amplify by a factor of 10 to 15. Thus, the choice of an optimal α is carried out by successive tests such that the forecast errors are substantially reduced. However, the maximum value of the initial perturbation cannot exceed the magnitude of an observation error or that might naturally occur in the real atmosphere. In our experiments the value 1/10 for the scaling factor was chosen.

3. Design of the sensitivity experiments

Generally, a sequence for performing a sensitivity experiment proceeds through the following steps:

- A non-linear forecast is carried out using the full physical parameterization schemes as the operational version (hereafter denoted reference or control run), and started from the same initial model state, $\mathbf{x}(t_0)$. This step is necessary for creating the trajectory containing the model state fields $\mathbf{x}(t_i)$, $t_0 \leq t_i \leq t$, at every time step (in fact this integration is already known at the case selection stage, however, it is needed to be repeated for storing the trajectory). The backward adjoint integration is to be performed around this trajectory.
- At the verification time, t, that is the end of the direct non-linear model integration, the difference between the forecast, denoted by $\mathbf{x}(t)$, and the

valid analysis, $\mathbf{x}^a(t)$, is used for computing the quadratic forecast error cost function (as defined in Eq. (4)) and its gradient. Since for the time when ALADIN model does not have its own operational data assimilation cycle, in our study, the valid analysis refers to the operational ARPEGE analysis. ARPEGE is the global spectral numerical weather prediction model of Météo France (*Courtier et al.,* 1991). The ALADIN model is the high resolution limited-area version of the ARPEGE model.

- A backward integration of the adjoint model is carried out in order to provide an estimate of the gradient of the forecast error cost function with respect to the initial conditions. This integration is performed around the trajectory computed at the first step. Generally, an adjoint model can be either completely adiabatic or it can enfold linearized physical parameterization schemes. In our studies, two schemes simulating the surface drag and vertical transport of momentum due to turbulent exchange were enforced in alternation. The first one, developed by *Buizza* (1993) for a low resolution global model, is a reduced and very simple scheme, because it assumes constant mixing coefficients. A second and more complex one is a package of simplified physical parameterization schemes proposed by *Janisková et al.* (1999), based on the vertical diffusion equation with a first-order closure for the exchange coefficients. Although it contains simplified schemes for radiation and moist processes, this study exclusively concentrates on the use of its dissipative part, namely vertical diffusion and surface drag. This package was developed for a global model too. Thus, a direct comparison between the two schemes is made possible. Hereafter, the simple physics as defined by Buizza will be called "reduced" physics, while the "dissipative part of the physics" will refer to the vertical diffusion and gravity wave drag schemes from Janisková.

- The final stage is the so-called sensitivity forecast. This is carried out starting from modified initial conditions, $\mathbf{x}(t_0)+\delta\mathbf{x}_0$, $(\delta\mathbf{x}_0=-\alpha\ \nabla_{\mathbf{x}(t_0)}J)$, by a new non-linear model integration including exactly the same physical parameterization package as for the control run. In such a way, the vector $\delta\mathbf{x}_0$ is used to diagnose the effect of the errors in the initial data based on forecast errors.

4. Analysis of the results

The integration domain utilized in our sensitivity experiments was the operational ALADIN/HU (ALADIN Hungary) model version, which covers mostly the Central European area. ALADIN/HU is a double nested high reso-

lution model (200 × 144 points horizontally with 31 vertical levels, $\Delta x = 8$ km) embedded into ALADIN/LACE (Limited-Area modelling for Central Europe, 240 × 216 points horizontally with 31 vertical levels, $\Delta x = 12.2$ km), which at its turn is embedded in the global model ARPEGE. Since our intention was to use the dissipative part of the simplified parameterization scheme for the gradients computation, a triple nested model version (80 × 80 horizontal points and 31 vertical levels, $\Delta x = 8$ km) embedded into ALADIN/HU was created as a zoom over Hungary. This appeared as a strong necessity due to computer memory limitations. The problem arrives when a complex parameterization scheme is used, because an additional trajectory at $t-\Delta t$ has to be stored in the computer memory (Δt is the time step of the physics). This extra storage is needed, because the tendencies and fluxes are entirely computed from the variables at previous time step.

As an example of sensitivity analysis, we consider a summer case covering the period between 12–18 UTC, June 22, 2001. From synoptic point of view, at 12 UTC, this case study pertains to a frontal activity linked to a moving low, which at ground level was situated in the western part of Ukraine. This cyclone had a well defined correspondent in the altitude. For instance, at 500 hPa (not shown), it was centered in the western part of Poland (about 800 km to the west). Over Hungary, the low was rapidly advecting cold air originating from the North Sea. Thus, the rapid air flow was found to be associated to a westerly jet stream having a maximum wind speed of about 35 m/s.

This case was selected, because the 6 hours precipitation forecast was overestimated especially in the eastern part of Hungary, over the Great Hungarian Plain. Although, there was an important amount of precipitation forecasted in the western part of the country, we are not concerned with this area due to the proximity of the Alpine region.

The operational numerical precipitation forecast is shown in *Fig. 1a*. A zoom over the region of main interest, i.e., the target area, in the south-eastern part of Hungary is presented in *Fig. 1b*. One can see that 16 mm/6h precipitation have been predicted whereas in that region a maximum of 2 mm/6h was reported by rain-gauge stations (not shown). The problem of such misforecasted precipitation should be seen as a complex one, where errors in initial conditions (e.g., analysis of humidity field, wind shears, or temperature gradients), or in lateral boundary conditions or model errors due to weaknesses in the formulation of the model physics and dynamics play an important role. However, in our study, we concentrate exclusively on the initial condition problem. We try to assess and correct the initial fields with the adjoint method, by focusing mainly on the dynamical processes at mesoscale.

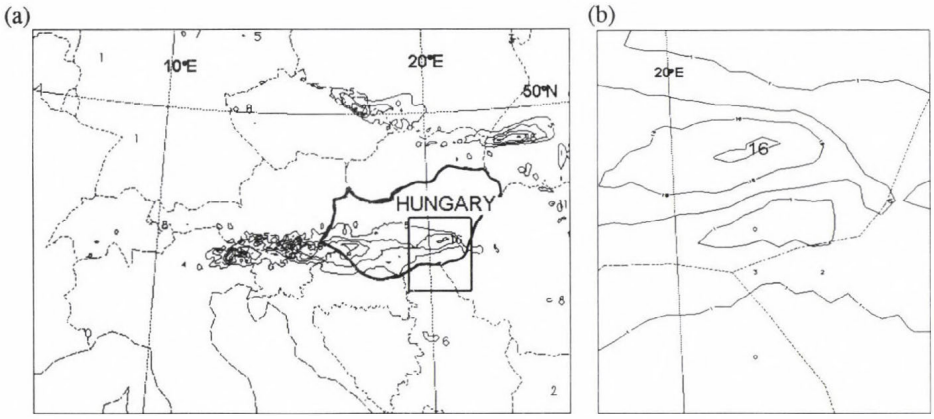

Fig. 1. (*a*) Field of 6 hours reference precipitation forecast over the ALADIN/HU domain. Contour intervals are at every 5 mm/6h. (*b*) Reference 6 hours precipitation field zoomed over the region of interest, i.e., south-eastern part of Hungary. Contour values are 1, 5, 10, and 15, respectively with units mm/6h.

Sensitivity experiments were carried out for 6 hours integration within the period mentioned above. The difference between the 6h forecast and the corresponding verification analysis was used to feed the adjoint model integration with the input gradient of the forecast error cost function. In order to isolate the origin of the forecast error of the misforecasted precipitation field in the eastern part of Hungary, the forecast error norm was computed over a target area inside the model integration domain. This subdomain is shown in *Fig. 1a*. This target area was subjectively chosen after analyzing the forecast error fields at +6h. In *Fig. 2a*, 500 hPa zonal wind speed difference between the control and verifying analysis is illustrated. It is revealed that already after 6 hours, the non-linear model underestimates by about 18 m/s the zonal wind speed in the area of interest. At the same time (as presented in *Fig. 2b*), the temperature difference is about 1.5 K indicating a warmer forecast, than the reality.

At the end of the adjoint integration, the retrieved initial sensitivity includes only the signal of main concern. *Fig. 3* illustrates the evolution of the gradients of the forecast error cost function with respect to zonal wind, $\nabla_U J$, on model level 20 (about 500 hPa), during an adjoint integration performed from +6h to +0h. One may see, how at the beginning of the adjoint integration (*Fig. 3a*) the initial gradient inside the target area is projected onto the integration domain. Further on, the gradient develops and is advected westward, upstream of the winds that tend to advect the perturbation eastward. At +4h (*Fig. 3b*), the sensitivity field was advected westward and located in

the middle of the domain, while at +2h, the gradient has already reached the western boundary of the integration area (*Fig. 3c*). For higher levels, one may anticipate that the gradient passes the border earlier, since its structure is characterized by a typical baroclinic tilt in the vertical. At the end of the adjoint backward integration, the gradient is concentrated near the western border of the domain (*Fig. 3d*).

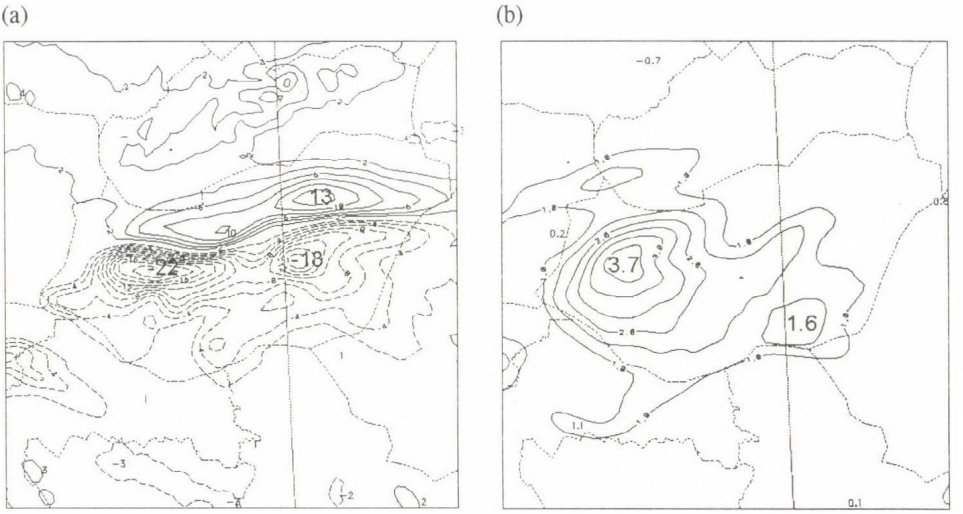

Fig. 2. (*a*) 500 hPa zonal wind difference between the +6 hours reference forecast and the verifying analysis valid at 18 UTC June 22, 2001. Contour intervals are at every 2 m/s. Positive (negative) value contours are continuous (dashed), and zero-valued contours are omitted. (*b*) As in Fig. 2a, except for the temperature. Contour intervals are at every 0.5 K. (Contour for values less than 1 K were omitted.)

In order to study the impact of the dynamics and physics in the sensitivity computation, a set of experiments has been performed using mainly the ALADIN/HU domain. Results from three different adjoint configurations have been compared. In the first run, the gradients have been computed adiabatically, without any physical process simulation, while in the second run, the reduced physics were used. The third run with the dissipative part of the simplified physical parameterization was carried out using the small integration domain.

Let us first analyze the results of the adjoint integration performed with adiabatic and reduced physics. *Figs. 4a–c* illustrate the gradients of the forecast error cost function with respect to the temperature, $\nabla_T J$, on the model level 29 (about 200 m). The figures are zoomed over Hungary

covering the same area as the small domain. The primary qualitative difference between panels (a) and (b) is that in *Fig. 4a* the gradients have larger values and look noisier than in *Fig. 4b*. The difference comes from the fact that the gradients plotted in *Fig. 4a* were computed with an adiabatic adjoint model, whereas in *Fig. 4b* the computation was performed with reduced physics.

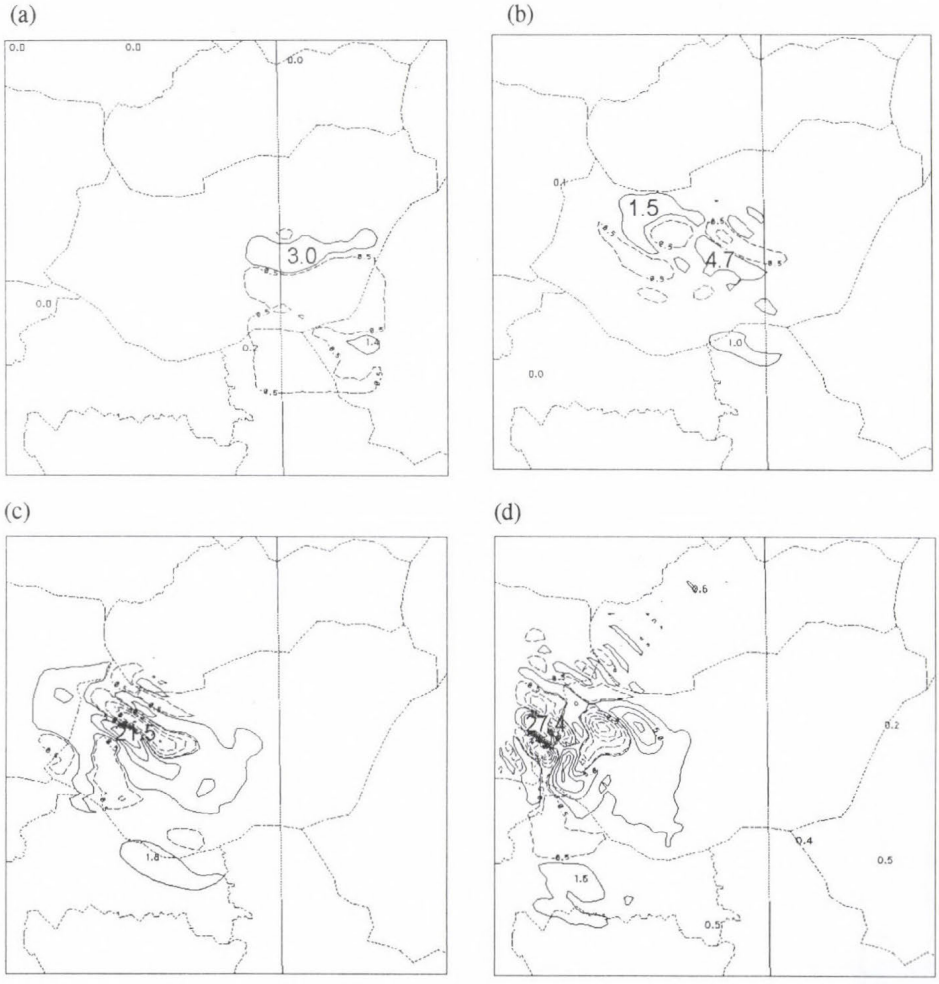

Fig. 3. Evolution of the gradients of the forecast error cost function with respect to zonal wind, $\nabla_U J$, on model level 20: (*a*) at the beginning of the backward adjoint integration, +6 hours; (*b*) +4 hours; (*c*) +2 hours; and (*d*) at +0 hours. Contour intervals are at every 4 Js/m for absolute values greater or equal to 4 Js/m. Contours are shown for absolute values less than 4 with intervals of 0.5 Js/m. Positive (negative) value contours are continuous (dashed), zero-valued contours are omitted.

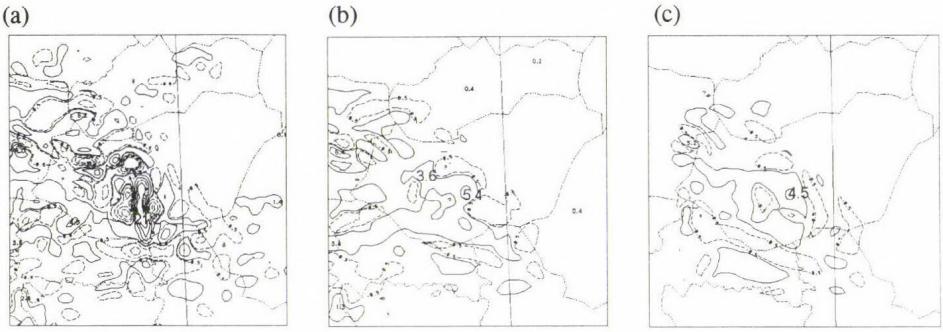

Fig. 4. Gradients of the forecast error cost function with respect to temperature, $\nabla_T J$, on model level 29 computed (*a*) adiabatically, (*b*) with reduced physics and (*c*) with the dissipative part of the simplified physical parameterization. Contour intervals are at every 5 J/K for absolute values greater or equal to 5 J/K except for the first contour plotted for absolute values equal to 0.5 J/K. Positive (negative) value contours are continuous (dashed); zero-valued contours are omitted.

In the latter case, the gradient field is one order of magnitude weaker than the adiabatic gradients. The gradients derived with the adiabatic adjoint model are not realistic in the sense that they contain non-meteorological fast growing structures confined only to the first model levels. Their time evolution must be similar to an error field evolution, and this is more realistically described when using reduced physics. It is known, that in the absence of any planetary boundary layer parameterization, the adiabatic model develops strong wind anomalies near the surface due to the lack of friction (*Buizza*, 1993). The importance of the physical description of the processes in the planetary boundary layer is highlighted by the results derived using the dissipative part of simplified physics as shown in *Fig. 4c*. Examination of *Fig. 4c* points out that the magnitude of the gradient has the same order than with reduced physics.

The sensitivity forecasts were performed using initial data perturbations following the procedure described in the previous section. The gradients of the forecast error cost function, computed adiabatically with reduced physics and dissipative part of the simplified physics, were normalized with a scaling factor $\alpha=0.1$ and added to the initial conditions. In this way, three new initial model states have been created, a priori each of them being "better" than the original one. The results of the sensitivity forecasts are presented in *Figs. 5a–c*. If compared with *Fig. 1b*, the general feature is that all sensitivity forecasts have improved the precipitation forecast. The introduction of a scaled gradient of the forecast error in the initial conditions has led to the reduction of the 6 hours precipitation amount with a maximum of about 7 mm in the case when the dissipative scheme has been used (*Fig. 5c*).

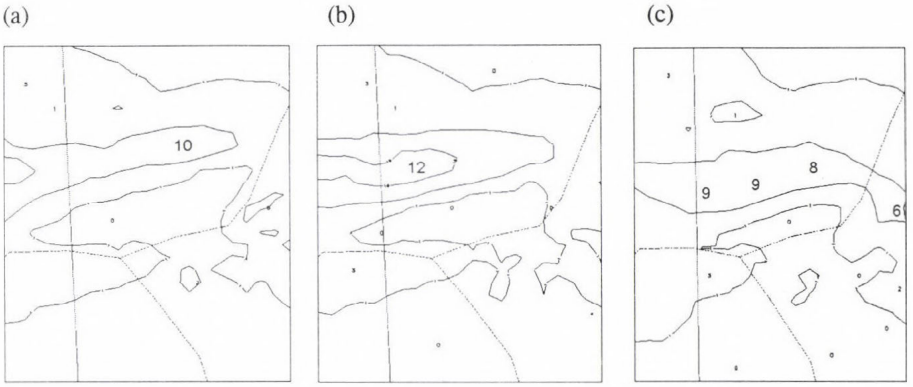

Fig. 5. Sensitivity precipitation forecasts – zoomed over the region of interest (target area) – performed starting from modified initial conditions with scaled gradients computed (*a*) adiabatically, (*b*) with reduced physics, and (*c*) with the dissipative part of the simplified physical parameterization. Contour values are 1, 5, and 10, respectively, with units mm/6h.

In *Figs. 5a* and *5b*, the precipitation fields from the sensitivity forecast run with the scaled gradients computed adiabatically, and with reduced physics, respectively, have been plotted. Surprisingly, the scaled gradients computed adiabatically have corrected the precipitation field as well (*Fig. 5a*). However, the perturbations introduced in the initial temperature field are relatively large in the first model levels. For example, at model level 29, the maximum value of the perturbation added was 3.5 K, while when gradients were computed with reduced physics, the magnitude was –0.6 K. For comparison, at the same level, when the gradients were calculated using dissipative physics, the maximum value of the perturbation was –0.5 K. These corrections of the initial dynamical model fields lead to a better match of the forecast with the verifying analysis. For example, *Figs. 6a–b* shows the difference of 500 hPa zonal wind and temperature, between the modified 6h forecast and verifying analysis. This experiment was run using the gradient computed with the reduced physics. Results obtained with the adiabatic adjoint model were very similar (not shown). *Fig. 6* has to be compared with *Fig. 2*. It can be seen that, in absolute values, the 500 hPa zonal wind difference between the sensitivity forecast and analysis has diminished by 2 m/s in the area of main concern, and by 4 m/s in the western part of Hungary. For other levels (not shown), it was noticed that the whole vertical structure of the wind field was changed. To be specific, there is a significant decrease of the vertical wind shear. Since this vertical shear is one crucial element to trigger convection,

this modification can at least partially explain the reduction of the activity of the system. Furthermore, the temperature has decreased as illustrated in *Fig. 6b*.

Since no moist parameterization was used in the adjoint model, the adjoint computation can be considered as dry. However, the correction of the precipitation field was substantial, so we do believe that, for this case, the evolution of the physical processes were partially driven by the dynamical forcing of precipitation.

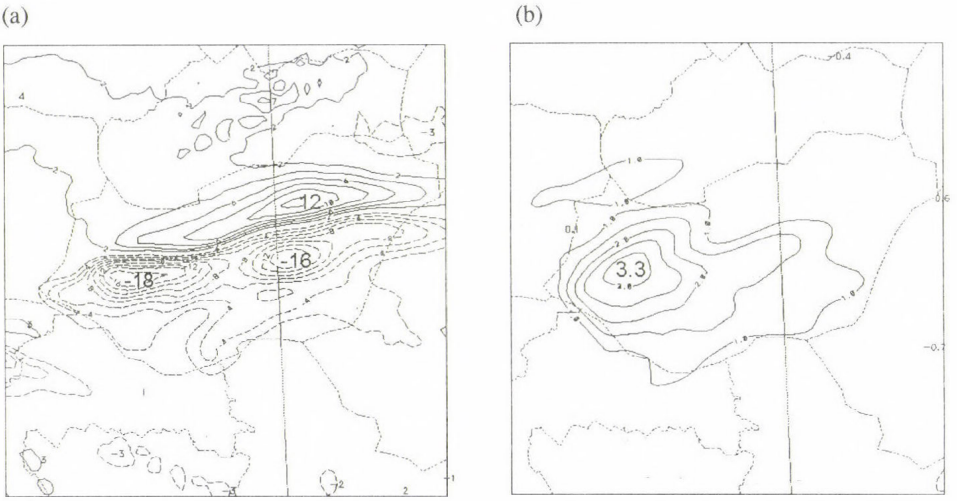

Fig. 6. (*a*) 500 hPa zonal wind difference between the +6 hours reference forecast and the verifying analysis valid at 18 UTC June 22, 2001. Contour intervals are at every 2 m/s. Positive (negative) value contours are continuous (dashed), and zero-valued contours are omitted. The sensitivity was computed with the adjoint model with reduced physics (*Buizza,* 1993). (*b*) As in Fig. 6a, except for the temperature. Contour intervals are at every 0.5 K. (Contour for values less than 1 K were omitted.)

5. Concluding remarks

In this paper, the adjoint model has served as a tool for calculating the sensitivity of 6 hours forecast errors to the initial conditions as measured by a dry total energy norm.

After describing briefly the mathematical basis of the adjoint method, results obtained for sensitivity experiments were presented. Special attention was devoted to the use of linearized physics such as vertical diffusion and surface drag during the adjoint integration.

The gradients computed with an adiabatic adjoint model, without any vertical diffusion and surface drag applied to the momentum equation, produce non-meteorological structures in the lowest model levels. For a 6 hours adjoint integration, their values can be one order of magnitude greater than if dissipative processes are taken into account. Including vertical diffusion and surface drag, the gradients are realistically improved.

In this study, when using the small domain, the sensitivity fields were located in the proximity of the western lateral boundary. This suggests the necessity of a larger integration domain, which may allow the enlargement of the sensitive area.

When computing mesoscale sensitivities using a high resolution adjoint model, their 6 hours amplification rate have the same order of magnitude as for the large scale gradients calculated by a low resolution adjoint model for larger time ranges (*Gustafsson* and *Huang*, 1996; *Rabier et al.,* 1996). This is why a scaling factor, $\alpha=0.1$, has proved to be optimal for the June 22, 2001 case study. Thus, it may suggest that there are mesoscale situations in which errors in the initial conditions may grow faster for a high resolution limited area model than for a low resolution one. For one selected case study, the sensitivity integration substantially improved the 6 hours precipitation forecast. However, this result should be carefully interpreted. Yet it does not allow to claim, that using a dry energy norm and a simplified physical parameterization without moist diabatic processes in the sensitivity computation, will always lead to a dramatic improvement of the precipitation field. Indeed, in other cases, the initial state modification based on dry gradients did not produce equivalently "desired" corrections in precipitation. An example is presented in *Fig. 7*, where the difference between the operational and sensitivity precipitation forecasts was plotted. This is a spring case, covering the period between 00–06 UTC, March 5, 2001, which was selected due to the fact that the operational precipitation forecast was overestimated by about 20 mm/6h. As one may see in *Fig. 7a*, the sensitivity forecast performed starting from the "improved" initial conditions (gradients computed with reduced physics and $\alpha=0.1$) was rather neutral, since the amount of precipitation was slightly increased by about 1 mm/6h in the area of main interest, i.e., the centre of the domain. For bigger α, the sensitivity precipitation forecast shows a degradation, when compared to the operational one (*Fig. 7b*), while for smaller values the gradient is negligible. Similar results were obtained using gradients computed adiabatically or with dissipative physics. Hence, the forecast failure cannot be attributed to errors in the initial conditions, but it has to be explained by some other reasons.

It is very likely that the good result obtained in the summer case is due to the fact, that the sensitive area was mainly over the Alps, a data-sparse

region, especially for vertical soundings. In this respect, however, detailed studies are to be performed with the goal of a better understanding of mesoscale gradients.

This study is understood as a first step for the evaluation of the benefit of adjoint computations in the frame of small scale and mesoscale numerical weather prediction. Indeed, while the adjoint approach (and the associated 4D-VAR assimilation) has been very successful for the representation of synoptic and sub-synoptic atmospheric flows, much needs to be done to evaluate its potential at smaller scales. The main interest then lies in the description of the humidity distribution inside a frontal system, or fine vertical profiles of all atmospheric fields to capture the boundary layer, capping inversions, convective areas, or inertia-gravity waves.

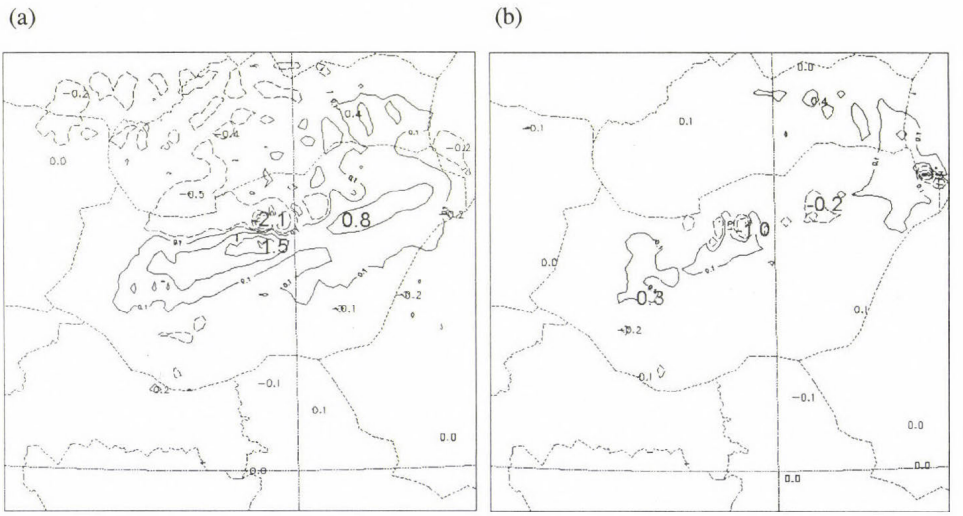

Fig. 7. (*a*) Difference between the 6 hours operational and sensitivity precipitation forecasts (valid at 06 UTC, March 5, 2001). Positive (negative) value contours are continuous (dashed), and zero-valued contours are omitted. The sensitivity was computed with the adjoint model with reduced physics. Contour values are 0.1, 0.5, 1, and 1.5, respectively, with units mm/6h. (*b*) As in Fig. 7a, except for α=0.75.

In the future work on sensitivity analysis, we will concentrate on the computation of the gradients of the forecast errors to the initial conditions by including the moist parameterization schemes in the ALADIN adjoint model. These moist linearized schemes will be useful for extracting meaningful sensitivity over the regions, where the evolution of the atmospheric flow is not only dictated by dynamical instability but also by strong local humid processes.

Acknowledgements—We thank Météo France and Hungarian Meteorological Service for scientific and technical support. This work was made possible thanks to ALATNET Grant HPRN-CT-2000-00057. ALATNET is supported by the TMR/IHP Programme of the European Community, but the information provided here is the sole responsibility of the ALATNET team and does not reflect the Community's opinion. The Community is not responsible for any use that might be made of data appearing here. *C. Soci* was on leave from the NIMH, Bucharest. ALADIN is an international NWP project (with presently 15 partner countries). We are grateful to all colleagues from the partner institutes who have contributed to maintain and develop the numerical tools used in this study. Also, we are grateful to the anonymous reviewers for their useful comments and suggestions, which resulted in a significant improvement of the paper.

References

Buizza, R., 1993: Impact of a simple vertical diffusion scheme and of the optimisation time interval on optimal unstable structures. *ECMWF Tech. Memo.* 192, 25 pp.

Courtier, Ph., Freydier, C., Geleyn, J-F., Rabier, F., and *Rochas, M.*, 1991: The ARPEGE project at Météo France. *ECMWF Seminar Proceeding, Reading*, Vol. II, 193-231.

Davies, H.C., 1983: Limitation of some common lateral boundary schemes used in NWP models. *Mon. Wea. Rev. 111*, 1002-1012.

Errico, R., 1997: What is an adjoint model ? *Bull. Amer. Meteor. Soc. 78*, 2577-2591.

Errico, R. and *Vukicevic, T.*, 1992: Sensitivity analysis using an adjoint of the PSU-NCAR mesoscale model. *Mon. Wea. Rev. 120*, 1644-1660.

Gustafsson, N. and *Huang, X.-Y.*, 1996: Sensitivity experiments with the spectral HIRLAM and its adjoint. *Tellus*, 48A, 501-517.

Horányi, A. and *Joly, A.*, 1996: Some aspects of the sensitivity of idealised frontal waves. *Beitr.Phys.Atmosph. 69*, 517-533.

Horányi, A., Ihász, I., and *Radnóti, G.*, 1996: ARPEGE/ALADIN: A numerical weather prediction model for Central-Europe with the participation of the Hungarian Meteorological Service. *Időjárás 100*, 277-301.

Janisková, M., Thépaut, J-N., and *Geleyn, J-F.*, 1999: Simplified and regular physical parametrizations for incremental four-dimensional variational assimilation. *Mon. Wea. Rev. 127*, 26-45.

Joly, A., 1995: The stability of steady fronts and the adjoint method: nonmodal frontal waves. *J. Atmos. Sci. 52*, 3081-3108.

Le Dimet, F-X. and *Talagrand, O.*, 1986: Variational algorithms for analysis and assimilation of meteorological observations: theoretical aspects. *Tellus 38*A, 97-110.

Rabier, F., Klinker, E., Courtier, Ph., and *Hollingsworth, A.*, 1996: Sensitivity of forecast errors to the initial conditions. *Quart. J. Roy. Meteor. Soc. 122*, 121-150.

IDŐJÁRÁS

Quarterly Journal of the Hungarian Meteorological Service
Vol. 107, No. 1, January–March 2003, pp. 67–83

Mesoscale atmospheric vortex generation over the Adriatic Sea

Branka Ivančan-Picek and **Vesna Jurčec**

Meteorological and Hydrological Service of Croatia,
Grič 3, 10000 Zagreb, Croatia; E-mail: picek@cirus.dhz.hr

(Manuscript received January 17, 2002; in final form July 3, 2002)

Astract—Circumstances under which the Adriatic mesoscale vortex was generated at the end of March, 1995 is investigated. Assuming that a mesoscale vortex can be isolated from the synoptic environment, the scale separation technique is employed. This provides the mesoscale orographic disturbances with characteristic quasi-antisymmetric dipolar structure across the Dinaric Alps. The mesoscale wind field contains a pronounced ageostrophic component with small-scale vortices of short duration and clearly marked convergence zones. Hence, the cyclonic vortex was generated over the middle Adriatic in a macroscale wind field as defined here, in which the smaller scale instabilities, as noise, are filtered out during the procedure. A very persistent mesoscale anticyclonic vortex is found in Pannonian Plain following the northerly flow around the eastern flank of Alps. This flow is responsible for the bora occurrence, but it also contributes to the Adriatic circulation, in which jugo wind in the southern and bora in the northern Adriatic lead to the vortex generation examined.

Key-words: mesoscale vortex, scale separation technique, bora, jugo, orographic pressure dipole.

1. Introduction

In recent years, mesoscale meteorology, and especially the orographic influence on mesoscale circulations and frontal deformations have received increasing attention of the scientific world. Many investigations in the Alpine area were motivated by the significant gap between very sophisticated high-resolution mesoscale models and poorly observed complex phenomena at the sea level. To provide datasets for the validation and improvement of high-resolution numerical weather prediction in mountainous terrain was one of the

main objectives of the MAP – Mesoscale Alpine Programm (*Binder* and *Schär*, 1996).

Vortex generation was observed in the western Mediterranean by *Gomis et al.* (1990) considering the composition of several lee cyclogeneses that occurred during the ALPEX SOP. Applying the scale separation method to 850 hPa level data, they isolated the subsynoptic/meso-β features from the "undisturbed" state characterizing the larger scale structure of this phenomenon. Vortices over the Adriatic Sea appeared in numerical simulation, but had never been shown by objective analysis with real surface data.

Jurčec et al. (1996) employed the same method using *the sea level observational data* in order to separate mesoscale features in the Adriatic area from the synoptic fields characterized by a cyclone in the gulf of Genoa and strong jugo wind over the Adriatic Sea. The complex structure of the mesoscale Adriatic fields with pronounced ageostrophic flow was clearly indicated, suggesting the need for further studies of this problem under different larger scale circumstances.

Our present study is dealing with objective analysis of two cases of Adriatic vortex generation at the end of March, 1995 marked by extremely strong bora wind. It was studied earlier by *Tafferner* (1995), *Brzović* and *Jurčec* (1997), *Ivančan-Picek* (1997), and *Brzović* (1999). The analyses include all available data in the Adriatic coast and islands in addition to ordinary synoptic data, aiming to separate the subsynoptic/meso-β scale features from the larger scale structures, using scale separation technique with known spatial filtering properties. We concentrate mainly on the wind field and search for cyclonic and anticyclonic vortices over the Adriatic Sea and surroundings.

Section 2 describes the Adriatic characteristics of cyclones (including low level shallow depressions by orography and thermal contrasts) and local winds, section 3 gives a synoptic overview, section 4 describes the scale separation, section 5 contains the results of macro- and mesoscale fields over the Adriatic area, and section 6 summarizes the conclusions.

2. Adriatic cyclones and wind characteristics

The Mediterranean area presents the highest concentration of real cyclogenesis (including low level shallow depressions by orography and thermal contrasts) in the world. The most famous is the Genoa cyclogenesis (*Buzzi* and *Tibaldi*, 1978). Nevertheless, there are other areas with quite frequent true cyclogenesis. One is located in the Adriatic (*Ivančan-Picek*, 1997). Mediterranean local winds (including Adriatic bora and jugo) can be seen as the results of the orographic mesoscale pressure perturbation induced by the

flow/mountain interaction. High and low pressure centres of the orographic disturbance (and/or the orographic pressure dipole as a whole) create local areas of strong pressure gradient, that provide intense local acceleration, leading to local wind generation (*Campins et al.*, 1995). The synergistic combination of intense cyclone and local wind generation can explain of the extreme violence of some of the strong wind events. Synoptic and local weather characteristics during the bora and jugo episodes are discussed in several studies, (e.g., *Ivančan-Picek* and *Tutiš*, 1996; *Jurčec et al.*, 1996, and references therein). However, there is an evidence of relationship between bora, jugo, and a cyclone in the Adriatic.

The obvious constraint on the spatial scales of an atmospheric system is the geometry of its boundaries. The Adriatic Sea is about 200 km wide and surrounded by the Alps on the north, Dinaric Alps on the eastern coast of Croatia, and the Apennines on the west in central Italy. Orographic effects are therefore essential for the Adriatic systems, particularly cyclones and wind characteristics. Northern Adriatic is frequently exposed to Alpine lee cyclogenesis. These cyclones move southeast along the Adriatic Sea, and usually deepen extending throughout the troposphere in the southern Adriatic. The first mesoscale numerical experiment in the Adriatic area, using the high-resolution ALADIN model, was performed by *Brzović* (1999) indicating the decisive role played by the Dinaric Alps on the maintenance of Adriatic cyclones and wind systems. Jugo (*jug* means *south* in Croatian), the strong southerly, warm, and humid wind appears ahead of the Adriatic cyclones or frontal zones, while the northeasterly cold bora wind is behind them.

Until recently, jugo was considered as a part of the sirocco wind family, which has the origin in the southern Mediterranean and northern Africa, characterized by dry and dusty air from the Sahara. Crossing the Mediterranean, the air picks up moisture, and reaching southern Italy it looses its force and energy, becoming a hot and humid wind (*Huschke*, 1959). However, jugo on the contrary could be very severe reaching the maximum speed over 40 m/s. Statistics and many case studies (*Jurčec et al.*, 1996) have indicated that jugo is associated mainly with Alpine lee cyclogenesis on synoptic scale in the western Mediterranean, whereas in the Adriatic Sea, subsynoptic scale analyses established the connection of jugo with mesoscale cyclones and fronts. Thus, jugo does not belong to the sirocco wind system, although, there may be some special cases of very strong southerly current ahead of the Mediterranean cyclone, which may bring a relatively dry air from the Sahara to the Adriatic area.

The best-known severe wind in the Adriatic area is the northeasterly bora wind, which is a down slope cold and gusty wind of the eastern Adriatic coast.

Until the ALPEX program in 1982, it was defined as a "falling wind", which accelerates as it moves down slope due to its low temperature and greater density. Results of the first aircraft observations of the bora in Croatia accomplished during the ALPEX project did not verify this popular idea of the bora as falling wind, since the aircraft measurements indicated an upstream acceleration too, which begins where the mountains begin to rise. This is explained by the conservation of mass flow between the rising terrain and descending isentropes toward the warm Adriatic Sea, which requires flow acceleration upstream from the mountaintop. From this analysis *Smith* (1987) introduced the internal hydraulic mechanism as a mathematical description of bora features.

For the ALPEX SOP (March–April 1982), the pressure drag exerted by the Dinaric Alps was evaluated by *Tutiš* and *Ivančan-Picek* (1991), *Ivančan-Picek* and *Tutiš* (1995), using data from mesoscale array of microbarographic stations. The pressure drag maxima were always connected with bora periods. In these cases we may compare the Dinaric Alps to the Alpine region in the drag value magnitudes. The orographic pressure dipole is a key phenomenon for the organization and intensification of the local bora wind. The pressure difference between the upstream and downstream regions during the bora periods can be greater than 10 hPa/50 km.

In our case study, we will describe some of these features in section 3. More details on this subject are presented by *Jurčec* and *Brzović* (1995, and references there), and a general description of the winds in the Adriatic area is given by *Poje* (1992).

3. Synoptic overview of the case study

Circumstances, under which the Adriatic mesoscale vortex is generated at the end of March 1995 are investigated. In a relatively short time period (March 28–30, 1995), two cold air outbreaks propagated towards Croatia, and resulted in two cyclogeneses over the northern Adriatic Sea. Abundant rain and snowfall were recorded over many parts of Croatia including Dalmatia, which is an extraordinary event for the last days of March. This situation has been chosen as an exceptional case of cold air outbreak over the Alps, which caused one of the strongest bora storms registered in the coastal region of Croatia.

The essential feature of this case study is a deep low in the Baltic area influencing the development in the Alpine region. On the first day, March 27, this low of 975 hPa was in southern Sweden with another center of the same intensity over the Barents Sea. These two lows, extending to the low troposphere, intensified the northerly flow over NW Europe and the W-SW

current over the Alpine area, Pannonian Plain, and Adriatic Sea. The frontal system from central Europe rapidly moved southward across the Alps, and a cold air outbreak influenced the pressure rise over Western Europe with a pronounced ridge to the north of the Alps. This process resulted in a strong cyclogenesis in the northern Adriatic on March 28 (*Fig. 1a*) with a front connecting this cyclone with the Baltic one, which moved to the east while deepening.

On March 29 the Baltic low decreased in size, and its influence on the Adriatic area gradually diminished (*Fig. 1b*). The cyclone from the Adriatic was already in the eastern Balkan, and a new weak low formed in northern Italy ahead of the frontal system approaching the Alpine area. This again intensified the Adriatic cyclone, which was moving toward the southern Adriatic, where it slowed down deepening and extending to the upper tropospheric levels (*Fig. 1c*). The intensification of the cyclone in this area is related to the upper level development in agreement with the conclusion by *Tafferner* (1990, 1994), who identified this process with other Alpine cyclogeneses.

Figs. 1 d–f show the 850 hPa charts for the same days. Due to the intensity of the Baltic low, the northerly current with strong winds did not encounter the Alpine region, which was, south of the front in *Fig. 1d*, under the influence of strong SW winds. This is not typical for the process of Alpine lee cyclogenesis, where the splitting current on the western Alps is missing. This was the reason why the cyclogenesis did not take place in the western Mediterranean but instead affected the north Adriatic through a very cold air outbreak circulating around the eastern flank of the Alps. This process was very fast marked by the *cross isobaric flow* over the Alpine area as a sign of increasing acceleration. On March 29 the Alpine area was again under the influence of lows (*Fig. 1e*), and on the last day (*Fig. 1f*), a deep low extended from the surface to higher tropospheric levels, and a ridge covered the western and middle Europe including the Alpine area.

Upstream conditions suitable for bora onset can be divided into two main groups (*Fig. 2*): (a) unidirectional northern flow throughout the troposphere; (b) shallow low-level bora flow below a critical level, defined either as the level of strong temperature inversion or level of flow reversal. This is demonstrated by the low and middle tropospheric changes in the sounding of Zagreb, characteristic for the upstream condition of the bora wind (see *Smith* (1987) for definition of upstream bora condition). The large temperature drop from 27th to 28th of March, with the changes of wind direction from SW to NE in the low level up to 2–3 km, covers the bora layer and explains the bora intensity in terms of hydraulic mechanism referred already in section 2.

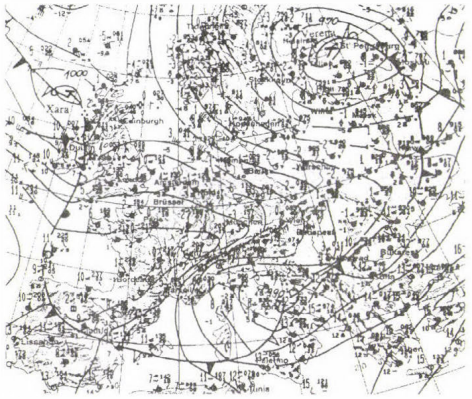

(a) March 28, 1995, 06 UTC, surface

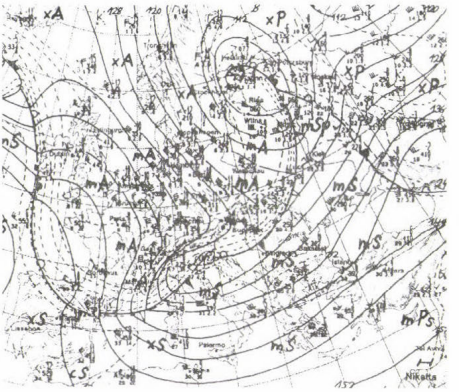

(d) March 28, 1995, 00 UTC, 850 hPa

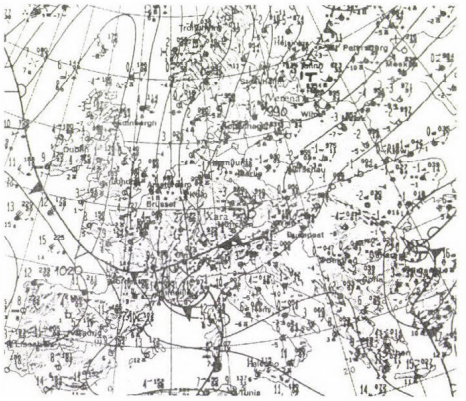

(b) March 29, 1995, 06 UTC, surface

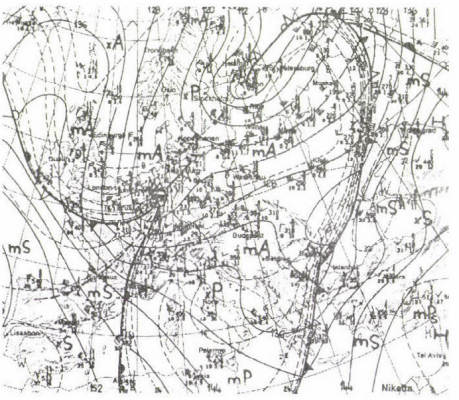

(e) March 29, 1995, 00 UTC, 850 hPa

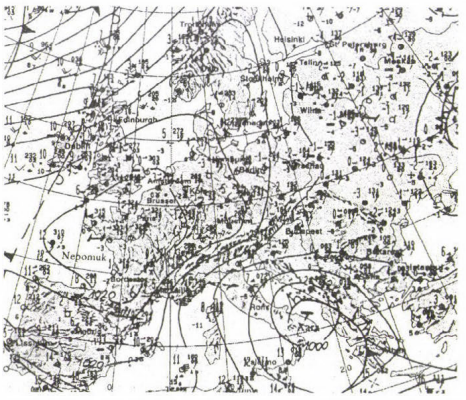

(c) March 30, 1995, 06 UTC, surface

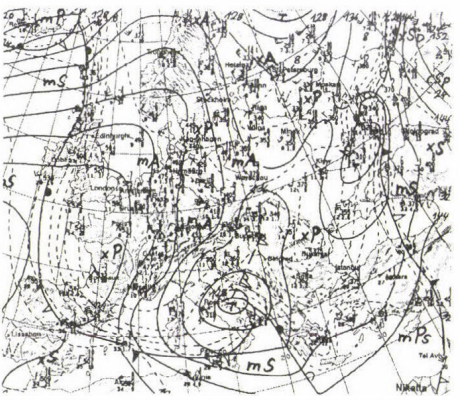

(f) March 30, 1995, 00 UTC, 850 hPa

Fig. 1. Subjective analysis of synoptic situation (from Berliner Wetterkarte).

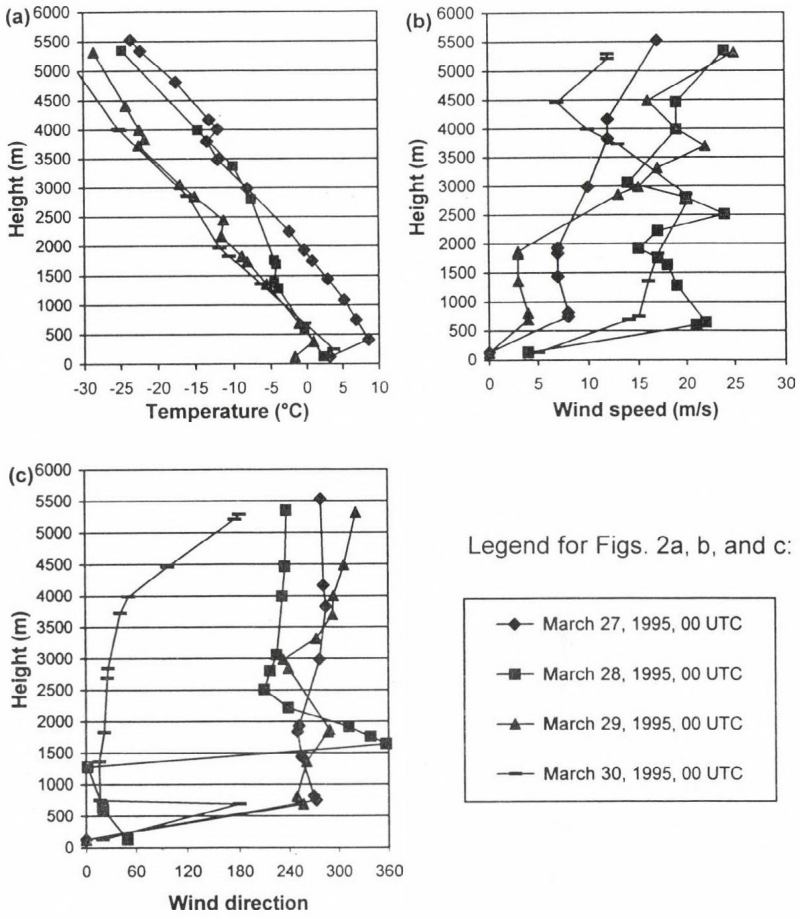

Fig. 2. Vertical profiles of temperature (*a*), wind speed (*b*), and wind direction (*c*) for Zagreb-Maksimir radiosounding station on March 27–30, 1995, 00 UTC.

Very strong bora events are illustrated in *Fig. 3* for Split in the middle Adriatic coast (see *Fig. 4*). It represents the daily courses of sea level pressure, temperature, and wind during the considered period. The striking feature is a large temperature drop following the pressure minimum on March 28, which coincides with the high increase of bora speed and gusts exceeding 45 m/s. The first bora event did not last long in comparison with the next episode of bora, which started at this location in the evening of March 29 with less variation in temperature. This is the result of both upstream and downstream influences, which is a known process under this condition in the southern Adriatic with a very deep and intense cyclonic activity (*Jurčec* and *Visković*, 1994).

(a)

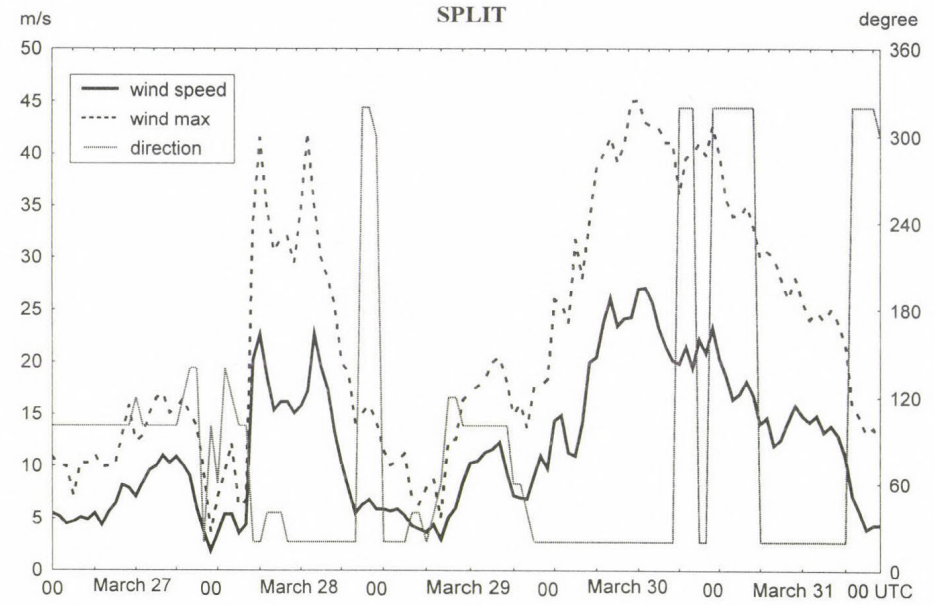

(b)

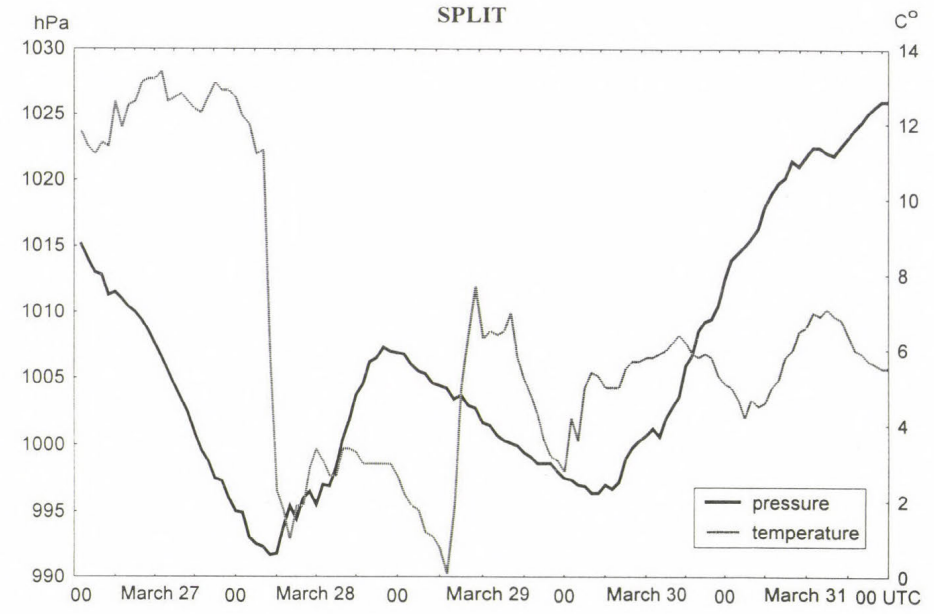

Fig. 3. Time courses of mean hourly wind speed, maximum wind gusts, wind direction (*a*), temperature and mean sea level pressure (*b*) in Split; March 27–31, 1995, 00 UTC.

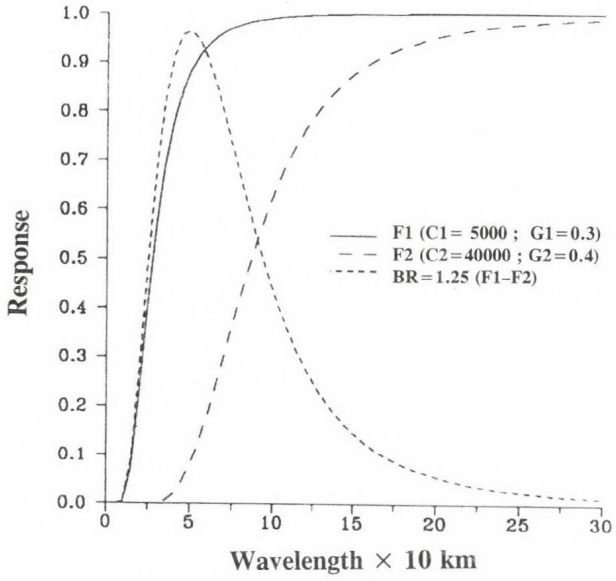

Fig. 4. Response curves for filters used in the objective scale separation technique (*Maddox*, 1980). Curves F1 and F2 are for low-pass filters used to define the bandpass (mesoscale) filter, curve BR. Response F2 also defines the macroscale field.

4. Data and computational method

The analysis technique employed here provides a scale separation successfully used by *Maddox* (1980), *Gomis* and *Alonso* (1988, 1990), *Gomis et al.* (1990), and *Jurčec et al.* (1996) in diagnosis of mesoscale structures. Briefly, the basic procedure is composed of two steps. The first step provides two macroscale fields after applying different low-pass filters. In the second step the subsynoptic (mesoscale) signal is obtained as a band pass field by subtracting those two macroscale fields. The total meteorological field is recovered as the sum of the macroscale and mesoscale fields, while the short wavelength noise is filtered out throughout the analysis.

There are two main features of the wavelength dependence of the analysis response: the cut-off wavelength for the large- and synoptic-scale contribution (hereafter referred to as "macroscale"), and the wavelenght at which the subsynoptic/meso-α contribution (hereafter referred to as "mesoscale") is centered. The response is controlled by a set of four parameters. Filtering and scale separation properties of the analysis, for the parameter values adopted in this work, are shown in Fig. 4. The mesoscale response retains the wavelengths in the range of about 500 km, and the response functions show the magnitude of damping of the shorter wavelengths, e.g., 50% damping at 250 km.

Our macroscale includes all features of wavelengths larger than approximately 900 km with damping of about 50% at 1000 km. Thus, both of our scales are much smaller than in the study of *Gomis et al.* (1990) at 850 hPa, where the mesoscale response describes wavelengths in the range of 500 –2000 km, and a macroscale response retains essentially wavelengths larger than about 2500 km. To minimize errors due to inhomogeneity of data distribution, we introduced the correction scheme as described briefly by *Gomis et al.* (1990), and in details by *Buzzi et al.* (1991).

Average data set contained 40 to 50 observations (*Fig. 5*), including data also from the climatological stations along the Adriatic coast and islands besides the conventional SYNOP observations. This data proved essential, particularly for the analysis of wind fields. To get reasonable values near the borders, stations outside the domain of the analysis were also included. The data were analyzed in a network of 25 × 25 grid points to a 0.5° longitude by 0.5° latitude grid extending from 38° to 50°N and 8° to 20°E (roughly 1100 × 900 km).

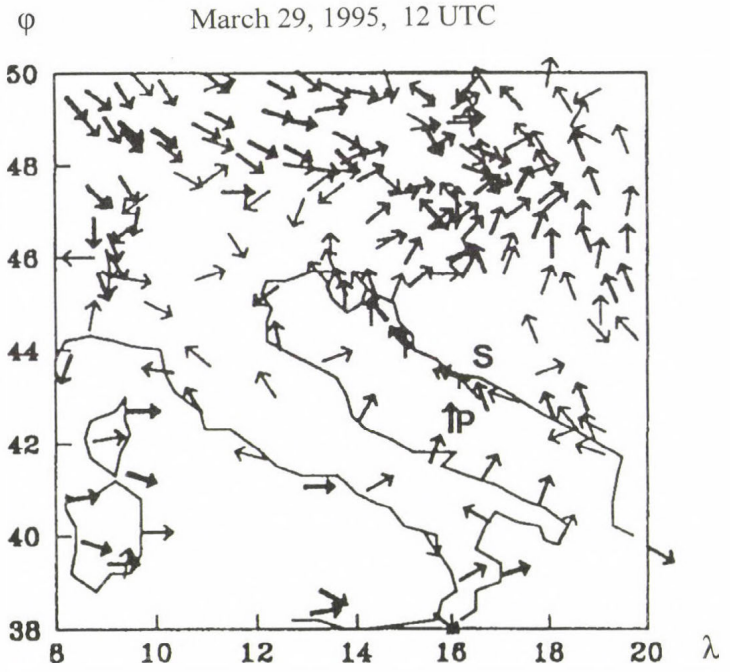

Fig. 5. Observed wind at available stations on March 29, 1995, 12 UTC. S and P indicate positions of Split and Palagruža. Thick arrows are for wind speed larger than 10 m/s, thinner arrows are for speed of 5–10 m/s, and thin arrows are for speed less than 5 m/s.

5. Results

Fig. 6a shows the total pressure field at 00 UTC on March 28 with a low center on the northern Adriatic. Across this low, the total wind field (*Fig. 6b*) indicates the convergence zone, which extends eastward and separates rather uniform N-NW winds in the north from the W-SW winds on the south. A relatively uniform wind structure at the northern (continental) and southern (Mediterranean) part of the considered area is typical for the macroscale wind field in the selected case study.

A strong dipolar structure is found in the mesoscale pressure field at that time (not shown), which is also seen across the Dinaric Alps at 06 UTC (*Fig. 6c*), when the mesoscale low extends to the middle Adriatic and central Italy toward the Tyrrhenian sea. The mesoscale wind field (*Fig. 6d*) at that time exhibits the convergence zone in the middle Adriatic and central Italy through the mesoscale low pressure. A small *cyclonic vortex* is seen in the northern Italy along the pressure trough. Notice that a cyclonic vortex is not found in the mesoscale wind field over the Adriatic sea, which is presumably the result of the warm sea intensifying the frontal zone and convergence at these zones only with possible appearance of very small and short-lived vortices.

On the contrary, the persistent vortex on this mesoscale field is the *anticyclonic vortex,* which also appears on the continent, e.g., on the eastern side of the Alps in the Pannonian Plain following the splitting current around the eastern flank of the Alps.

The mesoscale pressure field intensifies during the next 6 hours with a deep low in the southern Adriatic and a separate low in the Tyrrhenian Sea close to the Italian coast (*Fig. 6e*). The convergence zone (*Fig. 6f*) remains in the mesoscale wind field along this low pressure. The anticyclonic vortex is still seen in the Pannonian Plain, but cyclonic center in northern Italy no longer exists. Instead, there is a convergence line in this area in the direction of Genoa bay, where a small-scale cyclonic vortex is found. This vortex also disappears during the next few hours.

Fig. 7a presents the mesoscale temperature field at 12 UTC. It shows cold air behind the low centers and convergence zone in the southern Adriatic and central Italy. A very strong temperature gradient along the southern Adriatic coast is associated with the descending isentropes from the coastal mountains to the warm sea. This produces a horizontal density gradient, which hydrostatically gives rise to a pressure gradient below. This pressure gradient is directly responsible for the flow acceleration and bora intensification (*Smith*, 1987; *Tutiš* and *Ivančan-Picek*, 1991).

Fig. 7b presents the vorticity field at 850 hPa indicating a strong cyclonic vorticity over the southern Adriatic low.

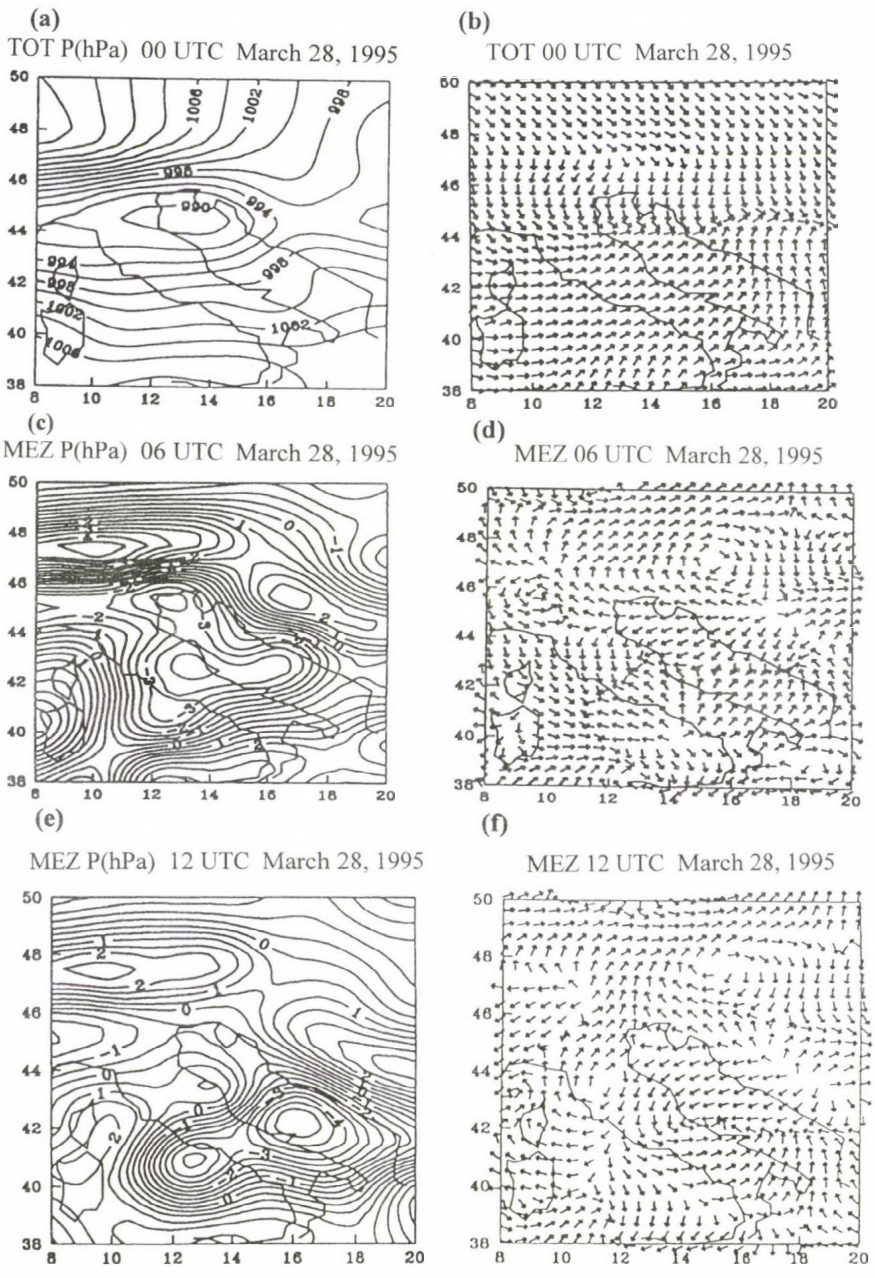

Fig. 6. Objective analysis of total pressure (*a*) and wind field (*b*) on March 28, 00 UTC; mesoscale presure (*c*) and wind field (*d*) on March 28, 06 UTC; mesoscale pressure (*e*) and wind field (*f*) on March 28, 12 UTC.

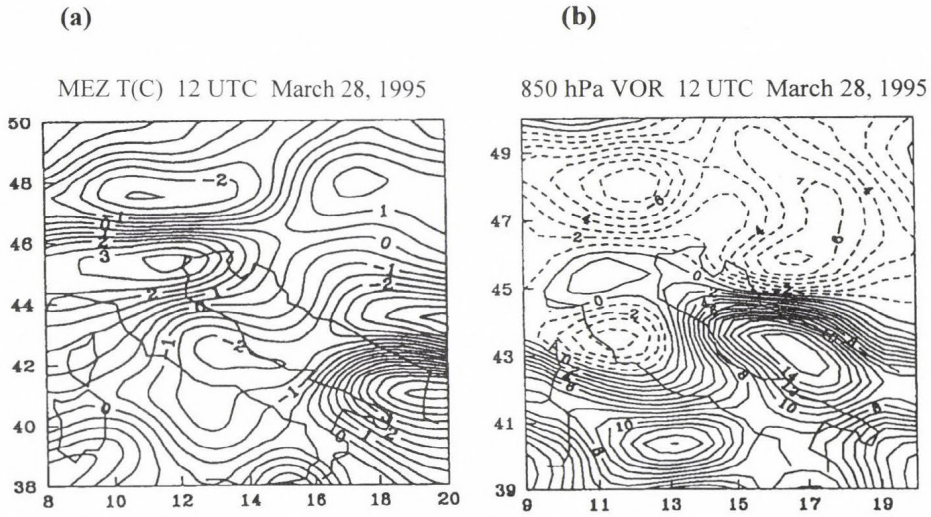

Fig. 7. Objective analysis of mesoscale temperature field (*a*) and relative vorticity (10^{-5}/s; solid lines are for positive values, dashed lines are for negative values) (*b*) on the 850 hPa level on March 28, 1995, 12 UTC.

Thus, this analysis does not indicate any vortex in the mesoscale wind field over the Adriatic area, leading to presumption that the marked fast moving front and strong bora wind along the *entire* Adriatic coast are not favorable for the vortex generation over the sea area. This is implied by the results of the second case study on the next day.

In this case we find the most essential feature of our analysis – the vortex generation in the middle Adriatic (*Fig. 8 a–d*). It is seen that this vortex is generated in the macroscale wind field to the north of macroscale pressure center. What is causing the cyclonic vortex generation in a macroscale wind field and why does it not appear on the mesoscale? The simplest answer would be that the mesoscale field is too much ageostrophic for such a process. Of course it is not surprising, that the vortex generation requires a more balanced condition similar to those found in larger scale field above the ground level as demonstrated by *Gomis et al.* (1990), where smaller scale *noise* is filtered out. Second, we noticed already more uniform currents over the middle Europe, to the north of Adriatic, as well as over the Mediterranean, with converging currents close to the Adriatic area. Third, the Adriatic basin and geometry of its boundary are convenient for the formation of *mesoscale atmospheric systems*. Finally, the specific condition for the observed Adriatic vortex is the appearance of strong bora in the northern, and jugo in the southern Adriatic. Using the same objective analysis, *Jurčec et al.* (1996) have shown that the

wind distribution in the southern Adriatic essentially changes if the strong jugo at Palagruža island (see Fig. 5) is included in the analysis. Therefore, the strong horizontal wind shear is convenient for the vortex generation, although it is not sufficient for such a process. Numerical simulation with dry and moist dynamics of this particular case study (*Brzović* and *Jurčec*, 1997) have revealed that jugo wind contains a humid air so that *diabatic effects could also contribute to the vortex formation*, although to a lesser degree that the orography.

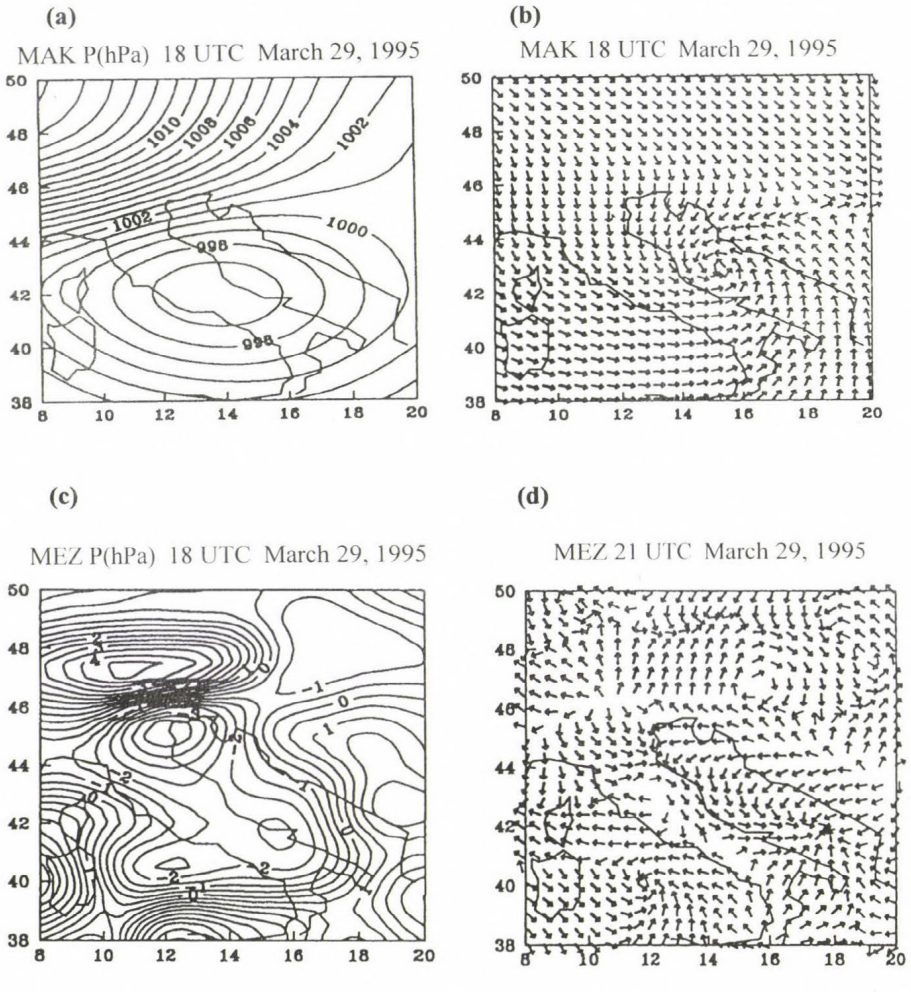

Fig. 8. Objective analysis of macroscale pressure field (*a*), macroscale wind field (*b*), mesoscale pressure field (*c*) on March 29, 1995, 18 UTC, and mesoscale wind field on March 29, 1995, 21 UTC (*d*).

On the other side, bora flow is mainly associated with the strong gravity wave breaking (*Glasnović* and *Jurčec*, 1990), and presumably the formation of Kelvin-Helmholtz instabilities influences the smaller scale motions over the sea (*Smith,* 1991). However, these instabilities as well as convective instability in a humid air occupied by jugo are filtered out as noise in our macroscale procedure. The bora intensified in the northern Adriatic at the low pressure as it can be seen in *Fig. 8c*.

The middle Adriatic vortex did not last long, since after 3 hours the bora flow occupied the entire eastern coast, and we found only a convergence zone in the southern Adriatic existing in both macro- and mesoscale wind fields (*Fig. 8d*).

6. Conclusions

- The objective sea level mesoscale analyses have shown, as expected, highly ageostrophic regime over the Adriatic Sea.
- Mesoscale fields are characterized by the dipole structure in wind, temperature, and pressure fields in the northern Adriatic. The same characteristics appear later on across the Dinaric Alps along the eastern Adriatic coast, influencing the low pressure centers, moving downstream, and intensifying together with the convergence zones in the wind field associated with these lows. Thus, these are clearly the *orogenic features mainly caused by orography*.
- This analysis intends to capture the Adriatic mesoscale vortices with wavelengths in the range of about 500 km and damping of the shorter wavelengths at 250 km, whereas the macroscale includes the features of wavelengths larger than approximately 900 km.
- Thus, no remarkable vortices were generated on selected mesoscale over the Adriatic Sea, except for temporary occurrence of very small size and short living vortices.
- Vortex centers in the mesoscale wind field over the entire area considered are displaced from the position of the corresponding pressure centers, indicating the existence of organized ageostrophic components of the flow. However, this ageostrophic flow in selected mesoscale is not solely to blame for the nonexistence of larger vortices over the Adriatic area. We find mesoscale vortices over the continent, such as cyclonic vortex over northern Italy, and especially a very persistent anticyclonic vortex in the Pannonian Plain. Therefore, warmer sea surface temperature must be responsible for the intensification of fronts and convergence lines with

frequent occurrence of very small vortices following the cold outbreaks from the north.

- The circumstance, under which the middle Adriatic vortex was generated, was the strong jugo wind in the southern and severe bora flow in the northern Adriatic. In the mesoscale, such vortex does not appear presumably for some of the following reasons: (1) due to ageostrophic condition, (2) warm sea surface increasing the frontal activities, (3) various instabilities on this scale, and (4) orographic effects leading to strong bora flow or jugo wind along the entire Adriatic coast.
- Jugo wind appears in the moist air, where convective activities are usually strong, and in this particular case the intensity of storm is accompanied by intensive rain and snow, even in the islands along Dalmatia.
- On the other side, strong and dry bora wind is well known in regions with strong turbulence ("dead regions"), and intensive gusts at the sea level are apparently caused by the Kelvin-Helmholtz instability (*Smith,* 1991). Since these instabilities, which are contained in the small wavelengths presenting the noise, are filtered out in the macroscale, this is considered as the main reason why the Adriatic vortex in this case study was generated in the macroscale and not mesoscale wind field defined in our procedure.
- This is, of course, only one case study, and more cases should be presented, particularly with numerical model simulations in order to corroborate these results. Scientific community expects significant observing efforts from the new project, MEDEX — Mediterranean Experiment on Cyclones that produce High Impact Weather in the Mediterranean (*Jansa et al.*, 2000). Thus, additional data should be focused to determine low-level distribution of wind, temperature, humidity and surface fluxes.

Acknowledgements—This study was partly supported by Ministry of Science and Technology of Croatia (project : 0004001). We appreciate very much *Prof. Werner Wehry* from Deutsche Meteorologische Gesellschaft and *Dr. Dražen Poje* for synoptic charts presented.

References

Binder, P. and *Schär, C.*, 1996: The Mesoscale Alpine Programme. Design Proposal, MeteoSwiss, 75 pp. (Available from the MAP Programme Office, MeteoSwiss, CH-8044, Zurich, Switzerland).

Brzović, N., 1999: Factors affecting the Adriatic cyclone and associated windstorms. *Contr. Atmos. Phys. 72*, No.1, 51-65.

Brzović, N. and *Jurčec, V.*, 1997: Numerical simulation of the Adriatic cyclone development. *Geofizika 14*, 29-46.

Buzzi, A. and *Tibaldi, S.*, 1978: Cyclogenesis in the lee of the Alps: a case study. *Quart. J. Roy. Meteorol. Soc. 103*, 135-150.

Buzzi, A. and *Alberoni, P.P.*, 1992: Analysis and numerical modelling of a frontal passage associated with thunderstorm development over the Po Valley and the Adriatic Sea. *Meteor. Atmos. Phys. 48*, 205-224.

Buzzi, A., Gomis, D., Pedder, M.A., and *Alonso, S.*, 1991: A method to reduce the adverse impact that inhomogeneous station distributions have on spatial interpolation. *Mon. Wea. Rev. 119*, 2465-2491.

Campins, J., Jansa, A., Benech, B., Koffi, E. and *Bessemoulin, P.*, 1995: PYREX observation and model diagnosis of the tramontane wind. *Meteorol. Atmos. Phys. 56*, 209-228.

Glasnović, D. and *Jurčec, V.*, 1990: determination of upstream bora layer depth. *Meteor. Atmos. Phys. 43*, 137-144.

Gomis, D. and *Alonso, S.*, 1988: Structure function responses in a limited area. *Mon. Wea. Rev. 116*, 2254-2264.

Gomis, D. and *Alonso, S.*, 1990: Diagnosis of a cyclogenetic event in the western Mediterranean using an objective technique for scale separation. *Mon. Wea. Rev. 118*, 723-736.

Gomis, D., Buzzi, A. and *Alonso, S.*, 1990: Diagnosis of mesoscale structures in cases of lee cyclogenesis during ALPEX. *Meteor. Atmos. Phys. 43*, 49-57.

Huschke, R.E. (ed.), 1959: Glossary of Meteorology. *American Meteorological Society*, 638 pp.

Ivančan-Picek, B., 1997: Adriatic cyclogenesis - mesoscale structures. *Proc. of the Int. Symposium on Cyclones and Hazardous Weather in the Mediterranean*, 14-17 April 1997, Palma de Mallorca, 267-272.

Ivančan-Picek, B. and *Tutiš, V.*, 1995: Mesoscale bora flow and mountain pressure drag. *Meteorologische Zeitschrift 4*, No. 3, 1-10.

Ivančan-Picek, B. and *Tutiš, V.*, 1996: A case study of severe Adriatic bora on 28 December 1992. *Tellus 48A*, 357-367.

Jansa, A., Alpert, P., Arbogast, P., and *Buzzi, A.*, 2000: Cyclones that produce high impact weather in the Mediterranean - MEDEX. *Preliminary research proposal to the WWRP*, http://www.inm.es/MEDEX/.

Jurčec, V. and *Visković, S.*, 1994: Mesoscale characteristics of southern Adriatic bora storms. *Geofizika 11*, 33-46.

Jurčec, V. and *Brzović, N.*, 1995: The Adriatic bora: Special case studies. *Geofizika 12*, 15-32.

Jurčec, V., Ivančan-Picek, B., Tutiš, V., and *Vukičević, V.*, 1996: Severe Adriatic jugo wind. *Meteorologische Zeitschrift*, N. F. 5, 67-75.

Maddox, R.A., 1980: An objective technique for separation macroscale and mesoscale features in meteorological data. *Mon. Wea. Rev. 108*, 1108-1121.

Poje, D., 1992: Wind persistence in Croatia. *Int. J. Climat. 12*, 569-586.

Smith, R.B., 1987: Aerial observations of the Yugoslavian bora. *J. Atmos. Sci.* 44, 269-297.

Smith, R.B., 1991: Kelvin-Helmholtz Instability in severe downslope wind flow. *J. Atmos. Sci. 48*, 1319-1328.

Tafferner, A., 1990: Lee cyclogenesis resulting from the combined outbreak of cold air and potential vorticity against the Alps. *Meteor. Atmos. Phys. 43*, 31-47.

Tafferner, A., 1994: Life cycle of the mountain generated Adriatic cyclone. *Proc. of Int. Symposium on the Life Cycles of Extratropical Cyclones. 27 June-1July 1994, Bergen, Norway*, 101-106.

Tafferner, A., 1995: The passage of the cold front of 27 March 1995 over the Alps: upper and lower-level flow features. *MAP-newsletter*, No. 3, October 1995, 75.

Tutiš, V. and *Ivančan-Picek, B.*, 1991: Pressure drag on the Dinaric Alps during the ALPEX SOP. *Meteor. Atmos. Phys. 47*, 73-81.

GUIDE FOR AUTHORS OF *IDŐJÁRÁS*

The purpose of the journal is to publish papers in any field of meteorology and atmosphere related scientific areas. These may be

- research papers on new results of scientific investigations,
- critical review articles summarizing the current state of art of a certain topic,
- short contributions dealing with a particular question.

Some issues contain "News" and "Book review", therefore, such contributions are also welcome. The papers must be in American English and should be checked by a native speaker if necessary.

Authors are requested to send their manuscripts to

Editor-in Chief of IDŐJÁRÁS

P.O. Box 39, H-1675 Budapest, Hungary

in three identical printed copies including all illustrations. Papers will then be reviewed normally by two independent referees, who remain unidentified for the author(s). The Editor-in-Chief will inform the author(s) whether or not the paper is acceptable for publication, and what modifications, if any, are necessary.

Please, follow the order given below when typing manuscripts.

Title part: should consist of the title, the name(s) of the author(s), their affiliation(s) including full postal and E-mail address(es). In case of more than one author, the corresponding author must be identified.

Abstract: should contain the purpose, the applied data and methods as well as the basic conclusion(s) of the paper.

Key-words: must be included (from 5 to 10) to help to classify the topic.

Text: has to be typed in double spacing with wide margins on one side of an A4 size white paper. Use of S.I. units are expected, and the use of negative exponent is preferred to fractional sign. Mathematical formulae are expected to be as simple as possible and numbered in parentheses at the right margin.

All publications cited in the text should be presented in a *list of references*, arranged in alphabetical order. For an article: name(s) of author(s) in Italics, year, title of article, name of journal, volume, number (the latter two in Italics) and pages. E.g., *Nathan, K.K.,* 1986: A note on the relationship between photo-synthetically active radiation and cloud amount. *Időjárás 90,* 10-13. For a book: name(s) of author(s), year, title of the book (all in Italics except the year), publisher and place of publication. E.g., *Junge, C. E.,* 1963: *Air Chemistry and Radioactivity*. Academic Press, New York and London. Reference in the text should contain the name(s) of the author(s) in Italics and year of publication. E.g., in the case of one author: *Miller* (1989); in the case of two authors: *Gamov* and *Cleveland* (1973); and if there are more than two authors: *Smith et al.* (1990). If the name of the author cannot be fitted into the text: *(Miller,* 1989); etc. When referring papers published in the same year by the same author, letters a, b, c, etc. should follow the year of publication.

Tables should be marked by Arabic numbers and printed in separate sheets with their numbers and legends given below them. Avoid too lengthy or complicated tables, or tables duplicating results given in other form in the manuscript (e.g., graphs)

Figures should also be marked with Arabic numbers and printed in black and white in camera-ready form in separate sheets with their numbers and captions given below them. Good quality laser printings are preferred.

The text should be submitted both in manuscript and in electronic form, the latter on diskette or in E-mail. Use standard 3.5" MS-DOS formatted diskette or CD for this purpose. MS Word format is preferred.

Reprints: authors receive 30 reprints free of charge. Additional reprints may be ordered at the authors' expense when sending back the proofs to the Editorial Office.

More information for authors is available: antal.e@met.hu

Information on the last issues: http://omsz.met.hu/irodalom/firat_ido/ido_hu.html

Published by the Hungarian Meteorological Service

Budapest, Hungary

INDEX: 26 361

HU ISSN 0324-6329

IDŐJÁRÁS

QUARTERLY JOURNAL
OF THE HUNGARIAN METEOROLOGICAL SERVICE

CONTENTS

****

http://omsz.met.hu/english/ref/jurido/jurido_en.html

VOL. 107 * NO. 2 * APRIL–JUNE 2003

IDŐJÁRÁS

Quarterly Journal of the Hungarian Meteorological Service

Editorial Office: P.O. Box 39, H-1675 Budapest, Hungary or
Gilice tér 39, H-1181 Budapest, Hungary
E-mail: prager.t@met.hu or *antal.e@met.hu*
Fax: (36-1) 346-4809

Subscription by

mail: IDŐJÁRÁS, P.O. Box 39, H-1675 Budapest, Hungary
E-mail: prager.t@met.hu or *antal.e@met.hu*; *Fax: (36-1) 346-4809*

Dr. Pál Ambrózy is 70

Dr. Pál Ambrózy has recently celebrated his 70th birthday. On this occasion we wish to congratulate him and also express our greatest honour for the enormous work he has completed during his carrier for the Hungarian meteorology and the society of Hungarian meteorologists.

He was born in 1933 in Rimaszombat. He completed his studies at the secondary school in Nyiregyháza, then he obtained a meteorologist diploma at the Eötvös Loránd University of Sciences (Budapest) in 1955. He obtained his university doctor degree in 1963. He devoted his entire life to the service of the Meteorological Service of Hungary and also the Hungarian Meteorological Society, for which he has been the President from 1991.

Just after finishing his studies he begins to work at the Meteorological Service. In the first years he works in a research team dealing with dynamical meteorology, where

he soon becomes the head. There he plays a significant role in the domestic implementation of numerical and graphic methods of weather forecasting, which were in the frontline of development of meteorological science at that time. He also participates in the establishment of objective methods of storm forecasting at Lake Balaton. In 1968 he spent one year in the United States and in the Soviet Union as a UN sponsored scholar. He serves as the head of the Central Office of the Service, then in 1974 he was appointed as the director of the Central Meteorological Institute. At that time this was the basic unit of the Service, whose tasks included the countrywide meteorological observations, data collection, and also climatological research. Under his direction many high quality scientific results were achieved in this institute, the recounting of that is beyond the limit of this short greeting note. The main thing is that he personally participates in scientific work and has many outstanding scientific results, like the mapping of climatic resources in Hungary, or the redaction of Climate Atlas of Hungary. He is one of the co-authors of the book "Register of small geographical regions of Hungary", which then won an Academic Award. The number of his scientific publications is over one hundred, and his name is fixed in the local macrosynoptic classification Ambrózy-Bartholy-Gulyás. He retired from the Service in 1991, but we cannot call this a retirement, because he is a most active worker of the Service even now.

He is the member of the Hungarian Meteorological Society from 1952. Under his presidency, as was mentioned before, the Society, which is an NGO, succeeded to survive the difficult period of the 1990's and now continues to work and develop properly, serving this way the interests of everybody, who is interested in the science of meteorology in Hungary. The Society now is a member of the European Meteorological Society, where he was elected as a council member.

For us Hungarian meteorologists a very important medium is the periodical "Légkör" ("Atmosphere") for which he is the Editor-in-Chief from 1978. Under his talented (I may say genial) supervision this periodical became and remains a central forum of distribution of information about meteorology for meteorologists and non-meteorologists in Hungary. It is a real pleasure to look at and read through every single issue of this journal.

Finally, we wish to mention, that he was awarded by the Steiner Lajos Memorial Prize in 1975, then with the Hungarian Scientific Societies Award in 1999, finally with the highest possible award for Hungarian meteorologists, the Schenzl Guido Award in 2000.

In the name of myself and the whole editorial board of the Időjárás I would like to wish "uncle Pali" good health and many further years of fruitful work for the interest of Hungarian meteorology.

Tamás Práger

IDŐJÁRÁS

Quarterly Journal of the Hungarian Meteorological Service
Vol. 107, No. 2, April–June 2003, pp. 85–114

Application of a cloud model in simulation of atmospheric sulfate transport and redistribution Part I. Model description

Vlado Spiridonov[1] and **Mladjen Ćurić**[2]

[1]*Institute of Physics, Faculty of Natural Sciences and Mathematics,*
St. Cyril and Methodius University,
Branislav Nusic 11-1/17, 1000 Skopje, Macedonia
E-mail: vspiridonov@meteo.gov.mk

[2]*Department of Meteorology, Faculty of Physics, University of Belgrade,*
11000 Belgrade, P.O. Box 550, Yugoslavia
E-mail: curic@ff.bg.ac.yu

(Manuscript received December 7, 2001; in final form September 25, 2002)

Abstract–The authors have incorporated the sulfur chemistry in a rather sophisticated three-dimensional compressible meso-scale cloud model with a standard bulk parameterization of microphysics. The governing equations of the model include momentum conservation equations, thermodynamic and pressure equations, four continuity equations for the various water substances, and the subgrid scale (SGS) turbulent kinetic energy equation (TKE). The chemical part is formulated in terms of the continuity equations in the gaseous, aqueous, and ice phases within the cloud. The absorption of a gas phase chemical species in the cloud water and rainwater is determined either by the equilibrium according to Henry's law or by mass transfer limitation calculations in order to include the possible non-equilibrium states. After dissolution into cloud water and rain, follows the transfer of a soluble compound through the microphysical processes that affect the parent hydrometeor. All dissolved compounds are retained during the conversion of liquid drops to frozen hydrometeors. Melting of ice, snow, or hail again totally transfers the dissolved matter to cloud water and rain. During sublimation of hail and snow, dissolved scalar is retained in the hail or snow, unless all hydrometeor mass is converted to gas phase. The calculation of the cloud water pH and rainwater pH is based on the equilibrium hydrogen ion concentration for $[H^+]$, which is given by the simple charge balance equation.

Part I of the paper gives the detailed description of the model including the chemistry. Results of case studies with the model are described in Part II of the present article, which will be published in a later issue of this journal.

Key-words: scavenging, oxidation, sulfate transport, redistribution, wet deposition.

1. Introduction

The interactions between clouds, atmospheric aerosols, and gases have important effects on the chemical composition of atmospheric hydrometeors and on the long-range transport of air pollutants. Deep convection significantly contributes to the transport and vertical redistribution of atmospheric pollutants (e.g., *Isaac et al.*, 1982, 1983). Many studies have been devoted to these issues in the past. Most of the early models are one-dimensional (e.g., *Hales,* 1982; *Walcek* and *Taylor,* 1986; *Taylor,* 1989a,b) constraining the physical interpretation of the model results. *Sarma* (1986) examined the in-cloud conversion of SO_2 for a single case using a two-dimensional Eulerian model. Studies by *Tremblay* and *Leighton* (1986) and *Niewiadomski* (1989) apply three-dimensional cloud chemistry models and their applications to redistribution of chemical species during convection, but they primarily focus on warm convective clouds. On the other hand, *Wang* and *Chang,* (1993a,b) have developed a three-dimensional cloud chemistry model focused on deep convection and chemical processes related to in-cloud transformations and redistribution of pollutants. *Flossmann* and *Wobrock* (1996), *Kreidenweis et al.* (1997) studied the transport of SO_2 in convective clouds and chemical reactions. *Skamorock et al.* (2000) have examined tracer transport in three-dimensional simulations using the Klemp-Wilhemson model. *Crutzen* and *Lawrence* (2000) used a three-dimensional global model to examine the impact of convective and large scale precipitation scavenging on the transport of trace gases. More recently *Barth et al.* (2001) examined the redistribution of gases with various solubility during deep convection, while *Yin et al.* (2001) examined the trace gas redistribution using a two-dimensional dynamic cloud model with detailed microphysics and spectral treatment of gas scavenging. *Table 1* gives a short review of studies, focused on deep convection and transport of various species, using cloud chemistry models with different dynamical, microphysical, and chemical frameworks.

Part I is focused on cloud model formulation and description of model dynamics, thermodynamics, and microphysics (Section 2). The microphysical and chemical processes of the sulfuric compounds are illustrated in Section 3. Chemical reactions of these compounds, their mass transfer between gas and liquid phases, and also their mass transfer between cloud hydrometeors, and finally calculation of pH are described.

2. Cloud model formulation and description

The present version of the model is a three-dimensional, nonhydrostatic, time-dependant, compressible system which is based on the *Klemp* and *Wilhelmson*

(1978) dynamics, *Lin et. al.* (1983) microphysics, *Orville* and *Kopp* (1977) thermodynamics, and *Taylor* (1989b) sulfate chemistry. The governing equations of the model include momentum conservation equations, thermodynamic and the pressure equations, four continuity equations for the water substances, a subgrid scale (SGS) turbulent kinetic energy equation (TKE), and continuity equations for chemical species associated with various cloud water species.

Table 1. A review of studies with brief description of their cloud-chemistry model formulations

Authors of separate studies→	***Taylor*** **(1989a,b)**	***Tremblay*** **and** ***Leighton*** **(1986)**	***Wang*** **and** ***Chang*** **(1993b)**	***Crutzen*** **and** ***Lawrence*** **(2000)**	***Barth et al.,*** **(2001)**	***Yin et al.*** **(2001)**	***Spiridonov*** **and** ***Curič*** **(present model)**
The basic characteristic of the model	1-D dimensional cumulus cloud model	3-D (warm cumulus cloud model)	3-D non-hydrostatic cloud model	3-D global model (MATCH)	3-D non-hydrostatic cloud model	2-D non-hydrostatic cloud model	3-D non-hydrostatic cloud model
Model dynamics and thermodynamics	1.5 D Eulerian model cloud TKE Local turbulent Kinetic energy	Compressible Cloud model	Compressible cloud model Ice-liquid potential temperature 1-order closure scheme	Global model for chemical transport	Compressible cloud model	Slab-symmetric	Compressible cloud model TKE 1- order closure scheme Prognostic equation for entropy
Model microphysics	Bulk-water microphysics	A simply bulk-parameterization warm microphysics	Semi-spectral microphysics scheme	Semi-explicit cloud microphysics scheme	Mixed phase. Particle microphysics	Detail microphysics. Method of multi moments	Bulk-water parameterization with significant improvements
Model chemistry	Sulfate chemistry parameterization	Liquid-gas phase chemistry	Gas phase and liquid-ice phase chemical reactions	Transport trace- gases Scavenging and dissolution in liquid phase	Transport and scavenging of tracers (highly soluble and passive tracers)	Spectral treatment of scavenging and redistribution of gases (tracers)	Liquid-ice phase chemical reactions (sulfate chemistry) inside clouds

2. 1 The model dynamics

2.1.1 The momentum equations

The momentum equations are derived from the Navier-Stokes equations with the aid of the moist equation of state:

$$p = \rho R_d T(1 + 0.608 q_v), \tag{1}$$

where p is the pressure; ρ is the density of moist air; R_d is the gas constant for dry air; T is the temperature; and q_v is the mixing ratio of water vapor. Re-written in terms of non-dimensional pressure or the Exner function Π :

$$\Pi = \left(\frac{p}{p_0} \right)^{R_d / c_p} = \left(\frac{R_d}{p_0} \rho \theta_v \right)^{R_d / c_v} \tag{2}$$

Here p_0 is the basic state pressure at the ground and θ_v is the virtual potential temperature. Using the Boussinesq-approximation for homogeneous and rotating fluid, taking into account advection, turbulent transport, buoyancy (either due to warming or loading hydrometeors), and pressure gradient force, the tensor form of the momentum equations could be written as:

$$\frac{d\vartheta_i}{dt} + c_p \theta_{\vartheta 0} \frac{\partial \pi'}{\partial x_i} = \left(\frac{\theta'}{\theta_0} + 0.608 q_{\vartheta}' - q_c - q_r \right) g \delta_{i3} - \varepsilon_{i3l} f \vartheta_l + F_{ui}. \tag{3}$$

In this equation ϑ_i $(i = 1,2,3)$ is the wind speed component along the ith coordinate axis; c_p is the specific heat at constant pressure of dry air; $\theta_{\vartheta 0} = c_p \theta_0 (1 + 0.608 q_{\vartheta 0})$; π' is the deviation of non-dimensional pressure or Exner function from the initial unperturbed state Π_0; θ' and q_{ϑ}' are the perturbations of the initial potential temperature and mixing ratio of water vapor; θ_0 is equilibrium value of the potential temperature; q_c and q_r are the mixing ratios of cloud water and rainwater, respectively; δ_{i3} is the delta function; g is the gravitational acceleration; ε_{i3l} is the appropriate tensor of third rang; f is the Coriolis parameter; and F_{ui} represents contribution of subgrid-scale processes to ϑ_i.

2.1.2 The pressure equation

The pressure equation is derived by taking substantial derivative of Eq. (2) using the compressible continuity equation,

$$\frac{\partial \rho}{\partial t} = -\frac{\partial}{\partial x_j}\overline{\rho u_j} - \frac{\partial}{\partial x_j}\overline{\rho'' u_j''}, \tag{4}$$

to eliminate $d\rho/dt$, and thermodynamic equation to eliminate $d\theta/dt$. The final equation has the following form:

$$\frac{\partial \pi'}{\partial t} + \frac{\bar{c}^2}{c_p \bar{\rho}\bar{\theta}_v^{\,2}}\frac{\partial}{\partial x_j}(\bar{\rho}\bar{\theta}_v u_j) = -u_j\frac{\partial \pi}{\partial x_j} + \frac{R_d \pi}{c_v}\frac{\partial u_j}{\partial x_j} + \frac{c^2}{c_p \theta_v^{\,2}}\frac{d\theta_v}{dt} + D_\pi . \tag{5}$$

Using the parallel tensor notation in the equations, $u_j\,(j=1,2,3)$ are the velocities u, v, w; $(\partial/\partial x_j)$ are partial derivatives along the axes (x,y,z); c is the speed of sound given by $c^2 = c_p R_d \Pi \theta_v / c_v$, and D_π is the subgrid scale contribution term for π'.

2.1.3 The thermodynamic equation

In the thermodynamic equation, the potential temperature derived by *Orville* and *Kopp* (1977) is used as a conservative variable for adiabatic processes. The flux-conserving form of the equation is

$$\begin{aligned}\frac{\partial \varphi'}{\partial t} &= -\vec{\vartheta}\cdot\nabla\varphi' + K_h\nabla\varphi' + \frac{L_f}{c_P T_{00}}(P_g' + P_s') + \frac{c_W}{T_{00}}(T - T_0)\,(P_{GMLT} + P_{SMLT}) \\ &- \frac{c_W}{T_{00}}\left[q_{CW}\vec{\vartheta}\cdot\nabla T + q_R(\vec{\vartheta} - \vec{k}U_R)\cdot\nabla T\right] - \frac{c_I}{c_P T_{00}}\delta\left[q_{CI}\vec{\vartheta}\cdot\nabla T + q_G(\vec{\vartheta} - \vec{k}U_G)\cdot\nabla T\right. \\ &\left. + q_S(\vec{\vartheta} - \vec{k}U_S)\cdot\nabla T\right],\end{aligned} \tag{6}$$

where φ' is the specific entropy of the moist air; K_h is the heat eddy coefficient; L_f is the latent heat of freezing; P_g' is the total production rate of hail; P_s' is the total production rate of snow; C_W is the specific heat of water; T_0 is the melting temperature; P_{GMLT} is the production rate of rain from melting of hail; P_{SMLT} is the production rate of rain from melting snow; $q_{CW}, q_{CI}, q_R, q_G, q_S$ are the mixing ratios of cloud water, cloud ice, rain, hail,

and snow; C_I is the specific heat of ice; and U_r, U_g, U_s represent terminal velocities for rain, hail, and snow, respectively. The first two terms on the right-hand side of Eq. (6) represent the advection and turbulent mixing effects. The third term shows the heating effect of liquid water freezing, or the cooling effect of melting. The fourth term indicates the energy needed to warm the melted hail and snow from 0°C to the ambient temperature. The last two terms represent the energy changes due to the various hydrometeors coming into thermal equilibrium with the environment as they move through a layer with changing temperature gradient.

2.1.4 The subgrid scale parameterization

The parameterization of subgrid scale fluxes is based on the solution of the turbulent kinetic energy (TKE) equation given in the form

$$\frac{\partial E}{\partial t}+\overline{\vartheta}_K\frac{\partial E}{\partial x_K}=\delta_{I3}g\,\overline{\vartheta_I'\left(\frac{\theta''}{\theta_0}+0.608q_v''-q_C'\right)}-\overline{\vartheta_I'\vartheta_K'}\frac{\partial\overline{\vartheta}_I}{\partial x_K}$$

$$-\frac{\partial}{\partial x_K}\overline{[\vartheta_K(E+c_p\theta_{v0}\Pi'')]}-\nu\,\overline{\frac{\partial\vartheta_I'}{\partial x_K}\frac{\partial\vartheta_I'}{\partial x_K}}, \tag{7}$$

where

$$E=\frac{1}{2}\overline{(\vartheta_i')^2} \tag{8}$$

is the subgrid-scale kinetic energy per unit mass. The terms on the right-hand side of Eq. (7) represent the effects of buoyancy, shear, diffusion, and dissipation. Eq. (7) is derived from momentum equation, Eq. (3), for incompressible fluid ($\rho = \text{const}$), performing Reynolds averaging on each of the prognostic variables and applying the first-order closure to the nearly conservative variables. Heat eddy coefficient is assumed to be proportional to the momentum eddy coefficient. Details could be found in study by *Klemp* and *Wilhemson* (1978).

2.2 Cloud microphysics

For the parameterization of the microphysical processes we use the integrated (bulk) water parameterization by *Lin et al.* (1983), with significant improvement of hail growth parameterization. Instead of using the hail size spectrum from zero to infinity (idealized spectrum), *Curic* and *Janc* (1995, 1997) proposed considering the hail size spectrum which includes only hail sized parti-

cles (larger than 0.5 cm in diameter; hereafter called realistic hail spectrum). Six types of water substances are included: water vapor, cloud water, cloud ice, rain, snow, graupel, and hail. Cloud water and cloud ice are assumed to be monodisperse, with zero terminal velocities. Cloud water droplets have identical mass $M_w = 4.19 \times 10^{-9}$ g, while cloud ice crystals have mass $M_i = 4.19 \times 10^{-10}$ g. Rain, hail, and snow have Marshall-Palmer type size distributions with fixed intercept parameters: $n_{0R} = 8 \times 10^{-2}$ cm^{-4}, $n_{0H} = 4 \times 10^{-4}$ cm^{-4}, and $n_{0S} = 3 \times 10^{-2}$ cm^{-4}. The assumed values for density of rain, hail, and snow are 1 g cm^{-3}, 0.9 g cm^{-3}, and 0.1 g cm^{-3}. The density of air is separately calculated. These six forms of the water substances interact mutually.

Four continuity equations for the various water substances

$$\frac{\partial q}{\partial t} = -\vec{\vartheta} \cdot \nabla q + \nabla \cdot K_h \nabla q - P_R - P_S - P_G , \tag{9}$$

$$\frac{\partial q_R}{\partial t} = -\vec{\vartheta} \cdot \nabla q_R + \nabla \cdot K_m \nabla q_R + P_R + \frac{1}{\rho} \frac{\partial}{\partial z} (U_R q_R \rho) , \tag{10}$$

$$\frac{\partial q_G}{\partial t} = -\vec{\vartheta} \cdot \nabla q_G + \nabla \cdot K_m \nabla q_G + P_G + \frac{1}{\rho} \frac{\partial}{\partial z} (U_G q_G \rho) , \tag{11}$$

$$\frac{\partial q_S}{\partial t} = -\vec{\vartheta} \cdot \nabla q_S + \nabla \cdot K_m \nabla q_S + P_S + \frac{1}{\rho} \frac{\partial}{\partial z} (U_S q_S \rho) , \tag{12}$$

where $q = r + q_{CW} + q_{CI}$; q_{CW}, q_{CI}, q_R, q_G, q_S, and r are the mixing ratios for cloud water, cloud ice, rain, hail/graupel, snow, and water vapor, respectively; K_h is the eddy heat diffusion coefficient; K_m is the eddy momentum diffusion coefficient; U_R, U_G, U_S are terminal velocities for rain, hail/graupel, and snow, and P_R, P_G, and P_S are production terms for rain, hail, and snow.

The source reference for the scheme to allow coexistence of cloud water and cloud ice in the temperature region of –40 to 0°C is derived from *Hsie et al.* (1980). Condensation and deposition of water vapor produce cloud water and cloud ice, respectively. Conversely, evaporation and sublimation of cloud water and cloud ice maintain saturation. Natural cloud ice is normally initiated by using a Fletcher-type equation for the ice nuclei number concentration. In this version of the model, cloud ice may also be produced by the Hallett-

Mossop ice multiplication. Bergeron-Findeisen process transforms some of the cloud water into cloud ice and, to a certain extent, both of them into snow.

Rain is produced by the auto-conversion of cloud water, melting of snow and hail, and shedding during the wet growth of hail.

Hail is produced by the auto-conversion of snow, interaction of cloud ice and snow with rain, and by immersion freezing of rain.

Snow may be produced by the auto-conversion, Bergeron-Findeisen growth of cloud ice, and interaction of cloud ice and rain. All types of precipitation elements grow by different forms of accretion. Evaporation (sublimation) of all types of hydrometeors is also simulated.

3. Microphysics and chemical processes of the sulfuric compounds

The chemical model is based on the sulfate chemistry taken from *Taylor* (1989b) and represents an extension of already published work concerning warm clouds from *Tremblay* and *Leighton* (1986).

To study the interactions between clouds, aerosols, and gases participating in sulfate production, the model is formulated in terms of continuity equations. If the concentration of the *i*th pollutant is expressed by the mixing ratio in the air, cloud water and cloud ice by $q_{i,a}$, rain by $q_{i,r}$, graupel or hail by (q_{i,g_h}), and snow by $q_{i,s}$, then the local change of each component separately is given by the following conserving forms which are consistent with the dynamics and thermodynamics formulations:

$$\frac{\partial q_{i,a}}{\partial t} + \vec{\vartheta} \cdot \nabla q_{i,a} = E_{i,a} + SM_{i,a} + Sq_{i,a} \qquad j = 1, 2, 3, \tag{13}$$

$$\frac{\partial q_{i,r}}{\partial t} + \vec{\vartheta} \cdot \nabla q_{i,r} - SF_{i,r} = E_{i,r} + SM_{i,r} + Sq_{i,r}, \tag{14}$$

$$\frac{\partial q_{i,g\_h}}{\partial t} + \vec{\vartheta} \cdot \nabla q_{i,g\_h} - SF_{i,g\_h} = E_{i,g\_h} + SM_{i,g\_h} + Sq_{i,g\_h}, \tag{15}$$

$$\frac{\partial q_{i,s}}{\partial t} + \vec{\vartheta} \cdot \nabla q_{i,s} - SF_{i,s} = E_{i,s} + SM_{i,s} + Sq_{i,s}, \tag{16}$$

where $\vec{\vartheta}$ is the wind velocity vector with components (u, v, w); $E_{i,a}$, $E_{i,c}$, $E_{i,r}$, E_{i,g_h}, and $E_{i,s}$ are the subgrid contribution terms; $SM_{i,a}$, $SM_{i,r}$, SM_{i,g_h}, and $SM_{i,s}$ are redistribution terms induced by microphysical conversion processes given by the relation

$$SM_{i,w} = q_{i,w}\, q_m(\mathrm{w} \rightarrow \mathrm{i})/q_w\,, \tag{17}$$

where $q_m(\mathrm{w} \rightarrow \mathrm{i})$ is the rate of microphysical transformation derived from the microphysical scheme. During transformation the water "w" is considered to lose mass and the category "i" to gain mass. $q_{i,w}$ is the mixing ratio of pollutant "i" associated with water "w" and q_w is the mixing ratio of water. $Sq_{i,a}$, $Sq_{i,r}$, Sq_{i,g_h}, and $Sq_{i,s}$ denote the chemical transformation terms, while the falling rates for hydrometeors $SF_{i,r}$, SF_{i,g_h}, and $SF_{i,s}$ are given by

$$SF_{i,r,g\_h,s} = \frac{1}{\bar{\rho}\rho}\frac{\partial}{\partial x_3}(\bar{\rho}\, U_{r,g\_h,s}\; q_{i,r,g\_h,s})\,, \tag{18}$$

where $\bar{\rho}$ is the initial unperturbed value of air density, $U_{r,g\_h,s}$ are terminal velocities of rain, graupel or hail, and snow, respectively.

3.1. The mass transfer between gas and liquid phases

The absorption of a gas phase chemical species in the cloud water and rainwater is determined either by the equilibrium according to Henry's law or by mass transfer limitation calculations in order to include the possible non-equilibrium states.

Gases (with an effective Henry's law constant $K_H^{*} < 10^3$ mol dm^{-3} atm^{-1}) in cloud water and rain are assumed to be in equilibrium with the local gas-phase concentrations. These liquid-phase concentrations of each chemical component "**i**" are calculated according to Henry's law, i.e.,

$$[\mathbf{i}] = K_H\, p_{\mathbf{i}}\,, \tag{19}$$

where **[i]** is given in units of mol **i**/L H_2O (M); K_H is the Henry's law coefficient (M atm^{-1}); and p_{i} is the partial pressure of the species "**i**" given in units atm. All equilibrium constants and oxidation reactions are temperature dependent according to van't-Hoff's relation

$$K_T = K_{T0} \exp\left(-\Delta H/R\,(1/T - 1/T_0)\right), \tag{20}$$

where ΔH is the increase of enthalpy induced by chemical reactions; K_{T0} is the equilibrium constant at a standard temperature T_0=298 K; and R is the universal gas constant. However, a chemical species may not attain equilibrium on the time scales of the cloud model because of slow mass transfer between phases. In that case a fully kinetic calculation of gas dissolution into the cloud droplets and raindrops is included in the model. The rate of mass transfer among gas species "**i**", spectra of drops with diameter α, and number concentration N_α (per mole air) could be expressed by the following relation by *Yin et al.* (2001):

$$\frac{dq_{d,i,a}}{dt} = \frac{12\eta D_{g,i} N_{Sh,i}}{RT\alpha^2}\left(V_\alpha N_\alpha P_i - \frac{q_{d,i,\alpha}}{K_H^*}\right), \tag{21}$$

where $q_{d,i,\alpha}$ is the rate of molar mixing ratio of gas species inside drops with diameter α to that in the air; K_H^* is the effective Henry's law constant of species "**i**"; R is the universal gas constant; T is the temperature; $D_{g,i}$ is the diffusivity of gases "**i**" in air which are taken from *Pruppacher* and *Klett* (1997); V_α is the volume of drops with diameter α; P_i is the partial pressure of gas species "**i**" in the environment; $N_{Sh,i}$ is the mass ventilation coefficient (Sherwood number); and η is a factor which is a function of the Knudsen-number K_n and sticking coefficient γ_i of gas species "**i**" on spherical drops.

3.2. Mass transfer between cloud hydrometeors

After dissolution into cloud water and rain, follows the transfer of a soluble compound through the microphysical processes that affect the parent hydrometeor.

The present cloud modeling study includes a freezing transport mechanism of chemical species based on *Rutledge et al.* (1986). Similar approach could be found in studies (e.g., *Wang* and *Chang*, 1993a; *Chen* and *Lamb*, 1994; *Kreidenweis et al.*, 1997).

It is assumed that all dissolved compounds are retained during the conversion of liquid drops to frozen hydrometeors. Melting of ice, snow, or hail again totally transfers the dissolved matter to cloud water and rain. During sublimation of hail and snow, dissolved scalar is retained in the hail or snow, unless all hydrometeor mass is converted to gas phase.

3.3. The sulfate chemistry parameterization terms

Microphysical processes and chemical conversions for SO_4^{2-} in air and different water substances, and the names associated with each of them in the model are demonstrated in *Fig. 1*. The equilibrium chemical reactions and reaction constants for these processes as well as for S (IV) oxidations (see 3.4) are listed in *Table 2*.

(1) PS1(SUL1) – S(IV) solution in cloud water

The total concentration of the S(IV) species for pH ≤ 5.5, which is typical for cloud and rain water, is predominantly in the form of $[HSO_3^-]$. Thus the concentration of $[HSO_3^-]$ is given by

$$[HSO_3^-] = (K_1 K_2 p_{SO_2}) / [H^+]. \tag{22}$$

By substitution of the rate coefficients, and using expression for the partial pressure of SO_2 (in Pascal's) given by

$$p_{SO_2} = p q_{SO_2} / \left(\frac{M_{SO_2}}{M_d} + q_{SO_2} \right), \tag{23}$$

the rate, at which SO_2 is removed from the atmosphere or return in gaseous phase, is written as

$$\text{PS1(SUL1)} = \frac{K_1 K_2}{[H_C^+]} p q_{SO_2} \frac{M_{SO_2}}{M_{HSO_3^-}} \frac{\delta q_c}{\delta t}, \tag{24}$$

where p is the air pressure; $(\delta q_c / \delta t)$ is condensation rate for cloud water; and $[H_C^+]$ is the equilibrium hydrogen ion concentration in cloud water. The molecular weights M_{SO_2} and $M_{HSO_3^-}$ for SO_2 and $[HSO_3^-]$ are included since SUL1 is a sink term for SO_2.

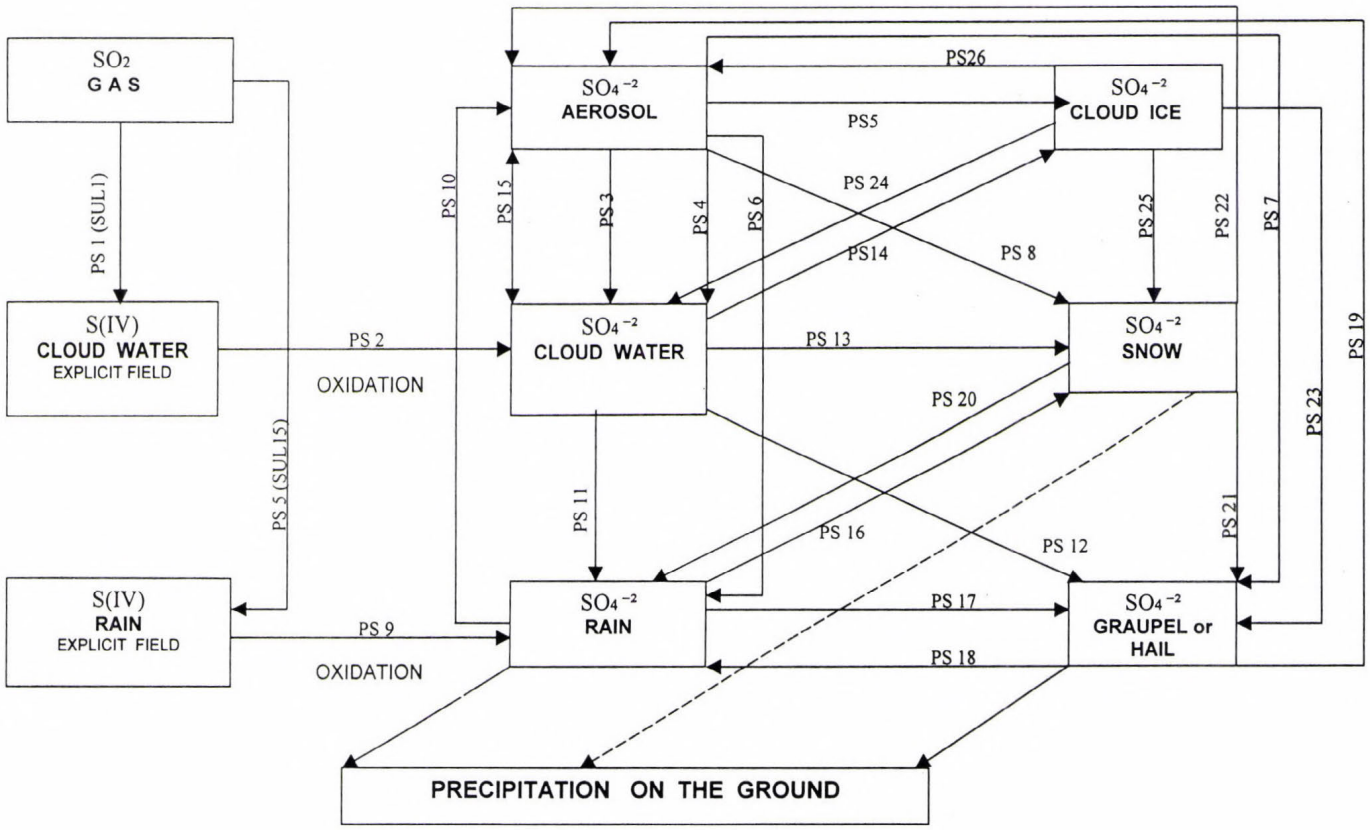

Fig. 1. Scheme of microphysics- and chemistry-related conversions for SO_4^{2-} in air and different water categories, and the names associated with each of them in the model.

Table 2. Equilibrium reactions, rate coefficients, S (IV) oxidations, and the corresponding coefficients

No.	Reactions	K_{298} (M or M atm^{-1})	$-H_{298}/R(K)$	References
1	SO_2 (g) $\Leftrightarrow$ SO_2 (aq)	1.2	3135	(1)
2	SO_2 (aq) $\Leftrightarrow$ $HSO_3^- + H^+$	1.3×10^{-2}	2000	(2)
3	$HSO_3^- \Leftrightarrow SO_3^{-2} + H^+$	6.3×10^{-8}	1495	(3)
4	O_3 (g) $\Leftrightarrow$ O_3 (aq)	1.13×10^{-2}	2300	(4)
5	H_2O_2 (g) $\Leftrightarrow$ H_2O_2 (aq)	7.1×10^4	6800	(5)
6	NH_3 (g) $\Leftrightarrow$ NH_4OH (aq)	75	3400	(6)
7	HNO_3 (g) $\Leftrightarrow$ HNO_3 (aq)	2.1×10^5	8700	(7)
8	CO_2 (g) $\Leftrightarrow$ CO_2 (aq)	3.4×10^{-2}	2420	(8)
9*	S(IV) + $O_3 \rightarrow$ S(VI) + O_2	3.7×10^5	5530	(9)
10*	S(IV) + $H_2O_2 \rightarrow$ S(VI) + H_2O	7.45×10^7	4751	(10)

* In case of non-equilibrium reactions 9 and 10 in the head of columns 2 and 3 ΔK_{298} (M s^{-1}) and $-\Delta H_{298}/R$ (K) should be understood;

(1), (2), (3), (9), and (10) are derived from values given by Hoffmann and Calvert (1985);

(4), (6), and (8) by *Pandis* and *Seinfeld* (1989); (5) by *Martin* and *Damaschen* (1981), and (7) by *Schwartz* and *While* (1981)

(2) PS2 - Oxidation by O_3 and H_2O_2 to SO_4^{2-} in cloud water

As it is listed in *Table 2*, PS2 term is a combination of oxidation reactions. In pH range of interest, S(IV) is predominately in form of HSO_3. Thus the oxidation of O_3 and H_2O_2 could be expressed by rate equation

$$\frac{d}{dt}[SO_4^{2-}] = K_{S(IV)} \left\{ [HSO_3^-][O_{3_{aq}}] + [HSO_3^-][H_2O_{2_{aq}}] \right\} . \tag{25}$$

The term $K_{S(IV)}$ is a modified Henry's law coefficient given by relation

$$K_{S(IV)} = K_1 \left(1 + \frac{K_2}{[H_C^+]} \right). \tag{26}$$

Here $[O_3\,aq]$ and $[H_2O_2\,aq]$ concentrations are calculated using Henry's law coefficients given in *Table 2*, respectively:

$$\begin{aligned} [O_3\,aq] &= K_9 p_{O_3}\,, \\ [H_2O_2\,aq] &= K_{10} p_{H_2O_2}\,, \end{aligned} \tag{27}$$

where p_{O_3} is the partial pressure. Taking into account this relation and the conversion factor $q_{SO_4^{2-}} = 0.0961[SO_4^{2-}]q_c$ given in *Taylor* (1989), the total rate of S(IV) conversion to SO_4^{2-} is given by

$$PS2 = K_{S(IV)} \frac{K_1 K_2}{[H_C^+]} p q_{SO_2} / \left(\frac{M_{SO_2}}{M_d} + q_{SO_2} \right) \{ K_9 p_{O_3} + K_{10} p q_{H_2O_{2C}} \} 0.0961 q_c \quad (28)$$

(3) PS3 - Nucleation scavenging of SO_4^{2-} aerosol by CCN

The term for nucleation scavenging of SO_4^{2-} aerosol by CCN simply shows primary activation of cloud condensation nuclei (CCN), based on numerical integration of the droplet growth equation. According to *Jensen* and *Charlson* (1984), in typical continental cloud condensation nuclei, most primary activation occurs few hundred meters of cloud basis. Also their work shows high nucleation efficiency, 80–100% of total aerosol mass is activated and incorporated into cloud drops. *Taylor* (1989b) has been approximated this process by following expression:

$$PS3 = \begin{cases} \dfrac{\varepsilon_{SO_4^{2-}} q_{SO_4^{2-}a}}{\delta t}, & \delta qc > 0 \\ 0, & \delta qc \le 0 \end{cases}, \quad (29)$$

where $\varepsilon_{SO_4^{2-}} = 0.55$ is the fractional nucleation efficiency; δqc is the condensation of cloud drops during the current time step in the model. Secondary activation of CCN is not included in the model since we use a bulk water parameterization and fixed droplet number in cloud model.

(4a) $PS4_{CB}$ - Scavenging of SO_4^{2-} aerosol by Brownian diffusion in cloud drops

Stationary drops capture aerosol particles by simple Brownian diffusion. The $PS4_{CB}$ term on this way approximates to

$$PS4_{CB} = 4\pi D_p N_C q_{SO_4 a} \alpha_C \bar{f}_p, \quad (30)$$

where D_p is the diffusion coefficient set to $D_p = 1.56 \times 10^{-8}$ m^2 s^{-1}, (*Pruppacher* and *Klett,* 1997), N_C is the cloud droplet concentration; α_C is the mean cloud droplet diameter; and $\overline{f}_p$ is the mean ventilation coefficient .

(4b) $PS4_{IB}$ - Scavenging of SO_4^{2-} aerosol by Brownian diffusion in cloud ice

This term is similar to previous term $PS4_{CB}$ but is related to cloud ice and scavenging of SO_4^{2-} aerosol by Brownian diffusion. This term is approximated as

$$PS4_{IB} = 4\pi D_p N_I q_{SO_4 a} \alpha_I \bar{f}_p , \tag{31}$$

where D_p is the diffusion coefficient set to $D_p = 1.56 \times 10^{-8}$ m^2 s^{-1} (*Pruppacher* and *Klett,* 1997); N_I is the cloud ice concentration; α_I is the mean cloud ice diameter; and $\overline{f}_p$ the mean ventilation coefficient.

(5) PS5 - Nucleation scavenging of SO_4^{2-} aerosol by ice nuclei (IN)

Although the effects of the nucleation scavenging by ice crystals have not been studied in field, the term for nucleation scavenging of SO_4^{2-} aerosol by ice nuclei (IN), is conditionally computed in an analogous fashion to PS3:

$$PS5 = \begin{cases} \dfrac{\varepsilon_{SO_4^{2-}} q_{SO_4^{2-}a}}{\delta t} , & \delta qI > 0 \\ 0, & \delta qI \le 0 \end{cases} , \tag{32}$$

where $\varepsilon_{SO_4^{2-}} = 0.55$ is the fractional nucleation efficiency; δqI is the initiating the ice phase during the current time step in the model.

(6) PS6 - Impact scavenging of SO_4^{2-} aerosol by rain

The impact scavenging of SO_4^{2-} by rain is computed for continuos collection processes

$$-\frac{\partial q_{SO_4a}}{\partial t} = \int_0^\infty \frac{\pi}{4} \alpha_R{}^2 U_R(\alpha_R) q_{SO_4a} \varepsilon_R n_d(\alpha_R, t) d\alpha_R \,. \tag{33}$$

Assuming exponential size distributions for the precipitation particles, PS6 is reduced:

$$\text{PS6} = \frac{\pi}{4} \Gamma(3.5) \varepsilon_R U_R n_{0R} \alpha_R{}^{3.5} q_{SO_4} \,, \tag{34}$$

where n_{0R} is the slope intercept parameter of the rain; α_R is the diameter of rain; U_R is the mass-weighted mean terminal velocity of rain; and ε_R is the collection efficiency.

(7) PS7 - Impact scavenging of SO_4^{2-} aerosol by graupel

Similar as previous term, impact scavenging of SO_4^{2-} aerosol by graupel is calculated assuming continuos collection, i.e.,

$$\text{PS7} = \frac{3\pi}{7} \varepsilon_G U_G N_{TG} \alpha_G{}^2 q_{SO_4a} \,, \tag{35}$$

where N_{TG} is the total number of graupels; α_G is the diameter of graupel; U_G is the mass-weighted mean terminal velocity of graupel; and ε_G is the collection efficiency.

(8) PS8 - Impact scavenging of SO_4^{2-} aerosol by snow

Impact scavenging of SO_4^{2-} aerosol by snow is computed on similar way to terms PS6 and PS7:

$$\text{PS8} = \frac{\pi}{4} \varepsilon_S U_S N_{TS} \alpha_S{}^2 q_{SO_4a} \,, \tag{36}$$

where N_{TS} is the total number of snow; α_S is the diameter of graupel; U_S is the mass-weighted mean terminal velocity of snow; and ε_S is the collection efficiency.

(9) PS9 - Oxidation of S(IV) by O_3 and H_2O_2 to SO_4^{2-} in rainwater

The term PS9, which represents oxidation of S(IV) in rain, is computed on similar way as term PS2:

$$PS9 = K_{S(IV)} \frac{K_1 K_2}{[H_R^+]} pq_{SO_2} / \left(\frac{M_{SO_2}}{M_d} + q_{SO_2} \right) \left\{ K_9 p_{O_3} + K_{10} pq_{H_2O_2 p} \right\} 0.0961 q_c \quad (37)$$

Here $[H_R^+]$ is the hydrogen ion concentration in rain; while $q_{H_2O_2 R}$ is the hydrogen peroxide rain water mixing ratio.

(10) PS10 - S(IV) Evaporation of rain

This term calculates the rate at which SO_2 returns to the atmosphere during evaporation of rain. Since the pH range of cloud and rain water S(IV) is predominantly in form of $[HSO_3^-]$, now the conversion from $[HSO_3^-]$ to SO_2 gas during evaporation of rain, could be expressed by relation

$$PS10 = \frac{K_1 K_2}{[H_R^+]} pq_{SO_2} \frac{M_{SO_2}}{M_{HSO_3^-}} P_{REVP}, \quad (38)$$

where P_{REVP} is the evaporation from rain.

(11) PS11 - SO_4^{2-} transfer from cloud water to rain

This term follows the microphysical transition and transfers SO_4^{2-} from cloud water to rain SO_4^{2-}.

$$PS11 = \frac{q_{SO_4 C}}{q_C} (P_{RAUT} + P_{RACW} + P_{SACW}), \quad (39)$$

where P_{RAUT}, P_{RACW}, and P_{SACW} are autoconversion of cloud water to form rain, accretion of cloud water by rain, and accretion of cloud water by snow, respectively producing snow if $T < T_0$ or rain if $T \geq T_0$. Also enhances snow melting for $T \geq T_0$.

(12) PS12 - SO_4^{2-} transfer from cloud water to graupel

This term follows the microphysical transition and transfers SO_4^{2-} from cloud water to graupel SO_4^{2-}:

$$PS12 = \frac{q_{SO_4C}}{q_C} P_{GACW}, \tag{40}$$

where P_{GACW} is accretion of cloud water by graupel.

(13) PS13 - SO_4^{2-} transfer from cloud water to snow

This term parallels the microphysical transition and transfers SO_4^{2-} from cloud water to snow SO_4^{2-}:

$$PS13 = \frac{q_{SO_4C}}{q_C} (P_{SACW} + P_{SFW}), \tag{41}$$

where P_{SFW} is the Bergeron process (deposition and riming) transferring cloud water to snow; and P_{SACW} is explained in the previous part.

(14) PS14 - SO_4^{2-} transfer from cloud water to cloud ice

This term follows the microphysical transition and transfers SO_4^{2-} from cloud water to cloud ice SO_4^{2-}:

$$PS14 = \frac{q_{SO_4C}}{q_C} (P_{IDW} + P_{IHOM}), \tag{42}$$

where P_{IDW} and P_{IHOM} are depositional growth of cloud ice at expense of cloud water, and homogeneous freezing of cloud water to form cloud ice, respectively.

(15) PS15 - SO_4^{2-} transfer from cloud water to aerosol

This term transfer the cloud droplet SO_4^{2-} to aerosol during evaporation of

cloud droplets. This transfer occurs in the model when mean cloud droplet diameter falls below 1 μm:

$$PS15 = \frac{q_{SO_4C}}{\delta t}. \tag{43}$$

(16) PS16 - SO_4^{2-} transfer from rain to snow

On analogous fashion, this term follows the microphysical transition and transfers SO_4^{2-} from rain to snow SO_4^{2-}:

$$PS16 = \frac{q_{SO_4R}}{q_R}(P_{IACR} + P_{SACR}), \tag{44}$$

where P_{IACR} is the accretion of rain by cloud ice, producing snow or graupel depending on the amount of rain and accretion of rain by snow; and P_{SACR} represents accretion of rain by snow. For $T < T_0$, it produces graupel if rain or snow exceeds threshold; if not, it produces snow. For $T \geq T_0$, the accreted water enhances snow melting.

(17) PS17 - SO_4^{2-} transfer from rain to graupel

Similarly to the computation of the term PS16, this term follows the microphysical transition and transfers SO_4^{2-} from rain to graupel SO_4^{2-}:

$$PS17 = \frac{q_{SO_4R}}{q_R}(P_{GACR} + P_{GFR} + P_{IACR} + P_{SACR}), \tag{45}$$

where P_{GACR} and P_{GFR} are the accretion of rain by graupel, and probabilistic freezing of rain to form graupel, respectively.

(18) PS18 - Transfer of SO_4^{2-} from graupel to rain

On analogous fashion, this term follows the microphysical transition and transfers SO_4^{2-} from graupel to rain SO_4^{2-}:

$$PS18 = \frac{q_{SO_4G}}{q_G} P_{GMLT}, \tag{46}$$

where P_{GMLT} is the melting of graupel to form rain, $T \geq T_0$. (In this regime, P_{GACW} is assumed to be shed as rain).

(19) PS19 - SO_4^{2-} transfer from graupel to aerosol

This term represents the microphysical transition and transfers SO_4^{2-} from graupel to SO_4^{2-} aerosol:

$$\text{PS19} = \frac{q_{SO_4G}}{q_G} P_{GSUB}, \tag{47}$$

where P_{GSUB} is the sublimation of graupel.

(20) PS20 - Transfer of SO_4^{2-} from snow to rain

On analogous fashion, this term follows the microphysical transition and transfers SO_4^{2-} from snow to rain SO_4^{2-}:

$$\text{PS20} = \frac{q_{SO_4S}}{q_S} P_{SMLT}, \tag{48}$$

where P_{SMLT} is the melting of snow to form rain, $T \geq T_0$.

(21) PS21 - Transfer of SO_4^{2-} from snow to graupel

The term PS21 follows the microphysical transition and transfers SO_4^{2-} from snow to graupel SO_4^{2-}:

$$\text{PS21} = \frac{q_{SO_4S}}{q_S} (P_{GAUT} + P_{GACS} + P_{RACS}) \tag{49}$$

where P_{GAUT}, P_{GACS}, P_{RACS} are the autoconversion (aggregation) of snow to

form graupel, accretion of snow by graupel, and accretion of snow by rain, respectively; produces graupel if rain or snow exceeds threshold and $T < T_0$.

(22) PS22 - Transfer of SO_4^{2-} from snow to aerosol

The term PS22 parallels the microphysical transition and transfers SO_4^{2-} from snow to SO_4^{2-} aerosol:

$$\mathrm{PS22} = \frac{q_{\mathrm{SO_4}S}}{q_S}(P_{SSUB} + P_{SDEP}), \tag{50}$$

where P_{SSUB} and P_{SDEP} are the sublimation of snow, and depositional growth of snow, respectively.

(23) PS23 - SO_4^{2-} transfer from cloud ice to graupel or hail

On analogous fashion, this term follows the microphysical transition and transfers SO_4^{2-} from cloud ice to graupel or hail SO_4^{2-}:

$$\mathrm{PS23} = \frac{q_{\mathrm{SO_4}I}}{q_I}(P_{GACI} + P_{RACI}), \tag{51}$$

where P_{GACI} and P_{RACI} are the accretion of cloud ice by graupel, and accretion of cloud ice by rain, respectively, producing snow or graupel depending on the amount of rain.

(24) PS24 - Transfer of SO_4^{2-} from cloud ice to cloud water

On analogous fashion, this term follows the microphysical transition and transfers SO_4^{2-} from cloud ice to cloud water SO_4^{2-}:

$$\mathrm{PS24} = \frac{q_{\mathrm{SO_4}I}}{q_I} P_{IMLT}, \tag{52}$$

where P_{IMLT} the melting of cloud ice to form cloud water, $T \geq T_0$.

(25) PS25 - SO_4^{2-} transfer from cloud ice to snow

This term parallels the microphysical transition and transfers SO_4^{2-} from cloud ice to snow SO_4^{2-}:

$$\mathrm{PS25} = \frac{q_{\mathrm{SO}_4 I}}{q_I}(P_{SAUT} + P_{SACI} + P_{SFI} + P_{RACI}), \tag{53}$$

where P_{SAUT}, P_{SACI}, and P_{SFI} are the autoconversion (aggregation) of cloud ice to form snow, accretion of cloud ice by snow, and transfer rate of cloud ice to snow through growth of Bergeron process embryos, respectively.

(26) PS26 - SO_4^{2-} transfer from cloud ice to aerosol

This term transfers the cloud ice SO_4^{2-} to aerosol during evaporation of cloud ice. This transfer occurs in the model when mean cloud ice diameter falls below 1 μm:

$$\mathrm{PS26} = \frac{q_{\mathrm{SO}_4 I}}{\delta t}. \tag{54}$$

3.4 Hydrogen peroxide, ozone, and sulfur dioxide source terms

The scheme of H_2O_2, O_3 and SO_2 reactions are presented in *Fig. 2*. The source terms for H_2O_2 and O_3 include: equilibration between gas and aqueous phases using Henry's law, reduction due to oxidation of S(IV) in cloud drops and rain, as well as the set of microphysical transfer and conversions among different water categories. SO_2 field is explicitly treated in the model. The source terms of S(IV) are solution in cloud water and rain water, and microphysical conversions.

(1) PH1, OHP1, SUL1 - Equilibration of H_2O_2, O_3, and SO_2 in cloud droplets

As SUL1 is a sink term for SO_2 described before, PH1 and OHP1 are terms representing equilibration of H_2O_2 and O_3 concentrations in cloud droplets. According to Henry's law, these terms could be expressed as

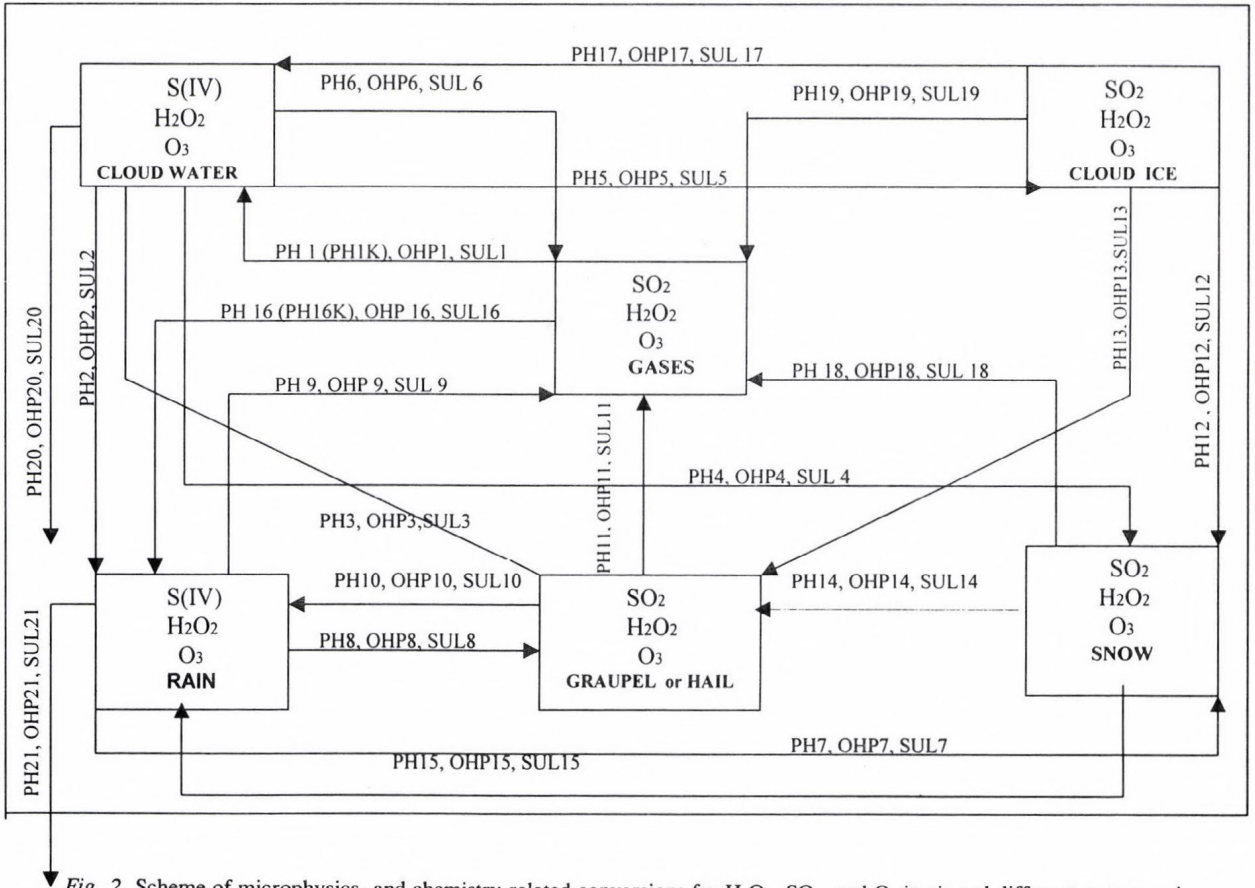

Fig. 2. Scheme of microphysics- and chemistry-related conversions for H_2O_2, SO_2, and O_3 in air and different water carriers, and the names associated with each of them in the model.

$$\mathrm{PH1,OHP1} = K_4 p q_{\mathrm{H_2O_2,O_3}C} \frac{\delta q_C}{\delta t}. \tag{55}$$

If condensation rate $\frac{\delta q_C}{\delta t} < 0$, in the computation of PH1 and OHP1 we take maximum available amounts of H_2O_2 or O_3, which is returned to the environment (*Taylor*, 1989), i.e.,

$$\mathrm{PH1,OHP1} = \max\left[K_4 p q_{\mathrm{H_2O_2,O_3}C} \frac{\delta q_C}{\delta t}, \frac{q_{\mathrm{H_2O_2,O_3}C}}{\delta t} \right]. \tag{56}$$

(2) PH2, OHP2, SUL2 - H_2O_2, O_3, and SO_2 transfer from cloud water to rainwater

This term follows the microphysical transition and transfers of H_2O_2, O_3, and SO_2 from cloud water to rain H_2O_2, O_3, and SO_2.

$$\mathrm{PH2,OHP2,SUL2} = \frac{q_{\mathrm{H_2O_2,O_3,SO_2}C}}{q_C} (P_{RAUT} + P_{RACW} + P_{SACW}), \tag{57}$$

where P_{RAUT}, P_{RACW}, and P_{SACW} are autoconversion of cloud water to form rain, accretion of cloud water by rain, and accretion of cloud water by snow; it produces snow if $T < T_0$, or rain if $T \geq T_0$. Also enhances snow melting for $T \geq T_0$.

(3) PH3,OHP3, SUL3 - H_2O_2, O_3, and SO_2 transfer from cloud water to graupel

$$\mathrm{PH3,OHP3,SUL3} = \frac{q_{\mathrm{H_2O_2,O_3,SO_2}C}}{q_C} P_{GACW}. \tag{58}$$

(4) PH4,OHP4,SUL4 - H_2O_2, O_3, and SO_2 transfer from cloud water to snow

$$\mathrm{PH4,OHP4,SUL4} = \frac{q_{\mathrm{H_2O_2,O_3,SO_2}C}}{q_C} (P_{SACW} + P_{SFW}). \tag{59}$$

(5) PH5,OHP5,SUL5 - H_2O_2, O_3, and SO_2 transfer from cloud water to cloud ice

$$\mathrm{PH5,OHP5,SUL5} = \frac{q_{\mathrm{H_2O_2,O_3,SO_2}C}}{q_C}\left(P_{IDW} + P_{IHOM}\right). \tag{60}$$

(6) PH6,OHP6, SUL6 - H_2O_2, O_3, and SO_2 transfer to gas phase from cloud water

$$\mathrm{PH6,OHP6,SUL6} = \frac{q_{\mathrm{H_2O_2,O_3,SO_2}\,G}}{\delta t}. \tag{61}$$

(7) PH7,OHP7,SUL7 - H_2O_2, O_3, and SO_2 transfer from rain to snow

In an analogous fashion, this term follows the microphysical transition and transfers H_2O_2, O_3, and SO_2 from rain to snow:

$$\mathrm{PH7,OHP7,SUL7} = \frac{q_{\mathrm{H_2O_2,O_3,SO_2}\,S}}{q_S}\left(P_{IACR} + P_{SACR}\right), \tag{62}$$

where P_{IACR} is the accretion of rain by cloud ice; produces snow or graupel depending on the amount of rain and accretion of rain by snow, and P_{SACR} represents accretion of rain by snow. For $T < T_0$, produces graupel if rain or snow exceeds threshold; if not, produces snow. For $T \geq T_0$, the accreted water enhances snow melting.

(8) PH8, OHP8, SUL8 - H_2O_2, O_3, and SO_2 transfer from rain to graupel

$$\mathrm{PH8,OHP8,SUL8} = \frac{q_{\mathrm{H_2O_2,O_3,SO_2}R}}{q_R}\left(P_{GACR} + P_{GFR} + P_{IACR} + P_{SACR}\right). \tag{63}$$

(9) PH9, OHP9, SUL9 - H_2O_2 evaporation from rain to aerosol

$$\mathrm{PH9,OHP9,SUL9} = \frac{q_{\mathrm{H_2O_2,O_3,SO_2}R}}{q_R}P_{REVP}. \tag{64}$$

(10) PH10, OHP10, SUL10 - Transfer of H_2O_2, O_3, and SO_2 from graupel to rain

$$PH10,OHP10,SUL10 = \frac{q_{H_2O_2,O_3,SO_2\,G}}{q_G} P_{GMLT} \cdot \quad (65)$$

(11) PH11, OHP11, SUL11 - H_2O_2, O_3, and SO_2 transfer from to gas phase graupel

$$PH11,OHP11,SUL11 = \frac{q_{H_2O_2,O_3,SO_2G}}{q_G} P_{GSUB} \cdot \quad (66)$$

(12) PH12,OHP12,SUL12 - H_2O_2, O_3, and SO_2 transfer from cloud ice to snow

$$PH12,OHP12,SUL12 = \frac{q_{H_2O_2,O_3,SO_2I}}{q_I} (P_{SAUT} + P_{SACI} + P_{SFI} + P_{RACI}) \cdot \quad (67)$$

(13) PH13 - H_2O_2, O_3, and SO_2 transfer from cloud ice to graupel

$$PH13,OHP13,SUL13 = \frac{q_{H_2O_2,O_3,SO_2\,I}}{q_I} (P_{GACI} + P_{RACI}) \cdot \quad (68)$$

(14) PH14,OHP14,SUL14 - Transfer of H_2O_2, O_3, and SO_2 from snow to graupel

$$PH14,OHP14,SUL14 = \frac{q_{H_2O_2,O_3,SO_2\,S}}{q_S} (P_{GAUT} + P_{GACS} + P_{RACS}) \cdot \quad (69)$$

(15) PH15, OHP15, SUL15 - H_2O_2, O_3, and SO_2 transfer from snow to rain

These terms transfer the snow H_2O_2, O_3, and SO_2 to rain during melting of snow:

$$PH15,OHP15,SUL15 = \frac{q_{H_2O_2,O_3,SO_2\,S}}{q_S} P_{SMLT} \cdot \quad (70)$$

(16) PH16, OHP16, SUL16 - Equilibration of H_2O_2, O_3, and SO_2 in rain drops

Like PH1, OHP1, these terms follows Henry's law equilibration between H_2O_2, O_3, SO_2, and rain drops,

$$PH16, OHP16, SUL16 = \max\left[K_{4,7,1}\ pq_{H_2O_2,O_3,SO_2R} P_{REVP}, \frac{q_{H_2O_2,O_3,SO_2R}}{\delta t} \right]. \tag{71}$$

The second term limits the amounts returning to the atmosphere through evaporation of rain drops.

(17) PH17, OHP17, SUL17 - Transfer of H_2O_2 from cloud ice to cloud water

$$PH17, OHP17, SUL17 = \frac{q_{H_2O_2,O_3,SO_2I}}{q_I} P_{IMLT}. \tag{72}$$

(18) PH18, OHP18, SUL18 - Transfer of H_2O_2, O_3, and SO_2 from snow gas phase

These terms transfer H_2O_2, O_3, and SO_2 from snow to gas phase:

$$PH18, OHP18, SUL18 = \frac{q_{H_2O_2,O_3,SO_2S}}{q_S} (P_{SSUB} + P_{SDEP}). \tag{73}$$

(19) PH19, OHP19, SUL19 - Transfer of H_2O_2, O_3, and SO_2 from cloud ice to gas phase

$$PH19, OHP19, SUL19 = \frac{q_{H_2O_2,O_3,SO_2S}}{\delta t}. \tag{74}$$

(20) PH20, OHP20, SUL20 - Reduction of H_2O_2 and O_3 in cloud droplets by SO_2

A part of the S(IV) conversion to SO_4^{2-} is due to oxidation in cloud drops and rain by H_2O_2. On this way, H_2O_2 is being reduced in cloud droplets and rain by SO_2. According to (*Taylor,* 1989), H_2O_2 is destroyed in aqueous reaction

$$HSO_3^- + H_2O_2 \Leftrightarrow O_2SOOH^- + H_2O. \tag{75}$$

The rate at which H_2O_2 is destroyed is parameterized in the same manner as for oxidations terms PS2 and PS9 formulated in the sulfate production:

$$\mathrm{PH20,OHP20} = K_{\mathrm{S(IV)}} \frac{K_1 K_2}{[\mathrm{H}_C^+]} pq_{\mathrm{SO_2}} \frac{M_{\mathrm{H_2O_2,O_3}}}{M_{\mathrm{SO_2}}} K_{4,7} pq_{\mathrm{H_2O_2,O_3}C} \cdot \qquad (76)$$

(21) PH21,OHP21, SUL21 – Reduction of H_2O_2 and O_3 in rain by SO_2

On similar way, parameterization of H_2O_2 destruction in rain is given by

$$\mathrm{PH21,OHP21} = K_{\mathrm{S(IV)}} \frac{K_1 K_2}{[\mathrm{H}_R^+]} pq_{\mathrm{SO_2}} \frac{M_{\mathrm{H_2O_2,O_3}}}{M_{\mathrm{SO_2}}} K_{4,7} pq_{\mathrm{H_2O_2,O_3}R} \cdot \qquad (77)$$

In addition, cloud and raindrops contain dissolved ammonium sulfate $(NH_4)_2SO_4$, which is not created or destroyed in the chemical reactions. The only transitions of $[NH_4^+]$ aerosol are from scavenging and those following the microphysical transfers (*Taylor*, 1989b).

3.5 Calculation of pH

The calculation of the cloud water pH and rainwater pH is based on the equilibrium hydrogen ion concentration for $[H^+]$, which is given by the simple charge balance equation (*Taylor*, 1989b):

$$[H^+] = 0.5\left\{2[SO_4^{2-}] - [NH_4^+] + \left((2[SO_4^{2-}] - [NH_4^+])^2 + 4K_H{}^* p_{SO_2} + 4K_W\right)^{0.5}\right\}. \qquad (78)$$

4. Summary and conclusions

We have developed and incorporated the chemical packet into a three-dimensional compressible cloud model combined with bulk water microphysics. The governing equations of the model include momentum conservation equations, thermodynamic and pressure equations, four continuity equations for the various water substances, subgrid scale (SGS) turbulent kinetic energy equation (TKE), and continuity equations for chemical species associated with various cloud water species.

The microphysics and chemistry modules have been formulated in terms of continuity equations, which represent the average microphysical and chemical properties of the cloud and cloud environment within elementary well-

mixed volumes. The simple sulfur chemistry and parameterization of chemical species included in sulfate budget are considered in detail. Processes occurring on smaller scales are parameterized in terms of these average properties. The utilized cloud-chemistry model uses explicit treatment of gases, and specifically, mass transfer limitation calculations for highly soluble gases. The set of three-dimensional runs with mixed phase microphysics and the modification of the hail growth equation in the microphysics parameterization scheme are also novel aspects of the model.

Acknowledgements–First of all we acknowledge to *Mr. Bosko Telenta*, for his support, giving insights and explanations concerning the technical aspects of this model. We also wish to express our gratitude to *Ms. Marija Andreevska* from Hydrometeorological Institue of Macedonia, for her help with some useful explanations of chemical aspects of the paper. The anonymous referees have made many substantial remarks that increased the completeness and clarity of the manuscript. We would like to express our special gratitude to *Dr. Tamás Práger*, for his important contribution giving constructive comments during final revision of the paper and allowance its publishing.

References

Barth, M.C., Stuart, A.L., and *Skamorock, W.C., 2001*: Numerical simulation of the July 10 Stratospheric-Tropospheric Experiment: Radiation, Aerosols, and Ozone/Deep Convection storm: Redistribution of soluble tracers. *J. Geophys. Res. 106*, 12, 381-12,400.

Chen, J.P. and *Lamb, D.*,1994: Simulation of cloud microphysics and chemical processes using a multicomponent framework, I. Description of the microphysical model. *J. Atmos. Sci. 51*, 2613-2630.

Crutzen, P.J. and *Lawrence, M.G.*, 2000:The impact of precipitation scavenging on the transport of trace gases: A three-dimensional model sensitivity study. *J. Atmos. Chem. 37*, 81-112.

Ćurić, M. and *Janc, D.*, 1995: On the sensitivity of the continuous accretion rate equation used in bulk-water parameterization schemes. *Atmos. Res. 39*, 313-332.

Ćurić, M. and *Janc, D.*,1997: On the sensitivity of hail accretion rates in numerical modeling. *Tellus 49A*, 100-107.

Flossman, A.I. and *Wobrock, W.*, 1996:Venting of gases by convective clouds. *J. Geophys. Res. 101*, 18,639-18,649.

Hales, J.M., 1982: Mechanistic analysis of precipitation scavenging using a one-dimensional time variant model. *Atmos. Environ. 16*, 177-1783.

Hoffmann, M.R. and *Calvert, J.G.*, 1985: *Chemical Transformation Modules for Eulerian Acid Deposition Models, Vol. 2.* The aqueous phase chemistry. Rep. EPA/600/3-85/017, U.S. Environ. Prot. Agency, Research Triangle Park. N. C.

Hsie, E.Y., Farley, R.D., and *Orville, H.D.*, 1980: Numerical simulation of ice-phase convective cloud seeding. *J. Appl. Meteor. 19*, 950-977.

Isaac, G.A., Strapp, J.W., Wiebe, H.A., Leaitch, W.R. Kerr, J.B., Anlauf, K.G., Summers, P.W., and *McPherson, J.I.*, 1982: The role of cloud dynamics in redistributing pollutants and the implications for scavenging studies. In *Precipitation Scavenging, Dry Deposition and Resuspension*. (Coords.: *H.R. Pruppacher, R.G. Semonin*, and *W.G.N. Slinn*). *Elsevier*, pp. 1-13.

Isaac, G.A., Joe, P.J., and *Summers, P.W.*, 1983: The vertical transport and redistribution of pollutants by clouds. In *The Meteorology of Acid Deposition*. (ed.: *P.J. Samson*). Air Pollution Control Association, pp. 496-512.

Klemp, J.B. and *Wilhelmson, R.B.*, 1978: The simulation of three-dimensional convective storm dynamics. *J. Atmos. Sci. 35*, 1070-1096.

Kreidenweis, S.M., Zhang, M., and *Taylor, G.R.*, 1997: The effects of clouds on aerosol and chemical species production and distribution 2. Chemistry model description and sensitivity analysis. *J. Geophys. Res. 102*, 23867-23882.

Lin, Y.L. Farley, R.D., and *Orville, H.D.*, 1983: Bulk water parameterization in a cloud model. *J. Climate Appl. Meteor. 22*, 1065-1092.

Martin, L R. and *Damaschen, D.E.*, 1981: Aqueous oxidation of sulfur dioxide by hydrogen peroxide at low pH. *Atmos. Environ. 15*, 191-195.

Niewiadomski, M., 1989: Sulfur dioxide and sulfate in a three-dimensional field of convective clouds: Numerical simulations. *Atmos. Environ. 23(2)*, 477-487.

Orville, H.D. and *Kopp, F.J.*, 1977: Numerical simulation of the history of a hailstorm. *J. Atmos. Sci. 34*, 1596-1618.

Pandis, S.N. and *Seinfeld, J.H.*, 1989: Sensitivity analysis of a chemical mechanism for aqueous-phase atmospheric chemistry. *J. Geophys. Res. 94(D1)*, 1105-1126.

Pruppacher, H.R. and *Klett, J.D.*, 1997: *Microphysics of Clouds and Precipitation*. 2nd ed. Kluwer Acad., Norwell, Mass.

Rutledge, S.A., Hegg, D.A., and *Hobbs, P.V.*, 1986: A numerical model for sulfur and nitrogen scavenging in narrow cold-frontal rainbands. Part 1: Model description and discussion of microphysical fields. *J. Geophys. Res. 91*, 14 385-14 402.

Sarma, R.A., 1986: *Numerical Simulation of the Formation and Transport of Sulfate in Convective Clouds. Ph.D. dissertation*. South Dakota School of Mines and Technology, Rep. No. SDSMT/IAS/R-86/04, 188 pp.

Skamorock, W.C. et al., 2000: Numerical simulation of the July 10 Stratospheric-Tropospheric Experiment: Radiation, Aerosols, and Ozone/Deep Convection experiment convective system: Kinematics and transport. *J. Geophys. Res. 105*, 19, 973-19,990.

Schwartz, S.E. and *White, W.H.*, 1981: *Solubility equilibrium of the nitrogen oxides and oxyacids in dilute aqueous solution*. In *Advances in Environmental Science and Engineering*, Vol. 4, (eds: *J.R. Pfafflin* and *E.N Ziegler*), 1-45. Gordon and Breach Science Publishers, NY.

Taylor, G.R., 1989a: Sulfate production and deposition in midlatitude continental cumulus clouds, Part I, Cloud model formulation and base run analysis. *J. Atmos. Sci. 46*, 1971-1990.

Taylor, G.R., 1989b: Sulfate production and deposition in midlatitude continental cumulus clouds, II, Chemistry model formulation and sensitivity analysis. *J. Atmos. Sci. 46*, 1991-2007.

Tremblay, A. and *Leighton, H.*, 1986: A three-dimensional cloud chemistry model. *J. Climate Appl. Meteor. 25*, 652-671.

Walcek, C.J. and *Taylor, G.R.*, 1986: Theoretical method for computing vertical distributions of acidity and sulfate production within cumulus clouds. *J. Atmos. Sci. 43*, 339-355.

Wang, C. and *Chang, J.S.*, 1993a: A three-dimensional numerical model of cloud dynamics, microphysics and chemistry, Part IV. Cloud chemistry and precipitation chemistry. *J. Geophys. Res. 98*, 116,799-16,808.

Wang, C. and *Chang, J.S.*, 1993b: A three-dimensional numerical model of cloud dynamics, microphysics, and chemistry, Part I. Concepts and formulation. *J. Geophys. Res. 98*, 14,827-17,844.

Yin, Y., Parker, D.J. and *Carslaw, K.S.*, 2001: Simulation of trace gas redistribution by convective clouds-Liquid phase processes. *Atmos. Chem. Phys. 1*, 19-36.

IDŐJÁRÁS

Quarterly Journal of the Hungarian Meteorological Service
Vol. 107, No. 2, April–June 2003, pp. 115–132

Validation of the Eulerian dispersion model MEDIA at the Hungarian Meteorological Service

Zita Ferenczi[1] and **István Ihász**[2]

Hungarian Meteorological Service
[1]*P.O. Box 39, H-1675 Budapest, Hungary; E-mail: ferenczi.z@met.hu*
[2]*P.O. Box 38, H-1525 Budapest, Hungary; E-mail: ihasz.i@met.hu*

(Manuscript received October 24, 2002; in final form May 16, 2003)

Abstract–This paper presents adaptation of the Eulerian dispersion model – MEDIA – at the Hungarian Meteorological Service. The model is part of the emergency response system of the Hungarian Meteorological Service, which can be operated by forecaster on request. The model calculates air concentration fields at 10 different sigma layers in lower and middle troposphere, and deposition field (dry and wet) for every 6 hours. The lead-time depends on the forecasting time of the driving numerical weather prediction model. Some new results of the investigation work are presented which provide the decision makers with new information about the time evolution of the polluted material. The influence of dry and wet deposition was examined separately. Model was launched without dry and wet deposition, and the final concentration fields were compared to the normal simulation. The influence of heavy rain was studied, and the concentration and deposition fields were compared to normal simulations as well. An interesting weather situation was selected to demonstrate our results.

Key-words: dispersion model, radioactive pollutant, concentration fields, dry/wet deposition, meteorological workstation, time series, vertical distribution, regional and continental scale transport.

1. Introduction

The aim of this paper is to describe a dispersion model, which has been used at the Hungarian Meteorological Service (HMS) in case of nuclear/industrial accident. Since 1990, foreward and backward trajectories have been calculated in emergency situation (*Ihász,* 1992, 1999). After the serious accident happened in Chernobyl, several air pollution models were developed in

Europe. The so-called MEDIA model was developed by Meteo France in 1989, and it was adapted by the HMS in 1997. Its aim is to provide forecasts for the dispersion of pollution in case of accidental release of potentially dangerous materials into the atmosphere. Since 1999, the model has been part of the emergency response system of the HMS, which can be operated on request. The model can be used in real time mode. The forecaster can choose the coordinate of the source point, the time of release, the type of pollutant, and the interval of emission. In Hungary the model is driven by meteorological input data provided by the ALADIN or ECMWF numerical weather prediction models (*Ihász,* 2000).

ALADIN is a short-range limited area model making weather forecasts up to 48 hours. ALADIN was developed by international co-operation of several European countries by leadership of France (ALADIN is French abbreviation: Aire Limitee Adaptation Dynamique Developement International (*Horányi et al.*, 1996). ECMWF (European Centre for Medium Range Weather Forecasts) is an international organization supported by 24 European countries, Hungary has a co-operation agreement since 1994. ECMWF operationally provides medium range deterministic and ensemble forecasts up to 10 days for its member states and co-operating states (resolution of deterministic model is 40 km, i.e., approximately 0.4 degrees) (*White*, 2000a-e).

All the simulations of MEDIA model that were performed reveal that the quality of the atmospheric transport model strongly depends on the quality of the driving numerical weather prediction model. Meteorological input data from the ALADIN/HU (version of ALADIN model running at the Hungarian Meteorological Service) numerical weather prediction model are used for the developing aim. The space resolution of these meteorological data are 0.1 by 0.15 degrees in latitude and longitude, the time resolution is 1 hour, so these data sets are much better for examination purposes than the data coming from ALADIN/LACE (LACE means Limited Area Model for Central Europe) or ECMWF models. ALADIN/LACE model was planned to be terminated on December 31, 2002, so in the future only ALADIN/HU model can be used on very high resolution. In this paper we will present some new results of the development work at the HMS and some interesting case studies.

2. Short description of MEDIA

Dispersion models can belong to two types, namely the Eulerian and Lagrangian models, or some kind of combination of them. Galmarini (*Galmarini et al.*, 2002) gives a summary about recently available dispersion models in Europe. If nuclear or chemical accident happens quite far from our

reception point, a continental or global model should be used, if it happens not so far from our reception point, fine mesh regional model can be preferable.

MEDIA is a three dimensional Eulerian type dispersion model for medium and long-range transport of emitted pollutant in the atmosphere. In this paper we give only a short review of the transport model. A complete description and validation of the model can be found in *Piedelievre et al.* (1990). The governing equation of the model is the diffusion equation, which is based on the mass conservation of the polluted material in the atmosphere in vectorial form:

$$\frac{\partial C}{\partial t} + \mathbf{V}(\nabla C) = \nabla(\mathbf{K}\nabla C) + \dot{S}_0 - \dot{S}_i \,, \tag{1}$$

$$\frac{\partial C}{\partial t} + u\frac{\partial C}{\partial x} + v\frac{\partial C}{\partial y} + w\frac{\partial C}{\partial z} = +\frac{\partial}{\partial x}\left(K_x \frac{\partial C}{\partial x}\right) + \frac{\partial}{\partial y}\left(K_y \frac{\partial C}{\partial y}\right) + \frac{\partial}{\partial z}\left(K_z \frac{\partial C}{\partial z}\right) + \dot{S}_0 - \dot{S}_i \,, \tag{2}$$

where C [Bq m^{-3}] is the air concentration of the pollutant at a given point at time t, u, v, w are three components of the wind velocity vector (**V**) [m s^{-1}], K_x, K_y ,K_z horizontal and vertical turbulent diffusion coefficients (diagonal elements of the **K** turbulent diffusion tensor), $\dot{S}_0$ and $\dot{S}_i$ are source and sink terms. The rate of decay of a radionuclide is described by its activity, namely by the number of atoms that decay per unit time. The unit of activity is becquerel (Bq), which is defined unit in International System (SI), defined as one disintegration or nuclear transform per second: 1 Bq = 1 s^{-1}.

2.1 Advection

The pollutant concentration is transported by the horizontal wind fields coming from the driving numerical prediction model.

2.2 Turbulent diffusion

The diffusion represents the mixing of the pollutant in the atmosphere due to the turbulent motions. In order to simplify the procedure and make it coherent with coupling model, the diffusion is modeled using exchange coefficients (first order closure). This choice means that the pollutant is assumed to be diffused in the same way as water vapor. In that case, **K** tensor is diagonal:

$$\nabla(\mathbf{K}\nabla C) = \frac{\partial}{\partial x}K_x\frac{\partial C}{\partial x} + \frac{\partial}{\partial y}K_y\frac{\partial C}{\partial y} + \frac{\partial}{\partial z}K_z\frac{\partial C}{\partial z} \,. \tag{3}$$

The diffusion is solved using the *K*-theory with horizontal coefficients (K_x, K_y) dependent on the grid size, and vertical coefficient (K_z) related to the stability of the layer according to *Louis* (1979), as follows:

$$K_z = l^2 \frac{\partial |\mathbf{V}_h|}{\partial z} F(Ri), \tag{4}$$

where $\mathbf{V}_h$ is the horizontal wind vector, l is the mixing length, Ri is bulk Richardson number,

$$l = \frac{\kappa z}{1 + \frac{\kappa z}{150}} \tag{5}$$

in which: κ is the Karman constant (0.4),

$$Ri = \frac{g}{\theta} \frac{\partial \theta}{\partial z} \left(\left(\frac{\partial u}{\partial z} \right)^2 + \left(\frac{\partial v}{\partial z} \right)^2 \right)^{-1}, \tag{6}$$

here: θ is the potential temperature, g is the gravitational acceleration.

$$F(Ri) = \frac{1}{1 + 3b\, Ri (1 + dRI)^{1/2}} \qquad \text{if } Ri > 0, \tag{7}$$

$$F(Ri) = \frac{1}{1 + 3bc \left[l^2 Ri^{1/2} / (z^2 \sqrt{27}) \right]} \qquad \text{if } Ri < 0, \tag{8}$$

where $b = c = d = 5$.

2.3 Sinks

Sinks can be wet and dry deposition and radioactive decay for radioactive pollutant.

2.4 Wet deposition

Wet deposition due to scavenging by precipitation is computed using a global coefficient of air-to-water transfer, which roughly describes dilution or catching. Despite its simplicity, this solution is generally used and is well

adapted to accuracy of precipitation predicted by the model. The rate of wet deposition D_W (Bq m^{-2} s^{-1})can be written in the next form:

$$D_w = \frac{C_m E P_r}{p_w} , \tag{9}$$

where C_m is average concentration in precipitating layer in concentration units (Bq m^{-3} for a radioactive cloud), $E=10^4$ is scavenging ratio, P_r is rate of precipitation (kg m^{-2} s^{-1}), p_w is specific mass of water (kg m^{-3}).

Since in coupling model precipitation fluxes are only available at ground level, we assume that the thickness of the precipitating layer is 3000 m, and that the scavenging is uniformly active in this part of the atmosphere. In the vertical it is distributed proportionally to the concentration. Four different types of precipitation can be defined in the model: rain and snow, which can be large scale or convective.

2.5 Dry deposition

Dry deposition describes uptake of a pollutant at the earth's surface by soil, water, or vegetation. This process is modeled using a coefficient that is dimensionally equal to a deposition velocity. The downward flux of radioactive material D_{dsoil} (Bq m^{-2} s^{-1}) can be written in the following way:

$$D_{dsoil} = V_d C_{soil} , \tag{10}$$

where C_{soil} is concentration in air near the ground (Bq m^{-3}), V_d is dry deposition velocity (m s^{-1}).

2.6 Radioactive decay

In case of a radioactive pollutant, the other factor of depletion is the radioactive decay, which is formulated by the well-known equation

$$\frac{dC}{dt} = -KC , \tag{11}$$

where $K = \ln 2/T$ is the splitting constant and T is the radioactive half-life time of the pollutant.

2.7 Source

In the source mesh, Gaussian distribution describes the diffusion on a subgrid scale:

$$\frac{dC}{dt} = \frac{Q(t)}{2\pi\sigma_n^2 H} \exp \frac{(-d^2)}{2\sigma_n^2}, \tag{12}$$

where d is distance from the source (m), Q is emission term (Bq s^{-1}), H is vertical extension of the pollutant cloud (m), σ_n^2 is surface of the mesh which includes the source (m^2).

The model has ten σ levels in the vertical ($\sigma = \frac{p}{p_s}$, where p is pressure and p_s is surface pressure in so-called Phillips terrain following co-ordinate system). Equidistant σ levels are located between 1 and 0.5 (*Table 1*).

Table 1. Relation between the σ levels of MEDIA and the typical heights above surface

σ levels of MEDIA	**Typical heights above surface level in m if p_s is 1013 hPa**
0.99	10.1
0.94	495.3
0.88	1004.5
0.83	1540.6
0.77	2106.8
0.71	2707.3
0.66	3347.2
0.60	4032.6
0.54	4771.6
0.49	5574.4

3. Description of the simulation

MEDIA dispersion model has been working operationally since 1999 at the HMS. The model was also tested in an accident happened in Algeciras, Spain, in May 1998. Several case studies have been investigated, now we will show a situation connecting to an interesting weather situation, when benefit of very fine mesh coupling numerical forecasting model can be specially seen.

The Hungarian a nuclear power plant near the town of Paks (46.8°N, 18.6°E) has been operating since 1982. This location was the source point in our experiment running. Four different geographical points were selected for the analysis of the time series. The first point is located near the source point in the path of the maximum concentration values. The other three points are

around the source point in different directions. Location of the source point and the four detection points can be seen in *Fig. 1.*

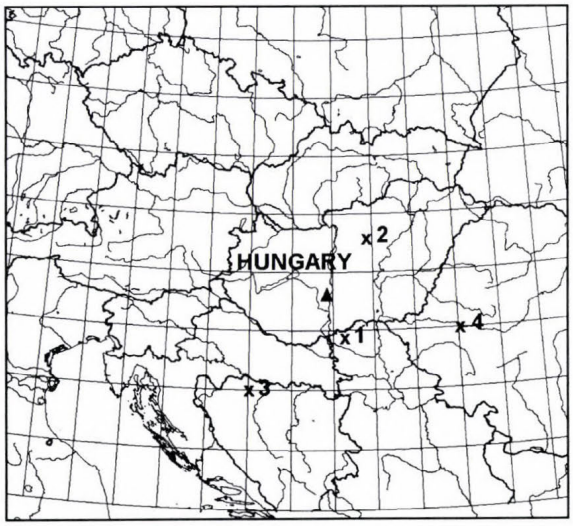

Fig. 1. Location of the source point and detection points (▲ indicates the source point, while the ×-s are the detection points).

The supposed release started at 00 UTC, December 11, 2001, and there was 2-hour explosion with an average hourly rate 5×10^{14} Bq h^{-1}. In the case of the extremely dangerous accident happened at Chernobyl, in April 26, 1986, maximum release was in this magnitude (*Piedelivre et al.*, 1990). The height of release was 10 to 120 m. The simulation was carried out for ^{137}Cs (the half time is 30 years). The dry deposition velocity was chosen to be equal to 10^{-3} m s^{-1}, which is compatible with the size of Caesium nuclides. The space resolution of the ALADIN/HU forecasted meteorological data were 0.1 by 0.15 degree in latitude and longitude, and the time resolution was 1 hour. The integration time step was 300 s, and the integration domain covers an area between 42.9° and 51.4°N; 6.4° and 24.55°E.

Weather situation in Central Europe at December 11, 2001:

There was an anticyclone in Europe, but over the eastern part of Europe there was a cyclone with an occluded front (*Fig. 2*). This frontal zone left Hungary late afternoon. In the territory of the Carpathian Basin, the weather was cold

and cloudy, there was snowing on many places. The wind was blowing from northwest to southeast. The wind speed near the ground level (at about 10 m height) was about 2–3 m s^{-1} (*Fig. 3*). In the upper air (at about 500 m height), the wind direction turned right and the wind speed was 3-4 m s^{-1} (*Fig. 4*). The wind moved the polluted material in the southeast direction. In the west part of Hungary, intensity of the precipitation was 2–3 mm day^{-1} (*Fig. 5*).

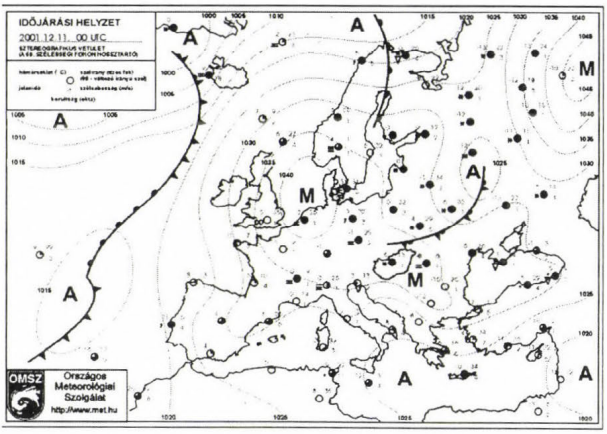

Fig. 2. Synoptic chart at 00 UTC, December 11, 2001.

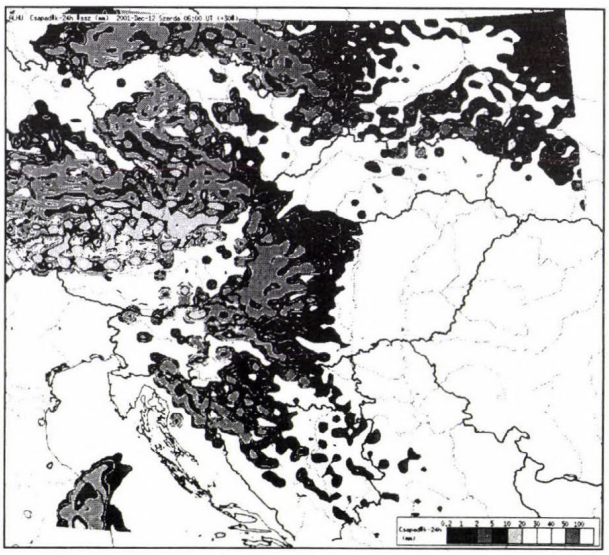

Fig. 3. Precipitation field between 00 UTC, December 11, 2001 and 00 UTC, December 12, 2001.

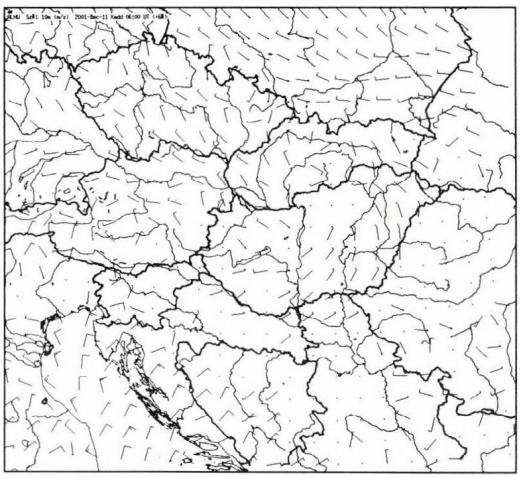

Fig. 4. Wind field at the 10 m height 00 UTC, December 11, 2001.

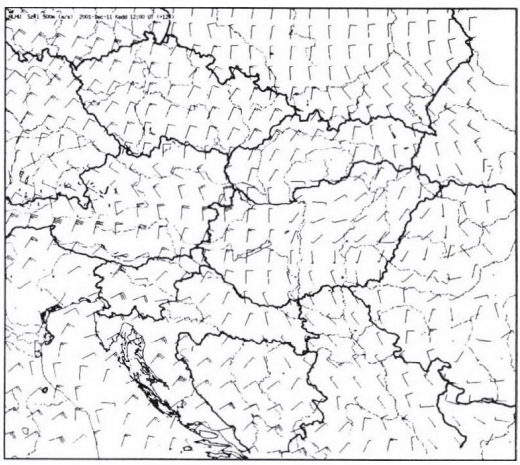

Fig. 5. Wind field at the 500 m height at 00 UTC, December 11, 2001.

4. Concentration fields at different vertical layers

The effect of horizontal and vertical wind fields and horizontal and vertical diffusion was studied in different vertical layers (*Figs. 6* and *7*). During postprocessing of the model, mean air concentration was determined for the standard layer (the average of concentration fields of the 2–5th sigma layers).

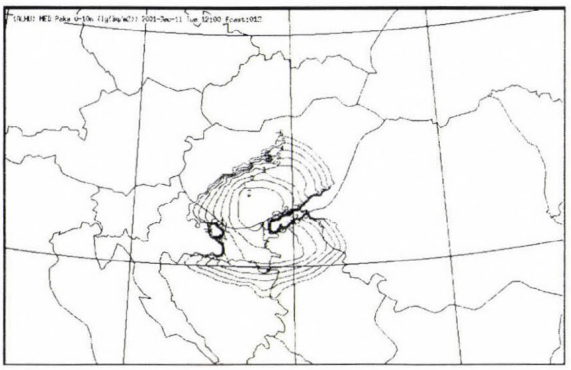

(a) first sigma level, maximum concentration is: 2.00 Bq m^{-3}

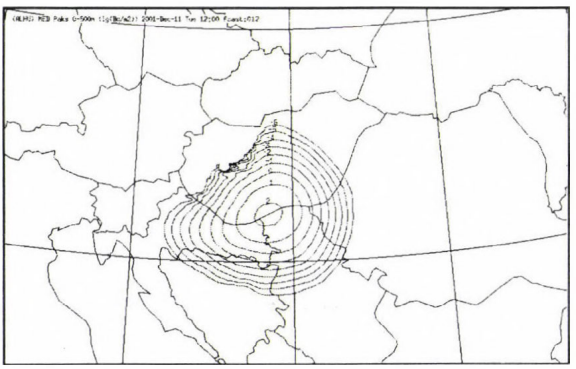

(b) second sigma level, maximum concentration is: 2.18 Bq m^{-3}

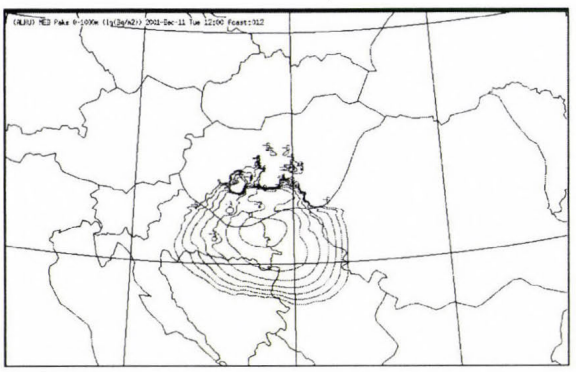

(c) third sigma level, maximum concentration is: 0.62 Bq m^{-3}

Fig. 6. Concentration fields 12 hours after the release at different vertical layers (isolines are $\log_{10}$C, and unit is in Bq m^{-3}) at 12 UTC, December 11, 2001.

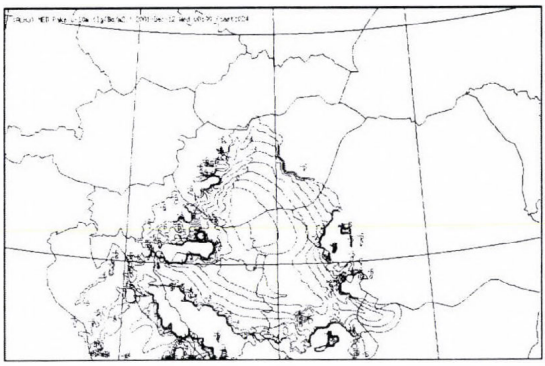

(a) first sigma level, maximum concentration is: 1.69 Bq m^{-3}

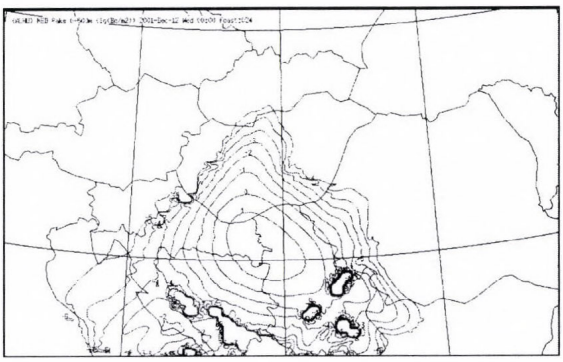

(b) second sigma level, maximum concentration is: 1.85 Bq m^{-3}

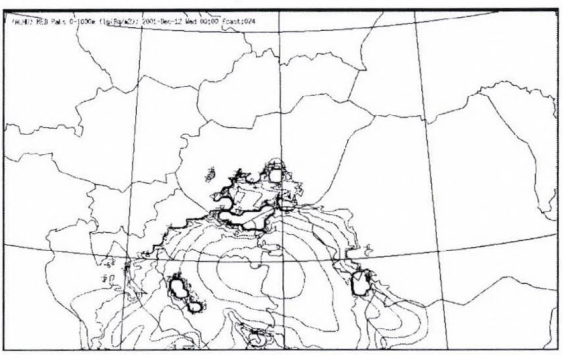

(c) third sigma level, maximum concentration is: 0.72 Bq m^{-3}

Fig. 7. Concentration fields 24 hours after the release at different vertical layers (isolines are $\log_{10}C$, and unit is in Bq m^{-3}) at 00 UTC, December 12, 2001.

In this experiment, this wide layer was divided to four sublayers (the 2nd, 3rd, 4th, and 5th sigma layers were separated). Dividing technique could be important near the surface layer (10–1000 m), because the concentration values here can be much higher than the mean values valid for the standard layer, and this concentration field influences directly the human beings.

The first three sigma layers were analyzed in detail. The effects of the terrain and wind field are reflected in the concentration field of the first sigma layer. 12 hours after the release, the plume covered almost the whole area of Hungary, and caused more than 10^{-10} magnitude of the concentration. 24 hours after the release, the situation in Hungary did not change essentially, but the contamination increased considerably in the countries, which are located in the south direction to Hungary. In the west part of Hungary, there was a significant amount of precipitation during the examination time. 24 hours after the release, the concentration field reflected the effect of wet deposition. The effect of wet and dry deposition will be examined in detail in section 6.

In the upper levels, the effect of the terrain is lower and lower, whilst the effect of the wind field becomes more and more important.

The maximum concentration values decrease continually in the first and second level 6 hours after the release. The situation is much more complex at the upper levels. This complexity can be observed in *Fig. 8*, in the case of station 1 (location of the station can be seen in *Fig. 1*) at the third and forth sigma level. At these upper levels, the shapes of the curves are not Gaussian, like in the lower levels, but they reflect the effect of vertical motion and diffusion.

As it was mentioned in the previous section, in MEDIA the value of the horizontal turbulent diffusion coefficient (K_x, K_y) is consistent with the grid resolution in metres (*Piedelievre et al.*, 1990). Parameterization of horizontal turbulent diffusion coefficient gives an universal solution in this way, when the time and spatial resolution of the driving numerical weather prediction models are different. In the previous version of the model, the values of these coefficients were fixed ($K_x=K_y=10^5$ m^2 s^{-1}) (*Bompay,* 1998). In the long-range dispersion models it is necessary to increase the horizontal diffusion, in order to include the advection fluctuations non-resolved by large-scale meteorological models (*Piedelievre et al.*, 1990). This effect is reflected in our case, when we used MEDIA in regional scale, so our horizontal turbulent diffusion coefficient must be smaller than 10^5 m^2 s^{-1}. In our experiment the grid resolution was 0.1 by 0.15 degrees in latitude and longitude, the north border was 51.4°N, the south border was 42.9°N of the driving model. This model resolution resulted in an $1.04\ 10^4$ - $1.22\ 10^4$ m^2 s^{-1} horizontal diffusion coefficient interval.

Parameterisation of the vertical turbulent diffusion coefficient (K_z) is better known than the horizontal diffusion coefficients. In MEDIA, this parameter depends on the stability of the layer. Determination of $F(R_i)$ is different when the value of R_i is higher (stable) or lower (instable) than zero (Eqs. 7–8). This thing causes that the values of the vertical turbulent diffusion coefficient change in wide scale. In our case, the magnitude of K_z changed from 10^{-15} to 10 $m^2 s^{-1}$.

5. Time series of the concentration values in specified geographical points

Four different geographical points were selected for the analysis of the time series. The first point is located southeast to the source point in the path of the maximum concentration values. The other three points are located 150–250 km far from the source point in different directions (southwest, east and northeast). Location of the source point and the four detection points can be seen in *Fig. 1*.

The figures with concentration fields give complex information about the situation of the pollution. Time series of the concentration values in discrete geographical points can be much more informative than the concentration fields, if we would like to know the time when the polluted cloud reaches or leaves a given town. With this program option we can predict the time series of the concentration values at different vertical levels. The original version of the model did not contain this option, but there were considerable claims to develop this tool. *Figs. 8* and *9* show some examples of application of this useful tool.

The highest values and concentrations were found in the first detector point (*Fig. 8*). In this point the highest concentration was detected at the second sigma layer 11 hours after the release, and after this time the concentration values decreased. The plume moved up in the 500 m height immediately, and from this layer the polluted material mixed up to the higher and lower layers. At every station the highest concentrations were detected at the 500 m height.

At the level of 500 m height, the concentration values were much higher than in the surface layer in the 22 hours interval after the release. After this time the situation was changed, the maximum values of the concentration of polluted material were at the surface layer. The diagrams show the concentration values at the 1000 m and 1500 m heights as well. At these levels the magnitude of concentration values is ten and hundred (or more) times lower than at the surface layer, except at station 3. At this station the highest values were detected at the third sigma layer.

The diagrams pointed that the considerable layer is the second sigma layer. This means that the concentration fields of this level should be visualized. The other important level is the surface level, where the concentrations can be dangerous for the biomass.

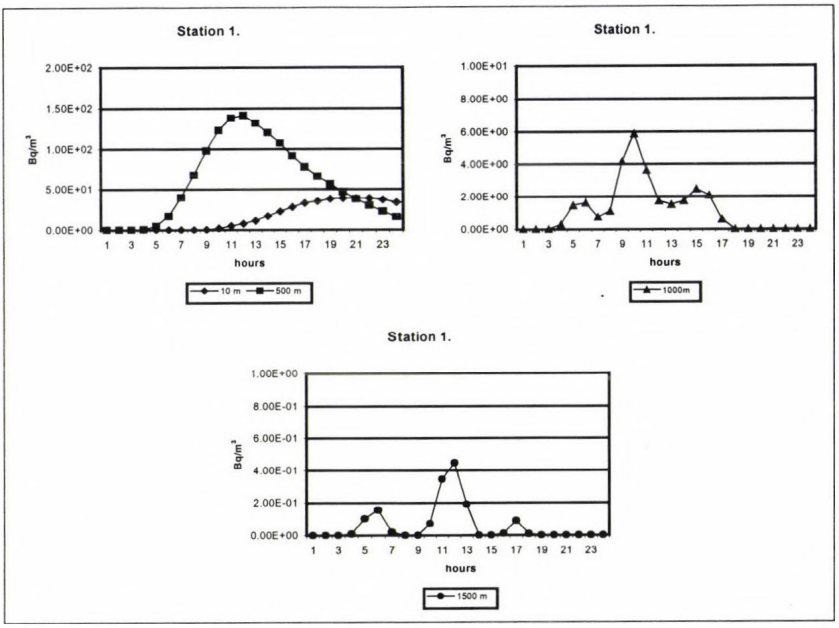

Fig. 8. Time series of calculated concentration on four different levels at station 1.

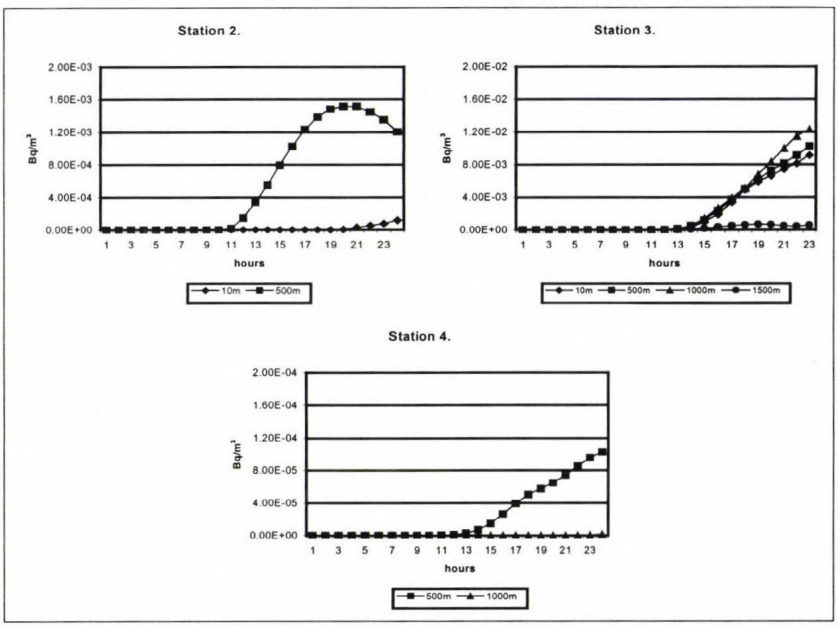

Fig. 9. Time series of calculated concentration on some selected levels at stations 2, 3, and 4.

6. Effects of wet and dry deposition

The deposition of airborne material to the underlying surface can follow two main pathways: dry and wet deposition. A further depletion process, where radionuclides are involved is, of course, the radioactive decay. Removal of material at the surface leads to plume depletion with distance, and to a modified vertical distribution of air concentration.

Dry deposition is the removal of gaseous or particulate material from the atmosphere by the surface or vegetation (or even water surfaces) through processes like absorption, implication, and sedimentation. For the pollutant plume is in contact with the ground, all the particles in the turbulent atmospheric boundary layer constitute a reservoir from which material can be deposited to the surface. This is calculated by means of a deposition velocity, which is related to the resistance of the underlying surface to the transfer. The parameterization of this process was described in section 2. Before running MEDIA, the value of deposition velocity must be set for a given radioactive nuclide emitted into the air.

Wet deposition – the removal of the radionuclides by the action of rain or snow – is a much more important process, and everyone is familiar with the notion of "hot spots" formed where a radioactive plume is intercepted by a burst of rain. There are two processes involved in wet deposition, washout: where pollutants are swept out of the air by falling rain, and the more efficient process of rainout, where the pollutant is taken up by the growing cloud droplets and is subsequently precipitated out. Representative coefficients for scavenging processes for large-scale and convective precipitation were given in the model. The model developers determined these coefficients and we have not changed their values.

In this experiment the influence of wet and dry deposition was studied. In the original version of the model only total (wet+dry) deposition field was produced at the final time step. After modifying the postprocessing scheme, it was possible to study the wet and dry deposition separately. It was found that in case of big amount of precipitation, wet deposition is the determinant process. This was the case in our investigated weather situation. The result can be seen in *Fig. 10.*

In the other case the dry deposition velocity was set to 0 and precipitation was set to 0 mm/12h as well in the grid points of the domain. Air concentration values were significantly higher in any vertical layers, than in normal case. Differences between the maximum concentration values became higher and higher in time.

In this experiment we found that the values of the dry deposition velocity and the intensity of precipitation are determinant in connection with the

concentration and deposition fields. It means that we have to set the value of dry deposition velocity and the intensity of precipitation as accurate as possible to get the best result of simulation.

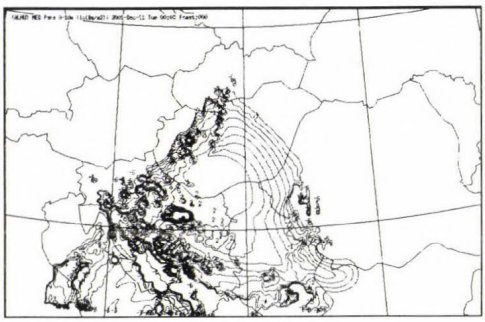

(a) Total deposition

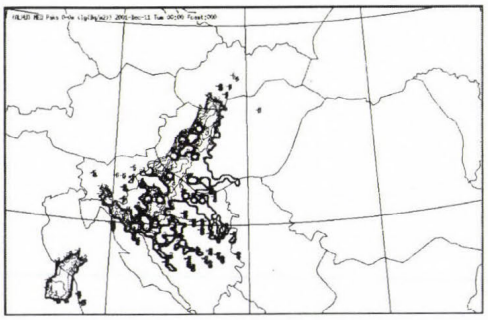

(b) Wet deposition

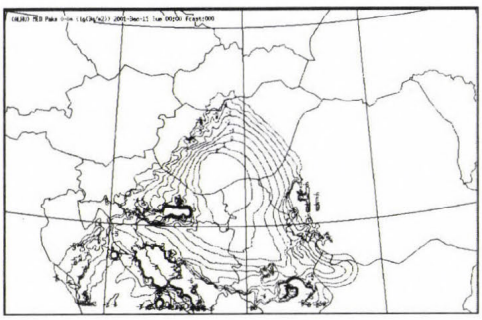

(c) Dry deposition

Fig. 10. Total, wet, and dry, 24-hour deposition fields (isolines are $\log_{10}$C, and unit is in Bq m^{-2}) between 00 UTC, December 12, 2001 and 00 UTC, December 12, 2002.

7. Conclusions

This study demonstrated the capability of MEDIA Eulerian type model to predict the time-evolution of a polluted material in the air considering wet and dry depositions.

Increasing the time and grid resolution of meteorological fields provided an improvement in the time and space resolution of the prediction of concentrations. This information is very important in case of emergency response applications. In the every day routine, ALADIN/LACE or ECMWF numerical weather prediction model results have been used as input meteorological data to drive MEDIA. Since the ALADIN/HU model gives data only for 36 hours with 1 hour time resolution; it could be very important in case of an emergency situation in regional scale, while deterministic ECMWF forecast can be preferable especially in continental scale. Due to the fact that computing capacity was significantly increased at the HMS in 2002, in the near future there is an opportunity to develop ensemble version of MEDIA dispersion model coupled by ECMWF ensemble model.

Acknowledgements–The authors gratefully acknowledge support and encouragement of *Francois Bompay* in Toulouse, and financial support of EU and the French government. Two anonymous referees are thanked for their insightful comments that helped improve the quality of manuscript.

References

Bompay, F., 1998. Evaluation of the METEO-FRANCE response in ETEX release 1. *Atmospheric Environment 32,* 4351-4357.

Galmarini, S., Bianconi R., Bellasio, R., and *Klug, W.*, 2002: ENSEMBLE: A system for ensemble dispersion forecast in case of nuclear emergencies. In *IRPA 2002*, Florence, 8-11 Oct., 2002.

Horányi, A., Ihász, I., and *Radnóti, G.*, 1996: ARPEGE-ALADIN: A numerical weather prediction model for Central-Europe with the participation of the Hungarian Meteorological Service. *Időjárás 100,* 277-300.

Ihász, I., 1992: Isobaric and isentropic objective analysis of meteorological fields for regional and continental scale trajectories. *Időjárás 96,* 81-91.

Ihász, I., 1999: The application of MEDIA dispersion model and 3D trajectory model using ALADIN/LACE, ALADIN/HU and ECMWF model products at the Hungarian Meteorological Service. *Proceedings of the 7th International ALADIN Workshop: Recent and planned operational exploitation of ALADIN model. Operational use and applications, verification. MAP.* 17-19 November 1999, Ljubljana, Slovenia.

Ihász, I., 2000: Large scale modelling of chemical and radioactive pollutant by joint use of ALADIN, ECMWF numerical weather forecasting models and MEDIA dispersion model at the Hungarian Meteorological Service (in Hungarian). In *Meteorológiai Tudományos Napok, 2000: A levegőkörnyezet monitoringja, állapotának értékelése és szabályozása*. Országos Meteorológiai Szolgálat, Budapest, 119-124.

Louis, J.F., 1979: A parametric model of vertical eddy fluxes in the atmosphere. *Boundary Layer Meteorology 17,* 187-202

Piedelievre, J.P., Musson-Genon, L., and *Bompay, F.,* 1990: MEDIA – An eulerian model of atmospheric dispersion: first validation on Chernobyl release. *J. of Applied Meteorology 29,* 1205-1220.

White, P., 2000a: IFS Documentation Part I: Observation Processing (CY21R4). *Meteorological Bulletin M1.5/2,* ECMWF, Shinfield Park, Reading, March 2000.

White, P., 2000b: IFS Documentation Part II: Data Assimilation (CY21R4). *Meteorological Bulletin M1.5/3*, ECMWF, Shinfield Park, Reading, February 2000.

White, P., 2000c: IFS Documentation Part III: Dynamics and Numerical Procedures (CY21R4). *Meteorological Bulletin M1.6/4*, ECMWF, Shinfield Park, Reading, March 2000.

White, P., 2000d: IFS Documentation Part V: The Ensemble Prediction System (CY21R4). *Meteorological Bulletin M1.6/6*, ECMWF, Shinfield Park, Reading, March 2000.

White, P., 2000e: IFS Documentation Part VI: Technical and Computational Procedures (CY21R4). *Meteorological Bulletin M1.6/7*, ECMWF, Shinfield Park, Reading, March 2000.

IDŐJÁRÁS

Quarterly Journal of the Hungarian Meteorological Service
Vol. 107, No. 2, April–June 2003, pp. 133–152

Surface ozone observations over Egypt

F. M. El-Hussainy[1], **W. M. Sharobiem**[2], and **M. D. Ahmed**[2]

[1]*Faculty of Science, Al-Azhar University, P.O. Box 11884, Cairo, Egypt; E-mail: el_hussainy@hotmail.com*

[2]*Meteorological Authority, P.O. Box 11784, Cairo, Egypt; E-mail: wafiek@yahoo.com*

(Manuscript received June 22, 2001; in final form January 21, 2002)

Abstract—Hourly data of surface ozone measurements at Cairo, Sidi Branni, and Hurghada were taken to compare the ozone concentration of polluted area with that of rural areas. The study showed that the maximum value of surface ozone concentration appears in the afternoon in all regions. While the maximum concentration of surface ozone appears in spring at Sidi Branni, and in summer at Cairo and Hurghada. Also, daily and monthly relationships between surface ozone and some meteorological elements were performed. Strong relationships between surface ozone and solar radiation were found for Cairo and Hurghada. Also, positive trend for surface ozone against wind speed was found in all regions.

Key-words: tropospheric ozone, regional pollution.

1. Introduction

Like water, ozone can be useful or dangerous atmospheric component, depending on the place and amount of it. Ozone in the stratosphere is very important as it acts as a shield for the mother planet, the Earth, and protects us against harmful UV-B radiation coming from the sun. However, the ozone in the atmosphere is a greenhouse gas, trapping the long wave radiation in 9.6 μm band, affecting the energy budget of the earth-atmosphere system. It is also a pollutant that is produced as a result of antropogenic activities such as fossil fuel burning, and has potential to affect human health (*Lippman,* 1989; *Tilton*, 1989), vegetation (*Woodman*, 1987) and animals (*Costa et al.*, 1989), if it is allowed to attain high concentration. It has been observed that the amount of ozone at the surface is increasing while in the stratosphere is decreasing with anthropogenic activities, and it is a serious problem (*Randriambelo et al.*, 1999).

Ozone close to the ground is produced on the account of photochemical reactions involving oxides of nitrogen, hydrocarbons, and sunlight. High ozone concentration at a particular place depends on the concentration of oxides of nitrogen and hydrocarbons. The source of oxides of nitrogen may be local or they can be transported from another source areas. Therefore, the monitoring of ozone concentration is very important, as it provides information about its formation, scavenging, and transport at a site or within an area (*Jain* and *Arya*, 2000).

Ozone measurements in the Mediterranean region (*Butkovic et al.*, 1990) indicate serious problems of photochemical air pollution in areas with more sunny days per year than in Central Europe. The special meteorological conditions, dominating almost in the whole year over the eastern Mediterranean (intensive sunlight, high temperatures, etc.), can enhance photochemistry and biogenic volatile organic compound emission into the atmosphere, and combined with low deposition velocities over the sea, they result in high ozone levels (*Kouvarakis et al.*, 2000; *Johnson et al.*, 2000).

Tropospheric ozone concentration in the tropics is believed to be low as compared to those in middle latitudes, because of inactive transport from stratosphere to troposphere (*Routhier et al.*, 1980). However, tropospheric ozone is supplied by photochemical reactions as well as transport from the stratosphere. We expect high photochemical activity in the tropics, where the solar radiation is intense. The land area provides potential sources for the precursor species of surface ozone formation in the tropics (*Crutzen et al.*, 1985), while the ocean does not seem to be a source (*Helas* and *Warneck*, 1981). Tropospheric ozone data imply that the marine air is lean in ozone (*Piotrowice et al.*, 1986).

Ozone formation in the greater Cairo (Egypt) area was studied in 1990 in a three weeks measurement period performed at three sites (Shoubra El-Khema, Mokattam Hill, and Helwan), covering a north–south direction of 27 km long. In 1991, from the beginning of April until the end of October, ozone was studied by measuring the seasonal variation of ozone at one site at El-Quobba (*Gusten et al.*, 1994). The sinusoidal shape in the diurnal volume fraction plots with peak values of 120 ppb and daily mean value of 50 ppb throughout the year indicates a substantial contribution of photochemical reactions to the ozone content of the atmosphere. Ozone is produced predominantly over the industrial area in the north and in the center of Cairo, and transported southward by the prevailing northerly winds. Contrary to many urban areas in Europe and North America, fairly high average ozone levels of 40 ppb are observed during the night in spring and summer. This may imply that health hazards and crop damages are higher in the greater Cairo area than in Central Europe.

This paper presents a comparative study between the formation and variation of surface ozone in a polluted area (Cairo) and rural areas (Sidi Branni and Hurghada). Also, it discusses the relationships between the surface ozone and each of the solar radiation, air temperature, wind, and relative humidity.

2. Observation sites and data

Hourly data of surface ozone (measured by Ozone Analyzer Model 49 manufactured by Thermo Environmental Inc.), solar radiation (measured by Epply Pyranometer), relative humidity, surface wind, and temperature at Cairo, Sidi Branni, and Hurghada are taken in the periods indicated in *Table 1*.

Table 1. Measuring period of the data with the latitude, longitude, and altitude of the stations

Stations	Latitude	Longitude	Altitude	Period
Cairo	30°02'N	31°12'E	16 meters	January–December 1999
Sidi Branni	31°22'N	25°32'E	24 meters	September 1999–August 2000
Hurghada	27°17'N	33°45'E	06 meters	October 1995–September 1996

Fig. 1 shows the location of surface ozone stations (Hurghada lies at the Red Sea and Sidi Branni at the Mediterranean Sea).

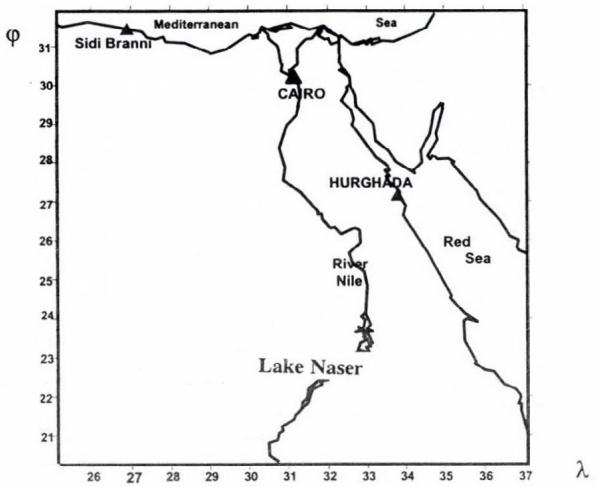

Fig. 1. Surface ozone stations in Egypt.

The Cairo station situates inside the buildings of Cairo University. Cairo encompasses 27% of the Egyptian population, 64% of the industry, and 45% of the motor vehicles. It is clear that the population of Cairo is exposed to an alarming level of air pollution (*Gusten et al.*, 1994). Hurghada station lies near the Red Sea, south from the natural gas burning at Ras Garb, Ras Shocker, and Oil Gulf regions, which extend from 70 to 150 km. Sidi Branni is a flat sandy area at the coast of the Mediterranean Sea. There is no industry in Sidi Branni with small population and few cars and trucks.

Table 2a–c represent the descriptive statistics for all measurements at Cairo, Sidi Branni, and Hurghada, respectively.

Table 2a. Descriptive statistics for daily data measured at Cairo

Elements	Number of valid obs.	Std. deviation	Mean value	Maximum value	Minimum value
Solar radiation (MJ/m^2/day)	256	6.61	19.43	29.00	4.90
Wind speed (m/s)	256	1.59	4.00	8.10	0.90
Rel. humidity (%)	256	7.13	65	89	47
Temperature (°C)	256	5.70	22.50	32.20	12.40
Surface ozone (ppb)	256	23.09	40.40	97.49	5.00

Table 2b. Descriptive statistics for daily data measured at Sidi Branni

Elements	Number of valid obs.	Std. deviation	Mean value	Maximum value	Minimum value
Solar radiation (MJ/m^2/day)	366	8.01	21.41	33.20	1.60
Wind speed (m/s)	366	2.49	4.23	16.80	1.00
Rel. humidity (%)	366	11.31	44	80	16
Temperature (°C)	366	4.90	21.60	34.70	10.60
Surface ozone (ppb)	366	6.58	48.56	70.59	27.90

Table 2c. Descriptive statistics for daily data measured at Hurghada

Elements	Number of valid obs.	Std. deviation	Mean value	Maximum value	Minimum value
Solar radiation (MJ/m^2/day)	365	7.43	22.55	32.68	1.96
Wind speed (m/s)	365	1.54	5.87	9.60	2.90
Rel. humidity (%)	365	12.76	39	75	14
Temperature (°C)	365	5.80	23.40	36.30	13.00
Surface ozone (ppb)	365	7.88	41.94	62.80	21.20

3. Results and discussion

Surface ozone has been measured on round the clock basis. According to *Table 1*, ozone was measured during different periods at the different locations using ozone analyzer to study diurnal as well as seasonal variation.

3.1 Diurnal variation of surface ozone concentration

The diurnal variation of surface ozone observed at Cairo, Sidi Branni and Hurghada is depicted in *Figs. 2a–e*. *Fig. 2a* represents the diurnal variation of average surface ozone concentration, while *Figs. 2b–e* represent the diurnal variation of seasonal surface ozone concentration in spring, summer, autumn, and winter, respectively.

There is a wide range between the day and night values of ozone at Cairo comparing to the other stations. This is due to the urbanization effect at Cairo (big industrial area) including the increasing vehicular traffic and big industries. Whereas Sidi Branni and Hurghada are considerable as rural regions with less human activities.

Generally, the minimum value of ozone concentration occurs in the early morning hours (before dawn at Hurghada), and its maximum occurs at around noon (late afternoon at Sidi Branni). The pattern of diurnal variation of surface ozone at Cairo results from daytime photochemical production and downward transport of ozone rich air from above, combined with ozone loss by dry deposition and reaction with nitric oxide (NO) at night, when photochemical production ceases and vertical transport is inhibited by an inversion of the normal temperature profile. In locations near large sources of NO (e.g., Cairo), the nighttime minimum in ozone can be quite pronounced (see *Table 2a*), because of the rapid reaction between ozone and NO. In fact, in many urban areas the NO source is strong enough to cause the complete nighttime disappearance of ozone (*Seinfeld* and *Spyros,* 1998). In addition to variations over a diurnal cycle, ozone concentration at these locations also can vary significantly from one day to the next, in particular, Cairo location has the maximum variation as indicated in *Table 2a*. It is not uncommon, for the daily maximum ozone concentration at an urban site (like Cairo), for instance, can vary by factor 2 or 3 from day to day, as local meteorological conditions change.

The maximum of the diurnal variation of surface ozone at Hurghada occurs at around 12:00 GMT. This is a typical type but its variation is not so big as in Cairo, which indicates that the photochemical activity is smaller. The diurnal variation changes from day to day due to advected ozone that produced from sources in north Hurghada (natural gas burning). Whereas, the diurnal variation of surface ozone in Sidi Branni is very little. This is because the

photochemical activity is smaller due to clean air conditions in this region (no human activities). But it is mainly vertically transported from the upper troposphere and has no definite pattern.

(a)

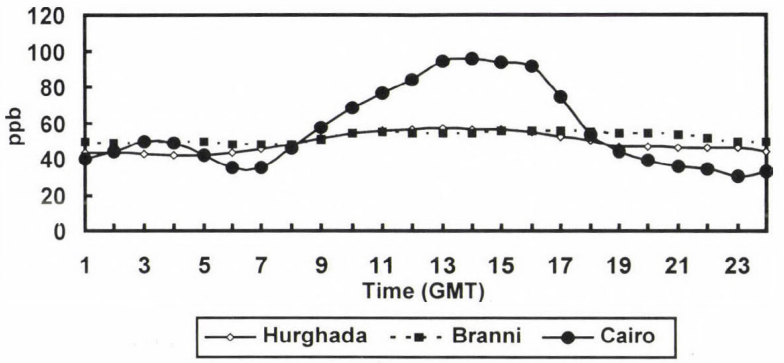

(b)

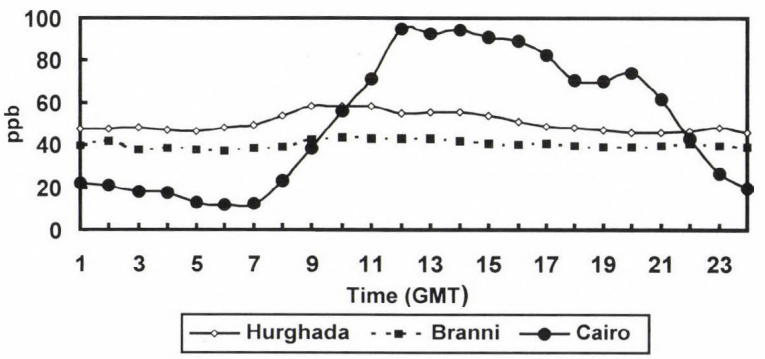

(c)

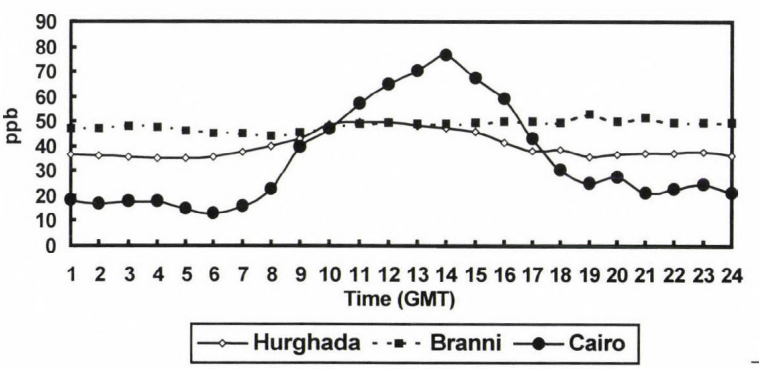

→

(d)

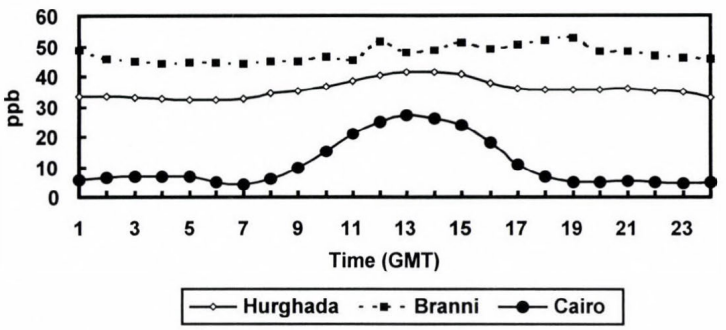

Fig. 2. Diurnal variation of surface ozone in Egypt (*a*) in spring, (*b*) in summer, (*c*) in autumn, (*d*) in winter.

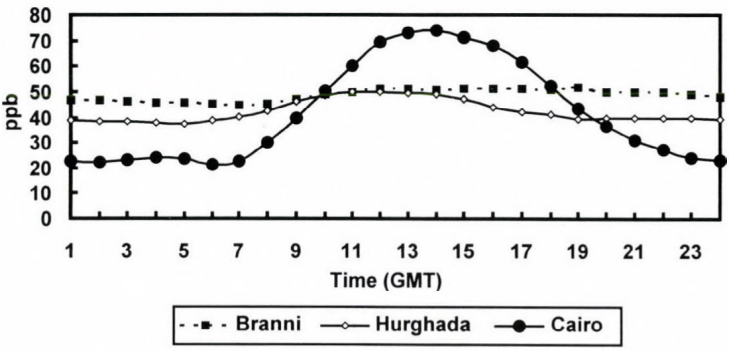

Fig. 2e. Diurnal variation of average surface ozone in Egypt.

On seasonal basis, surface ozone has small concentration at Cairo in wintertime. This is due to low solar radiation intensity and high emissions of reductive substances like NO. The latter characterizes the city all year. In contrast, the other stations do not depend on the effect of photochemical reactions as mentioned before. In spring, the pattern for Cairo goes up to higher concentrations, in particular daytime, due to the increasing solar radiation intensity. In summer and autumn the patterns of surface ozone concentration at Cairo seem to be the same.

3.2 Monthly variation of surface ozone concentration

The monthly average variation of surface ozone concentration at Cairo, Sidi Branni, and Hurghada are depicted in *Fig. 3a*. The variation of maximum and minimum values of surface ozone concentration at Cairo, Sidi Branni, and Hurghada are depicted in *Figs. 3b* and *3c*.

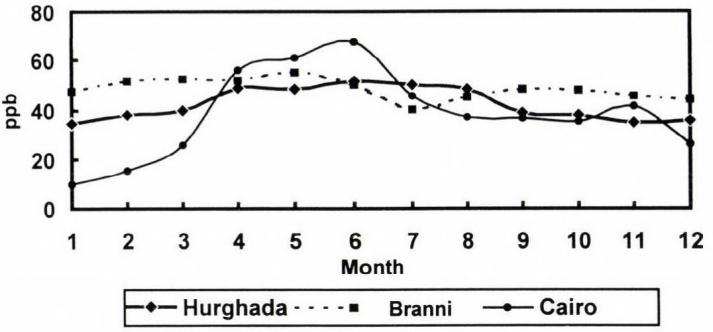

Fig. 3a. Monthly variation of average surface ozone in Egypt.

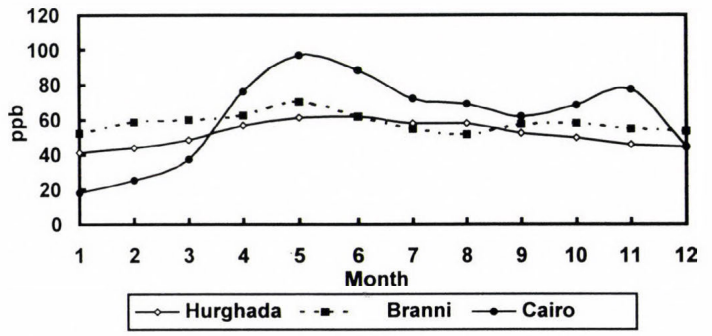

Fig. 3b. Monthly variation of maximum surface ozone in Egypt.

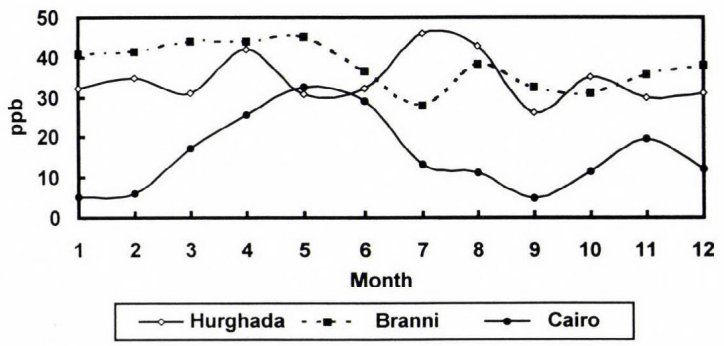

Fig. 3c. Monthly variation of minimum surface ozone in Egypt.

Fig. 3a shows that Cairo has a maximum concentration in June and the minimum occurs in January. This follows the seasonal solar radiation cycle.

A secondary maximum in November seems to appear occasionally, due to rice straw burning in 1999. Monthly variation at Hurghada mainly depends on solar intensity change from summer to winter. Sidi Branni has a maximum in spring, and the minimum occurs in July. The spring maximum follows the seasonal variation of total amount of ozone in middle latitudes, while the minimum occurs due to northerly wind, which blows from the Mediterranean Sea.

It can be noticed, that Cairo has the same pattern with large amplitude (see *Figs. 3b* and *3c*). The maximum pattern for Hurghada and Sidi Branni takes the same shape as the average pattern, but the minimum pattern for each station has no definite aspect.

In spite of low human activity at Sidi Branni, the concentration of surface ozone is higher than the background stations in Europe, which varies from 20 to 40 ppb. This is due to the permanent subtropical high pressure with the subsidence of air, which causes the intrusion of surface ozone from higher altitudes to the surface.

3.3 Relationship between surface ozone and solar radiation

As proposed by *Frenkiel* (1959), the main source reaction for photochemically produced ozone is photodissociation of NO_2 by solar radiation with wavelength $\lambda < 400$ nm

$$NO_2 + h\nu \rightarrow NO + O\,(^3P) \qquad \lambda < 400 \text{ nm}. \tag{1}$$

This reaction provides the needed O atoms for ozone production. The UV (ultraviolet) portion is about 3–4% of total global radiation. Strong relationship between UV radiation and global solar radiation over Cairo was found by *El-Hussainy* (1986). Therefore, global solar radiation can be used because UV radiation measurements are not available at all stations in Egypt.

Figs. 4.a1, 4.b1, and *4.c1* show the monthly variation of surface ozone concentration and solar radiation at Cairo, Sidi Branni, and Hurghada, respectively, while *Figs. 4.a2, 4.b2*, and *4.c2* represent the relation between surface ozone concentration and solar radiation at these stations.

Table 3 gives the daily correlation between surface ozone concentration and global solar radiation at Cairo, Sidi Branni, and Hurghada. There is a significant relation at Cairo and Hurghada with 1% significance level, while for Sidi Branni there is no significant relation (with 5% significance level). This indicates that the surface ozone concentration in Cairo and Hurghada depend on the photochemical reactions producing surface ozone. Also, the family of curves (*Figs. 4.a1, 4.b1, 4.c1*) and trends (*Figs. 4.a2, 4.b2, 4.c2*) are ascertained the above fact. The trend line for Sidi Branni shows that the vertical transport of ozone from the upper troposphere is the effective source.

(a1)

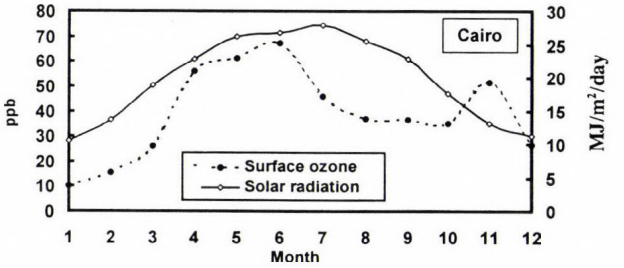

(b1)

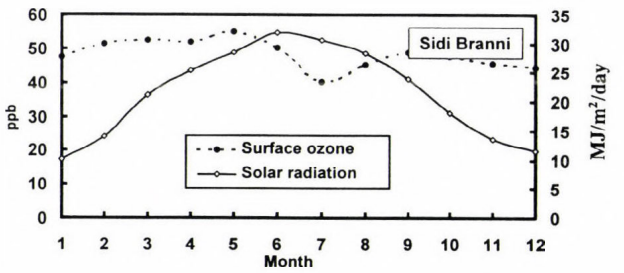

(c1)

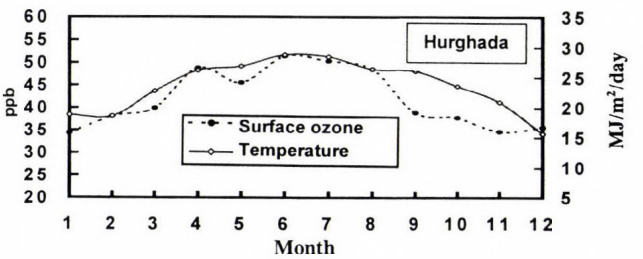

Fig. 4.a1–c1. Monthly variation of surface ozone and solar radiation at Cairo, Sidi Branni, and Hurghada.

(a2)

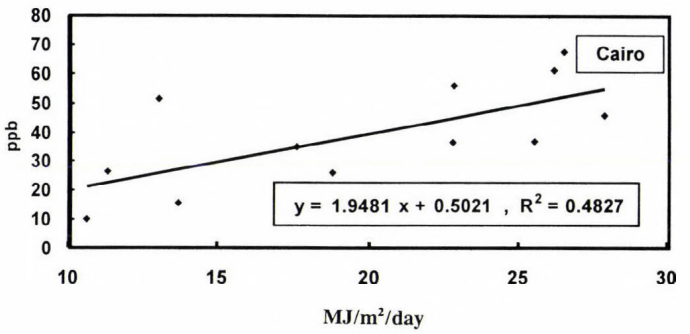

→

(b2)

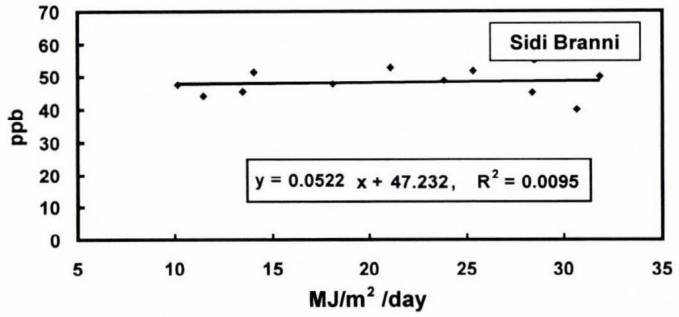

(c2)

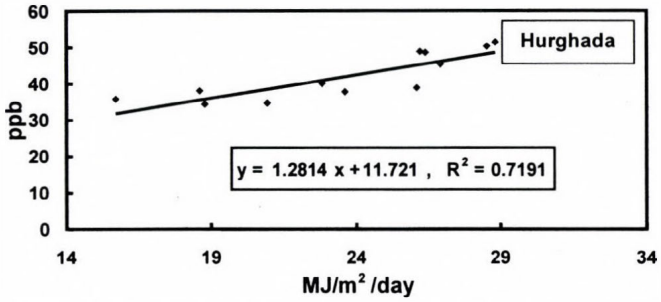

Fig. 4.a2–c2. Relation between surface ozone and solar radiation at Cairo, Sidi Branni, and Hurghada.

Table 3. Correlation coefficients between surface ozone against relative humidity, wind speed, temperature and solar radiation at Cairo, Sidi Branni, and Hurghada

Daily correlation	Rel. humidity	Wind speed	Temperature	Solar radiation	All*
Ozone (Cairo)	-0.26	+0.37	+0.54	+0.59	0.61
Ozone (Sidi Branni)	-0.12	+0.11	-0.27	+0.05	0.40
Ozone (Hurghada)	-0.54	+0.15	+0.53	+0.53	0.40

*All: multiple correlation for all elements with surface ozone

3.4 Relationship between surface ozone and surface wind

We are aware that surface wind is only a rough approximation of horizontal transport of ozone and its precursors. The situation becomes even more complicated, because solar radiation should play an important role in the photochemical ozone production. *Figs. 5.a1, 5.b1*, and *5.c1* represent the monthly variation of surface ozone and wind speed at Cairo, Sidi Branni, and

Hurghada, respectively, while *Figs. 5.a2, 5.b2*, and *5.c2* show the relation between surface ozone and wind speed at the same stations. On monthly basis, it is noticed from these figures, that there is a positive correlation between the surface ozone concentration and surface wind speeds in the range of 2–7 m/s. The noticeably clear correlation at Cairo is due to several existing sources of pollutants. On daily basis, it is noticed from *Table 3* that there is a negative correlation with a significant level better than 1 % for Cairo and Hurghada, and there is no significant correlation for Sidi Branni.

(a1)

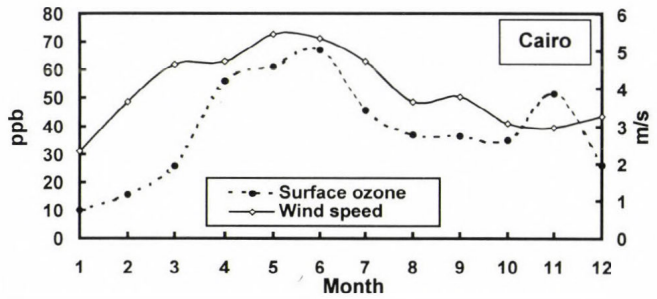

(b1)

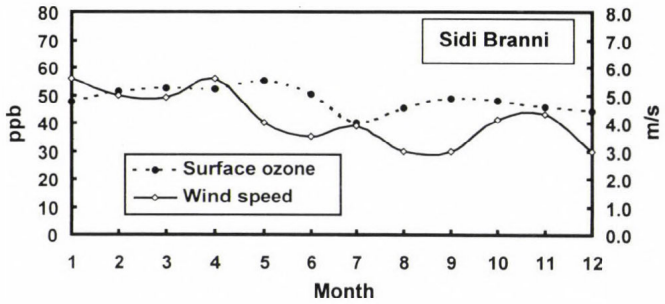

(c1)

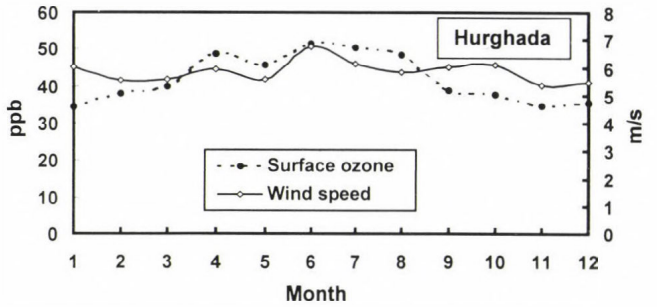

Fig. 5.a1–c1. Monthly variation of surface ozone and wind speed at Cairo, Sidi Branni and Hurghada.

(a2)

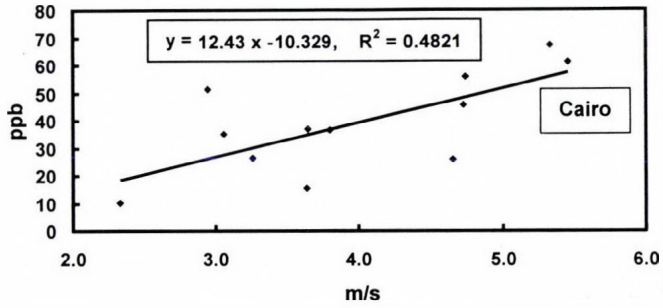

(b2)

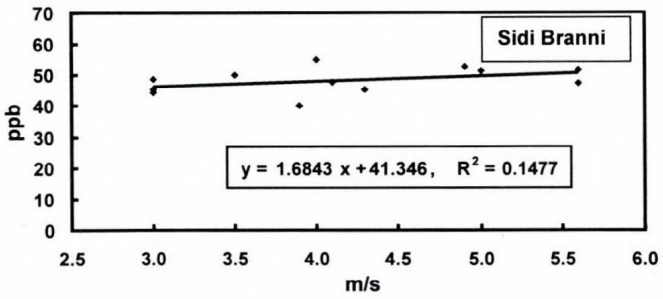

(c2)

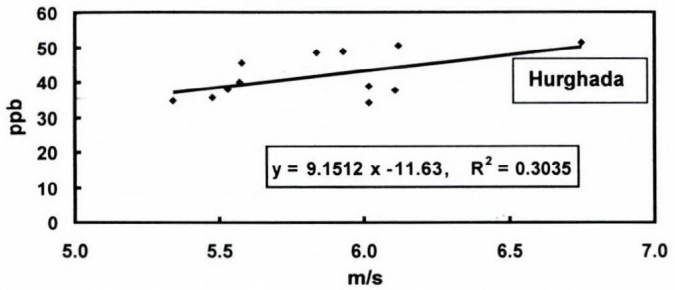

Fig. 5.a2–c2. Relation between surface ozone and wind speed at Cairo, Sidi Branni, and Hurghada.

Fig. 5d shows that for Hurghada the surface ozone concentration takes high values when the wind direction is northeast, while low values of surface ozone concentration occur when the wind is northwest. At Sidi Branni, the surface ozone concentration takes low values when the wind direction is north or northeast, and high values occur when the wind is southeast or northwest. The wind direction is not significant for concentration of surface ozone at Sidi Branni. For Cairo, high values of surface ozone concentration occur when the wind direction is northwest and low values occur at northeast, wind (see *Gusten et al.*, 1994).

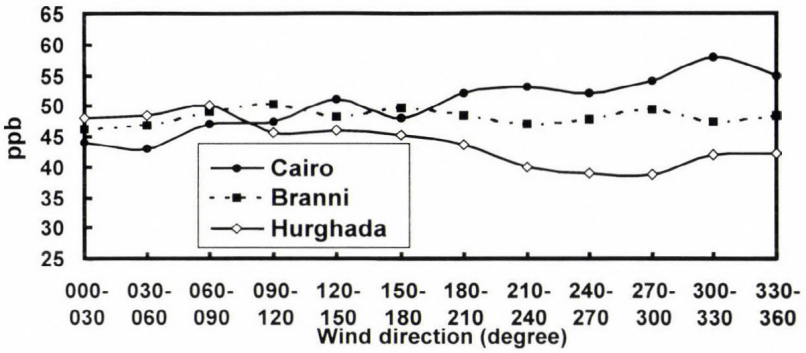

Fig. 5d. Variation of surface ozone and wind direction at Egypt.

3.5 Relationship between surface ozone and relative humidity

The principal photochemical sink of O_3 in the troposphere can be written by the following reactions:

$$O_3 + h\nu \rightarrow O(^1D) + O_2, \quad (2)$$

$$O(^1D) + M \rightarrow O + M, \quad (3)$$

$$O(^1D) + H_2O \rightarrow 2OH. \quad (4)$$

Since this removal path depends on the concentration of water vapor, it is most effective at low latitudes and low altitudes, where the radiation is intense and the humidity is high. Ozone destruction occurs whenever an $O(^1D)$ reacts with H_2O, since this removes $O(^1D)$ from the system; otherwise $O(^1D)$ is just quenched back to O in reaction (2), and O immediately reforms O_3 by reaction:

$$O + O_2 + M \rightarrow O_3 + M, \quad (5)$$

where M represents N_2, O_2 or another third molecule that absorbs the excess vibrational energy and thereby stabilizes the O_3 molecule formed (*Seinfeld* and *Spyros*, 1998).

Figs. 6.a1, 6.b1, and *6.c1* represent the monthly variation of surface ozone and relative humidity at Cairo, Sidi Branni, and Hurghada, respectively, while *Figs. 6.a2, 6.b2*, and *6.c2* show the relation between surface ozone and relative humidity at the same stations. There is a negative trend for the surface ozone against relative humidity, which is in agreement with the findings by *Seinfeld* and *Spyros* (1998).

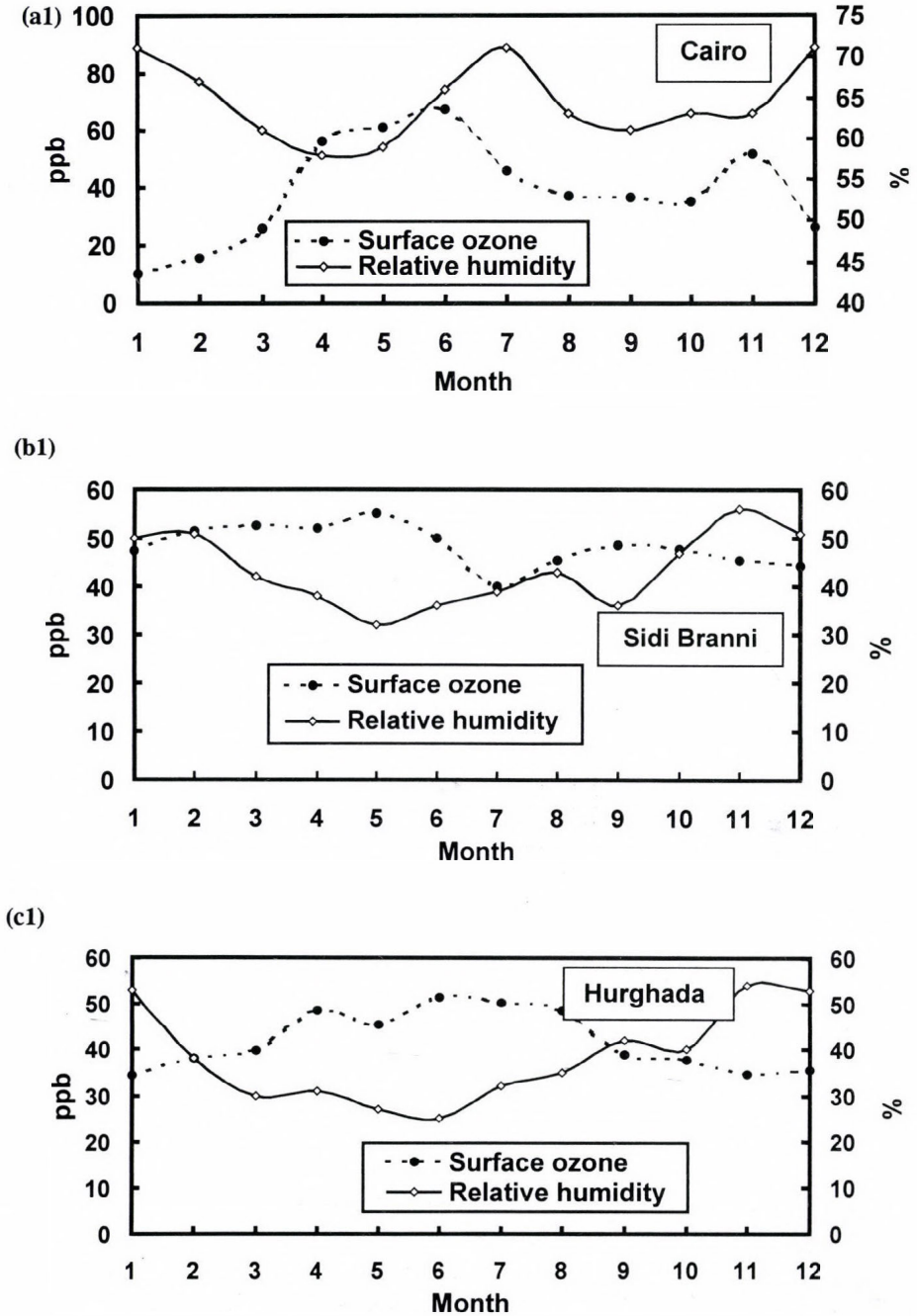

Fig. 6.a1–c1. Monthly variation of surface ozone and relative humidity.

(a2)

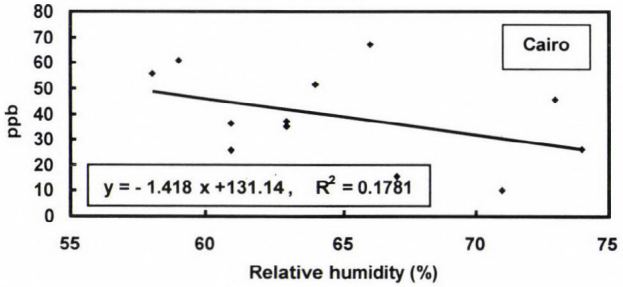

(b2)

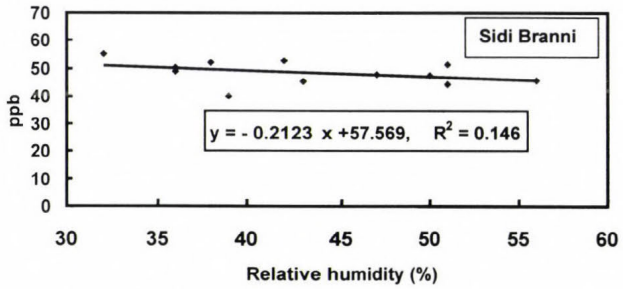

(c2)

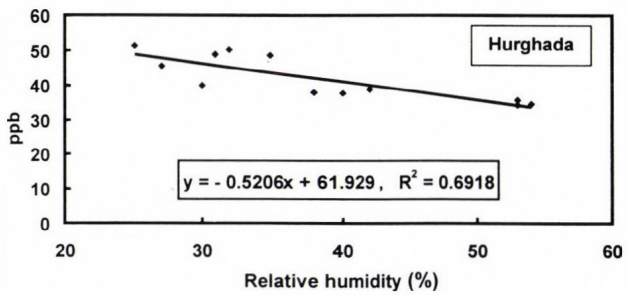

Fig. 6.a2–c2. Relation between surface ozone and relative humidity.

3.6 Relationship between surface ozone and temperature

Figs. 7.a1, 7.b1, and *7.c1* represent the monthly variation of surface ozone concentration and temperature at Cairo, Sidi Branni, and Hurghada, respectively, while *Figs. 7.a2, 7.b2*, and *7.c2* show the relation between surface ozone and temperature at the same stations. It is noticed, that there is a strong similarity among the family of curves, trends, correlation of surface ozone concentration against surface air temperature, and correlation of surface ozone concentration against solar radiation. This is due to the strong relationship between solar radiation and air temperature over Egypt (*El-Hussainy* and *Essa*, 1997).

(a1)

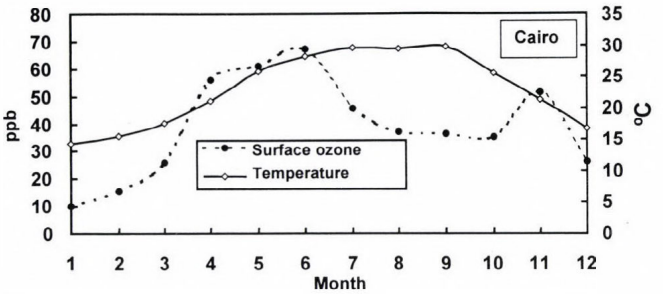

(b1)

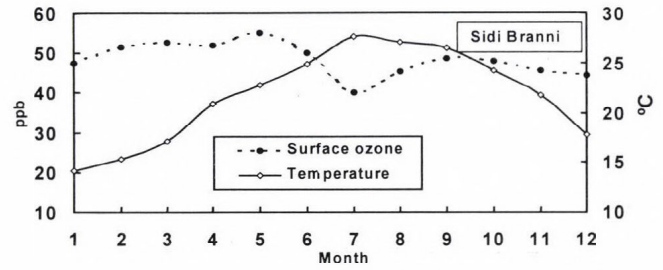

(c1)

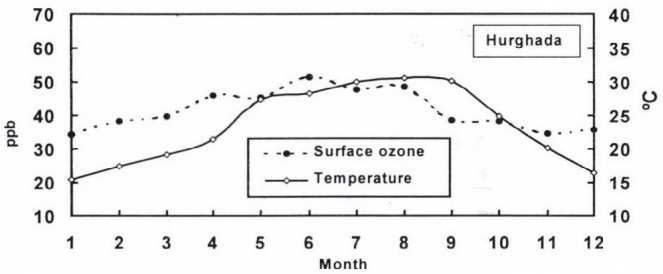

Fig. 7.a1-c1. Monthly variation of surface ozone and temperature.

(a2)

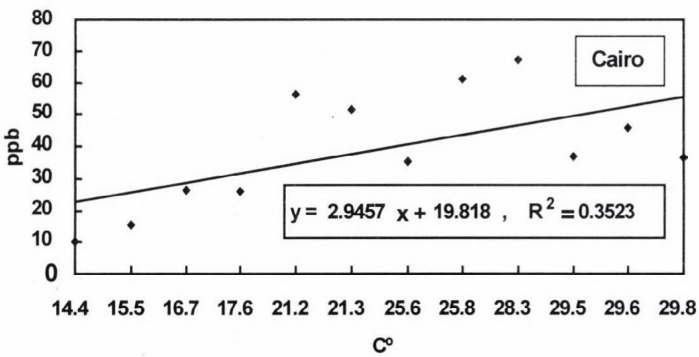

→

(b2)

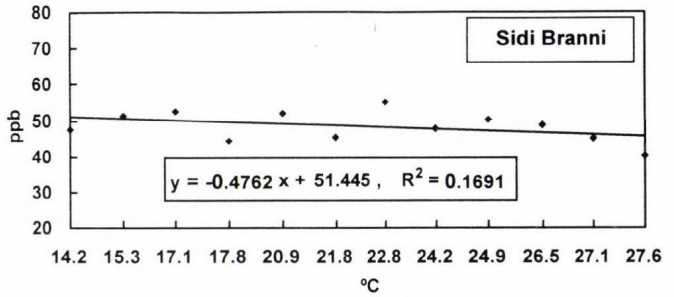

(c2)

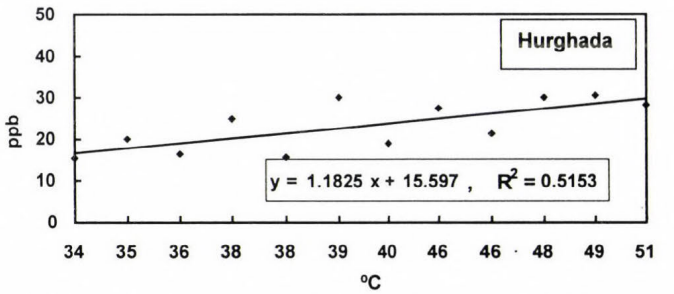

Fig. 7.a2–c2. Relation between surface ozone and temperature.

3.7 Relative importance of different weather elements affecting surface ozone

The relative importance of solar radiation (R), air temperature (T), relative humidity (H), wind speed (S), and wind direction (D) in the formation of surface ozone (Z) will be studied by using multiple regression analysis (*Snedecor* and *Cochran,* 1980) as

$$Z = b_0 + b_1 X_1 + b_2 X_2 + b_3 X_3 + b_4 X_4 + b_5 X_5 + E, \tag{6}$$

where X_1 , X_2 , X_3 , X_4, and X_5 represent R, T, H, S, and D, respectively. E represents the residual (errors).

The equations for Cairo, Sidi Branni, and Hurghada, respectively, are

$$Z = 16.39 + 2.40R + 1.71T - 0.48H + 2.60S, \tag{6a}$$
$$Z = 59.83 + 0.25R - 0.65T - 0.06H + 0.03S, \tag{6b}$$
$$Z = 45.48 + 0.16R + 0.29T - 0.19H + 1.12S - 0.05D. \tag{6c}$$

The standard deviation of errors for Eqs. (6a) to (6c) are 6.01, 6.08, and 5.94, respectively.

The variance for Eq. (6) is

$$\sigma^2_Z = b^2_1\,\sigma^2_1 + b^2_2\,\sigma^2_2 + b^2_3\,\sigma^2_3 + b^2_4\,\sigma^2_4 + b^2_5\,\sigma^2_5 + \sigma^2,$$

where σ^2_i denotes the variance of X_I, and σ^2 denotes the variance of the residual.

The quantity $b^2_I\,\sigma^2_i\,/\sigma^2_Z$ measures the fraction of the variance of Z (surface ozone) attributable to its linear regression on X_i. This fraction can reasonably be regarded as measure of the relative importance of X_I as shown in *Table 4*.

Table 4. Relative importance of different weather elements affecting surface ozone formation at Cairo, Sidi Branni, and Hurghada

Stations	Wind direction	Wind speed	Relative humidity	Temperature	Solar radiation	Residual
Cairo	0.00	0.01	0.05	0.15	0.23	0.56
Sidi Branni	0.00	0.00	0.01	0.22	0.07	0.71
Hurghada	0.06	0.06	0.12	0.06	0.01	0.70

Cairo and Sidi Branni have lowest values in wind speed and direction. This means that wind speed and direction have high relative importance in the formation of surface ozone concentration. While the solar radiation has high relative importance at Hurghada.

4. Conclusions

It is found that photochemical reactions are the effective sources at Cairo and mainly at Hurghada, whereas the upper troposphere is the effective source at Sidi Branni. Higher values of concentration of surface ozone at Sidi Branni and Hurghada comparing to Europe (20–40 ppb) are due to the Azores high belt, which lies at this area making large scale subsidence which causes the transportation of ozone from upper air. For areas of anthropogenic activity (Cairo), the amplitude of diurnal variation is large, and concentrations at daytime can affect the human health (i.e., concentration exceeding 80 ppb).

There is a positive/negative trend for surface ozone concentration against solar radiation/relative humidity for all stations. The relation between wind speed and surface ozone concentration takes a positive trend in the range of 2-7 m/s.

Acknowledgements–The authors thank the Egyptian Meteorological Authority for the data and valuable assistance to prepare this material. Also, thank *Dr. A. S. Zaki* and *Mr. M. A. Dawood* for cooperation and help.

References

Butkovic, V., Cvitas, T., and *Klasinc, L.,* 1990: Photochemical ozone in the Mediterranean. *Sci. Total Environ. 99,* 145-151.

Costal, D.L., Highfill, E.G., Stevens, J., and *Tepper, J.S.,* 1989: Pulmonary function studies in the rate addressing concentration versus time relationship of ozone. In *Atmospheric Ozone Research and its Policy Implications* (eds.: *T. Schneider, S.D. Lee, G.J.R. Wolters* and *L.D. Grant*), 733-743.

Crutzen, P.J., Delany, A.C., Greenberg, J., Haagenson, P., Heidt, L., Lueh, R., Pollack, W., Seiler, W., Wurthurg, A., and *Zimmeimem, P.,* 1985: Tropospheric chemical composition measurement in Brazil during the dry season. *J. Atmos. Chem. 2,* 233-256.

El-Hussainy, F.M., 1986: The spectral composition of the global solar radiation at Cairo and Bahtim. *ASRE 86, 1,* 13-23 *March* 1986, *Cairo, Egypt.*

El-Hussainy, F.M. and *Essa, K.S.M.,* 1997: The phase lag of temperature behind global solar radiation over Egypt. *Theor. Appl. Climatol. 58,* 79-86.

Frenkiel, F.N., 1959: Tropospheric ozone. Symposium on Atmospheric Ozone. July 1959, Oxford. *IUGG Monograph* No. 3, 33-36.

Gusten, H., Heinrich, G., Weppner, J., Abdel-Aal, M.M., Abdel-Hay, F.A., Ramadan, A.B., Tawfik, F.S., Ahmed, D.M., Hassan, G., Cvitas, T., Jeftic, J., and *Klasinc, L.,* 1994: Ozone formation in the greater Cairo area. *The Science of the Total Environment 155,* 285-295.

Helas, G. and *Warneck, P.,* 1981: Background NO_x mixing ratio in air masses over North Atlantic Ocean. *J. Geophys. Res. 86,* 7283-7290.

Jain, S.L. and *Arya, B.C., 2000*: Measurement of surface ozone at NPL, New Delhi. *Q. Ozone Symposium. Atmospheric Ozone.* July 2000, Sapporo, Japan.

Jonson J.E., Kylling, A., Berntsen, T., Isaksen, I.S.A., Zerefos, C.S., and *Kourtidis, K.,* 2000: Chemical effects of UV fluctuations inferred from total ozone and tropospheric aerosol variations. *J. Geophys. Res. 105,* 14561-14574.

Kouvarakis, G., Tsigaridis, K., Kanakidou, M., and *Mihalopoulos, N.,* 2000: Temporal variations of surface regional background ozone over Crete Island in southeast Mediterranean. *J. Geophys. Res. 105,* 4399-4407.

Lippman, M., 1989: Health effects of ozone: a critical review. *J. Air. Pollut. Control Ass. 39,* 672-695.

Ogawa, T. and *Kamala, N.,* 1989: Diurnal and seasonal variations of the tropospheric ozone in tropical Asia. Ozone in the atmosphere. *Ozone Symposium.* Göttingen, Germany, 437-440.

Piotrowicz, S.R., Boran, D.A., and *Fischer, C.J.,* 1986: Ozone in the boundary-layer of the equatorial Pacific-Ocean. *J. Geophysical Res. 91,* 13113-13119.

Randriambelo, T., Baray, J.L., Baldy, S., Bremaud, P., and *Cautenet, S.,* 1999: A case study of extreme tropospheric ozone contamination in the tropics using in-situ, satellite and meteorological data. *Geophy. Res. Let. 26,* 1287-1290.

Routhier, F., Dennett, R., Daves, D.D., Wartburg, A., Haagenson, P., and *Delany, A.C.,* 1980: Free tropospheric and boundary-layer airborne measurement of ozone over the latitude of 58 S to 70 N. *J. Geophysical Res. 85,* 7307-7321.

Seinfeld, J.H. and *Sypros, N.,* 1998: *Atmospheric Chemistry and Physics from Air Pollution to Climate Change.* John Wiley and Sons. Inc., New York, London, Sydney, Toronto.

Snedecor, G.W. and *Cochran, W.G.,* 1980: *Statistical Analysis.* 7th edition. The Iowa State University Press.

Titlon, B.E., 1989: Health effects of tropospheric ozone. *Environment Science Technology 23,* 257-263.

Woodman, J.N., 1987: Pollution induced injury to North American forests and suspicions. *Tree Physiol 3,* 1-15.

IDŐJÁRÁS

Quarterly Journal of the Hungarian Meteorological Service
Vol. 107, No. 2, April–June 2003, pp. 153–170

Temporal change of some statistical characteristics of wind direction field over Hungary

Károly Tar[1] and **Emese Verdes**[2]

[1]*Department of Meteorology, University of Debrecen*
P.O. Box 13, H-4010 Debrecen, Hungary; E-mail: tark@tigris.klte.hu

[2]*Department of Sociology, University of Debrecen*
P.O. Box 11, H-4010 Debrecen, Hungary; E-mail: verdese@tigris.klte.hu

(Manuscript received March 26, 2002; in final form January 22, 2003)

Abstract–The objective of this study is to assess whether changes in the surface pressure field over Europe are reflected in the statistical structure of the wind direction field over Hungary. The data basis consists of hourly wind direction data measured at ten meteorological stations of the country in 1968–1972 and 1991–1995. Relative frequency, relative energy, average speed, and average duration of the wind directions were analysed in the above two periods, in winter and summer, over plains and mountains of the country. We investigated the difference of the relative frequencies with the so-called pi-star index. We gave the definition of the characteristic wind directions and we investigated their energy content and average speed compared to those of the non-characteristic wind directions. Then we detailed the quality of connections between the above-mentioned four parameters of the wind directions. Our main result is that the alterations of the statistical structure of wind direction field over Hungary depend on the features of the terrain and seasons.

Key-words: wind directions, relative frequency of wind directions, relative energy content of wind direction, pi-star index, characteristic wind directions.

1. Introduction

The rise in global surface air temperature, due to the increase of the atmospheric concentration of greenhouse gases, has probably induced a redistribution of the surface pressure field. According to *Schönwiese et al.* (1994) and *Meyhöfer et al.* (1996), this process has occurred in Europe: in the winter half-year the average values of surface pressure, converted to sea level, increased in the south and decreased in the north of the continent between 1961 and 1990, whereas in the summer half-year there were no significant changes.

On the other hand, *Metaxas* et al. (1991) and *Bartzokas* and *Metaxas* (1996) found that the average intensity of influx of cold air masses in summer, coming from the north and north-west to the south-east of Europe, had increased. Therefore, according to their investigations, the summer circulation system is also changing, as a consequence of the redistribution of the surface pressure field in summer, as well. In the above-mentioned authors' view, it is clear that such changes may affect Central-Europe to a relatively less degree than the northwestern and southeastern regions of our continent.

In continental Europe, in winter, the direction of the average pressure gradient is from south to north (*Justyák*, 1994). Thus, according to the previously mentioned results, this gradient itself is also increasing, which might also give rise to changes in the circulation system, e.g., the frequency or average speed of westerly winds may increase during this season. The spatial distribution of annual and monthly average sea level pressure fields in Hungary is due to the so called "basin character": roughly in the middle of the Great Hungarian Plain, a pressure minimum can be found. This is caused by strong warming in summer and frequent passing through of the Mediterranean cyclones in winter (*Dobosy* and *Felméry*, 1971).

The aim of our former investigations (*Tar*, 1998a, 1998b, 1999, 2001; *Mika et al.*, 1999; *Tar et al.*, 2000, 2001a, 2001b; *Makra et al.*, 2000a, 2000b) was to decide whether or not the observed changes in the pressure field over Europe could be detected in the statistical structure of the wind field over Hungary, in spite of the specific pressure field over the country. Change in the wind field, apart from climatic effects, also produces changes, among other things, of deflation and wind energy.

Our aim in this paper is to demonstrate possible marked changes in the statistical structure of the wind direction field over Hungary. The data basis of our investigations consists of hourly wind direction data of ten meteorological stations in Hungary, measured in periods 1968–72 and 1991–95. *Fig. 1* shows the locations and geographical coordinates of the stations. Since our data basis is not continuous, trends, autocorrelations, etc., cannot be determined.

2. Distribution of the wind directions and pi-star index

From the relative frequencies of wind directions of two critical seasons, over the ten stations, in the two five-year periods, we can see that the bigger deviations are in the winter, the significant differences are not presumable in a few cases in the summer.

The statistical test performed to evaluate differences was the χ^2 test of homogeneity. As the observed hours of different wind directions turned to be

quite large numbers, this test showed significant difference in the distributions in each case, which was not very surprising taking into account the sensitivity of the χ^2 test for sample size. The critical value of the χ^2 distribution at 0.05 significance level with 14 degrees of freedom is 23.65, which was highly exceeded in our examples, so we can conclude that wind direction field has changed remarkably. Note, however, that there were very big differences in the computed χ^2 values, which means that the magnitude of difference in hours of wind directions depended on the locations, seasons, and year very much, as *Table 1* shows.

Station	φ	λ	h_1 (1968-72)	h_2 (1991-95)	h_{a1} (1968-72)	h_{a2} (1991-95)
Szombathely	47°16'	16°38'	224	224	9	9
Keszthely	46°46'	17°14'	117	117	15	15
Győr	47°41'	17°38'	119	116	10	10
Pécs	46°00'	18°14'	202	202	10	10
Budapest	47°27'	19°13'	130	130	12	12
Szeged	46°15'	20°06'	83	83	9	9
Miskolc	48°08'	20°48'	118	233	15	15
Békéscsaba	46°41'	21°10'	88	88	9	10 and 20.6
Debrecen	47°30'	21°38'	111	108	10	10
Kékestető	47°52'	20°01'	1010	1010	26	26

h_1, h_2: height of the observatory above the sea level (m);
h_{a1}, h_{a2}: height of the anemometer above ground level (m)

Fig. 1. Location and geographical coordinates of the meteorological stations.

To remove the effect of sample size, we performed an another test, which is not so traditional as the χ^2 test, but has the advantages of not depending on sample size and giving a nice impression of discrepancy between model and data. This test is not a test of significance, rather an index between zero and one, and it is called pi-star index.

Table 1. Results of the χ^2 test

Station	Winter	Spring	Summer	Autumn	Year
Békéscsaba	710	271	148	259	528
Debrecen	1177	468	249	841	1613
Szeged	1178	468	232	398	813
Budapest	1036	627	617	630	2036
Győr	1848	1035	1489	1602	4695
Szombathely	1691	979	576	433	2671
Keszthely	1517	1437	941	1524	4484
Pécs	1451	240	618	611	1511
Miskolc	843	734	662	873	2044
Kékestető	1374	484	315	267	979

The pi-star index of fit was introduced by *Rudas et al.* (1994) for contingency table analysis. The original definition is

$$\pi^* = \pi^*(P, M) = \inf\{\pi : P = (1-\pi)F + \pi Q, \quad F \in M, \quad 0 \le \pi \le 1\}, \tag{1}$$

where P, F and Q denote cell probabilities of two-way contingency tables of the same size and M is a model. Although this definition is for two-way tables, it can be extended to contingency tables of any size with any model, moreover, to any known statistical model.

Roughly speaking, here the observations are decomposed into two parts: a first part, that fits the model exactly, and a second one, which is unrestricted, so that the sum of the observations in the first part will be maximal. Then the ratio of the observations in the second part is the pi-star index. This is the fraction of the sample that cannot be described by the model in the best case. Hence, if the pi-star index is small, we will conclude, that we are close to the model, as only a small fraction of the sample cannot be described by the model. On the contrary, if π^* is big, we will conclude, that we are not so close to the model.

In our case the null hypothesis was that the distribution of the hourly wind direction was the same in the two time periods. Putting it in another way, we had to examine in what extent the measurements in the second period could be described by those of the first period. Again, small π^* values indicated smaller differences, and bigger π^* values meant greater discrepancy in the distributions. According to this, we could conclude, that even removing the effect of sample size, we found big differences in the distributions due to quite big π^* values, but here also we could make differences among the ten stations and seasons examined.

Table 2. Values of π^*

Station	Winter	Spring	Summer	Autumn	Year
Békéscsaba	0.59	0.28	0.24	0.44	0.28
Debrecen	0.55	0.48	0.40	0.58	0.39
Szeged	0.55	0.48	0.39	0.31	0.25
Budapest	0.60	0.65	0.65	0.49	0.60
Győr	0.72	0.64	0.62	0.47	0.54
Szombathely	0.71	0.49	0.47	0.44	0.44
Keszthely	0.71	0.61	0.53	0.61	0.51
Pécs	0.73	0.41	0.47	0.45	0.47
Miskolc	0.46	0.59	0.56	0.55	0.53
Kékestető	0.67	0.50	0.53	0.31	0.50

Seasonal and yearly values of π^* are listed in *Table 2*. It can be seen from the table, that these values are bigger in the majority of cases in winter. This confirms that we wrote about this season in the introduction. The values also show that the temporal change of the distribution of wind directions is more marked in Transdanubian stations. In summer, values commensurable with winter ones can be seen in the no lowland-stations (Szombathely, Keszthely, Pécs, Miskolc, Kékestető), e.g., in the more complex geographical/orographical environment. All these suggest the alteration of directional distributions of summer wind, too, during about 20 years. This also is claimed by Mediterranean authors, *Metaxas* et al. (1991), *Bartzokas* and *Metaxas* (1996). First of all they are speaking about the Etesian wind, which can be considered as part of the summer monsoon circulation. It is possible that the change of features of this wind causes the increase of frequency of northerly directions over Hungary, too. In spring and autumn, the values of π^* cannot be classified from geographical/orographical or other point of view. It is possible that the measure of marked alteration of frequency distribution of wind directions can rather be connected to the circulation/macrosynoptic situations.

Conclusions about the above differences were made by these two (χ^2 and π^*) statistical analyses. Most of the cases they show similar results, however, sometimes they do not move paralelly, because they measure different things. The χ^2 statistic is a sum of the deviances in the observations in the 16 cells measured in two time periods, however, the pi-star index measures the amount of maximum deviance in the above cells.

3. Some other statistical characteristics of wind direction

By our former investigations (*Tar,* 2001), the frequency distribution of wind directions can be in close relation with the relative energy content, average

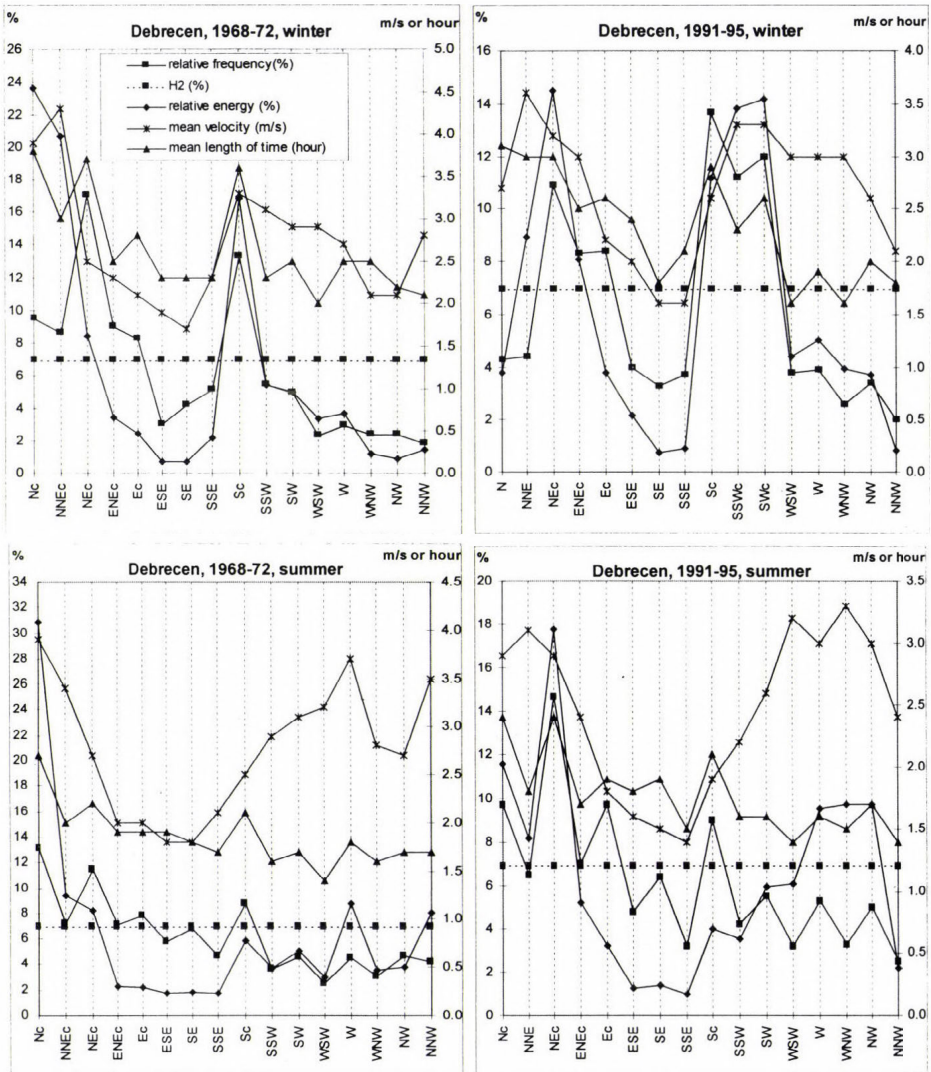

Fig. 2. Some statistical characteristics of wind direction in Debrecen (*c:* characteristic wind direction).

speed, and average duration of wind directions. This can be seen in *Fig. 2* and *Fig. 3.* These figures show the above-mentioned characteristics in winter and summer, in a lowland and a Transdanubian station (Debrecen and Szombathely), which are on about the same geographical latitude. One can see, there are some wind directions where these characteristics differ markedly from the characteristics of other directions.

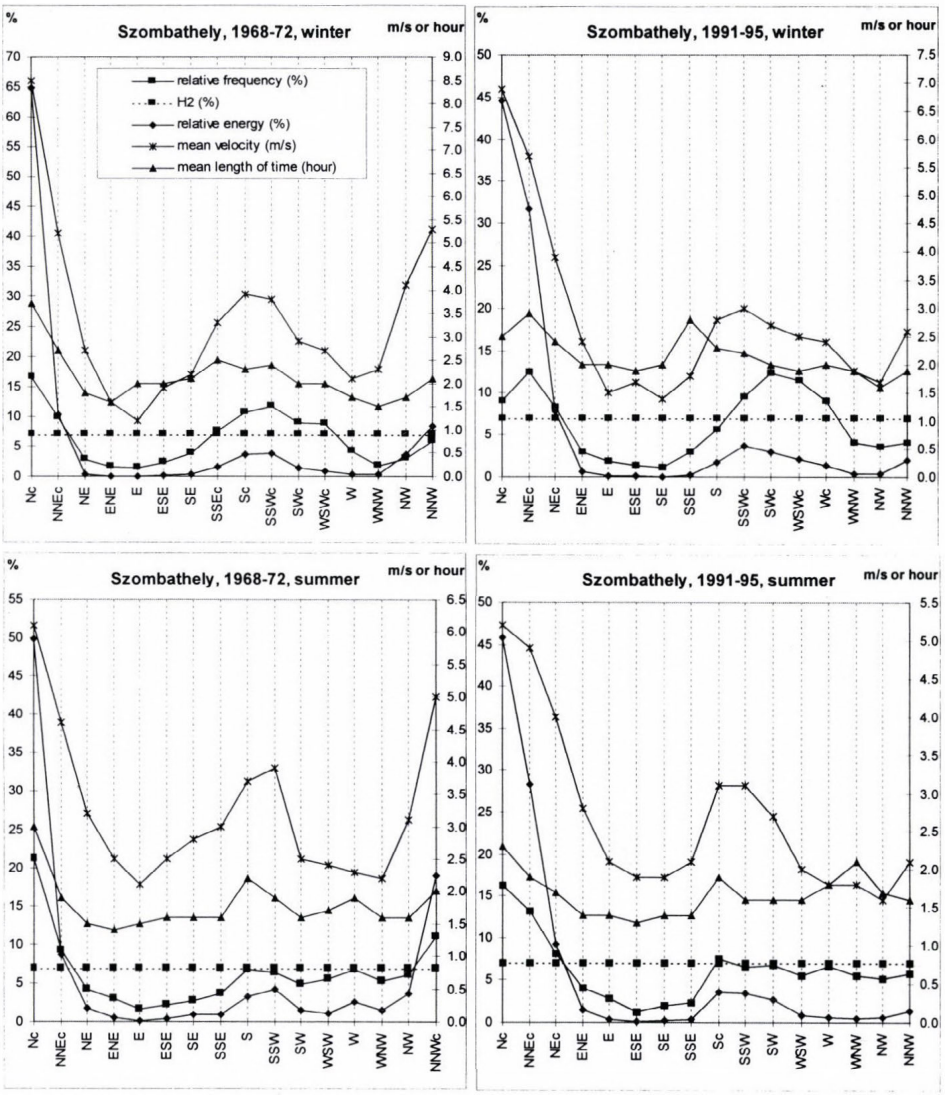

Fig. 3. Some statistical characteristics of wind direction in Szombathely (*c:* characteristic wind direction).

3.1 Characteristic wind directions

The hypothesis on the evenness of the frequency distribution of wind direction was verified in the following way (*Tar*, 1991): let h_1 and h_2 be

$$h_1 = p_0 n - u_\varepsilon \sqrt{n p_0 (1 - p_0)}, \tag{2}$$

$$h_1 = p_0 n + u_\varepsilon \sqrt{n p_0 (1 - p_0)}, \tag{3}$$

where p_0 is equal to $1/16=0.0625$, as we used 16 wind directions, n is the number of cases. u_ε satisfies the equation

$$2\Phi(u_\varepsilon) - 1 = 1 - \varepsilon, \tag{4}$$

where Φ(x) is the distribution function of standard normal distribution. So, if $\varepsilon=0.0027$ (*Péczely*, 1957), then $u_\varepsilon=2.28$.

Let f_D be the relative frequency of direction D, where $D=\{$N, NNE, NE, ENE, E, ESE, SE, SSE, S, SSW, SW, WSW, W, WNW, NW, NNW$\}$. If $f_D \geq h_2$, then D is called characteristic wind direction (CWD), else it is a non-characteristic wind direction (NWD) on $1-\varepsilon$ probability level. If f_D is given in percents, then the limits of the critical interval are $H_1=100\ h_1/n$, $H_2=100\ h_2/n$. *Fig. 2* and *Fig. 3* show the value of H_2, where the characteristic wind directions are denoted by „c" on axis x.

In the following we will compare the energy content and average speed of characteristic wind directions to those of the other wind directions. The average energy content of a D wind direction for a time period (season, year) can be determined with the mean specific wind power, namely with the equation

$$P_{f1}(D) = \frac{\rho}{2} \sum_{j=1}^{k} \frac{f_{Dj}}{N} v_j^{\,3}. \tag{5}$$

Here f_{Dj} is the frequency of the speed of D wind within the $(v_j - 0.5\Delta v, v_j + 0.5\Delta v)$ interval, k is the number of intervals and N is the number of the days of time period, respectively. Let P_{f1} denote the mean specific wind power of time period, which is independent of the wind directions, then the ratio

$$p(D) = \frac{P_{f1}(D)}{P_{f1}} \tag{6}$$

is equal to the relative energy content of the given D wind direction. The average speed of this direction is

$$\bar{v}(D) = \sum_{j=1}^{k} \frac{f_{Dj}}{N} v_j. \tag{7}$$

Value of the last parameter strongly depends on the height of anemometer. This height is regularly 10 meters at the meteorological stations, but it can happen that the wind speed is measured on a lower or higher level. In these cases the height correction is done by the following equation:

$$v_h = v_{10}\,[0.233 + 0.656\,\lg(h + 4.75)] \tag{8}$$

(*Mezősi* and *Simon*, 1981), where v_h is the measured wind speed on $h \neq 10$ m and v_{10} is the calculated wind speed on 10 m. In some selected cities it had happened that the measurements were carried out on height differing from 10 m, or the stations was moved to another place, or the instrument was changed for an automatic one. In the last two cases the height of the sensor was changed, too. In all of these stations we produced the 10-meter wind speed by the above equation.

We investigated in detail the number of characteristic wind directions (CWD), common relative frequencies (CWD_F), common and mean relative energy contents (CWD_E and CWD_{E1}), and average speeds (CWD_{V1}) of these wind directions, mean relative energy content (NWD_{E1}) and average speed (NWD_{V1}) of non-characteristic wind directions, and the seasonal (independently of the wind directions) average wind speed (AWD_{V1}), respectively, in winter and summer of the two five-year periods. The stations were grouped by the following way: stations over plain terrain (Debrecen, Békéscsaba, Szeged, Budapest, Győr), which are opened by geographically, stations over hilly or mountainous territory (Szombathely, Keszthely, Pécs, Miskolc), in which the orography modifies the airflow strongly, and Kékestető, because it belongs to an other current of air, that we have to take into consideration comparing the average wind speeds. We are able to compare only the relative quantities of Miskolc, because the meteorological station was removed to the Avas-mountain in the second time period, and its height above sea level increased markedly.

Our results at stations over plain terrain show that

- the value of CWD is between 3 and 9, CWD_F is between 33 and 81% (Békéscsaba, 1968–72, winter and Győr, 1991–95, winter, respectively),
- CWD_E is between 91% (Győr, 1991–95, winter) and 42% (Debrecen, 1991–95, summer),
- CWD_{E1} (the energy content of one CWD) is between 18.6% (Győr, 1991–95, summer) and 8.3% (Debrecen, 1991–95, summer),
- the maximum values of the above parameters are in Győr, but the minimum value of CWD_{V1} is also here (1991–95, summer). The maximum of the latest parameter is in the Great Hungarian Plane, Szeged, 1968–72, winter,

- relative energy content of an other, non-characteristic wind direction (NWD_{E1}) is between 5.3% (Debrecen, 1991–95, summer) and 1.2% (Győr, 1991–95, winter). The time and place of extreme values of NWD_{V1} agree with those of CWD,
- the average wind speed of seasons (AWD_{V1}) alters from 3.5 m/s (Szeged, 1968–72, winter) to 1.9 m/s (Győr, 1991–95, summer).

Table 3. Territorial averages: average values of CWD, common relative frequency (CWD_F) and relative energy content (CWD_E) of characteristic wind directions, average energy content (CWD_{E1}) and average speed (CWD_{V1}) of one characteristic wind direction, average energy content (NWD_{E1}) and average speed (NWD_{V1}) of one non-characteristic wind direction, averages of wind speed (AWD_{V1})

Average of	CWD	CWD_F (%)	CWD_E (%)	CWD_{E1} (%)	CWD_{V1} (m/s)	NWD_{E1} (%)	NWD_{V1} (m/s)	AWD_{V1} (m/s)
Stations over plain terrain								
Yearly	**5.3**	**53.7**	**63.5**	**12.4**	**2.9**	**3.4**	**2.4**	**2.7**
1968–72	5.3	53.0	63.8	12.2	3.1	3.4	2.5	2.8
1991–95	5.3	54.3	63.3	12.5	2.8	3.3	2.3	2.6
Winter	**5.5**	**55.1**	**66.3**	**12.4**	**3.1**	**3.1**	**2.4**	**2.8**
1968–72	5.0	51.7	62.8	12.7	3.2	3.3	2.6	2.9
1991–95	6.0	58.6	69.7	12.1	3.0	2.9	2.3	2.8
Summer	**5.1**	**52.2**	**60.8**	**12.4**	**2.7**	**3.6**	**2.4**	**2.6**
1968–72	5.6	54.3	64.7	11.7	3.0	3.4	2.5	2.7
1991–95	4.6	50.1	56.9	13.0	2.5	3.8	2.2	2.4
Stations over no-plain terrain								
Yearly	**5.1**	**54.2**	**68.9**	**14.3**	**3.6**	**2.8**	**2.6**	**3.2**
1968–72	4.6	51.8	65.1	14.9	4.0	3.0	2.9	3.5
1991–95	5.3	56.6	72.6	13.6	3.3	2.6	2.3	2.9
Winter	**5.5**	**58.2**	**68.1**	**12.4**	**3.8**	**3.0**	**2.8**	**3.4**
1968–72	5.0	56.4	62.9	12.6	4.1	3.3	3.1	3.6
1991–95	6.0	60.1	73.3	12.3	3.5	2.6	2.6	3.2
Summer	**5.0**	**50.2**	**69.6**	**16.1**	**3.5**	**2.6**	**2.4**	**2.9**
1968–72	4.2	47.3	67.3	17.2	4.0	2.7	2.7	3.3
1991–95	5.0	53.0	72.0	14.9	3.1	2.6	2.1	2.5

Table 3 shows the average values. (The average number of CWD is important from the point of view of other parameters only.) Based on the part concerning the stations over plain terrain of this table we can say that

- there is no considerable difference between the "yearly" (winter +summer) parameters, given in percents, in the two five-year periods at these stations. The ratio of energy content of one CWD to that of one

NWD (CWD_{E1}/NWD_{E1}) is 3.6 in the first five-year period and 3.8 in the second five-year period. The average speed of CWD (CWD_{V1}) is larger than NWD_{V1} with 0.5 m/s, and with 0.2 m/s than the "yearly" average wind speed,

- note, that the decrease of different average wind speeds is 0.2–0.3 m/s to the second period,
- the number of CWD increased with 1, CWD_F and CWD_E also increased with about 7% according to this in winter,
- on the other hand CWD_{E1}, NWD_{E1}, and all the average speed decreased, the latest parameters with 0.1–0.3 m/s in winter,
- the ratio of energy content of different direction groups increased with 3.8–4.2 to the second period, it is equal to 4 on average in winter,
- the number of CWD decreased with 1, CWD_F and CWD_E also decreased with about 4 or 8% according to this in summer,
- the different average wind speeds decreased with 0.3–0.5 m/s in summer, i.e., more considerably than in winter,
- the ratio of energy content of different direction groups increased somewhat to the second period, it is equal to 3.4 on average in two summers.

Our results at stations over no-plain terrain show that

- the number of CWD is between 3 (Szombathely, 1968–72, summer) and 7, the last number occurs in more cases,
- CWD_F is between 74% (Szombathely, 1968–72, summer) and 41% (in more cases), CWD_E is between 94 and 38%,
- CWD_{E1} and CWD_{V1} are between 26–7.6%, and 5.5–1.8 m/s, respectively. In the last case we considered only 3 stations (Szombathely, Keszthely, and Pécs). Note, however, that the average speeds in Szombathely are commensurable with those in Kékestető,
- the maximum of above-mentioned parameters occurs in Szombathely. This value of NWD_{E1} occurs in Pécs (1968–72, winter) among the five stations, and here is the maximum of NWD_{V1} among the considered three stations,
- average wind speed of the seasons is the largest in Szombathely, too. It is interesting that these values decreased in the first three stations in all cases and in Kékestető in summer with 0.9–0.2 m/s to the second period, but they stagnate in Kékestető in the winter.

Based on the part concerning the stations over no-plain terrain of *Table 3*, we can find the following results.

In "yearly average" (winter+summer),

- the number of CWD, CWD_F, and CWD_E increased in order with about 1, 5 and 7%, but in contrast with this

- CWD_{E1} decreased by 1.3% to the second period,
- the above yearly value exceeds that of the stations over plain terrain by about 2% in average, 2.7% in the first, and 1.1% in the second period,
- the value of NWD_{E1} also decreased,
- the ratio CWD_{E1}/NWD_{E1} is equal to 5.1 at these stations in contrast with 3.6 at stations over plain terrain.

In winter,

- the number of CWD increased by 1, CWD_F and CWD_E also increased by about 4%, and 10%, according to this, respectively,
- the values of CWD_{E1} did not change,
- these values are equal to the corresponding values of plain terrain in average and by periods, too,
- NWD_{E1} somewhat decreased. The ratio CWD_{E1}/NWD_{E1} increased here and now, too, but to essentially higher degree than on the plain terrain.

In summer,

- the average number of CWD increased, CWD_F and CWD_E also increased by about 6%, and 5%, according to this, respectively,
- the value of CWD_{E1} decreased by more than 2%, but
- the above mentioned numbers are larger than those at the stations over plain terrain. Therefore, at the stations over no-plain one characteristic wind direction carries more than 3% energy in average. This surplus is 5.5% in summers of 1968–72 and about 2% in summers of 1991–95,
- for the stations over plain terrain there is no considerable difference in the winter and summer values of the above mentioned parameters. For the stations over no-plain terrain, the value of CWD_{E1} is larger by about 4% in summer.
- the ratio CWD_{E1}/ NWD_{E1} is the largest over no-plain terrain in summer, it is 6.2 in average of periods, 6.4 for summers of 1968–72, 5.7 for summers of 1991–95. It is in contrast with the stagnating summer values on plain terrain.

Different average wind speeds are determined, except Miskolc. Based on the part concerning the stations over no-plain terrain of *Table 3*, we can find that,

- in the "yearly average", the value of CWD_{V1} is larger by exactly 1 m/s than NCW_{V1} and 0.4 m/s than the average wind speed of the "year" (in last column, AWD_{V1}: average speed of all wind directions),
- in the period 1991–95 these differences are the same, in the period 1968–72 they are 1.1, and 0.5 m/s, respectively,
- these differences do not change essentially in winter,

- but in summer the difference CWD_{V1}-NCW_{V1} is equals to or larger than 1 m/s, CWD_{V1}-AWD_{V1} is equal to or larger than 0.6 m/s. The maximum of two differences is in the summers of 1968–72,
- all average wind speeds are decreasing, to the highest degree, 0.9 m/s, in the case of summer characteristic wind directions. This value is equal to 0.5 m/s on the plain terrain.

In *Table 4* we give the ratios of time and terrain average energy content of one characteristic and one non-characteristic wind direction (CWD_{E1}/NWD_{E1}). It can be established, that these ratios

- have orographic differences on the annual and summer averages,
- are larger on the plain terrain in winter, and on the no-plain terrain in summer, respectively.

The yearly ratios of two five-year periods do not show considerable differences in the two groups of stations. But these ratios have significant differences in the two groups in winter and on the no-plain terrain stations in summer. According to the table, the ratio does not increase period-by-period in summer, even it decreases on the no-plain terrain stations in this season.

Table 4. The ratios of CWD_{E1}/NWD_{E1}

	Stations over	
	Plain terrain	**No-plain terrain**
Yearly	3.6	5.1
1968–72	3.6	5.0
1991–95	3.8	5.2
Winter	4.0	4.1
1968–72	3.8	3.8
1991–95	4.2	4.7
Summer	3.4	6.2
1968–72	3.4	6.4
1991–95	3.4	5.7

3.2 Relationship between the frequency, energy content, average speed, and average duration of wind directions

As it can be seen in *Fig. 2* and *3*, some curves of values connected to wind directions (frequency, energy content, average speed, and average duration) are roughly parallel to each other. This refers to the linearity of their stochastic connection, so we determined the values of linear correlation coefficient (r). They are given in *Table 5* and *6* in stations over plain and no-plain terrain to the winter and summer of the two five-year periods. The critical value of r, belonging to 16 number of cases, on 0.05 significance level, $r_{0.05}$ equals to 0.4973 (*Dobosi* and *Felméry*, 1971).

Table 5. Values of the linear correlation coefficient in stations over plain terrain (*italic:* significant value)

Debrecen, winter					**Debrecen, summer**				
1968-72	**rel.freq.**	**rel. energ.**	**mean sp.**	**mean dur.**	**1968-72**	**rel.freq.**	**rel. energ.**	**mean sp.**	**mean dur.**
rel.freq.		*0.5984*	0.3266	*0.8722*	**rel.freq.**		*0.6453*	0.0253	*0.9547*
rel. energ.	*0.8580*		*0.8741*	*0.7982*	**rel. energ.**	*0.5676*		*0.6794*	*0.7868*
mean sp.	0.3889	*0.7524*		0.4922	**mean sp.**	0.0193	*0.7619*		0.1816
mean dur.	*0.5929*	*0.5554*	0.3183		**mean dur.**	*0.9114*	0.4940	-0.0481	
1991-95	**rel.freq.**	**rel. energ.**	**mean sp.**	**mean dur.**	**1991-95**	**rel.freq.**	**rel. energ.**	**mean sp.**	**mean dur.**
Békéscsaba, winter					**Békéscsaba, summer**				
1968-72	**rel.freq.**	**rel. energ.**	**mean sp.**	**mean dur.**	**1968-72**	**rel.freq.**	**rel. energ.**	**mean sp.**	**mean dur.**
rel.freq.		*0.8674*	*0.5139*	*0.9484*	**rel.freq.**		*0.6820*	0.2999	0.4669
rel. energ.	*0.9836*		*0.8280*	*0.8628*	**rel. energ.**	*0.8444*		*0.8541*	-0.0084
mean sp.	*0.7940*	*0.7765*		*0.5285*	**mean sp.**	*0.5861*	*0.8606*		-0.4259
mean dur.	*0.8558*	*0.8419*	*0.5264*		**mean dur.**	*0.8486*	*0.6944*	0.4484	
1991-95	**rel.freq.**	**rel. energ.**	**mean sp.**	**mean dur.**	**1991-95**	**rel.freq.**	**rel. energ.**	**mean sp.**	**mean dur.**
Szeged, winter					**Szeged, summer**				
1968-72	**rel.freq.**	**rel. energ.**	**mean sp.**	**mean dur.**	**1968-72**	**rel.freq.**	**rel. energ.**	**mean sp.**	**mean dur.**
rel.freq.		*0.8793*	*0.7232*	*0.7775*	**rel.freq.**		*0.9213*	*0.8119*	*0.8711*
rel. energ.	*0.8099*		*0.9113*	*0.7324*	**rel. energ.**	*0.9241*		*0.9093*	*0.6938*
mean sp.	0.4926	*0.7570*		*0.6297*	**mean sp.**	*0.5521*	*0.7566*		*0.5368*
mean dur.	*0.9016*	*0.7501*	0.4186		**mean dur.**	*0.8172*	*0.6425*	0.2182	
1991-95	**rel.freq.**	**rel. energ.**	**mean sp.**	**mean dur.**	**1991-95**	**rel.freq.**	**rel. energ.**	**mean sp.**	**mean dur.**
Budapest, winter					**Budapest, summer**				
1968-72	**rel.freq.**	**rel. energ.**	**mean sp.**	**mean dur.**	**1968-72**	**rel.freq.**	**rel. energ.**	**mean sp.**	**mean dur.**
rel.freq.		0.3862	0.2789	*0.9285*	**rel.freq.**		*0.8212*	*0.6517*	*0.9041*
rel. energ.	0.4469		*0.9248*	*0.5818*	**rel. energ.**	*0.8022*		*0.9347*	*0.8050*
mean sp.	0.3089	*0.9473*		0.4348	**mean sp.**	0.3678	*0.7413*		*0.6852*
mean dur.	*0.9011*	0.3372	0.2072		**mean dur.**	*0.9394*	*0.7206*	0.3576	
1991-95	**rel.freq.**	**rel. energ.**	**mean sp.**	**mean dur.**	**1991-95**	**rel.freq.**	**rel. energ.**	**mean sp.**	**mean dur.**
Győr, winter					**Győr, summer**				
1968-72	**rel.freq.**	**rel. energ.**	**mean sp.**	**mean dur.**	**1968-72**	**rel.freq.**	**rel. energ.**	**mean sp.**	**mean dur.**
rel.freq.		*0.7970*	0.3713	*0.6007*	**rel.freq.**		*0.9345*	0.4608	*0.8253*
rel. energ.	*0.7994*		*0.7886*	*0.5146*	**rel. energ.**	*0.8652*		*0.6831*	*0.8373*
mean sp.	*0.6648*	*0.8829*		0.2303	**mean sp.**	0.4389	*0.6314*		*0.5187*
mean dur.	*0.6867*	*0.6164*	*0.5108*		**mean dur.**	*0.9025*	*0.8393*	0.4449	
1991-95	**rel.freq.**	**rel. energ.**	**mean sp.**	**mean dur.**	**1991-95**	**rel.freq.**	**rel. energ.**	**mean sp.**	**mean dur.**

The most important conclusions from *Table 5* concerning to stations over the plain terrain are:

- All number of significant cases ($r > r_{0.05}$) are 74% in the year, 75% in winter, and 73% in summer. Therefore, there is no considerable seasonal difference.
- The numbers of significant cases do not differ considerably from each other in the seasons of two periods: it is 77% in 1968–72 and 73% in

Table 6. Values of the linear correlation coefficient in stations over no-plain terrain (*italic:* significant value)

Szombathely, winter					**Szombathely, summer**				
1968-72	**rel.freq.**	**rel. energ.**	**mean sp.**	**mean dur.**	**1968-72**	**rel.freq.**	**rel. energ.**	**mean sp.**	**mean dur.**
rel.freq.		*0.6786*	*0.7797*	*0.8492*	**rel.freq.**		*0.9560*	*0.8751*	*0.9284*
rel. energ.	0.4830		*0.8566*	*0.8420*	**rel. energ.**	*0.9022*		*0.8531*	*0.8918*
mean sp.	*0.6253*	*0.9557*		*0.8218*	**mean sp.**	*0.8655*	*0.8877*		*0.8224*
mean dur.	0.3392	*0.5975*	*0.6234*		**mean dur.**	*0.8319*	*0.6764*	*0.5469*	
1991-95	**rel.freq.**	**rel. energ.**	**mean sp.**	**mean dur.**	**1991-95**	**rel.freq.**	**rel. energ.**	**mean sp.**	**mean dur.**
Keszthely, winter					**Keszthely, summer**				
1968-72	**rel.freq.**	**rel. energ.**	**mean sp.**	**mean dur.**	**1968-72**	**rel.freq.**	**rel. energ.**	**mean sp.**	**mean dur.**
rel.freq.		*0.6606*	*0.6539*	*0.8576*	**rel.freq.**		*0.8653*	*0.7997*	*0.8377*
rel. energ.	*0.7496*		*0.9347*	*0.7963*	**rel. energ.**	*0.8224*		*0.9159*	*0.8103*
mean sp.	*0.6966*	*0.8792*		*0.7209*	**mean sp.**	*0.5748*	*0.8159*		*0.7999*
mean dur.	*0.9010*	*0.8937*	*0.8891*		**mean dur.**	*0.7705*	*0.8052*	*0.7653*	
1991-95	**rel.freq.**	**rel. energ.**	**mean sp.**	**mean dur.**	**1991-95**	**rel.freq.**	**rel. energ.**	**mean sp.**	**mean dur.**
Pécs, winter					**Pécs, summer**				
1968-72	**rel.freq.**	**rel. energ.**	**mean sp.**	**mean dur.**	**1968-72**	**rel.freq.**	**rel. energ.**	**mean sp.**	**mean dur.**
rel.freq.		0.4683	0.1163	*0.8819*	**rel.freq.**		*0.8411*	*0.5724*	*0.6756*
rel. energ.	*0.5967*		*0.8659*	*0.5679*	**rel. energ.**	*0.7262*		*0.8737*	*0.6381*
mean sp.	0.1946	*0.7915*		0.3267	**mean sp.**	0.3151	*0.8094*		*0.5874*
mean dur.	*0.7193*	0.4252	0.2774		**mean dur.**	*0.8260*	*0.7219*	0.3534	
1991-95	**rel.freq.**	**rel. energ.**	**mean sp.**	**mean dur.**	**1991-95**	**rel.freq.**	**rel. energ.**	**mean sp.**	**mean dur.**
Miskolc, winter					**Miskolc, summer**				
1968-72	**rel.freq.**	**rel. energ.**	**mean sp.**	**mean dur.**	**1968-72**	**rel.freq.**	**rel. energ.**	**mean sp.**	**mean dur.**
rel.freq.		*0.5031*	0.0466	*0.7001*	**rel.freq.**		*0.8412*	0.1503	*0.6116*
rel. energ.	*0.5638*		*0.7380*	*0.6524*	**rel. energ.**	*0.8762*		*0.5916*	*0.5826*
mean sp.	0.4584	0.7941		0.3880	**mean sp.**	0.4432	*0.7148*		0.3475
mean dur.	*0.9115*	*0.6530*	*0.6420*		**mean dur.**	*0.8289*	*0.7290*	*0.5445*	
1991-95	**rel.freq.**	**rel. energ.**	**mean sp.**	**mean dur.**	**1991-95**	**rel.freq.**	**rel. energ.**	**mean sp.**	**mean dur.**
Kékestető, winter					**Kékestető, summer**				
1968-72	**rel.freq.**	**rel. energ.**	**mean sp.**	**mean dur.**	**1968-72**	**rel.freq.**	**rel. energ.**	**mean sp.**	**mean dur.**
rel.freq.		*0.8857*	*0.6121*	*0.8336*	**rel.freq.**		*0.9483*	*0.6743*	*0.8953*
rel. energ.	*0.9161*		*0.8550*	*0.6888*	**rel. energ.**	*0.8767*		*0.8038*	*0.8972*
mean sp.	*0.8441*	*0.8478*		0.3769	**mean sp.**	*0.7431*	*0.7700*		*0.7733*
mean dur.	*0.6222*	*0.7576*	*0.7428*		**mean dur.**	*0.8204*	*0.8552*	*0.7377*	
1991-95	**rel.freq.**	**rel. energ.**	**mean sp.**	**mean dur.**	**1991-95**	**rel.freq.**	**rel. energ.**	**mean sp.**	**mean dur.**

- 1991–95, in winter and summer. Namely, the ratio of significant cases decreased by about 4% to the second period at stations over the plain terrain.

The most important conclusions from *Table 6* concerning the stations over the no-plain terrain are:

- All number of significant cases are 80% in winter, 92% in summer, 86% altogether. Therefore, there is considerable seasonal difference at these stations.

- The ratios of significant cases differ from each other in the seasons of two periods: it is 80% in winter, 93% in summer of 1968–72, 80% in winter, 90% in summer of 1991–95. Namely, the number of significant cases did not change considerably to the second period in the seasons at these stations.

The most important conclusions from the two tables are:

- The connection of the relative frequency and relative energy content is not significant only in four cases. They are all winter cases. There are no orographical and temporal differences.
- There is no seasonal difference in connection of the relative frequency and mean velocity. There is a temporal difference in the stations over no-plain terrain: the number of significant cases decreased by 10% to the second period. The orographical differences are marked: the number of significant cases are more with 30% (1968–72), 20% (1991–95), and 25% (together), respectively, than those in the stations over no-plain terrain.
- The connection of relative frequency and average duration is significant except two cases, which is not surprising.
- The connection of relative energy and average speed is significant in every case, since they are in a complicated functional relation through the hourly wind speed.
- The connection between relative energy and average duration is completely random, of course. The number of significant cases is larger by 10% in the stations over no-plain terrain, considering all the cases or periods. There is a temporal difference, too: such cases decreased by 10% to the second period in both territories. There are no seasonal differences.
- All three kinds of differences are noticeable in connection of the average speed and average duration. Considering all the cases, we can establish twice as many significant cases in the stations over no-plain terrain than in the other territory (70% and 35%, respectively). The difference is only 10% in the first period, but it is 60% in the second one. Namely, the number of significant cases considerably decreased at the stations over plain terrain and considerably increased at the stations over no-plain terrain to the second period. At the same time, the number of significant connections is more in summer in the first period and in winter in the second period.

4. General conclusions

Temporal change of the frequency distribution of wind directions, which is in connection with the global warming, during the two selected period (1968–72, 1991–95), is not investigable by traditional statistical tests. The χ^2-test cannot

be applied because of the large sample size. The π^* index shows seasonal and orographical differences but only in the comparison of its values, there is no significant threshold value. Its outstanding winter values, in Győr, Szombathely, Keszthely, and Pécs, refer rather to geographical differences than orographical ones. They indicate the connection with the NW steering flow, i.e., the seasonal large-scale processes (for example with the change of the see-level pressure in Europe). Its summer values are less, they show the less marked change without geographical and/or orographical differences.

The energy carried by the wind directions depends on the season and orography. This is verified by our investigations concerning the characteristic wind directions: in summer their energy content is less at the stations over plain terrain, more at the stations over no-plain terrain than in winter. The energy content of a characteristic wind direction increases in both territory in winter, decreases in the no-plain terrain in summer, to the second period. One characteristic wind direction carries about four times more energy than one non-characteristic wind direction on the yearly and winter averages, and about five times more than the summer average in Hungary.

There are seasonal and orographical differences in relations of the different parameters (relative frequency, relative energy content, average speed, average duration) of wind directions. In summer the number of significant cases is more than in winter in the plain terrain, they are almost equal to each other in the no-plain terrain. We could not establish considerable temporal differences between the two periods.

With the above results and establishments we would like to contribute to more exact and detailed knowledge of wind climate in our country, and to scientifically/climatologically established utilization of the wind energy .

Acknowledgements–The authors wish to express thanks to OTKA (Hungarian Scientific Research Found) and the Ministry for Environmental Protection for the sponsorship of researches connected the subject of this study, as well as to the Hungarian Meteorological Service for putting the data basis at their disposal.

References

Bartzokas, A. and *Metaxas, D.A.*, 1996: Northern Hemisphere gross circulation types. Climatic change and temperature distribution. *Meteorol. Zeitschrift*, N.F. 5, 99-109.

Dobosi, Z. and *Felméry, L.*, 1971: *Climatology* (in Hungarian), Tankönyvkiadó, Budapest, 500 p.

Justyák, J., 1994: *The Climate of Europe* (in Hungarian). Egyetemi Jegyzet. Debreceni Egyetem, 135 p.

Makra, L., Tar, K., and *Horváth, Sz.*, 2000a: Some statistical characteristics of the wind energy over the Great Hungarian Plane. *Int. J. Ambient Energy 21*, No. 2, 85-96.

Makra, L., Tar, K., and *Lukácsovicsné Horváth, Sz.*, 2000b: Analysis of wind speed data series in Hungary by using a new statistical test and conclusions in connection with climate change.

Scientific Meeting on Detection and Prediction of Contemporary Climate Change and their Effects in a Regional Scale, Tarragona, Spain, 29-31st May, 2000.

Metaxas, D.A., Bartzokas, A., and *Vitsas, A.*, 1991: Temperature fluctuations in the Mediterranean area during the last 120 years. *Int. J. Climatol. 11*, 897-909.

Meyhöfer, S., Rapp, J., and *Schönwiese, C.D.*, 1996: Observed three-dimensional climate trends in Europe 1961-1990. *Meteorol. Zeitschrift*, N.F. 5, 90-94.

Mezősi, M. and *Simon A.*, 1981: The theory and practice of meteorological wind measurements (in Hungarian). *Meteorológiai Tanulmányok*, No. 36. Országos Meteorológiai Szolgálat, Budapest.

Mika, J., Kircsi, A., and *Tar K.*, 1999: Some statistical characteristics of daily maximum wind gusts in the Great Hungarian Plain (in Hungarian). *Meteorológiai Tudományos Napok 1999*. Orsz. Meteorológiai Szolgálat, 207-213.

Rudas, T., Clogg, C.C., and *Lindsay, B.G.*, 1994: A new index of fit based on mixture methods for the analysis of contingency tables. *J. Royal Statistical Society*, Ser. B 56, 623-639.

Schönwiese, C.D., Rapp, J., Fuchs, T., and *Denhard, M.*, 1994: Observed climate trends in Europe 1891-1990. *Meteorol. Zeitschrift*, N.F. 3, 22-28.

Tar, K., 1998a: Statistical characteristics of the wind field over Hungary, in connection with the global warming (in Hungarian). In *Klimaváltozás és következményei*. Orsz. Meteorológiai Szolgálat, 249-258.

Tar, K.,1998b: Alteration of the statistical structure of the wind field in Hungary in connection with the climatic change. *2nd European Conference on Applied Climatology*, Central Institute for Meteorology and Geodinamics, Nr. 19, (CD-ROM, ISSN 1016-6254) Vienna, Austria.

Tar, K., 1999: Temporal change of statistical charcateristics of wind field over the Great Hungarian Plain (in Hungarian). *Change of landscape in the Carpathian Basin*. Proc. of Scientific Conference, Nyíregyháza, November 4-6, 1998. (ed.: *Gy. Füleky*), Gödöllő, 225-230.

Tar, K., 2001: Alteration of the statistical structure of the wind field in Hungary in connection with the conditional climatic change. *OTKA Research Paper* (T023765), University of Debrecen (in Hungarian).

Tar, K., Makra, L., and *Horváth, Sz.*, 2000: Some statistical characteristics of the wind energy in Hungary in connection with climatic change. *3rd European Conference on Applied Climatology* (CD-ROM, ISBN 88-900502-0-9), Pisa, Italy

Tar, K., Makra, L., and *Kircsi, A.*, 2001a: Temporal change of some statistical characteristics of wind speed in Hungary. In *Detecting and Modelling Regional Climate Change* (eds.: *M.B. India* and *D.L. Bonillo*). Springer-Verlag, 251-262.

Tar, K., Makra, L., Horváth, Sz., and *Kircsi, A.*, 2001b: Temporal change of some statistical characteristics of wind speed in the Great Hungarian Plane. *Theoretical and Applied Climatology*, Vol. 69, No. 1-2, 69-79.

BOOK REVIEW

Barry, R. G. and *Carleton, A. M.*, 2001: **Synoptic and Dynamic Climatology.** Routledge (Taylor and Francis Group), London and New York, 620 pages, with 15 color and black-and-white plates, nearly 300 figures and didactic illustrations, extended topical index.

The book provides a comprehensive account of the dynamical behavior and mechanisms of the global climate system and its components, together with a modern survey of synoptic scale weather systems in the tropics and extratropics, including the methods and applications of synoptic classification.

Roger G. Barry is Professor of Geography and Director of the National Snow and Ice Data Center at the University of Colorado. *Andrew M. Carleton* is Professor of Geography at Pennsylvania State University. This fact largely determines the key value of the book for meteorologists and other scientists. Scrolling through the book, the reader gets a scholarly description of the atmospheric circulation from the smallest to largest scales of atmospheric motions.

Twenty-seven years have elapsed since the publication of *Synoptic Climatology: Methods and Applications* (*Barry* and *Perry*, 1973), and the field has advanced considerably during that time. Computer-based classifications have become the rule, and the ready availability of extensive climatic data bases has permitted diverse analytical studies to be carried out. Results from these studies now allow us to state more confidently the most useful procedures for the synoptic classification and analysis of regional or local climatic conditions. The book differs very much from the one appeared three decades before. Only the last Chapter ("Synoptic climatology and its applications") remind us to the book-ancestor which is not coincidental and is accompanied by displaying *Prof. Allen H. Perry*, as co-author of the present chapter, as well.

The widespread practical applications of these studies is illustrated, with particular emphasis on the linkages between regional and global-scale climate processes. The latter relation, most likely an unresolved task required by climate change impacts but not yet available with fully dynamical models, makes the book especially valuable. Downscaling studies frequently based on objective classifications of the circulation systems, but sometimes using just formal statistics and (easily available) low resolution fields, could improve a lot by assimilation of the corresponding chapters, too.

Part I provides an introduction to the global climate system and the space-time scales of weather and climate processes, followed by a chapter on climate

data and their analysis. *Part 2* describes and explains the characteristics of the general circulation of the global atmosphere, planetary waves and blocking behavior, and the nature and causes of global teleconnection patterns. *Part 3* discusses synoptic weather systems in the extra-tropics and tropics, and satellite based climatologies of synoptic features. It also describes the methods and applications of synoptic climatology and summarizes current climatic research and its directions.

The scale and scope of this undertaking is remarkable. Each chapter makes it clear what is known and what has still to be investigated. This is coupled with a fascinating insight into the development of ideas over the past centuries and the way in which investigations have become increasingly scientific, utilizing the most sophisticated technologies available. Some of the figures are interesting because we know other interpretations expressing the same idea. A part of the figures are a little old, however, which is acceptable with tolerance in case of a textbook. In some cases, however, the print of the drawings does not correspond to the present typographical technology.

Summarizing, the authors provided a much-needed bridge between classical synoptic climatology and the more recent developments in dynamical and statistical meteorology. This book will serve as a valuable reference for climate researchers. It will also provide an excellent textbook for climate related courses at the graduate and post-graduate levels.

J. Mika

GUIDE FOR AUTHORS OF *IDŐJÁRÁS*

The purpose of the journal is to publish papers in any field of meteorology and atmosphere related scientific areas. These may be

- research papers on new results of scientific investigations,
- critical review articles summarizing the current state of art of a certain topic,
- short contributions dealing with a particular question.

Some issues contain "News" and "Book review", therefore, such contributions are also welcome. The papers must be in American English and should be checked by a native speaker if necessary.

Authors are requested to send their manuscripts to

Editor-in Chief of IDŐJÁRÁS

P.O. Box 39, H-1675 Budapest, Hungary

in three identical printed copies including all illustrations. Papers will then be reviewed normally by two independent referees, who remain unidentified for the author(s). The Editor-in-Chief will inform the author(s) whether or not the paper is acceptable for publication, and what modifications, if any, are necessary.

Please, follow the order given below when typing manuscripts.

Title part: should consist of the title, the name(s) of the author(s), their affiliation(s) including full postal and E-mail address(es). In case of more than one author, the corresponding author must be identified.

Abstract: should contain the purpose, the applied data and methods as well as the basic conclusion(s) of the paper.

Key-words: must be included (from 5 to 10) to help to classify the topic.

Text: has to be typed in double spacing with wide margins on one side of an A4 size white paper. Use of S.I. units are expected, and the use of negative exponent is preferred to fractional sign. Mathematical formulae are expected to be as simple as possible and numbered in parentheses at the right margin.

All publications cited in the text should be presented in a *list of references*, arranged in alphabetical order. For an article: name(s) of author(s) in Italics, year, title of article, name of journal, volume, number (the latter two in Italics) and pages. E.g., *Nathan, K.K.,* 1986: A note on the relationship between photo-synthetically active radiation and cloud amount. *Időjárás 90,* 10-13. For a book: name(s) of author(s), year, title of the book (all in Italics except the year), publisher and place of publication. E.g., *Junge, C. E.,* 1963: *Air Chemistry and Radioactivity*. Academic Press, New York and London. Reference in the text should contain the name(s) of the author(s) in Italics and year of publication. E.g., in the case of one author: *Miller* (1989); in the case of two authors: *Gamov* and *Cleveland* (1973); and if there are more than two authors: *Smith et al.* (1990). If the name of the author cannot be fitted into the text: *(Miller,* 1989); etc. When referring papers published in the same year by the same author, letters a, b, c, etc. should follow the year of publication.

Tables should be marked by Arabic numbers and printed in separate sheets with their numbers and legends given below them. Avoid too lengthy or complicated tables, or tables duplicating results given in other form in the manuscript (e.g., graphs)

Figures should also be marked with Arabic numbers and printed in black and white in camera-ready form in separate sheets with their numbers and captions given below them. Good quality laser printings are preferred.

The text should be submitted both in manuscript and in electronic form, the latter on diskette or in E-mail. Use standard 3.5" MS-DOS formatted diskette or CD for this purpose. MS Word format is preferred.

Reprints: authors receive 30 reprints free of charge. Additional reprints may be ordered at the authors' expense when sending back the proofs to the Editorial Office.

More information for authors is available: antal.e@met.hu

Information on the last issues: http://omsz.met.hu/irodalom/firat_ido/ido_hu.html

Published by the Hungarian Meteorological Service

Budapest, Hungary

INDEX: 26 361

HU ISSN 0324-6329

IDŐJÁRÁS

QUARTERLY JOURNAL
OF THE HUNGARIAN METEOROLOGICAL SERVICE

CONTENTS

****

http://omsz.met.hu/english/ref/jurido/jurido_en.html

VOL. 107 * NO. 3 - 4 * JULY - DECEMBER 2003

IDŐJÁRÁS

Quarterly Journal of the Hungarian Meteorological Service

Editorial Office: P.O. Box 39, H-1675 Budapest, Hungary or
Gilice tér 39, H-1181 Budapest, Hungary
E-mail: prager.t@met.hu or *antal.e@met.hu*
Fax: (36-1) 346-4809

Subscription by

mail: IDŐJÁRÁS, P.O. Box 39, H-1675 Budapest, Hungary
E-mail: prager.t@met.hu or *antal.e@met.hu*; *Fax: (36-1) 346-4809*

Prof. Dr. Gábor Szász is 75

Professor Dr. Gábor Szász has recently celebrated his 75th birthday. On this occasion we wish to publish a special number of the journal Időjárás devoted to him and his lifetime activity. The articles of this number are written by their colleagues who shared the work with him under his long and extremely successful career, and by students who were educated by him to be such devoted persons to meteorology and especially agrometeorology as he was and remains all the time of his life. We can say without any reservation that he is one of the leading personalities of Hungarian meteorology and one of the rare ones who could build and can maintain efficient contacts with other sciences, which gives us – the community of Hungarian meteorologists – a living joint to the engineering practice of agronomy and industrial use of microclimatology. He was extremely successful in building a school and creating a unit at the Agricultural University of Debrecen dealing with these branches of our science. He has undertaken important leading positions at the mentioned university including the rector and prorector position for a long time, and this way he was an important personality of the country's scientific policy, and also a leading personality of science in the region.

In the name of the Editorial Board, the authors of this issue and all representatives of other disciplines, whose activities were encouraged and supported by Professor Szász, I wish to send our greetings to him and wish many good and successful years in his professional and personal life.

Prof. Dr. Gábor Szász's scientific career

He was born in 1927 in Békés. After finishing his studies in the course of biology and geography at the University of Debrecen, he obtained his teacher's degree in 1950. Already in the years 1948–1950, he worked for the Meteorological Institute of the University where he started his professional career. He was an aspirant between 1952 and 1955, then he obtained his CSc degree in 1956. In this period he also finished the course of mathematics-physics (1958). He became the doctor of the Hungarian Academy of Sciences in 1999.

His long scientific career he devoted to research in the field of agrometeorology, and inside it he dealt with macro- and micrometeorological problems of water supply of plant. For the aim of this research, in 1962 he developed, with significant investment, the climatic station of the – now already 100 years old – Debrecen-Pallag Agricultural Academy into a high level and even now state-of-the-art observatory, for which he is the head. His scientific work was always the part of some large country-wide scientific programs, presently he works on two big projects in the frame of the Széchenyi plan. In the years 1970–1980 he worked out the system of agroecological regions of Hungary, that is in constant use from that time in decision-making practice of the Ministry of Agriculture and Regional Policy. He maintained and continues to maintain intensive scientific contacts and co-operation with research institutions and universities from a wide range of countries, like Germany, the Netherlands, USA, etc., mainly in micrometeorology. Some specific areas of his research include

- *the characteristics and representativity of plant canopy climate,*
- *the role of micro-advection and turbulent diffusion in formation of plant canopy climate,*
- *the transport of energy and substances within plant canopy,*
- *the role of macro- and micrometeorological conditions in plant development and crop yield,*
- *the use of remote sensing in determining the water supply of plant canopies.*

During his entire professional life, he had affiliation with universities and never left Debrecen. From 1951 to 1956 he worked as lecturer in the Department of Meteorology, then became scientist at the same place. In 1961 he changed to the College of Agrarian Science, where he continued to work in the same capacity. He became associated professor in 1963, then professor in 1971. At both of his workplaces he was the lecturer of agrometeorology, but also made lectures in climatology, micrometeorology, hydrometeorology, and agroecology for decades. In the frame of the reform of the University he organized and became the leader of a multidisciplinary PhD educational program and postgraduate school in agroecology. He always actively participated in the public life of the Debrecen universities, held a number of leading positions. For ten years he was the dean of a faculty, then for nine years the rector and the prorector of the Agricultural Univerisity of Debrecen. From the end of the 1970s he was an active initiator of the integration of the universities in Debrecen, and in consequence he led for two years the Union of Debrecen Universities, or – simply – the Universitas. His long participation in scientific policy has given us such results, like the computer network connecting the universities, or the harmonization of education and research through bringing them nearer to practice. In 1997 he formally retired from education, and presently he is professor emeritus of the University. He is member of numerous scientific organizations, e.g., for 10 years he was the president of the Hungarian Meteorological Society. He is the author of a very long list of scientific publications whose number exceeds 140, with 3 big monographs among them. He was honored for his work with numerous orders and prizes, like the Order of Labor (two times), the Officers' Cross of the Order of Republic, Eötvös Loránd, Pázmány Péter, and Schenzl Guidó Prizes, Steiner L., Hatvani I., Bocskai I., Pro Universitatis Memorial Medals, etc.

IDŐJÁRÁS

Quarterly Journal of the Hungarian Meteorological Service
Vol. 107, No. 3–4, July–December 2003, pp. 173–188

Effects of the weather and climate to the evapotranspiration of crop canopies

Emánuel Antal

Hungarian Meteorological Service,
P.O. Box 39, H-1675 Budapest, Hungary; E-mail: antal.e@met.hu

(Manuscript received October 3, 2003; in final form October 30, 2003)

Abstract—Water demand, water consumption and water efficiency of crop canopies are affected by numerous factors. Plant species, variety, developing phase, plant canopy density, leaf area, fertilizer- and water supply play important roles. On the other hand, changes in these active factors are controlled by the weather and climatic conditions.

This paper presents the relationships between the features characterizing crop canopies and the optimal evapotranspiration affected by the weather (the water demand of crop canopies), on the base of few decades agrometeorological experiments.

Key-words: evapotranspiration, water demand, water supply of crop canopy, water balance, irrigation water demand, surface water surplus.

1. Introduction

At a given place, crop canopy water balance is regulated by the plant properties and, significantly, by the meteorological and climatic factors. Under Hungarian climatic conditions, precipitation plays significant role in the shaping of water demand and water supply of plants. Precipitation, capriciously spreaded in time and space, often does not satisfy the water demand of plant canopies, on the other hand, from time to time water surplus is generated which can be resulted in inland waters. In dry, drought-stricken years different amounts of irrigation water are needed to enhance the yield safety. The crop canopy water balance is exposed primarily to the permanently changing weather. The role of the climate becomes conspicuous when we are interested in the changes in space or in the effects of a climate change or fluctuation.

Examination of the plant-water-atmosphere system is always a current topic in our country, but nowadays it gets to the center of interest all the more, since it is considered that the dry, droughty periods are more frequent and intense in the last one or two decades, affecting the crop canopy water balance. Also, global warming became a timely problem in the last 10–15 years, whose expectable consequences can cause more unfavorable agricultural water balance in our country. It is obvious, that these suppositions or facts arouse the interest of competent experts whether it can be expected a sensible (favorable or unfavorable) change in the plant-water-weather-climate system in the future in our country. The starting point of these kind of examinations is the survey of the present situation, to which the expectable future situation can be compared.

On the other hand, the research activity has significantly decreased on this field in Hungary. There are very few studies demanding financial and material resources, though, the spread and direct practical use of recent measuring instruments and computing techniques, as well as modeling techniques would make the more exact description and more correct biological and physical explanation of the soil-plant-atmosphere system possible.

This paper gives a short overview of the relationships between the crop canopy water balance and the weather, based on the results of agrometeorological researches carried out at the Hungarian Meteorological Service. We try to make a comprehensive study on the questions and answers raised in the course of the examination of evapotranspiration.

For an objective analysis of the effects of an expectable global warming on the evapotranspiration, and irrigation water demand it is essential to clear the possible answers given to the following questions.

2. How does the permanently changing weather influence the water demand (optimal evapotranspiration) of crop canopies?

There is an objective answer for this question only if the characteristic parameters of crop canopies (variety, plant density, fertilizer- and water supply) in the field experimental researches are the same year by year, whilst the weather conditions are changing. We had been carrying out studies for different species planted in compensatory evapotranspirometers for years (*Antal*, 1966). The water consumption of different plant species had been measured from sowing to harvest by lysimeters with good water supply. From the experimental series we chose maize and potato from the period of 1963–1968 (variety, fertilizer supply, plant canopy density, and water supply were the same during this period). There were extremely hot and dry (1963, 1968) as well as cold and wet (1965, 1966) years in the field experimental period.

Figs. 1 and *2* definitely show that the water demand changes within wide bounds depending on the weather conditions. (The same experimental conditions and varying weather conditions in the course of period 1963–1968). The water demand of both the potato and maize canopies is 30–40 percents higher in a hot and dry growing season than in a cold and wet vegetation period. The influence of the weather parameters is more obvious if we examine the course of the daily water demand in the growing season in years with different weather conditions (*Antal*, 1966, 1998) (*Figs. 3* and *4*).

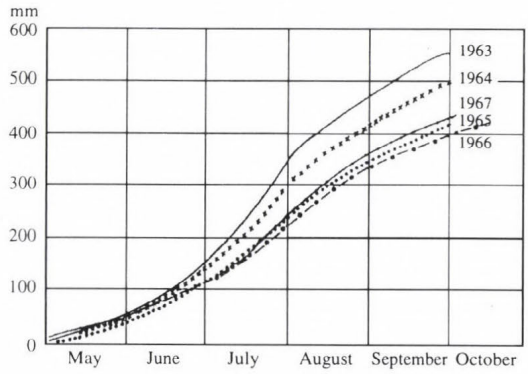

Fig. 1. Accumulated water demand (ET_{opt}) of maize canopy in the years 1963–1967 with different meteorological conditions (Szarvas).

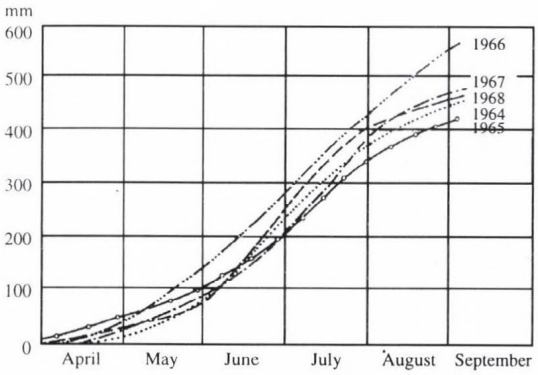

Fig. 2. Accumulated water demand (ET_{opt}) of potato canopy in years 1963–1967 with different meteorological conditions (Szarvas).

As *Fig. 3* shows, in the period between sowing and spring, the optimal evapotranspiration (ET_{opt}) of potato canopy is 1.5–2.0 mm/day, which is

practically equal to the evaporation of moist soil surface. After this period, water consumption increases with the quick growing of the plants. In the critical development phase (blooming and intensive tuber growth), daily maximum of the water demand is 4–6 mm depending on the weather. On certain hot and dry days, the daily water loss was as high as 8 mm, while on cool and cloudy days it did not exceed the value of 2–3 mm, even in the period of apex development. After the ending of blooming, the daily water demand of potato canopy quickly decreases, and it less depends on the weather conditions.

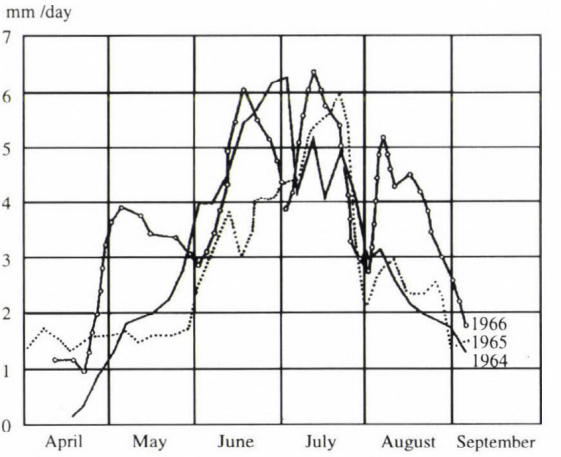

Fig. 3. The annual course of potato ET_{opt} in the period 1964–1966 with different weather conditions.

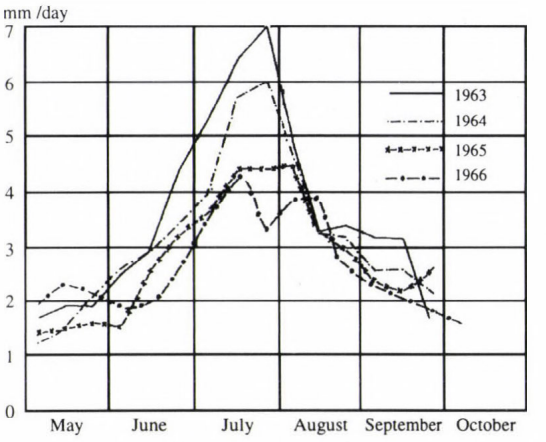

Fig. 4. The annual course of maize ET_{opt} in the period 1964–1966 with different weather conditions.

Similar conclusions can be drew on the water consumption of maize canopy (*Fig. 4*), with the difference that in the period following the critical development phase (head flowering, tasseling) of the individual years, the water consumption of maize canopy is less dependent on the weather conditions than the evapotranspiration (ET) of potato canopy.

Data presented in *Table 1* gives an other evidence on the considerable dependence of the water demand of crop canopies on the day by day changing quantity of the heat reversible to evaporation and, indirectly, on the temperature (*Antal*, 1972, 1981, 1998, 2003).

From the blooming and hand flowering phases those periods (3–4 days) were chosen, when there was a quick temperature increase or decrease after a frontal passage. Based on the data of the table it can be concluded, that the temperature change of 7–10°C resulted in an overnight 50–80% change in the water consumptive use of maize canopy, without any change in the soil moisture content of the root zone.

Table 1. Changes of the daily water consumptive use of potato- and maize canopy as a function of the air temperature (Szarvas, silty clay soil)

Period	Water demand of potato mm/day	Temperature daily average °C	Period	Water demand of maize mm/day	Temperature daily average °C
1964 June 28	7.1	24.2	1963 June 26	10.0	25.9
29	7.7	23.2	29	2.3	17.5
30	4.3	11.5	30	3.5	17.8
1965 June 24	6.2	23.4	1964 July 22	9.4	27.1
25	6.4	24.4	24	3.1	20.8
28	2.6	16.5	25	3.6	19.7
1966 June 3	2.8	14.4	1965 July 26	7.1	22.6
July 1	2.4	16.7	27	2.4	16.9
July 5	7.1	24.6	28	3.7	18.0
1967 June 8	7.0	22.0	1966 July 20	7.3	24.0
9	1.3	17.3	23	1.7	17.0
10	1.4	16.5	1967 Aug 7	2.2	18.8
11	0.6	11.4	10	8.2	25.3
1968 June 9	7.4	22.9	1968 July 15	11.0	24.7
10	2.5	13.1	18	2.5	17.1
11	2.0	12.4	19	2.7	16.1

The above presented temperature dependent water demand fluctuations could be detected also in vegetable-, fruit-tree-, and vineyard canopies (*Cselőtei*, 1959; *Gergely* and *Stollár*, 1980; *Stollár* and *Gergely*, 1978; *Füri* and *Kozma*, 1975, 1978).

On the base of the above described results, a general answer can be formulated for the first question. Namely, *the yearly and year-by-year changes of the weather are definitely followed by a change in the optimal evapotranspiration, i.e., water demand of crop canopies, even if the soil moisture content availability in the root zone is optimal in irrigated circumstances.*

An other question raised in connection with the determination of the irrigation water demand was the role of the species, variety, and developing phase in the shaping of water consumption of crop canopies. Therefore, the second basic question was the following:

3. How do the species, variety, and developing phase effect the shaping of the water demand (optimal evapotranspiration)?

There are many ways to study the effects for getting an answer to this question. A definite and quantitative answer can be given only on the base of the results of a water balance and ET measurements, which are carried out under the same meteorological conditions. On the base of the few decades long evapotranspirometer experiments carried out at the agrometeorological observatory of Szarvas, a definite answer can be given for the above expressed question. *Fig. 5*, which was drawn in our earlier studies (*Antal*, 1966, 1998), presents the accumulated curves of the optimal evapotranspiration (water demand) of five different plant species. The curves suggest that there is a significant difference in the water demand of individual crop canopies, even with the same soil texture, water supply, and meteorological conditions. If in thought we transform the sowing times into the same point of time, there are still decided differences among the accumulated curves. For example, the winter wheat finished its vegetation period with 400 mm accumulated water consumption, while the sugar beet used 25% more water in its vegetation period, and the accumulated water consumption of the alfalfa crop canopy was about 700 mm, in the same year. The most evident differences among the individual species appear in the accumulated water consumption. On the other hand, since all the field experimental conditions were the same, the possible cause of the significant differences experienced in the water demand can be searched in the different biological and plant physiological features, as well as in the individual characteristics of the crop canopy type (plant canopy density, leaf area, different radiation balance).

The effect of the plant species difference on the water demands are more clearly demonstrated by the curves of *Fig. 6*, which presents the daily amounts

of the optimal evapotranspiration in case of different plant species (*Antal*, 1966, 1972, 1998, 2003; *Antal* and *Szesztay*, 1996).

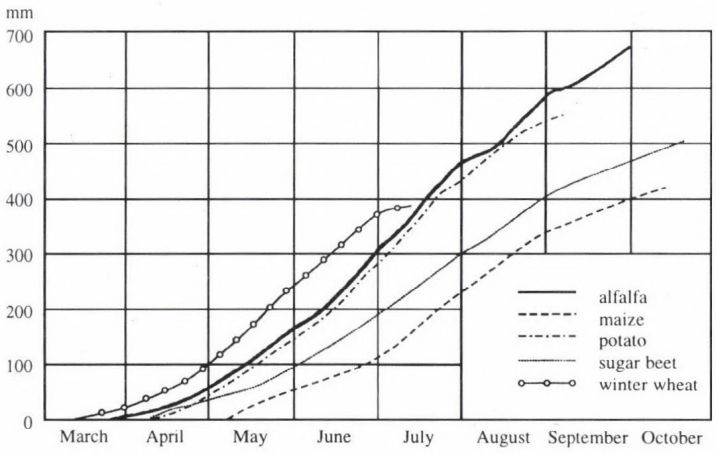

Fig. 5. Accumulated curves of the ET_{opt} in case of different plant canopies (Szarvas, 1966).

Three basic conclusions can be derived from the course of the curves of *Fig. 6*:

- there are definite differences between the daily water demands of the species (on certain days, a plant canopy with higher water demand uses 2–3 times more water than a plant with lower water demand, e.g., in the middle of May);
- the water demand of all crop canopies remarkably fluctuates during the growing season, which indicates the effect of changing meteorological conditions;
- it can be stated, too, that the maximum of daily water demand coincides with the critical development phase in the case of all species (it is not obvious in the case of pasture as it is mown a few times in the vegetation period).

Therefore, there is an unambiguous answer for the second question: *there are significant differences in the water demand and water consumption of the individual plant species, even in the same periods and meteorological conditions, and the period of maximal water demand definitely coincides with the time of the critical development (usually blooming) phase.* Taking into account these facts is of vital importance in the irrigation farming.

In both irrigation- and natural farming, the role of the plant canopy density in the formation of the yield harvest and water demand is a matter of many disputes. In irrigated conditions, the size of the optimal plant number per hectare is influenced by the light supply, whilst in circumstances without irrigation it is influenced by the soil moisture content in the root zone. This discussion emerged the third question of the evapotranspiration researches:

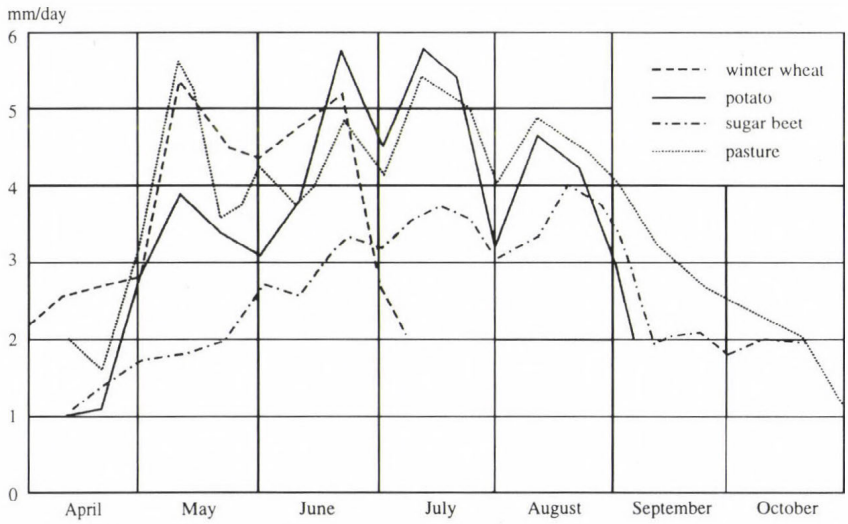

Fig. 6. Dependence of the daily ET_{opt} on the different plants species in course of the growing season (Szarvas, 1966).

4. What kind of relationship can be found between the plant canopy density and the development of water demand?

It is obvious, that in this case every effecting factors (water- and fertilizer supply, variety) have to be the same. Our study was based on data measured by evapotranspirometers in maize canopies with different plant density (*Antal et al.*, 1974, 1975).

The main features of the relationship between the evapotranspiration and plant stem density are summarized in *Table 2*.

The table shows that with increasing plant density (from 4 to 6 stems per m^2) the water demand raised with 19%. It means, that the corn canopy of 60,000 plant numbers per hectare used 1050 m^3 more water than that of 40,000.

It was not possible to determine an optimal plant density for water consumption and yield without any doubt. In cooler years with less sunshine, the less dense plant canopy assured more yield and water consumption, while in warmer vegetation periods, which were rich in sunshine (for example in 1968, see *Table 2*), the most dense corn canopy produced the biggest yield and water consumption.

Table 2. Optimal evapotranspiration measured by evapotranspirometers in corn canopy with different plant stem density per m^2, mm (Szarvas, 1968)

Month	Plant number per m^2			
	4	5	6	7
April	10	11	11	11
May	43	48	54	54
June	135	145	154	187
July	189	209	229	284
August	126	138	150	176
September	61	65	69	99
October	5	6	7	11
April–October	569	622	674	822

Note: April and October are fragmented months (few days only)

Therefore, there is no definite answer for the third question to the experts of irrigation. Results of the examinations can be summarized only generally: *with increasing plant number per hectare, the water demand definitely increases, however, the plant canopy can not be given with a particular value, since it depends on the probable weather of the vegetation period, and this dependency can not be compensate even with the most favorable water- and fertilizer supply*. It would help if a weather prediction with acceptable accuracy would be given in the time of sowing at least to the end of the critical development phase, and the sowing plant number per hectare would be determined as a function of that.

Development of the irrigation emerged the so far actual question, that farms working on soils with good productivity need to be preferred to those with weak productivity in the course of irrigation investments. An objective decision postulates studies on numerous economic, market, social, and farming technologic aspects. Experts of this field ask the fourth question concerning the water balance of the plants:

5. Does the fertilizer supply influence the water cycle of plant canopies, if yes, in what extent?

The question can not be narrow down to the analysis of interaction between the nutrition supply and water consumption, since the crop result appears as a standard of value. On this field, evapotranspirometer investigations have been carried out for years in Szarvas and Keszthely, examining few plant species with different amounts of combined nitrogen, phosphorus, potassium artificial fertilizers (NPP) (*Antal et al.*, 1975; *Endrődi*, 1978; *Tóth*, 1978).

From the decade long measurement series we pick out the results concerning maize canopy. In this case, we tried to give an answer on the basis of four measuring series with different fertilizer supply (0, 120, 240, 480 kg/hectare NPP efficient substance) and three series with different water treatment (*Antal et al.*, 1975; *Tóth*, 1978; *Posza* and *Tóth*, 1978).

Fig. 7 shows the accumulated curves of the optimal evapotranspiration (ET_1, ET_2, ET_3) of corn canopy in the case of different fertilizer supply, as well as the actual evapotranspiration of the plant canopy with natural water supply (precipitation) in the surroundings of the evapotranspirometers ($ET_ø$). The upper curve is the calculated potential evapotranspiration (PE).

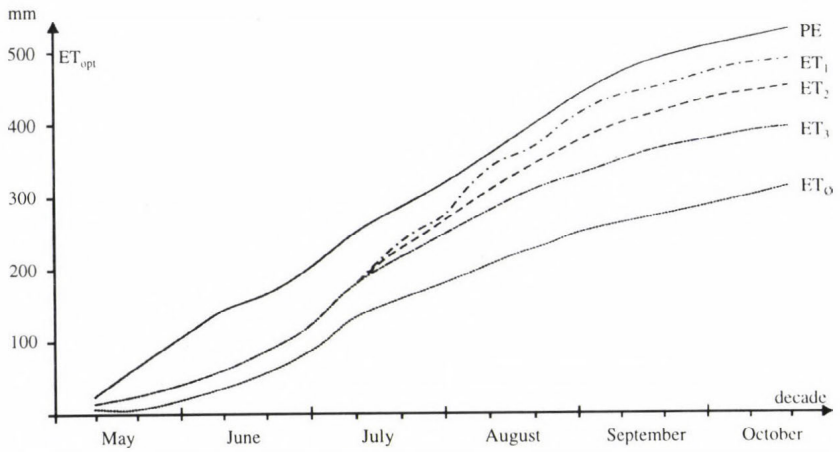

Legend: PE potential evapotranspiration; ET_1 and ET_2 optimal evapotranspiration in case 480 and 240 kg NPP with irrigation; ET_3 optimal evapotranspiration of irrigated canopy without NPP; ET actual evapotranspiration of controlling plot (no irrigation, no NPP).

Fig. 7. Accumulated curves of the maize canopy evapotranspiration at the different NPP supply (Keszthely, 1973).

The results of investigations can be summarized as follows. In the case of medium fertilizer supply (240 kg/hectare NPP), the water demand of maize canopy increased with 13%, in the case of large amount (480 kg/hectare NPP), the water demand increased with 22% comparing to the plant canopy without fertilization. However, the excess fertilizer did not increased the water demand in the same degree, which is proved by *Table 3*.

Table 3. Increase of the water demand of maize canopy comparing to the controlling plot

Year	Increase of water demand, 240 kg/hectare NPP, %	Increase of water demand, 480 kg/hectare NPP, %
1971	14	22
1972	8	9
1973	7	13
Average	**9.7**	**14.7**

Effects of the nutrition supply to the water demand is well demonstrated by the water consumption coefficient as well (to be expressed in liters of water used to corn cob yield production), which is presented by *Table 4* on the base of the experiments (*Antal et al.*, 1975).

Table 4. Maize water consumption coefficient in the case of different fertilizer supply

Year	Controlled plant liter/kg	240 kg/hectare NPP liter/kg	480 kg/hectare NPP liter/kg
1971	592	431	412
1972	1090	467	430
1973	1404	539	445

The maize water consumption coefficient changes from year to year depending on the meteorological conditions. Similar results arised from examining the transpiration coefficient of vegetable canopies (*Cselőtei*, 1964).

It can be seen, that excess fertilizer makes the water efficiency better by means of bigger crop results (on the controlling parcel the water consumption coefficient declines from year to year, since the crop result decreases in the lack of fertilizer supply).

The answer for the fourth question is the following: *Increasing of the NPP doses leads to the increase of the water demand and water consumption, nevertheless, the irrigation demand depends on the year-by-year changing meteorological conditions.* Moreover, irrigation can be built into the farming technology only if it is rewarding in average of many years. As our investigations pointed out (*Antal et al.*, 1975), beyond a certain extent, even the increasing of either the artificial fertilizer or irrigation water was not resulted in the efficiency of the yield.

A widely discussed question is the role of leaf area in water consumption of plant canopy. The majority of formulas, developed to evaluate ET, do not contain this feature of plants, nevertheless, many researchers tried to involve it in the computational methods more or less successfully. It is an understandable aspiration, as the leaf area projected to 1 m^2 soil surface changes within wide limits depending on species, canopy plant density, and developing phase. While the leaf area of a well developed maize canopy is 2.5–3.5 m^2/m^2 soil surface, leaf area of a closed, well developed alfalfa crop canopy is much bigger.

In this case the following question is raised:

6. What role does the leaf area play in the change of evapotranspiration amount of crop canopies?

Leaf area plays twofold role in influencing the evapotranspiration. On the one hand, it increases the transpiration area, on the other, by interception of precipitation and sprinkler irrigation water it decreases the water income of the root zone, because the interception water evaporates from the plant without utilization.

In this case the question is raised in the following form: what order of magnitude of the water, first intercepted from the precipitation and sprinkler irrigation by the leaf area, is evaporated without utilization, and whether this amount should be taken into account in drawing up of irrigation timetable. How should this water amount be taken into account in determination of irrigation water norm, single irrigation water dose, and irrigation time (day or night).

The evaporation deficit of the sprinkler irrigation is composed of the accumulated amounts of water evaporated from the irrigated water drops, plants, and soil surface. The quantity of the deficit depends on the leaf- and steam surface of plant canopy, as well as on the evaporative demand of atmosphere. On cloudy, cool days and in the night hours the evaporation deficit is minimal, under hot, dry, clear, windy weather conditions it can

maximally reach the value of net radiation of the plant canopy expressed in water millimeter.

In Hungary, in the summer months, under average weather conditions the daily net radiation of plant canopies is 150–250 MJ/m^2 depending on the plant species (*Dávid et al.*, 1990). The evaporative equivalent of this value is 3.3–6.0 mm/day. Thus, in the case of continuous daytime irrigation, the maximum evaporation can fluctuate within this limits, supposing that the net radiation is fully consumed by the evaporation, i.e., the heat converted to warming up the soil and air is zero.

Comparing the 3.3–6.0 mm maximum amount of evaporative water to the 30 mm irrigation dose, the evaporation deficit of the irrigation water is given to be 11–20%, i.e., 24–27 mm water reaches the root zone from the 30 mm irrigated water. *Using smaller irrigation water doses, the relative evaporation loss (expressed in % units)is greater, with bigger water doses the loss is less. It is obvious, that in the case of plant canopies with bigger leaf area and under highly evaporative weather conditions, 10–20 % evaporation loss of the sprinkler irrigation needs to be taken into account in determining the amount of irrigation water.*

The above discussed questions can be numerically and objectively answered only by experimental measurements and analysis. These kind of investigations will be requisite in the future as well, as the results up till now have to be strengthened and corrected, and the continuously developing farming technologies emerge further questions. On the other hand, analyzing conditions of the water cycle of plant canopies improve, since the measuring instruments and data processing and analyzing methods are developed very quickly, too. It can also be supposed, that our membership in the European Union will be a great challenge for the Hungarian food industry as regards farming efficiency as well as qualitative expectations. Since under Hungarian climatic conditions the precipitation supply is a limiting factor for both efficiency and quality, prospectively the farmers, leaders of the management of water-supplies of the agriculture, and experts will claim for correct and reliable research results regarding water- and irrigation water demand as well as economical and effective water supply of plant canopies. Our researchers can fill these expectations if the concerning special fields take the initiative in closer co-operation. That is, as the above discussed tasks made it perceptible, analysis of the effects of the weather and climate to the soil-plant-water system is an interdisciplinary task.

7. The role of the climate in shaping of water demand and irrigation water need of plant canopies

As it was mentioned in the introduction, climatic features play important role in planning of the irrigation system of plant canopies. During the planning of the irrigation system (irrigation canal, pump capacity, size of the irrigated area, etc.), a claim is raised to necessary basic data, which are well-established in climatic point of view. Such data are, among others, the average of many years, expectations with different probabilities, fluctuation in time, areal distribution, etc., of the water demand and irrigation water need of plant canopies.

Based on the climatic database, being at our disposal, the parameters are suitable to be calculated for as long time as possible (possibly for 50, 100 years), partly for avoiding the presence of short time climate fluctuations in the averages and particular frequency threshold values. The other reason is that building up of the irrigation system for long time needs basic climatological data representing few decades.

For well-established planning of irrigation systems, the basic irrigation water need data have to be determined by regions and plant species. The most expedient method is to derive empirical distribution functions from the time series, as the function curves represent the irrigation water need expected with any possibilities.

As an example, *Fig. 8* presents the empirical distribution function of irrigation water need calculated from the almost 100 years long data base of our earlier studies (*Antal*, 1991, 1998), for three different climatic zones in Hungary and two plant species. Irrigation water need expected with any percentage frequencies and the average value belonging to the 50% can be read from the curves. The ending points of the curves indicates the maximum and minimum values occurred in the processing period.

If the irrigation water need data calculated for every vegetation period are put in order of magnitude and the year of occurrence is signed, we can reply to the question whether the droughty growing seasons were more frequent in the last one or two decades. Because of the size of the data table, detailed values are not presented, we only note that all of the three climatological stations reported more occurrences of extreme irrigation water need in the last two decades than in any other two decades of the 20th century.

Summarizing our investigations on water demand, water consumptive use, and irrigation water need of plant canopies, we can say that these features change by climatic zones and plant species depending on the weather conditions. Consequently, the recent irrigation systems have to be based on the following up the dynamically changing water demand and water deficit of the

given plant canopy. The basis of planning of irrigation system developments can be the irrigation water norm determined by farming regions and plant species from long climatological time series. The average values and expectations with different probabilities of the irrigation water norm have to be known as well.

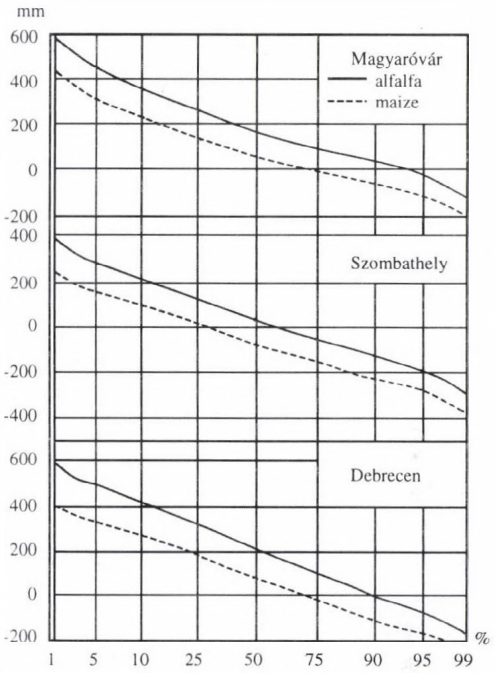

Fig. 8. Empirical distribution function of the irrigation water requirement of alfalfa- and maize canopies in the period of 1901–1995.

References

Antal, E., 1966: Potential evapotranspiration of particular agricultural plants (in Hungarian). *Öntözéses Gazdálkodás 4* (1), 69-86.

Antal, E., 1972: Is plant growth determined by internal water balance and turgor in the cells or by external factors? *Acta Agronomica Academiae Scientiarium Hungaricae*, Tomus 21 (1-2), 458-468.

Antal, E., 1981: Irrigation. *Acta Agronomica Academiae Scientiarium Hungaricae*, Tomus 30 (1-2), 87-222.

Antal, E., 1988: Comparative analysis of the irrigation water requirement and aridity conditions. In *Identifying and Coping with Extreme Meteorological Events* (eds.: *E. Antal* and *M.H. Glantz*). Országos Meteorológiai Szolgálat, Budapest, 205-254.

Antal, E., 1991: Possible effect of the climate change on the droughts in Hungary (in Hungarian). *Acta Geographica Debrecina 1989-1990,* Tomus XXVIII-XXIX, 17-28.

Antal, E., 1998: Relation of the weather and climate to the water balance of crop canopies (in Hungarian). In *Meteorológiai Tudmányos Napok '98.* Országos Meteorológiai Szolgálat, Budapest, 15-28.

Antal, E., 2003: Question marks on the atmospheric water cycle in Hungary regarding the global climate change (in Hungarian). In *Anyagáramlások és hatásaik a természetben* (ed.: *F. Glatz*). MTA Társadalom Kutató Központ, Budapest, 9-71.

Antal, E. and *Szesztay, K.*, 1996: Climate and water in plant ecology. *Időjárás 100,* 193-206.

Antal, E., Posza, I. and *Tóth, E.*, 1974: Relationship between the heat- and water balance system of maize canopy and irrigation water need (in Hungarian). *Beszámolók az 1971-ben végzett tudományos kutatásokról.* Országos Meteorológiai Szolgálat, Budapest, 142-158.

Antal, E., Posza, I., and *Tóth, E.*, 1975: The effect of weather and climate on the fertilizer efficiency (in Hungarian). *Időjárás* 79, 95-104.

Cselőtei, L., 1959: Effect of temperature on the water circulation of vegetable plant canopies (in Hungarian). *Növénytermesztés 4*, 333-348.

Cselőtei, L., 1964: Water usage of vegetable plant canopies (in Hungarian). *GATE Mezőgazdasági Karának Közleményei*, 203-226.

Dávid, A., Takács, O., and *Tiringer, Cs.*, 1990: *Spatial Distribution of Radiation Balance in Hungary on the Basis of the Data During 1951-1980 Period.* Országos Meteorológiai Szolgálat Kisebb Kiadványai 66.

Endrődi, G., 1978: Evapotranspiration of potato canopy as a function of artificial fertilizer supply (in Hungarian). *Beszámolók az 1976-ban végzett tudományos kutatásokról.* Országos Meteorológiai Szolgálat, Budapest, 171-180.

Füri, J. and *Kozma, F.*, 1975: Evapotranspiration of vineyard canopy (in Hungarian). *Időjárás 79,* 112-120.

Füri, J. and *Kozma, F.*, 1978: Effective evapotranspiration and irrigation water need of vineyard canopy (in Hungarian). *Beszámolók az 1975-ben végzett tudományos kutatásokról.* Országos Meteorológiai Szolgálat, Budapest, 181-194.

Gergely, I. and *Stollár, A.*, 1980: Investigations on the water consumptive use of apple plantations and trees cultivated in growing pan (in Hungarian). *Beszámolók az 1978-ban végzett tudományos kutatásokról.* Országos Meteorológiai Szolgálat, Budapest, 138-145.

Posza, I. and *Tóth, E.*, 1978: Shaping of the evapotranspiration of maize canopy as the function of water- and fertilizer supply (in Hungarian). *Beszámolók az 1974-ben végzett tudományos kutatásokról.* Országos Meteorológiai Szolgálat, Budapest,175-176.

Stollár, A. and *Gergely, I.*, 1978: Evapotranspiration of the young apple plant canopy (in Hungarian). *Beszámolók az 1976-ban végzett tudományos kutatásokról.* Országos Meteorológiai Szolgálat, Budapest, 206-215.

Tóth, E., 1978: Evapotranspiration, yield, and water utilization of maize canopy under different fertilizer- and water supplies (in Hungarian). *Beszámolók az 1975-ben végzett tudományos kutatásokról.* Országos Meteorológiai Szolgálat, Budapest, 241-255.

IDŐJÁRÁS

Quarterly Journal of the Hungarian Meteorological Service
Vol. 107, No. 3–4, July–December 2003, pp. 189–198

Seasonal changes of soil moisture in Hungary

Zoltán Varga-Haszonits and **Zoltán Varga**

University of West-Hungary, Faculty of Agricultural and Food Sciences
Vár 2, H-9200 Mosonmagyaróvár, Hungary
E-mail: vargahz@mtk.nyme.hu

(Manuscript received March 28, 2003; in final form September 30, 2003)

Abstract—Soil moisture is a basic enviromental factor determining the water supply of plants. Amount of this meteorological element is influenced by precipitation and evaporation. When rainfall exceeds water loss, water content of soil increases, and this time spell is called as wet period. In a period dominated by evaporation, water uptake of plants becomes more difficult and it is designated as dry period. A critical period from agricultural point of view is when the water shortage in soil can coincide with a high temperature stress, since this phenomenon can be a serious risk factor for plant production.

We can see that seasonal changes in water balance of soil can be determined by the help of climatological data of precipitation and evaporation. This calculation is based on water balance equation, which can be described by models of different complexity. First, the different indices expressing changes in water supply were studied, then wet and dry periods of an average year were determined by the help of an index called relative evaporation.

Climatological data measured in observational network of Hungarian Meteorological Service during the time period of 1951 and 1990 were used for studying the question.

Key-words: soil moisture, relative evaporation, dry and wet period, drought, seasonal changes.

1. Introduction

The plants are fixed in soil by their roots, and their green parts are surrounded by air over the surface, therefore, the value of soil moisture and humidity of the air, as well as evaporative power of the air (potential evaporation) moving water from the soil to the assimilating organs (mainly to leaves) are equally important for them. Besides, the water plays role in moving nutrition solved in water to assimilating organs. Therefore, water supply of plants should be

continuous. This is based on soil moisture, which is varying according to the rainfall amount and evaporation. In a wet period, when the rainfall amount exceeds the water loss, the water income is determinant, and the water content of soil is increasing. In a period without precipitation, the evaporation becomes prevailing, and the water content of soil begins to decrease.

The seasonal changes of precipitation and quantity of incoming energy determine the annual course of soil moisture, too. This is of basic importance for agricultural crops because of the knowledge of irrigation water need. Hence, an agroclimatological analysis of this phenomenon is essential in a country dealing with plant breeding.

2. Material and methods

Seasonal changes in water balance of soil can be determined by the help of climatological data of precipitation and evaporation. This calculation is built on water balance equation, which can be described by models of different complexity. A relatively simple model was elaborated earlier for Hungary using climatological data (*Dunay et al.*, 1968, 1969). This model makes up the data of observational network including potential evaporation data of pan „A", which are very useful for practical purposes (*Stanhill, 2002).*

A simple form of water balance equation is the following:

$$W = W_0 + P - E\,, \tag{1}$$

where W is the soil moisture measured at the end of investigated period, W_0 is the soil moisture measured in the beginnig of the examined period, P is the rainfall amount, and E is the actual evaporation of the same period. Using this model we have to assume, that there is no water flow in horizontal direction, there is no capillary rise, and the water surplus over field capacity will infiltrate to lower layer of soil, under the plant root zone. It is important to build up a water balance model, which can be run with readily available inputs (*Ritchie,* 1985*; Brisson et al.*, 1992).

It is practical to characterize the soil moisture conditions by the aim of relative value of soil water balance. This method is based on radiation aridity index (*ARI*) elaborated by *Budiko* (1956), and can be written in general form as

$$ARI = \frac{E_0}{P}\,, \tag{2}$$

where E_0 is potential evaporation and P is the precipitation. The ratio of potential evaporation and precipitation was represented in graphical form and

designated as climate diagram of *Walter* (1985) for characterizing of different types of climate. Earlier we have analyzed the values of this index for Hungary (*Varga-Haszonits,* 2002).

For a long time, it is usual to calculate the water balance of soil by using relative evaporation (*RE*) or evaporation index, which is ratio of actual evaporation to potential evaporation and can be written as

$$RE = \frac{E}{E_0}. \tag{3}$$

This value is in very close connection with the water content of soil. Therefore, it is a useful method for describing the seasonal changes of soil moisture.

Sometimes it is practical to use the crop water stress index (*CWSI*), which is a version of relative evaporation expressing the ratio of the difference between potential and actual evaporation to the potential evaporation (*Jackson,* 1982), that is

$$CWSI = \frac{E_0 - E}{E_0}. \tag{4}$$

The values of *CWSI* make the values of relative evaporation up to the value of 1. This is the reason why it is sufficient to use only one of two. In this paper, the relative evaporation is calculated.

Climatological data measured in observational network of Hungarian Meteorological Service during the time period of 1951 and 1990 were used for studying the water balance of soil.

3. Results

3.1 Effect of precipitation and evaporation on the change of soil moisture

The rainfall is the main source of water income of soil. Amounts of rainfall vary significantly during the year as *Fig. 1* indicates. The annual course of precipitation is very similar over the whole territory of Hungary. Differencies are found only in the amount of rain. South-western part of the country has the highest amount of rainfall, and southern part of central Hungary has the lowest values.

The evaporation is the basic loss of water content of soil. Potential evaporation shows what amount of water can be evaporated from the free water surface. The amount of evaporated water is mainly depending on solar energy reaching the surface, water vapor deficit in the air, and wind speed. As

we can see in *Fig. 1*, potential evaporation indicates a seasonal variability within the year, which follows the annual course of solar radiation. The annual course of potential evaporation is similar in the whole territory of Hungary, but the amount of evaporation differs from area to area. Highest values of evaporation occur in the southern part of central Hungary, and the lowest are found in the south-western part of the country.

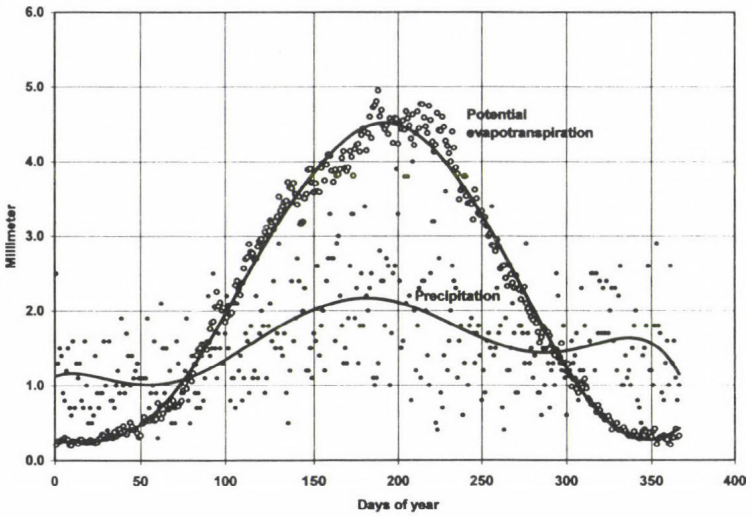

Fig. 1. Annual course of potential evapotranspiration and precipitation in Mosonmagyaróvár (1901–2000).

As we can see in *Fig. 1*, the rainfall amount during the cool period (from November to March) exceeds the amount of evaporation, therefore, this period is a wet period. In this period the rain water can be accumulated in soil. From March the evaporation exceeds the rainfall, thus, soil moisture continuously decreases. This period is called dry period and lasts to the November, when the rainfall amount becomes higher than the evaporation. During this time, the water is primarily the most important environmental factor for plants, and this is why the plant breeders have an increasing risk according to the drought.

Drought can be defined as a significant water shortage for a longer period (*Palmer*, 1965). Only shortage of rainfall itself does not cause dryness. Dry period, however, begins with a low level or total lack of rainfall. Especially in warm period of the year, the low level of rainfall is coupled with intensive radiation and low relative humidity of air, therefore, the evaporation is increasing. This is the reason why the soil water content is decreasing to such

an extent, that plants suffer from water deficiency. Generally, the dryness results from the combination of low precipitation and high evaporation (*Larcher*, 2003).

Finally, rather close relationships can be determined between drought and crop yield. On the basis of these relationships we are able to characterize economically the drought as risk factor (*Varga-Haszonits* and *Harnos,* 1988).

3.2 Seasonal changes in the indices of relative evaporation

In many cases, the soil moisture conditions were characterized by relative evaporation. This was expressed — as we mentioned earlier — by the ratio of actual evaporation to the potential evaporation, where the actual evaporation was calculated as evaporation of bare soil, and the potential evaporation was determined as the evaporation of free water surface (measured by pan „A") under given meteorological conditions. This index value is in a very close connection with soil moisture.

We calculated the average daily values of relative evaporation from 40 years data series for Zalaegerszeg, which is in the wettest area of Hungary, and for Szeged, which is in the dryest territory in Hungary. We can see in *Fig. 2* that in the winter time, when precipitation amount exceeds the amount of evaporation, the values of relative evaporation vary most intensively. In this period, the values in both stations are very close to the maximum values. Consequently, there are no essential differences between the wettest and dryest area in the respect of the length of wet period. After the maximum in February, however, the values of *RE* decrease continuously to the minimum in August. The dryest part, Szeged, indicates a double minimum in August and September. In autumn the values of *RE* begins to rise again to the maximum at the end of winter, but variability of the values increases.

The curve of annual course shows a rise in values of *RE* between 150th and 180th days of the year. In this time a rainfall maximum is found in Hungary. In the area with various moisture content, the differences in soil moisture content are the highest in autumn. The reason of this fact is that in summer time precipitation falls mainly in the form of shower, that means a lot of quantity of rainfall in a short time, then a long dry and warm period follows with high evaporation values. Soil moisture decreases in this latter time. The values of evaporation also strongly decrease, the values of *RE* indicate low evaporation too.

It is worth noting, that annual course of *RE* can be represented by a polinom of six degree with a determination coefficient $r^2 = 0.97$ (as can be seen in *Fig. 3*). This shows a very close relationship. It makes possible to model this phenomenon climatologically.

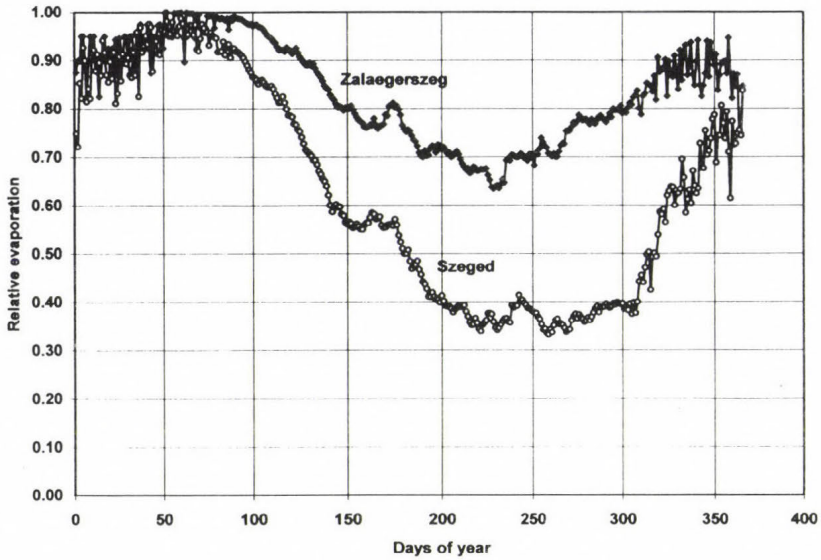

Fig. 2. Annual course of relative evaporation in a moist (Zalaegerszeg) and dry (Szeged) area (1951–1990).

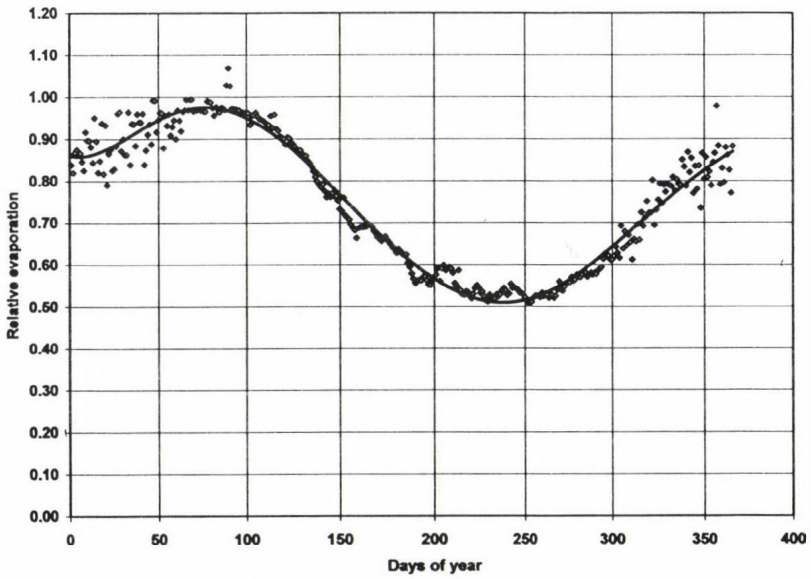

3. ábra. Annual course of relative evaporation in Mosonmagyaróvár (1951–1990).

3.3 Seasonal changes of soil moisture

Finally, we determined the seasonal changes of soil moisture content by using a soil moisture model elaborated earlier *(Dunay et al.,* 1968*; Dunay et al.,* 1969). We calculated the daily average values of water content of soil from 40 years long (1951–1990) data series.

It is important to note, that the average values in winter months are very close to the maximum values of 40 years data series. From the beginning of spring, when the soil moisture begins to decrease, the mean values come more and more nearer to the minimum values. The minimum can be found nearly in the middle of August. The soil moisture values can, therefore, be characterized by the help of values of *RE*.

The southwestern part of Hungary is the wettest area of the country, where the maximum values of soil moisture are very close to the field capacity throughout the year (*Fig. 4*). A short dryer time can be found in the beginning of July and in September, but the dry period in September is more significant because of intensity of dryness and length of time spell. In the dryest area of the country, the maximum values could sometimes be quite low, near to 80% from the middle of summer to the end of autumn, even in some cases they fall short of 80% (*Fig. 5*).

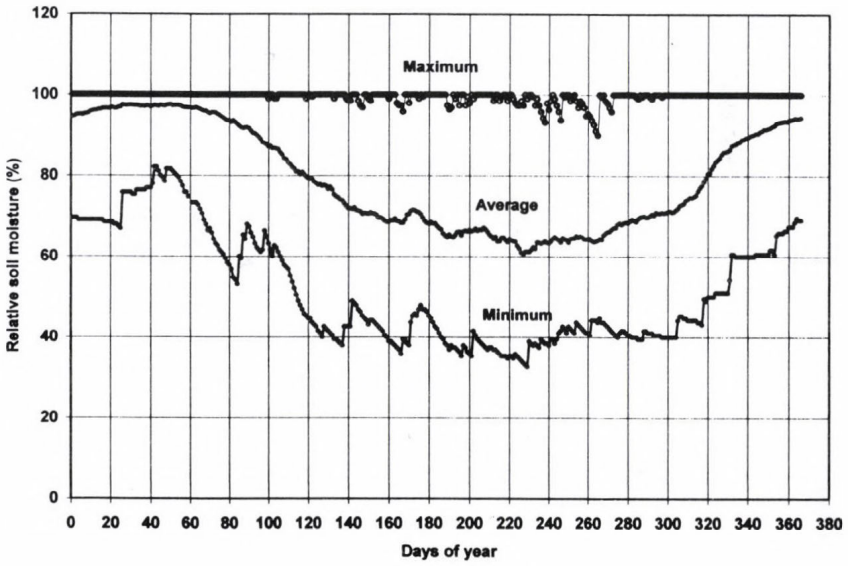

Fig. 4. Annual course of minimum, average, and maximum values of relative soil moisture in a moist area (Zalaegerszeg, 1951–1990).

Seasonal changes of minimum values are very similar to those of averages and maximum. Minimum values fall down under 40% only in the middle of summer in the wettest area, but in the dryest area the minimum values under 40% can occur from the end of spring to the end of autumn.

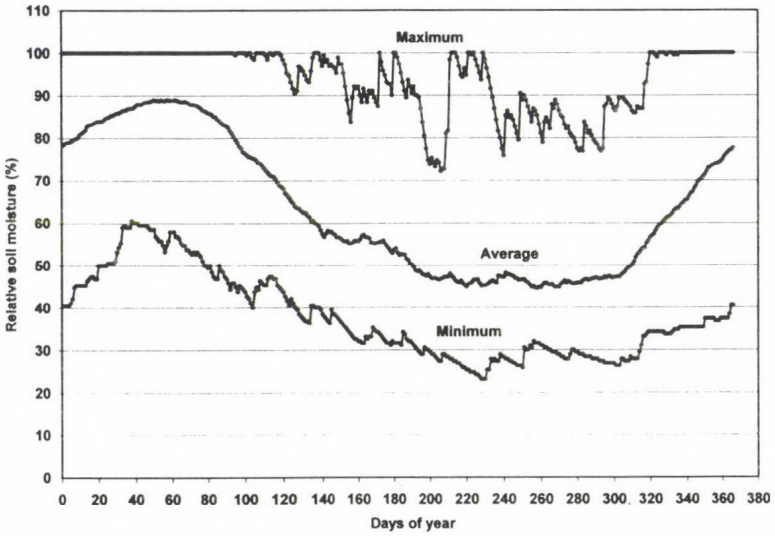

Fig. 5. Annual course of minimum, average, and maximum of relative soil moisture in a dry area (Szeged, 1951–1990).

4. Conclusions

An important feature in the climate of our country — as it can be seen in *Fig. 1* — is the length of period, when the amount of rainfall exceeds the amount of evaporation. This time spell begins with the secondary maximum of mediterranean type of rainfall. After the secondary maximum of rainfall in November, the rainfall is more than evaporation, therefore, if soil is not frozen, water continuously infiltrates into the soil. If soil is frozen and the precipitation falls in the form of snow, the water would infiltrate into the soil after melting. This is the reason why the maximum value of soil moisture occurs at the end of February and in the beginning of March (*Fig. 6*).

In spring the amount of rainfall rises intesively to the maximum of that element in June, but evaporation increases more rapidly because of the strongly rising quantity of energy, thus, soil moisture is gradually decreasing. Summer precipitation falls mostly in the form of shower, and long warm

periods without rainfall can cause significant water shortage from the middle of summer to the end of autumn. It is a critical period from agricultural point of view, because the water shortage in soil coincides with a high temperature stress, and this phenomenon is able to rise the risk factor in plant breeding of our country.

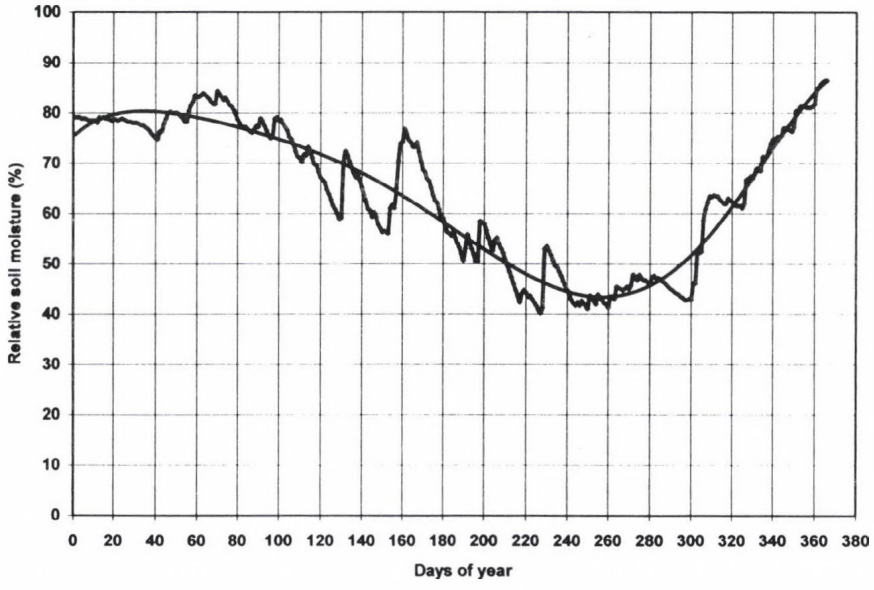

Fig. 6. Annual course of relative soil moisture in Mosonmagyaróvár (1950–1990).

Acknowledgements—The authors express their thanks to the Hungarian Scientific Research Fund (OTKA) and National Research Development Program (NKFP) for financially supporting this project (under the number T 034592 of OTKA, and under the number of OM-3B/0057/2002).

References

Brisson, N., Seguin, B., and *Bertuzzi, P.*, 1992: Agrometeorological soil water balance for crop simulation models. *Agricultural and Forest Meteorology 59*, 267-287.

Budiko, M.I., 1956: Heat balance of surface (in Russian). Gidrometeoizdat, Leningrad, 254 pp.

Dunai, S., Posza, I., and *Varga-Haszonits, Z.*, 1968: A simple method for determining actual evapotranspiration and soil water content. Part I. Meteorology of evaporation (in Hungarian). *Öntözéses Gazdálkodás 6* (2), 39-48.

Dunai, S., Posza, I., and *Varga-Haszonits, Z.*, 1969: A simple method for determining actual evapotranspiration and soil water content. Part II. Actual evaporation (in Hungarian). *Öntözéses Gazdálkodás 7* (2), 27-38.

Jackson, R.D., 1982: Canopy temperature and crop water stress. *Advences in Irrigation 1*, 43-85.

Larcher, W., 2003: *Physiological Plant Ecology. Ecophysiology and Stress Physiology of Functional Groups*. Fourth edition. Springer Verlag, Berlin, 513 pp.

Palmer, W., 1965: Meteorological Drought. Research Paper No. 45. US Department of Commerce, Washington. 58 pp.

Ritchie, J.T., 1985: A user-oriented model of soil water balance in wheat. In *Wheat Growth and Modeling* (eds.: *E. Fry* and *T.K. Atkin*). NATO-ASI Series. Plenum, New York, 293-305.

Stanhill, G., 2002: Is the Class A evaporation pan still the most practical and accurate meteorological method for determining irrigation water requirements? *Agricultural and Forest Meteorology 112*, 233-236.

Varga-Haszonits, Z., 2002: Water supply of growing seasons and maize production. *Időjárás 106*, 89-101.

Varga-Haszonits, Z. and *Harnos, Zs.*, 1988: Effect of climate variability and drought on wheat and maize production. In *Identifying and Coping with Extreme Meteorological Events* (eds.: *E. Antal* and *M.H. Glantz*). Orsz. Meteorológiai Szolgálat, Budapest, 138-166.

Walter, H., 1985: *Vegetation of the Earth and Ecological Systems of the Geo-biosphere*. Third, revised and enlarged edition. Springer-Verlag. Berlin and New York, 318 pp.

IDŐJÁRÁS

Quarterly Journal of the Hungarian Meteorological Service
Vol. 107, No. 3–4, July–December 2003, pp. 199–204

On the pointing error of pyrheliometers

György Major

Hungarian Meteorological Service,
P.O. Box 39, H-1675 Budapest, Hungary
E-mail: gmajor@met.hu

(Manuscript received July 21, 2003)

Abstract—In this paper the results of calculations are shown on the error caused by the mispointing of pyrheliometers. The penumbra functions of three pyrheliometers (absolute cavity, KIPP, and NIP) are used for two atmospheric situations (high solar elevation and low turbidity as well as low solar elevation and high turbidity) to calculate the output values of pyrheliometers as functions of the pointing error.

Key-words: cavity pyrheliometer, NIP pyrheliometer, KIPP pyrheliometer, penumbra function, pointing error

1. Introduction

The direct radiation is the shortwave (solar) radiation coming from the solid angle determined by the solar disk. The pyrheliometers are designed to measure the direct radiation. Their view limiting angles (slope, opening, and limit angle) are larger than the visible radius of the solar disk. This is partly due for the easier tracking of the Sun: if the limiting angles are larger than the solar disk, it is not necessary to follow the Sun quite precisely.

How large pointing errors or inaccuracies occur in the everyday practice? Let us take a hand-operated pyrheliometer. If its adjustments are made once in a minute, its largest mispointing in azimuth angle would be one quarter of a degree. The deviation from the right position in elevation angle is in the same order. Regarding the pointing devices of the pyrheliometers, 1 mm deviation of the illuminated spot from its proper position could be regarded as large mispointing. Depending on the length of the pointing path, this deviation means about half a degree of pointing error.

The purpose of this document is to present calculated values of the errors in the output of pyrheliometers caused by pointing uncertainty up to 2 degrees.

Two atmospheric conditions are taken into account:

- mountain aerosol, optical depth: 0.07, solar elevation: 60 degrees, direct radiation: 1000 W/m^2;
- continental background aerosol, optical depth: 0.23, solar elevation: 20 degrees, direct radiation: 461 W/m^2.

The calculations have been made for 3 pyrheliometers: the Packrad size cavity instrument (ABS), the KIPP and NIP pyrheliometers. Their slope angles are: 0.75, 1.0, and 1.78 degrees, respectively.

2. The method of calculation

The calculation is based on the Pastiels' theory (see, for example, in *Major,* 1994). The irradiance given by a circular pyrheliometer can be written as:

$$I = \frac{V}{KS} = \pi \int_0^{z_l} F(z)\, L(z) \sin(2z)\, dz\,, \tag{1}$$

where V is the output of the pyrheliometer,
K is the average sensitivity of the receiver,
S is the area of the receiver,
z_l is the limit angle of the pyrheliometer,
$F(z)$ is the penumbra function of the pyrheliometer,
$L(z)$ is the radiance (=sky function) and
z is the angle between the direction of radiance and the optical axis of the pyrheliometer.

Circular pyrheliometer means that all the view limiting diaphragmes and the receiver are circular in shape, that is the whole pyrheliometer has a rotational symmetry around its optical axis. In the equation, the same rotational symmetry is supposed for the solar disk and the circumsolar sky.

If the optical axis of the pyrheliometer is not directed to the solar center, then the angle measured from the solar center ($z1$) differs from the angle measured from the optical axis (z). The transformation is

$$\cos(z1) = \cos(d)\cos(z) + \sin(d)\sin(z)\cos(\varphi), \tag{2}$$

where d is the deviation between the solar center and the optical axis, that is the pointing error,
φ is an azimuth angle measured in the plane of the receiver, it is zero if the radiance comes from the solar center.

2.1 Radiance along the solar disk

Photospheric models of the Sun produce one-dimensional radiance distribution across the solar disk, that is the so called limb darkening function. According to theoretical calculations (*Allen*, 1985; *Zirin*, 1988), the radiance depends near linearly on the cosine of the zenith angle at the solar "surface". Taking into account some observations too (*Zirin*, 1988) and using $z1$ as variable instead of the aforementioned zenith angle, the following radiance distribution along the solar disk has been used:

$$L(z1) = L_0[0.3 + 0.7\, SQR\,[1 - (z1/0.26)^2]]\,, \tag{3}$$

where L_0 is the radiance at the solar center,
0.26 is the radius of the solar disk in degrees.

This way the atmosphere affects the absolute value of the radiance coming from the solar disk, but not the relative distribution along it. If the direct radiation is 1000 W/m^2, then $L_0 = 2.01565 \cdot 10^7$ W/(m^2 sr), while at 461 W/m^2 it is $9.29216 \cdot 10^6$. Since the gradient at the solar edge is very large, the step of integration in Eq. (1) has to be 0.0001 degree to obtain 0.1 W/m^2 accuracy.

2.2 Radiance along the circumsolar sky

For several atmospheric aerosol contents and solar elevation angles the radiances coming from the circumsolar sky have been calculated by *Putsay* (1995). To make our calculation more practical, second order polynoms have been fitted to the logarithm of the two selected circumsolar sky functions. The fit is not quite perfect, but it is not significant since we want to obtain the effect of the shift caused by the uncertain pointing.

In *Fig. 1* the whole (solar and circumsolar) sky functions are shown for the two selected atmospheric models.

2.3 The penumbra functions

To make the computations faster, the penumbra functions have been approximated by third order polynoms in the interval between the slope and limit angles. Again, the fit is not perfect, but this has small effect on the deviations of the values calculated for different pointing uncertainty.

3. Results

In the calculations the effect of the solar disk and that of the circumsolar sky could be separated. In *Figs. 2* and *3* the actually direct irradiance of the pyrheliometric sensor can be seen. If the pointing error is smaller than the slope

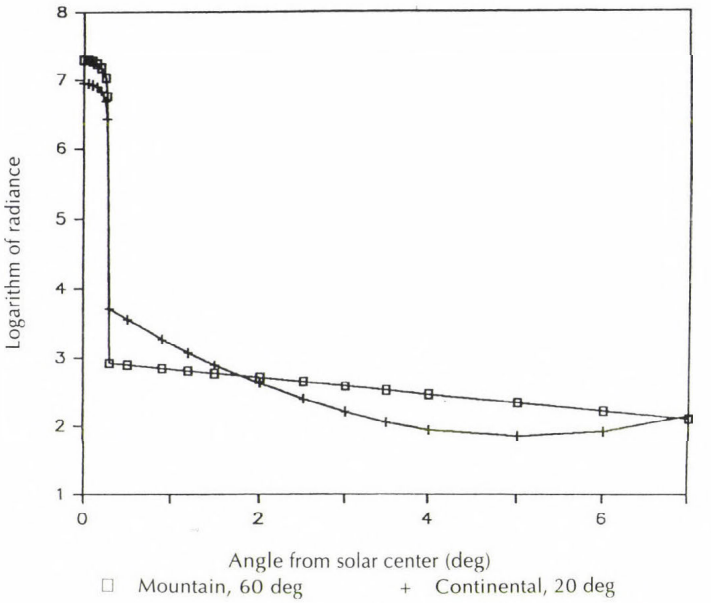

Fig. 1. The sky functions used in this calculation.

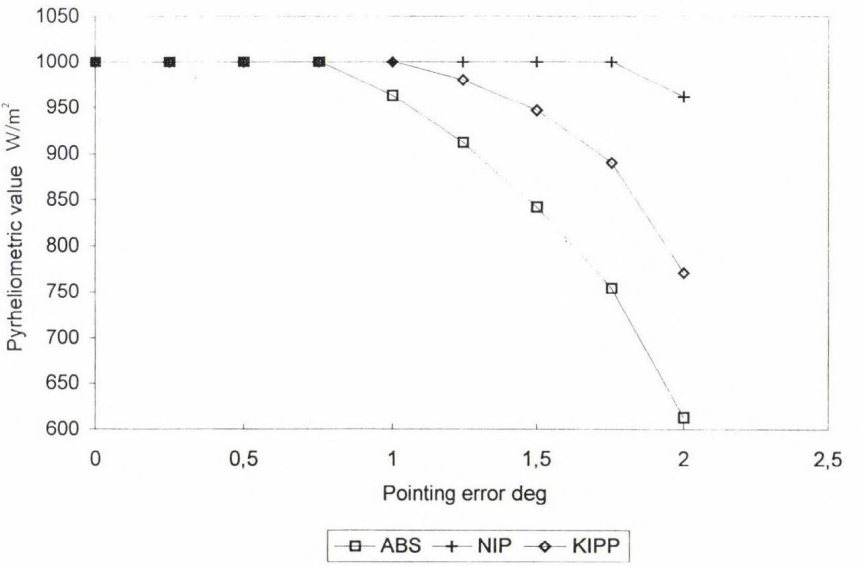

Fig. 2. The contribution of the solar disk to the irradiance of pyrheliometric sensors depending on the pointing error. Case of mountain aerosol and 60 degrees solar elevation.

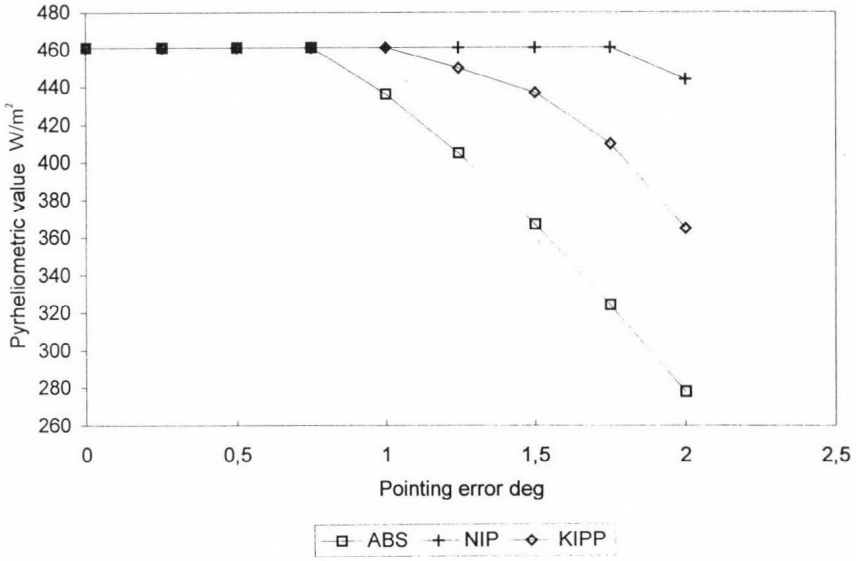

Fig. 3. Same as Fig. 2 except that the case is continental background aerosol and 20 degrees solar elevation.

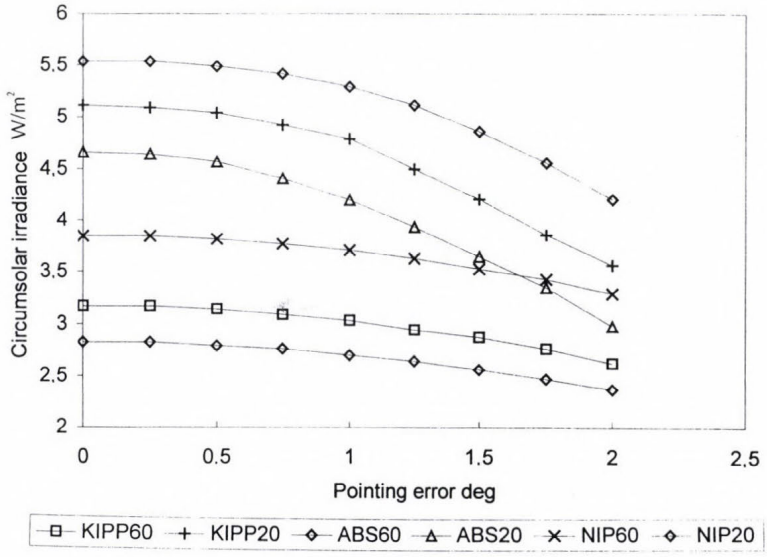

Fig. 4. The contribution of the circumsolar sky to the irradiance of pyrheliometric sensors. The upper 3 curves belong to the case of continental background aerosol and 20 degrees solar elevation, the lower 3 curves belong to the case of mountain aerosol and 60 degrees solar elevation. In both group of curves the instruments are from the top to down: NIP, KIPP, and ABS.

angle, the irradiance is not affected. If the solar disk is in the penumbra region of the pyrheliometer, the irradiance decreases rapidly with the increasing pointing error.

In *Fig. 4* the irradiance coming from the circumsolar sky is seen for all pyrheliometers and both atmospheric conditions. The decrease is continuous, but the effect is not significant compared to that of the solar disk.

4. Conclusions

- If the pointing error of a pyrheliometer is smaller than its slope angle, the effect is negligible.
- If the pointing error of a pyrheliometer is larger than its slope angle, the irradiance of the pyrheliometric sensor decreases rapidly with increasing mispointing. The value can be estimated using *Fig. 2* and *3*.

References

Allen, C.W., 1985: *Astrophysical Quantities*. The Athlone Press, London.

Major, G., 1995: Circumsolar Correction for Pyrheliometers and Diffusometers. WCRP, WMO/TD-No.635.

Putsay, M., 1995: Circumsolar radiation calculated for various aerosol models. *Időjárás 99*, 67-76.

Zirin, H., 1988: Astrophysics of the Sun. Cambridge University Press, Cambridge-New York-London-New Rochelle-Melbourne-Sydney.

IDŐJÁRÁS

Quarterly Journal of the Hungarian Meteorological Service
Vol. 107, No. 3–4, July–December 2003, pp. 205–211

Data on the short wave radiation balance and temperature of the Síkfőkút forest

János Justyák

Department of Meteorology, University of Debrecen
P.O. Box 13, H-4010 Debrecen, Hungary

(Manuscript received 30 August, final form 30 September 2002)

Abstract—Radiation and temperature measurements were carried out between 1978 and 1994 in oak forest at Síkfőkút, Hungary. The experimental station is located on the southwestern part of the Bükk Mountains at a height of 270–290 meters above sea level. Since about 1980, the forest decay has affected 50–60% of the sessile oak trees (Quercus petrea), which is the most important species (85% of the trees belong to that species); while Turkey Oak trees (Quercus cerris) have not been damaged. The impacts of the deforestation are detectable on the radiation balance and temperature regime. The healthy forest (July 1978) let through 8% of the incoming short wave radiation and absorbed 92% of that. The decayed forest (July 1994) let already 22% of short wave radiation and absorbed 78%. The annual and summer mean temperatures have increased more rapidly in the forest than above the neighboring treeless grassland during the 17 years period examined here. The ten years summer mean temperatures have increased by 2.2°C inside the forest and by 1.8°C above the treeless area. This fact can be explained partly by that the deforestation have decreased the tree density of the forest and partly by the higher frequency of warm years in the examined period. In the leafless forest, high temperatures can be found at the level of the crown of the trees and at the soil surface as well, while in the leafy forest high temperatures can only be found in the foliage. Because of the forest decay, sometimes when skies are clear and weather is calm in the afternoon, a second warm air layer can form near the surface.

Key-words: forest, forest decay, short wave radiation balance, temperature.

1. Introduction

The Department of Meteorology of the University of Debrecen (previously Kossuth Lajos University) joined in the complex ecological study of the Síkfőkút forest (*Jakucs*, 1973) in 1978, when a 25 meters tall meteorological tower had been completed. The project was started by the Department of Ecology.

The forest is situated on a slope of 2–3 degrees, which has a southern exposure at a height of 270–280 meters above see level. It is placed in the Bükk Mountains in Hungary. The average height of the trees was 19.5 meters at the beginning of the ecological studies. The experimental area is a homogenous Turkey-Sessile oak forest (Quercus-petrea-cerris). 84.5% of the woodland consists of Sessile oak (Quercus petrea). About 63% of the mass of the foliage of the forest can be found at the height between 14 and 21 meters. This layer absorbs a considerable amount of precipitation and incoming solar (global) radiation. In the forest there are two shrub levels that are not very thick, at heights of 0.5–1.0 and 1.5–2.0 meters.

The 25 meters high meteorological tower was mounted on the study area, which has an area of 1 hectare, while on the treeless area (grassland) a weather station was mounted (*Fig. 1*).

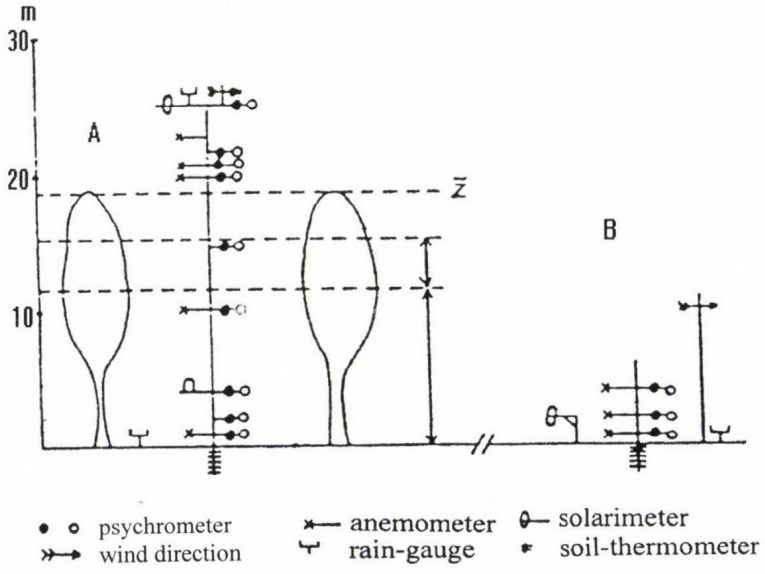

Fig. 1. The mounting of the meteorological instruments, and the levels of measurements inside the forest (A) and above the treeless grassland (B) at Síkfőkút.

Inside the forest, a digital data logger with 80 channels was installed in a wooden cabinet. It carried out meteorological measurements (radiation, temperature humidity, wind velocity, etc.) along a vertical profile inside the forest and above the treeless area. Data had been recorded on telex tape. Later digital data logging had been used (*Justyák*, 1995).

Forest decay appeared in about 1980 in Hungary. In the Síkfőkút forest 50–60% of the Sessile oak decayed until 1995, and a part of the trees had fallen causing detectable changes in the climate of the forest. In the followings we deal with the impacts of the forest on the radiation and temperature elements.

2. Solar radiation

Data on the short wave radiation balance of the Síkfőkút forest can be found in *Table 1*. It can clearly be seen that in 1978, when the forest was healthy, in leafless state (April), the lower layer (2 meters) of the foliage let the 48% of the global radiation through the forest, while the branches and trunks of the trees absorbed 52%. Many years later, in April 1994, 54% of global radiation were let through and 46% were absorbed due to the decay and fall of the trees. Therefore, the healthy forest lets through less and absorbs more radiation. In the decaying forest the situation is reversed. In both cases enough energy reaches the surface under the forest to form its *own independent energy balance* (the air of the forest warms up mostly from beneath). Since the near-surface level of the forest is abundant in light and heat, the growth of the plants in that level is accelerated.

Table 1. Short wave radiation components in the Síkfőkút forest (1978–1994), MJ m^{-2}

Years	Forest leafless (April)					Forest leafy (July)				
	G	r	G–r	A	T	G	r	G–r	A	T
1978	369	48	321	154	167	548	86	462	425	37
1980	367	47	320	160	160	536	83	453	399	54
1982	386	49	337	172	165	555	85	490	421	69
1984	397	50	347	180	167	570	89	4487	404	83
1986	399	49	350	186	164	581	81	500	4056	95
1988	395	49	346	183	163	609	86	523	429	94
1990	400	50	351	190	161	556	78	478	382	96
1992	411	50	361	195	166	625	86	540	416	124
1994	378	47	331	179	153	628	85	453	424	119
Average	**389**	**49**	**340**	**177**	**163**	**579**	**84**	**487**	**412**	**82**

Legend: G= global radiation, which reaches the surface of the forest, r=reflex radiation from the surface of the forest, G–r=short wave radiation balance of the forest, A=the amount of radiation absorbed by the forest, T=the amount of radiation let through by the forest, measured at a height of 2 meters in the forest.

In leafy state (July), the forest let through 8% and absorbed 92% of the global radiation in 1978. In the decayed forest in 1994, 22% were let through and 78% were absorbed. These figures mean that energy transport processes in the lower level of the healthy forest are restricted and *an independent energy balance can not form there* (*Justyák,* 1987). On the other hand, in the near-surface level of the decayed forest an *independent energy balance can develop* due to the additional incoming radiation. For this reason, the decayed forest in cloudless dry and hot days gets heat not just from the sides and above but from the warming surface beneath.

3. Temperature

In the trunk space (at a height of 2 meters) of the Síkfőkút forest, usually lower temperatures occur than above the neighboring treeless area (*Table 2*). The annual mean temperature of the forest is 10.0°C, while that of the treeless area is 10.3°C. In the coolest year (1980), the annual mean temperature in the forest canopy was 8.4°C, while above the treeless area it was 8.8°C. In the warmest year (1994), the annual mean temperature in the forest was 11.3°C, while above the treeless area it was 11.5°C. The difference between the coolest and warmest year in the forest was 2.9°C, while above the grassland area it was 2.9°C. The warming up was only a little bit stronger in the forest than its environment.

Table 2. Annual and seasonal mean air temperatures (°C) inside the forest and above the treeless grassland at a height of 2 meters (1978–1994)

Temperature	**Forest**				
	Year	**Winter**	**Spring**	**Summer**	**Autumn**
Maximum	11.3	1.8	12.7	22.9	11.8
Minimum	8.4	–4.1	8.4	17.3	8.0
Average	**10.0**	**–0.5**	**10.6**	**19.6**	**10.0**
	Treeless area				
Maximum	11.5	1.8	12.5	23.6	12.4
Minimum	8.4	–4.1	8.2	18.2	8.4
Average	10.3	**–0.4**	**10.7**	**20.3**	**10.4**

In *Fig. 2* the changes of the annual mean temperatures, their trend lines, the equations of the trend lines, and the R^2 values are presented during the studied period inside the forest canopy and above the treeless area. On the base of the figure, it is visible that during the 17 years of the studied period, the

annual mean temperature increased faster in the forest than above the treeless area: the ratio of steepness of the lines is 1:13. The ratio of the temperature increase in a 10 years period is 1.0°C. The increase of the mean temperatures in the forest stand can be explained by two reasons. One of them is that the forest stand became rare due to the decay of the trees. The other reason is that there had been some years warmer than the average during the studied period. As it is visible, at the beginning of the period the difference between the two trends is 0.4°C, while at the end it is only 0.2°C.

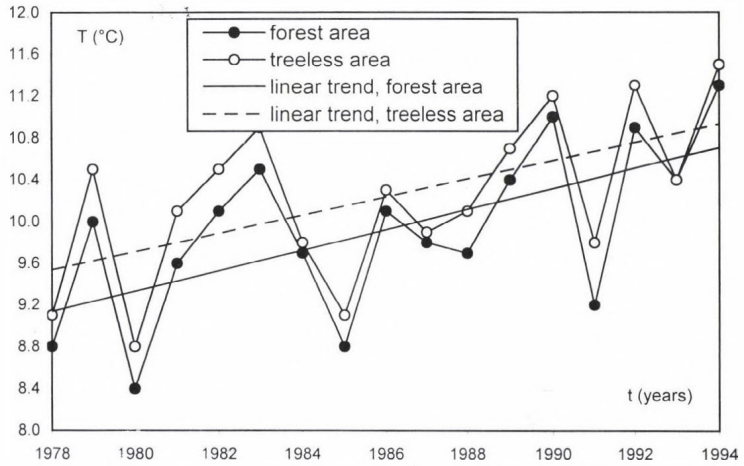

Fig. 2. Fluctuations and trends in the annual mean temperature in the oak forest.

In the forest the mean temperature in the summer period (Jun–Aug) is 19.6°C, above the treeless area it is 20.3°C. In the coolest summer (1978) it was 17.3°C in the forest and 18.2°C above the treeless area. In the warmest summer (1994) the mean temperature was 22.9°C and 23.6°C above the treeless area. The difference between the warmest and coolest summer was 5.6°C, while in the case of the treeless area it was 5.4°C. In this case there was a stronger warming up in the forest again.

As it can be seen in *Fig. 3*, the increase of the mean temperatures is the most rapid and significant in summer. The 10 years average increase of the mean temperatures in the treeless area is 1.8°C, while in the forest it is 2.2°C and R^2 reaches its highest values in this case. The ratio of steepness (1.19) is maximum as well. The ratio of the increase is more than double of the increase the annual mean temperatures: the ratios of the corresponding lines are 2.18 in the forest and 2.08 above the treeless area (*Tar*, 1995; *Antal et al.*, 1997).

In the studied period (1978–1994) it is characteristic for the decayed Síkfőkút forest, that its heat balance system had been altered, and its microclimate had become similar to the microclimatic system of the treeless area (*Justyák*, 1995; *Justyák* and *Víg*, 1997).

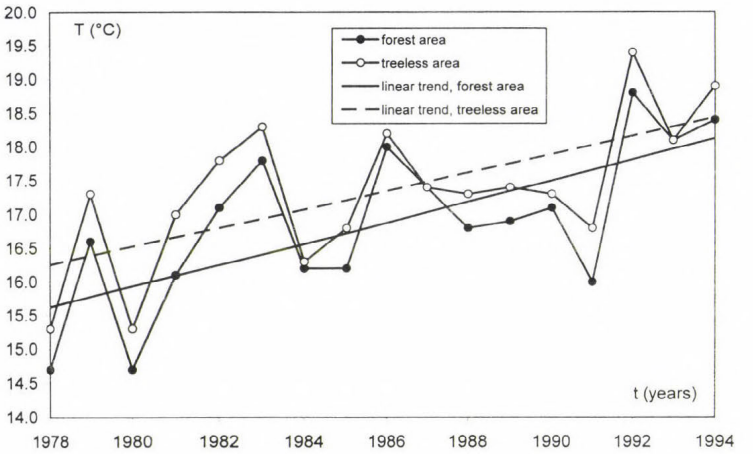

Fig. 3. The change and trend in the summer mean temperatures in the oak forest.

In both the healthy and decayed forest in leafless state, the warmest (active) surfaces can be found in the level of the leafless crowns and on the soil surface of the forest. In the leafless forest more solar energy reaches the soil surface warming it up, and the surface emits heat into the surface layer of the atmosphere (see part A in *Fig. 4*).

In both the healthy and decayed forest, the air temperature is lower under the foliage of the forest than over it, because the foliage absorbs and retains considerable amounts of solar radiation and heat. The active surface, which transfers the heat, is the foliage. In leafy state, only one active surface forms. The 19.5 meters high level of the foliage takes the place of the soil surface in warming the lower layer of the atmosphere (see part B in *Fig. 4*).

Heat is emitted into both layers: the air over the forest and inside the forest from that level of the foliage. For this reason, daytime and in the summer the air is cooler under the active surface of the foliage than inside the upper level of the foliage.

Nevertheless, in the decayed forest, where 50% of the trees had perished, especially in early afternoon in the drought-stricken '90's, when the weather was clear and calm, sometimes another active warm layer formed in the lower

air layer of the forest. In such cases two active surface developed: *one* in the upper level of the foliage and *another* in the level of the dry fallen leaves and soil surface. In such weather conditions, a heat surplus of 1.0–2.0°C formed at a height of 2 meters compared to the treeless grassland.

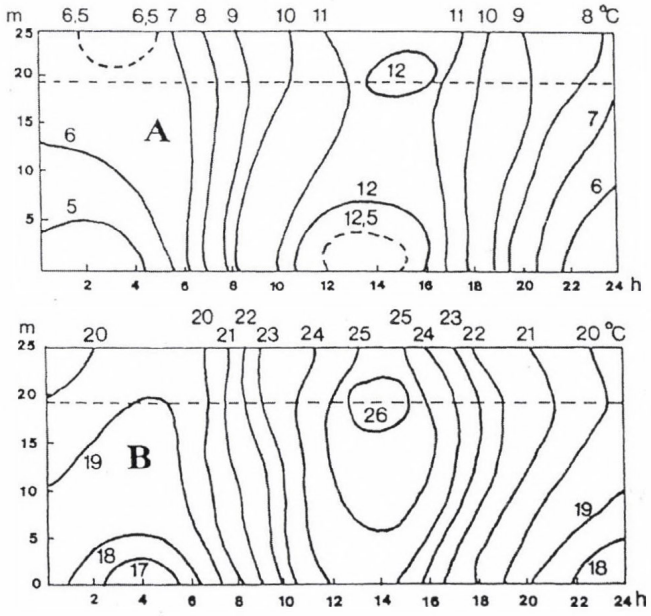

Fig. 4. The diurnal changes of air temperature profile in the leafless (A) and leafy (B) oak forest.

References

Antal, E., Berki, I., Justyák, J., Kiss, Gy., Tar, K., and *Vig, P.*, 1997: *The Examinations on the Heat and Water Balance of the Forest Stand of Síkfőkút in the Mirror of the Forest Fading and Climate Change* (in Hungarian). KLTE, Debrecen.

Jakucs, P., 1973: The „Síkfőkút Project". Environmental Biological Research of an Oak forest Ecosystem in the Frame of the Biosphere Program (in Hungarian). *MTA Biol. Oszt. Közl. 16*, 11-25.

Justyák, J., 1987: Energy balance measurements in an oak forest (in Hungarian). *Időjárás 91*, 131-146.

Justyák, J., 1995: Results of microclimate measurements in a Turkey Oak-Sessile oak forest ecosystem (in Hungarian). In *Erdő és Klíma*, KLTE, Debrecen, 28-37.

Justyák, J. and *Vig, P.*, 1997: Microclimate of the forest (in Hungarian). In *Meteorológia mezőgazdáknak, kertészeknek, erdészeknek* (eds.: *G. Szász* and *L. Tőkei*). Mezőgazda Kiadó, Budapest, 543-561.

Tar, K., 1995: The statistical structure of the temperature of the Síkfőkút Forest. In *Erdő és Klíma*, KLTE, Debrecen, 100-105.

IDŐJÁRÁS

Quarterly Journal of the Hungarian Meteorological Service
Vol. 107, No. 3–4, July–December 2003, pp. 213–224

Relationship between the stability of wind directions and the mean wind velocity under various weather conditions

Károly Tar and **Sándor Szegedi**

Department of Meteorology, University of Debrecen
P.O. Box 13, H-4010 Debrecen, Hungary
E-mail: tark@puma.unideb.hu; szegedis@tigris.klte hu

(Manuscript received March 28, 2003; in final form October 6, 2003)

Abstract—In this study we summarize the initial results of our examinations on the wind climate of the growing season. We have selected those weather conditions, when wind directions are stabile and wind velocity is low. These are preconditions for effective irrigation or spraying. These conditions – theoretically – cannot be satisfied at the same time, for this reason we have selected those ones, where the stochastic relationship is weak – it does not differ significantly from 0 – between the stability of the wind directions and mean wind velocity. The database consists of the 5-year (1991–95) hourly wind direction and velocity records of three meteorological stations: Debrecen, Békéscsaba, and Szeged. Analysis had been carried out for each weather station for the whole data set, for the growing season (from April 1 to September 30), and for certain subsets of them. These subsets had been established on the base of macrosynoptic type groups and the so-called central types described by Péczely. We can state that the most favorable for spraying and irrigation is macro synoptic type A and the MS type group. The time of irrigation and spraying can be planned a few days in advance, on the base of the results of the studies on the lifetime of the types, time pattern of their fluctuations, and fluctuations of their transitions into each other.

Key-words: stability of wind direction, index of stability, growing season, irrigation, spraying, macrosinoptic type by Péczely.

1. Introduction

"When dealing with the microclimates of the plant stands, it is not advisable to separate the characteristics of the inner microclimatic spaces of the plant stands from the features of the microclimatic spaces over the plant stands, especially from the wind velocities there. Wind velocity and radiation are the governing factors of the fluxes, which develop in microclimatic spaces. It means that the

before mentioned elements control the formation of fluxes." (*Szász,* 1995). Therefore, the wind conditions inside the plant stand, which have an effect on the thermal conditions of the plant stand for instance, are not independent from the characteristics of the wind field over the plant canopies. On the base of this idea, we started the detailed analysis of the wind conditions during the growing season in Hungary. In a previous paper (*Tar* and *Szegedi,* 2002) we dealt with the initial results on meteorological conditions of the sprinkling irrigation and sprinkling, which are in direct connection with the developing of the plants. In the present paper we focus on those questions that were not answered there, for instance, the clustering of the data (the establishment of subsets).

2. The aim of our research

For effective sprinkling irrigation or sprinkling, those weather conditions are suitable, when wind directions are stabile (less variable) and wind velocity is low. These two preconditions are contradictory, since presumably, those wind directions are stabile that have high velocities. How can we select those macro-synoptic situations, when conditions are suitable for the irrigation or sprinkling? The aim of our research is to select those weather situations, where the stochastic relationship between the measure of the stability of the wind directions and mean wind velocity does not differ significantly from zero or very weak.

3. Database

The database consists of the 5-year (1991–95) hourly wind direction and velocity records of three meteorological stations: Debrecen, Békéscsaba, and Szeged, which was made available for us by the Hungarian Meteorological Service. The dataset – according to the climatologic standard – consists of 16 wind directions. When preparing the data for the analysis, it was taken into consideration, that not each value was measured at the standard 10 meters height. In those cases data were transformed to the 10 meters height using the equations proposed for meteorological wind measurements (Mezősi and Simon, 1981).

Analysis had been carried out for each weather station for the whole data set, during the growing season (from April 1 to September 30), and for certain subsets of whole data set and growing season. These subsets had been established on the base of the macro synoptic type groups described by Péczely. In opposition to *Péczely* (1983), the central types are handled separately on the base of its obviously different air flow characteristics. According to this, the following categories are used: meridional northern (MN), meridional southern (MS), zonal western (SW), zonal eastern (ZE) type

groups, and anticyclone center (A) and cyclone center (C) types. Their characteristics are summarized in *Table 1*.

Table 1. Codes, letter codes, and short descriptions of the Péczely's macrosynoptic types

No.	Code	Description
		Types connected with northerly current (type group MN)
1	mCc	Hungary lies in the rear of an Eastern European cyclone
2	AB	anticyclone over the British Isles
3	CMc	Hungary lies in the rear of a Mediterranean cyclone
		Types connected with southerly current (type group MS)
4	mCw	Hungary lies in the fore part of a Western European cyclone
5	Ae	anticyclone in the east from Hungary
6	CMw	Hungary lies in the fore part of a Mediterranean cyclone
		Types connected with westerly current (type group ZW)
7	zC	zonal cyclonic
8	Aw	anticyclone extending from the west
9	As	anticyclone in the south from Hungary
		Types connected with easterly current (type group ZE)
10	An	anticyclone in the north from Hungary
11	AF	anticyclone over the Fennoscandinavian region
		Types of pressure centers
12	A	anticyclone over the Carpathian Basin
13	C	cyclone over the Carpathian Basin

As it can be seen, the base of the classification is the place of the cyclone or anticyclone centers as compared to Hungary. The types, when a cyclone governs the weather of Hungary, can be grouped in the cyclonal type group (CG). The types of the CG are: 1, 3, 4, 6, 7, 13. Anticyclone type group (AG) can be defined similarly; its elements are: type 2, 5, 8, 9, 10, 11, and 12. For the classification of the individual days, we used the macrosynoptic codes of *Károssy* (1998). The size (the number of days) of the macrosynoptic types/type groups for the whole five years long period and for five growing season together is shown in *Table 2*. It can be seen that in the frequency of the occurrence of the macrosynoptic types/type groups, the greatest differences (4–5%) are in the meridional group: the number of the days in the MN group has increased, while in the MS group it has decreased relative, to the whole period. It is remarkably that in the relative frequency of the cyclonal and anticyclonal type groups there are practically not differences between the whole period and growing season.

Table 2. The number of days of the various type groups (days), and their length relatively to the whole length of the period (%) in the whole 5-year period (1991–95), and in the growing season

Type	1991–1995		Five growing seasons	
groups	days	%	days	%
MN	401	22.0	244	26.7
MS	434	23.8	161	17.6
ZW	390	21.4	182	19.9
ZE	235	12.9	142	15.5
A	269	14.7	120	13.1
C	97	5.2	66	7.2
SUM	**1826**	**100.0**	**915**	**100.0**
AG	1259	68.9	627	68.5
CG	567	31.1	288	31.5
SUM	**1826**	**100.0**	**915**	**100.0**

4. Methods

On the diurnal changes of the wind directions in Hungary, *Hegyfoky* (1904a-d) had published data first. On the base of the records of ten weather stations, he established that near the surface layer of the atmosphere there is a positive change in the wind directions in the morning, and a negative change in the afternoon, if we determine positive direction as a clockwise turn facing the wind. He assumed that the reason for this phenomenon is the mechanical effect of the air pressure system drifting to the east on one hand, and the diurnal changes of the temperature conditions on the other hand. Based on this, in a previous paper we studied the change of the wind direction as a random variable (*Tar*, 1980) using the five years long dataset (1968–72) of five weather stations situated on the Great Hungarian Plane (Kisvárda, Debrecen, Kecskemét, Békéscsaba, and Szeged), which are affected by orography to a lower degree. The method of the examinations, which we follow in the present paper, too, is that we create elemental events from the hourly wind directions. The wind direction of the t hour of a day of a given period (subset) is compared to that of the previous $(t-1)$ hour. If these are uniform (that is the difference between them expressed in degrees is lower than $360/16=22.5$), then the t hour is considered to be a *stable (permanent) point of time* from the aspect of the change of the wind directions, and it is marked by S_t. Otherwise, the t hour is an unstable (fluctuating) point of time, and the event is I_t. The wind direction of the first hour of the day is compared to the 24th hour of the

previous day, even though it belongs to another subset. If in each hour of a given time interval the wind direction is stable or unstable, it is considered to be a stable or instable period.

Therefore, in our case the maximal daily number of stable or instable hours can be 24. This should be considered as a lower limit from any aspect. The number of stable or instable hours increases if the number of observations and/or wind direction categories increases. Both are true, for instance, for the case of automatic weather stations. Our results would obviously change if we used such datasets, that would have not only climatological consequences but effects on the utilization of wind energy as well (*Tar,* 2003).

5. The measures of the stability of the wind directions

First we define the measure of the stability of the wind directions, i.e., the *stability index*. It is the ratio of hours with stabile wind direction in a given period to the whole length (in hours) of that period. The values of the stability index for the whole studied period growing season, as well as different type groups are presented in *Table 3*. Generally it can be stated, that on the Great Hungarian Plane wind directions show a stronger trend to be stable than to fluctuate, since, with the exception of three cases (the ZE type group, types A and C in Békéscsaba during the growing season), they take 0.5 or higher values. It can also be seen in the table, that in Békéscsaba the stability indexes are lower than those in the same subsets at the two other stations for the years and growing season, with the exception of the ZW type group. That is because the bent for fluctuation is the strongest there. The reason for this is presumably orografic, because that station is the nearest to the Carpathian Mountains, therefore, the development of thermal circulations is the most possible there. This fact and that the sequence (from the lowest to the highest) of the stability indexes for almost all cases is: Békéscsaba-Debrecen-Szeged, are quite in line with the observations of Péczely (*Péczely,* 1963) on mountain and valley winds.

From the table it is also visible, that stability indexes for all subsets and stations are lower during the growing season than in the whole year. The strong fluctuation of the wind directions during the growing season presumably has thermal reasons, because the mean temperatures during the growing season are much higher than in the whole year. The five-day mean temperatures are between 10 and 20°C during the growing season and under 10°C in the other part of the year (*Szász,* 1988).

The minimum of the stability index in the whole year occurs – understandably – at all the three stations in the C type. During the growing season the picture is not so simple: in Békéscsaba and Debrecen this value in type A is near the

minimum. The logic of the maxima generally speaking is the following: in a north-south direction through the zonal (ZW, ZE) type groups it arrives to the meridional southern type group (MS). This logic is disturbed by the values of the whole year in the A type in Szeged and the values of the growing season in the MN type in Debrecen. The absolute maximum occurs in both periods in the MS type group in Szeged, but these values are very close to those of type A.

Table 3. Stability index (st.i), mean wind velocity (v_{mean}), and mean daily number of stabile hours (st.h) in various periods

Stations	Characteristics	Whole	MN	MS	ZW	ZE	A	C	AG	CG
					Year					
	st.i.	0.56	0.55	0.57	0.56	**0.59**	0.56	*0.53*	0.57	0.54
Debrecen	v_{mean} (m/s)	2.7	3.1	2.4	2.9	2.8	*2.0*	**3.3**	2.5	3.2
	st.h.	13.5	13.1	13.6	13.5	**14.1**	13.4	*12.6*	13.7	13.1
	st.i.	0.54	0.54	0.55	**0.56**	0.53	0.52	*0.51*	0.54	0.55
Békéscsaba	v_{mean} (m/s)	2.8	3.2	2.6	3.1	2.5	*2.0*	**3.5**	2.7	3.4
	st.h.	13.0	13.0	13.2	**13.4**	12.7	12.5	*12.3*	12.9	13.2
	st.i.	0.58	0.55	**0.61**	0.58	0.57	**0.61**	*0.54*	0.59	0.56
Szeged	v_{mean} (m/s)	3.1	3.5	3.3	3.2	2.8	*2.2*	**3.9**	2.9	3.7
	st.h.	14.0	13.3	**14.6**	13.9	13.8	14.5	*12.9*	14.2	13.4
					Growing season					
	st.i.	0.52	**0.54**	0.52	0.51	**0.54**	*0.50*	0.51	0.53	0.51
Debrecen	v_{mean} (m/s)	2.6	3.0	2.4	2.6	2.6	*2.0*	**3.2**	2.5	3.0
	st.h.	12.5	**12.9**	12.5	12.3	**12.9**	*12.0*	12.2	12.6	12.3
	st.i.	0.50	0.50	0.51	**0.52**	*0.48*	*0.48*	*0.48*	0.50	0.50
Békéscsaba	v_{mean} (m/s)	2.9	3.1	2.9	2.9	2.7	*2.5*	**3.3**	2.7	3.2
	st.h.	12.0	12.1	12.1	**12.5**	*11.5*	*11.6*	*11.5*	12.0	12.0
	st.i.	0.54	0.52	**0.56**	0.55	0.54	0.55	*0.51*	0.55	0.52
Szeged	v_{mean} (m/s)	3.0	3.3	3.2	3.0	2.7	*2.2*	**3.6**	2.8	3.4
	st.h.	12.9	12.5	**13.5**	13.2	13.0	13.1	*12.2*	13.1	12.5

bold: the maximum value, *italic:* the minimum value in the macrosynoptic type groups and types

On the base of the data in the table, the strength and trend of the stochastic relationships between the stability indexes and average wind velocities for the individual subsets (MN, MS, ZW, ZE, C, A) can be determined. It can be stated, that the linear correlation coefficient does not differ from 0 significantly in any cases, since its absolute value does not reach the critical value ($r_{0.05}$=0.81) of the probability level of 0.05. The closest to

the critical value occurs in Szeged in the case of the year (–0.706). On the base of the before mentioned facts, we can establish that type C is quite unsuitable from the aspect of the sprinkling irrigation of the plant, because in that type low stability indexes are combined with high wind velocities. On the other hand, there are no types or type groups where the opposite is true, that is, where maximal stability indexes and minimal wind velocities occur. To find the solution, we have to analyze the relationships between the *daily* parameter of stability and *daily* mean wind velocity.

6. The relationship between the stability and daily mean wind velocity

As daily characteristic parameter of the stability, we choose the daily number of hours with stabile wind directions. Its average values are presented in *Table 3*. The relationships between daily stability and mean wind velocities are examined by two methods. In the first case we correlate the *actual* daily number of stabile hours of the periods with the mean wind velocity of the same day. Two examples for this are presented in *Fig. 1* and *Fig. 2*, where the regression line is presented as well (it will be called *case of day-to-day* in the followings). In the second method we gather the days that have the same number of stabile hours, and then we correlate their mean wind velocity with the daily number of stabile hours (*case of classification*). The frequency of those days, that have the same number of stabile hours, their daily mean wind velocities and the regression line applied for them are presented in *Fig. 3*. In *Table 4,* linear correlation coefficients determined by the two methods, and their critical values at the significance level of 0.05 ($r_{0.05}$) are shown in the different cases.

Critical values – the minimal values of the correlation coefficient that significantly differs from 0 –, up to about 100 sample elements, can be most simply determined using the Fisher-Yates table, in some cases by interpolation (*Dobosi* and *Felméry*, 1971). Dealing with more than 100 elements – that occurs using the first method – the significance analysis must be carried out using the *t*-test that is $r_{0.05}$ was calculated from the value of $t_{0.05}$. Therefore, the test function is

$$t = \frac{r}{\sqrt{1-r^2}}\sqrt{n-2}\ , \tag{1}$$

where n is the number of the elements (*Yule-Kendall*, 1964). The critical t values ($t_{0.05}$) of the 0.05 probability level over 400 elements are 1.96–1.97 – they practically do not change –, but because of the different number of the elements, the $r_{0.05}$ changes. The critical values of the correlation coefficient between the daily number of the stabile hours and mean wind velocity of the

same day (case of day-to-day) are the same in the three stations, because the number of the elements is the same. It is not true for the clustering of the days that show the same stability (case of classification), since the number of stabile hours – that theoretically can take values between 0 and 24 – can be different in each case (subset) and each station. The occurrence of low (0, 1, 2) and high (22, 23, 24) values can even be 0.

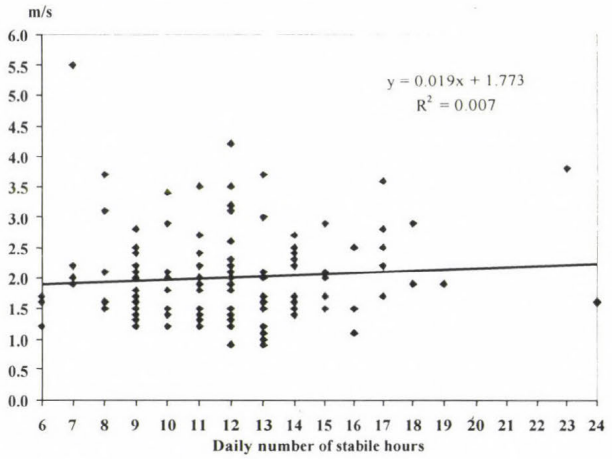

Fig. 1. Linear regression and correlation between the daily mean wind velocity (m/s) and daily number of stabile hours in the case of day-to-day (growing season, the case of minimum correlation: Debrecen, type A).

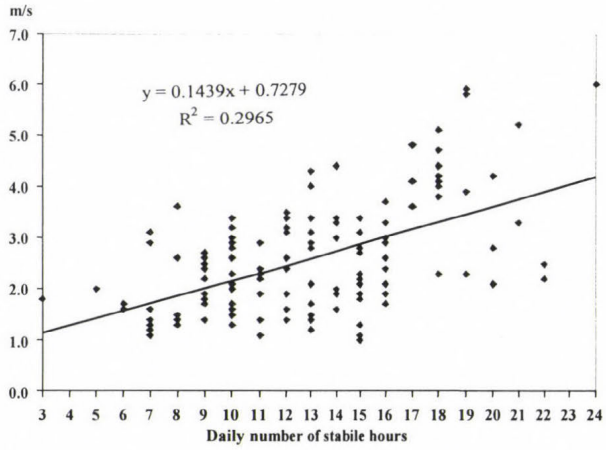

Fig. 2. Linear regression and correlation between the daily mean wind velocity (m/s) and daily number of stabile hours in the case of day-to-day (growing season, the case of maximum correlation: Debrecen, type group ZE).

On the base of *Table 4* it can be stated, that in the *case of day-to-day,* values of the correlation coefficient between the daily number of the stabile hours and daily mean wind velocities in the six subsets (MN, MS, ZW, ZS, C, and A) of both the whole year and growing season are the lowest in type A at all the three stations, and they are not significant in Debrecen (see *Fig. 1*) and Szeged. The "second lowest" but significant values at all the three stations occur in type group MS. In the *case of classification* there are slight differences between the whole year and growing season: for the whole year there are not significant correlation coefficients in type A, in Debrecen and Szeged (see *Fig. 3*), in Békéscsaba the lowest value can be found in type group ZE. The next correlation coefficient by the value is in type group ZW in Debrecen, it falls into type group MS in Békéscsaba and Szeged, but it is not significant in Szeged. The picture is more clear during the growing season: it is similar to the daily event with the exception of that in Szeged in the case of type group MS and type C the values are not significant.

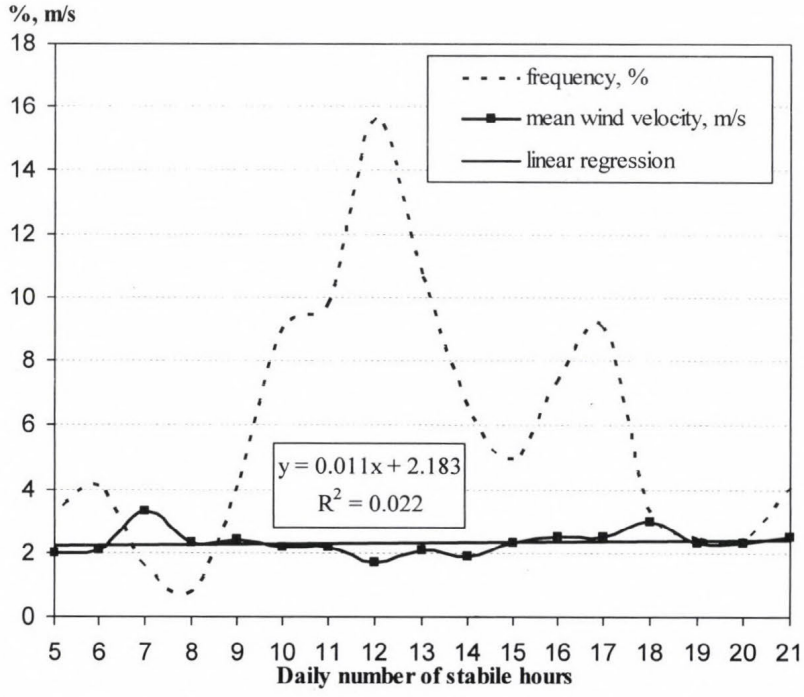

Fig. 3. Frequency of days having the same number of stabile hours (%), as well as the linear regression and correlation between the mean wind velocity (m/s) and daily number of stabile hours in the case of classification of the days (Szeged, type A, growing season).

Table 4. Linear correlation coefficients and their critical values at the 0.05 significance level in the case of day-to-day and classification of the days, in various periods

Method of the data groups	Whole	MN	MS	ZW	ZE	A	C	AG	CG
Year									
Debrecen									
Day-to-day	0.29	0.42	0.27	0.27	0.46	**0.11**	0.41	0.30	0.36
Classification of the days	0.91	0.94	0.88	0.80	0.87	**0.43**	0.82	0.87	0.95
Békéscsaba									
Day-to-day	0.44	0.56	0.39	0.48	0.44	0.34	0.53	0.32	0.33
Classification of the days	0.88	0.91	0.88	0.96	0.80	0.91	0.90	0.92	0.77
Szeged									
Day-to-day	0.21	0.39	0.20	0.21	0.32	**0.03**	0.38	0.19	0.38
Classification of the days	0.84	0.79	**0.27**	0.62	0.60	**0.20**	0.60	0.78	0.90
Critical values – day-to-day	0.05	0.10	0.09	0.10	0.13	0.12	0.20	0.06	0.08
Critical values – classification of the days									
Debrecen	0.40	0.42	0.42	0.44	0.42	0.45	0.50	0.42	0.42
Békéscsaba	0.41	0.41	0.44	0.44	0.42	0.42	0.47	0.41	0.41
Szeged	0.43	0.43	0.43	0.44	0.43	0.45	0.43	0.43	0.41
Growing season									
Debrecen									
Day-to-day	0.37	0.440	0.26	0.37	0.54	**0.08**	0.40	0.41	0.35
Classification of the days	0.89	0.92	0.67	0.86	0.75	**0.07**	0.79	0.78	0.92
Békéscsaba									
Day-to-day	0.34	0.41	0.26	0.35	0.33	0.26	0.44	0.35	0.36
Classification of the days	0.80	0.85	0.48	0.78	0.90	0.77	0.58	0.80	0.62
Szeged									
Day-to-day	0.25	0.32	0.20	0.29	0.36	**0.17**	0.33	0.27	0.29
Classification of the days	0.80	0.820	**0.32**	0.73	0.67	**0.15**	**0.19**	0.59	0.62
Critical values – day-to-day	0.06	0.130	0.16	0.14	0.16	0.18	0.24	0.08	0.11
Critical values – classification of the days									
Debrecen	0.42	0.47	0.43	0.52	0.47	0.53	0.50	0.42	0.43
Békéscsaba	0.43	0.47	0.44	0.50	0.47	0.50	0.50	0.44	0.44
Szeged	0.41	0.48	0.48	0.47	0.48	0.48	0.50	0.43	0.41

bold: no significant coefficients

For both periods examined here it can be stated, that the stronger correlations can be found for the case of day-to-day in Békéscsaba in the whole year, and at the two other stations during the growing season. Higher correlations can be found at all the three stations during the growing season only in the antyicyclonal type group (AG). In the AG and CG groups and A and C types, considering the whole period in the case of classification, the situation is the opposite: the correlations for the whole year are stronger. Consequently, our assumptions discussed in Chapter 2 are not true for type C, because in that type two fronts appear together.

7. Conclusions

It can be stated, that on the Great Hungarian Plane the conditions for the sprinkling and sprinkling irrigation are the most favorable in the A type and MS type group (its elements can be found in *Table 2*). In these cases there is no correlation, or only very weak linear correlation can be found between the parameter characteristic for the stability of the wind directions, daily number of stabile hours, and daily mean wind velocity. On the base of the studies on the life span of the macrosynoptic types (*Péczely,* 1983), time patterns of their fluctuations (*Tar* and *Kircsi*, 2002), and frequencies of their transformations into each other (*Mika* and *Domonkos*, 1994), the time of the sprinkling or sprinkling irrigation can be planned in a few days in advance.

We have proved that the increase of the size of the subsets (groups) decreases the amount of information useful for solving the problem (see, e.g., type groups AG and CG). Presumably, we could gain better results in this aspect carrying out the above detailed analysis for the individual macrosynoptic types. This analysis, however, requires more abundant database.

The relationship between the wind conditions and water supply of plant canopies can be examined from a completely different point of view. Wind machines, which use wind energy for water pumping, are suitable for dripping irrigation. It is proven that the specific wind power is in a – not obviously linear – stochastic relationship with the stability of the wind directions.

Acknowledgements—The authors thank the Hungarian Meteorological Service for providing the necessary database for the analysis.

References

Dobosi, Z. and *Felméry, L.*, 1971: *Climatology* (in Hungarian). Tankönyvkiadó, Budapest.

Hegyfoky, K., 1904a: The turn of the wind at Ógyalla (in Hungarian). *Athmosphera VIII,* 219-221.

Hegyfoky, K., 1904b: The turn of the wind at some Hungarian weather stations (in Hungarian). *Athmosphera VIII*, 285-301.

Hegyfoky, K., 1904c: The turn of the wind at Bjelasnica and at some peaks (in Hungarian). *Athmosphera VIII*, 321-327.

Hegyfoky, K., 1904d: The turn of the wind and its reasons (in Hungarian). *Athmosphera VIII*, 353-364.

Károssy, Cs., 1998: Péczely's classification of macrosynoptic types and catalogue of weather situations (1992-1997). In *Light Trapping of Insects Influenced by Abiotic Factors*. Part II. (ed.: *L. Nowinszky*), Savaria University Press, Szombathely, 117-130.

Mika, J. and *Domonkos, P.*, 1994: Statistical characteristics of local weather within Péczely's macrosynoptic classification and its modified version. *Annales Universitetis Scienticaum Budapestiensis de Rolando Eötvös nominate*. Sectio geophysica et meteorologica. Tomus X, 73-91.

Mezősi, M. and *Simon, A.*, 1981: The theory and practice of meteorological wind measurements (in Hungarian). *Meteorológiai Tanulmányok*, No. 36., Országos Meteorológiai Szolgálat, Budapest.

Péczely, Gy., 1983: *The Catalogue of the Macrosynoptic Types of Hungary (1881-1983)* (in Hungarian). Országos Meteorológiai Szolgálat Kisebb Kiadványai, 53. kötet, Budapest.

Szász, G., 1988: *Agrometeorology* (in Hungarian). Mezőgazdasági Kiadó, Budapest.

Szász, G., 1995: The role of the wind velocities in the control of the thermal conditions of plant stands (in Hungarian). In *Berényi Dénes professzor születésének 95. évfordulója tiszteletére rendezett tudományos emlékülés előadásai*. KLTE-MMT-MTA, Debrecen, 7-33.

Tar, K., 1980: Statistical examinations on the time patterns of the fluctuations of the wind directions (in Hungarian). *Időjárás 84*, 151-159.

Tar, K. and *Kircsi, A.*, 2002: The connections between wind energy and weather conditions (in Hungarian). In *ÖKOENERG' 2002. Energiahatékonysági és hulladékgazdálkodási konferencia*, Kecskemét, 41-46.

Tar, K. and *Szegedi, S.*, 2002: The stability of the wind directions in the growing season under different weather conditions (in Hungarian). In *Levegő-növény-talaj rendszer*. Debreceni Egyetem–Agrártudományi Centrum, Debrecen, 103-113.

Tar, K., 2003: Relationship between the energy and the change of directions of the wind (in Hungarian). In *Környezetvédelmi mozaikok–Tiszteletkötet Kerényi Attila 60. születésnapjára. Debreceni Egyetem,* Debrecen, 391-406.

Yule, G.U. and *Kendall, M.G.*, 1964: *An Introduction to the Theory of Statistics* (in Hungarian). Közgazdasági és Jogi Könyvkiadó, Budapest.

IDŐJÁRÁS

Quarterly Journal of the Hungarian Meteorological Service
Vol. 107, No. 3–4, July–December 2003, pp. 225–236

An evapotranspiration calculation method based on remotely sensed surface temperature for agricultural regions in Hungary

Zoltán Dunkel

Hungarian Meteorological Service,
P.O. Box 38, H-1525 Budapest, Hungary; E-mail: dunkel.z@met.hu

(Manuscript received October 20, 2003; in final form November 3, 2003)

Abstract—The surface temperature measured by satellite can be the basis of evapotranspiration (ET) computation. The possibility of the daily sum of the regional ET using surface temperature was examined under Hungarian weather conditions. Simplified relationship, namely $R_{nd} - ET_d = A + B(T_C - T_A)$, which relates to the daily ET and daily net radiation with one measurements of surface and air temperature was used for the calculation. No information was obtained about the surface inequality using NOAA AVHRR satellite data. To collect any information describing the distribution of surface temperature, infrared thermometer was used to scan the surface from the board of a hang-glider, ultra-light-aeroplane, and light aeroplane. The limited field observations were made during the vegetation period of 1992, 1993, and 1994. In eastern part of the country, a homogeneous field (1 km × 1 km) and a larger, and relatively homogenous area was scanned, before noon and afternoon. In the western part of the country, a much larger area (45 km × 45 km) was investigated. The distribution of the surface temperature in special cases is shown. The paper presents a calculation system which can produce the daily sum of evapotranspiration using the daily maximum surface and standard air temperature. The results of a simplified validation method proves the usefulness of the shown method. The limitation of the use and possible development of the method concludes the paper.

Key-words: evapotranspiration, latent heat flux, near-surface measurements, satellite born information, surface temperature.

1. Introduction

One of the basic task of agricultural meteorology is the determination of water supply of plants using simply measurable meteorological elements. The ratio of transpired water and potential evaporation shows the plant water supply, the measure of plant water stress. Determining the water stress status of the plant,

agrometeorology can give useful information to the users. Nowadays, three great changes have happened in meteorology. The first two are connected with the instrument and measurement technique, the third one is related to the data transfer and processing. The operative application of remote sensing gives new, previously impossible methodology to the agrometeorology. The satellite born information promotes the regional investigation as much as it was not possible earlier. The computer technique and data transfer allow so quick data process which was unthinkable 10–15 years ago.

The application of remote sensing in agrometeorology started when the first instruments were issued to measure the surface temperature. The equation using the surface temperature (*Jackson et al.*, 1977, 1981, 1988), the developed methods are valid for more or less small field experiment places. The question we have to answer is how to use the results of field experiments for larger scale processes (*Caselles et al.*, 1992, *Hurtado et al.*, 1994). Two demands triggered the present work. The first one was the investigation of possible use of directly measured surface temperature in agricultural meteorology (*Dunkel et al.*, 1989). The second one (*Kerényi* 1993, 1994) was the demand of ground truth for calibration of satellite born surface temperature measurements. Hungarian experiments (*Dunkel* and *Vadász*, 1993) were carried out to determine the water stress status of plants using the surface temperature.

The investigations were continued not in this direction. Previously the application of satellite born surface temperature for calculation of evapotranspiration was investigated. More or less the same approach is how to exploit the recent meteorological development in agricultural meteorology. The present study gives the methodology of the calculation of areal evapotranspiration. Neither the important calibration problems of the measurement of surface temperature close to the surface nor the evaluation of evaporation calculation methods are shown. To choose surface control method we had to evaluate few classic calculation methods, but only the result of the comparison with *Antal* (1968) method is presented. Combining the different systems, a method was developed which is suitable for calculation of daily areal evapotranspiration.

The surface temperature measured by remote sensing can be the basis of territorial investigation of water stress status of any kind of canopy. ET can be calculated following *Seguin* and *Itier* (1983) or *Lagouarde* (1991) by solving the surface energy equation in a simplified way, or *Jackson et al.* (1981, 1988) calculating directly the water stress status of the canopy. In the present paper water stress map is not shown. An example for calculation of territorial ET for Hungary is presented. There is no information about the changes within a pixel. There is no information about the emissivity of the investigated surface.

Knowledge about the water vapor content and its influence on the measured surface temperature is poor. Surface reference values to calibrate the ET calculation equation are inadequate. To answer at least partly the problem, a surface controlled measurement was made in Hungary.

2. Description of the field experiments

In order to get a better spatial resolution for estimating the temperature distribution, a near-surface trial was executed during the vegetation period of 1992, 1993, and 1994. KT-24 type infrared thermometer was used every year. The instrument was put on board of a hang-glider in 1992, a light (CESSNA 105), and ultra-light (TUCANO) aeroplane in 1993. Later, in 1994 and 1995, the measurement program was extended to measuring, besides the surface temperature short wave reflected, and the long wave irradiated radiation, by Kipp-Zonen CM-5 type radiometer, and Eppley pyrgeometer, respectively. In the first two years, the data were collected using one-channel data-logger. In 1994, the instruments were built into the wing of an AN-2 type aeroplane, and the data were loaded directly to a PC. The cruising height was 100 m in case of the hang-glider, and 500 m in case of the aeroplane. To understand the effect of water vapor on surface temperature, the runway was scanned from 600, 400, 200, and 20 m heights.

As reference to ET for surface control measurements in 1992 and 1993, only the class A-pan evaporation observation was used. The ET reference value, using empirical formula derived for Hungarian climate was calculated. In 1994, it was possible to measure the latent heat flux directly using Bowen ratio system, however, for only one place. In 1992, the basic goal was to investigate the temperature change within one field. Two fields were chosen as control area. Their size was about 1 km × 1 km. In the eastern part of Hungary sometimes such a large field with approximately homogeneous vegetation was found. In the present investigation the surface temperature scanning over irrigated and non-irrigated maize canopy was executed. The scanning routes had north-south direction in 1993 and 1994. In 1992, a relatively small area was scanned in the eastern part of Hungary close to the town Szarvas, where an agrometeorological observatory was maintained by the Hungarian Meteorological Service (HMS). The scanned surfaces were maize and wheat canopies. We tried to measure a more or less homogeneous surface as large as it could be identified in the satellite picture. In 1993, the philosophy was changed. We tried scan as large area as it was possible. The length of one scanning route was 45 km. The experiment area was in the western part of the country. Eleven scanning routes completed the examination area. Few

scanning route crossed the lake Balaton. In 1994, the place of the field experiments was the Hortobágy puszta in the eastern part of the country close to Debrecen, the second biggest city of Hungary. The surface of the "puszta" is more less natural grass, it looks like a steppe. The assumption of homogeneous surface worked more or less in this case as well. The length of scanning route was shorter in 1994, 25 km.

To calibrate the infrared thermometer, a "black body" model was used. This "black body" was a sooty copper plate. The instrument and the "black body" were placed together into a climate chamber. The near-surface temperature measurements were not all simultaneous. Because of the achieved cruising speed, the time-leg between the first and last measured value could be few hours. If a comparison of the result with any kind of satellite picture is desired, the measured values need to be homogenized. Following *Sellers et al.* (1986), a simplified model was used for this purpose (*Dunkel et al.*, 1991). The main problem in the use of the suggested model is the estimation of heat capacity of the canopy. The calculated and measured surface temperatures were compared for sunflower canopy under different experimental conditions. Using the developed diurnal temperature change model, the measured surface temperature values were homogenized for the same time. This homogenization is necessary, because airborne measurements are not synchronous.

Comparing the morning and near afternoon temperature distribution along one cruising route during the 1993 field experiments, characteristically different distribution was observed. Few hours after sunrise almost no change in canopy temperature was observed, nevertheless, the swamp can be well identified, and of course the surface of the lake Balaton shows characteristic values.

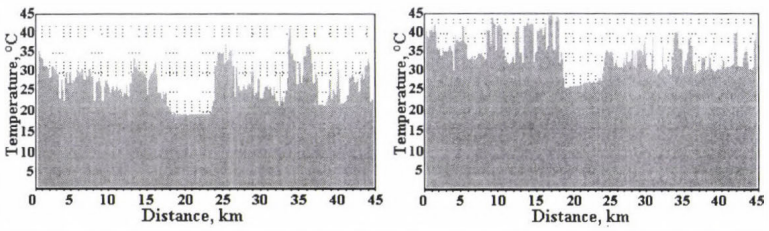

Fig. 1. The distribution of the surface temperature along a Balaton crossing route. July 9 and August 5, 1993.

The hypothesis before the flight was that no change would be found in the water surface temperature. As *Fig 1.* shows, the surface temperature of the shallow lake is not homogeneous, but comparing with the other surfaces it is

much more characteristic. Repeating the flight over that area near noon, opposite situation was observed. The swamp was much cooler than the surrounding area, and the variation in temperature was more than 10 degrees. The temperature distribution shows the same change along the same route during July–August across the lake Balaton. The lake surface temperature shows almost no change. The temperature difference outside the lake could be more than 10 degrees, but the results of the scanning showed that the homogeneous surface conception is not valid even in case of a shallow lake such as Balaton.

3. The model

The calculation method is based on the simplified surface energy balance equation. The energy balance equation of any given surface could be written as

$$R_n = D + G + J + \mu A + H + LE\,, \tag{1}$$

where R_n is the net radiation, D is the horizontal energy transfer, G is the soil heat flux, J is the energy storage in the "surface", μA is the energy used for biochemical processes, H is the sensible heat flux, LE is the latent heat flux. In our terminology the evapotranspiration expressed in W m^{-2} unit, later converted into traditional unit mm. A very simple and useful solution of the equation was suggested by *Jackson et. al* (1977). Later *Seguin* and *Itier* (1983) used only the larger elements of energy budget and neglected the smaller terms, namely μA (*Hunkár,* 1985), the rate of energy stored biochemically, and G, the ground heat flux is more or less zero on a daily basis. After the simplification the equation shows the following form:

$$R_n = H + LE\,. \tag{2}$$

The term H, the sensible heat flux could be expressed in the near-surface layer as,

$$H = -\rho\, c_p \frac{T_C - T_A}{r_A}, \tag{3}$$

where T_C is the surface temperature, later to be determined using satellite information, and T_A is the near-surface temperature practically to be taken equal with the air temperature measured in the standard wind screen above the surface in 2 m height at the synoptic station. The ρ is the density, c_p is the heat capacity of the air at constant pressure, r_A is the air resistance in the lower layer. In the present approximation every value is instantaneous. After the

simplification, we have found a linear expression between the temperature difference latent heat flux, and net radiation difference, as

$$LE - R_n = -b^* (T_C - T_A), \tag{4}$$

where all physical constants are united into one parameter, b^*. We would like to calculate the daily evapotranspiration, but only instantaneous values are measured. The field experiments, in case of cloudless day, proved that the presented linear expression is good approximation (*Seguin* and *Itier*, 1983; *Lagourde*, 1991) for the calculation of daily sum of evapotranspiration using only one temperature difference as it is shown in *Fig. 2*. The final expression will be

$$ET_d - R_{nd} = A + B (T_C - T_A) \qquad \text{(mm/day)}, \tag{5}$$

changing the LE abbreviation to ET, as usually accepted in agricultural meteorology for the searched quantity, and signing the daily values with d. In the expression A and B, parameters can be estimated by linear regression, T_C is the surface (canopy, skin) temperature measured by satellite or any kind of remote sensing technique, and T_A is the near-surface (daily maximum) temperature. The determination of T_C, the surface (canopy, skin) temperature measured by satellite, is one of the basic tasks of satellite meteorology (*Becker* and *Li*, 1990; *Kerényi*, 1994).

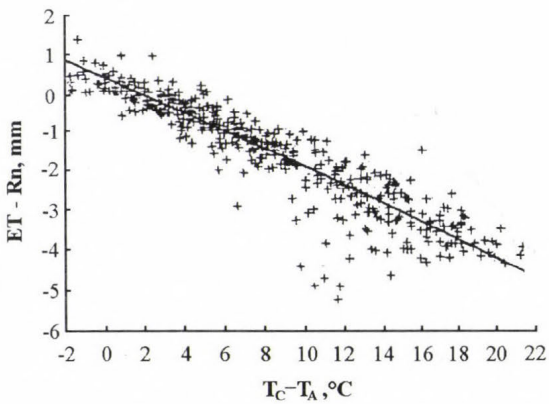

Fig. 2. The relationship between the two differences, ten-day average (*Lagourde*, 1991).

The parameters can be estimated experimentally, simulated, or calculated by a combination of the two methods. The regression coefficients depend on the surface roughness as it is shown in *Table 1*.

Table 1. The value of "A" intersection (mm day^{-1}) and "B" slope (mm day^{-1} $grad^{-1}$) by *Lagourde* (1991), z_0 is the roughness coefficient

z_0	A	B
0.001	0.41	0.145
0.002	0.43	0.166
0.005	0.47	0.204
0.01	0.5	0.244
0.02	0.53	0.296
0.05	0.55	0.394
0.1	0.59	0.498

The simple linear regression between the daily sum of ET and the midday difference of surface temperature minus air temperature is proven by many investigators (*Caselles et al.*, 1992; *Jackson et al.*, 1977, 1981, 1989; *Hurtado et al.*, 1994; *Kustas et al.*, 1982; *Lagourde* 1991; *Sandholt* and *Andersen*, 1993).

4. Calculation method

Satellite Research Laboratory of HMS has been receiving NOAA-AVHRR data digitally, since 1992. The data are calibrated and geographically identified. For the ET calculation, NDVI is derived from Channel 1 and 2, which is the calculation procedure widely used all over the world. The surface temperature was calculated by split-window method from the data of Channel 4 and 5 (*Kerényi* and *Putsay*, 2000). The calculated and measured surface temperature were compared in case of few situations during summer time. For estimation of ET, following *Seguin* and *Itier* (1983) suggestion, besides the midday surface temperature, the maximum air temperature measured by standard meteorological network is also needed. During the 1995/96 period, the traditional meteorological observations were replaced by automatic synoptic stations. If the observation time was very different from the date of maximum air temperature, a shifting correction was applied following the *Sellers et al.* (1986) model.

The basic goal of the research was to establish a method which could be used in operative practice to determine the daily sum of evapotranspiration. The base of the method is a simplified solution of surface energy balance equation as it was introduced earlier in Eq. (5). This equation is valid not only for instantaneous but longer period, namely for daily values, too, as showed by many field experiments. If we apply this equation for the whole day, the daily evaporation minus net radiation is the linear function of maximal air and surface temperature difference. To apply the method in the practice, we need several further informations.

The elements of the calculation system are shown in *Fig 3*. The near-surface air temperature and surface temperature are measured by HMS operatively. The necessary A and B constants are originated partly from field experiments and mainly from the cited literature, because we had possibility to carry out the necessary field experiment only in few cases of the possible land surface covering situations. The air-born surface temperature measurements were carried out above different parts of Hungary, as it was mentioned in the previous chapter. The measurements were done in summer during the time of well developed vegetation. We tried to carry out the measurements above homogeneous surface and use as large experimental area as it could be identified on satellite picture.

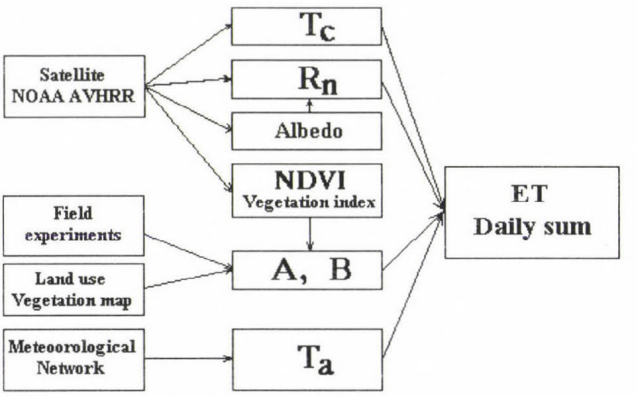

Fig. 3. The flow-chart of daily evapotranspiration calculation.

The satellite born surface temperature could be useful for our purpose if they were done near noon. Sometimes we need the temporal change of surface temperature. Using the surface energy equation, a simplified solution was developed to calculate the surface temperature. The calculation method was controlled using lysimeter data derived from the experimental sites. The evaporation calculation system could be compared with other calculation methods. Few potential evaporation calculation formula were evaluated to decide which one could be used for our evaluation. Taking into consideration the difficulties of many ET calculation methods, the comparison with the *Antal* (1968) potential ET calculation method is shown as verification of the method. For the calculation we used only the meteorological stations equipped with standard A pan. In *Fig. 4*, the stations are shown where Pan A open water evaporation is measured operatively by HMS.

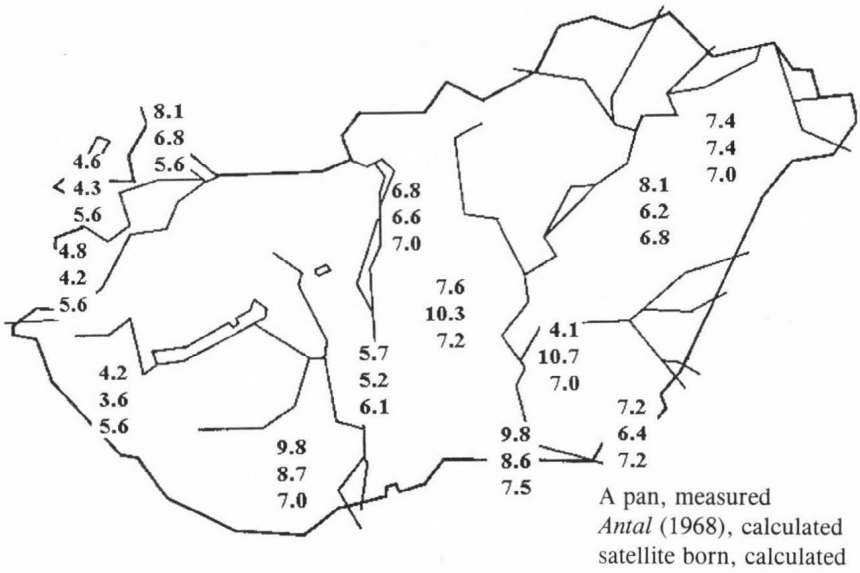

Fig. 4. Comparison of values derived from satellite data with surface measurements and calculation, July 23, 1998.

The calculation were carried out in dry and wet years as well. In present paper the results of the 1998 year are shown. The main problem concerning the application of the method is whether it is possible to determine realistically the daily sum of evapotranspiration using only one daily maximum value. The other problematic case is when the radiation balance will not follow sinus function when any kind of cloudiness appears. In this situation, to calculate the daily sum of ET using only one instantaneous value of temperature does not seem to be correct approach.

Nevertheless, when areal conditions are optimal for application of the method, the accuracy limit is approximately ±1 mm day^{-1}. It does not seem to be very good approach, if we take into consideration that the maximum value of daily evapotranspiration exceeds 10 mm day^{-1} very few times. But the accuracy of any classic method is more or less the same. We can accept this limitation, because in agrometeorological practice the 10 days time step is the standard, and on this time scale the calculation error seems to be not so bad.

Anyway, our basic approach is to exploit the standard meteorological observation system as simple as possible and the introduced method is applicable. *Fig. 3* summarizes the structure of the whole methodology of the introduced method.

5. Validation of the method

The introduced method produces areal values. The resolution of the prepared ET map is equal to the resolution of the satellite images. Practically, we can calculate with an approximately 3 km resolution. It means that we have got cca. 9,000 data every day for the whole territory of the country. The only possibility of the validation is, if the satellite born data are compared with the measured values in individual points. We have got only few places where A-pan measurements are available. For these stations the ET values using *Antal* (1968) method were calculated and compared with the satellite born values. As an example, the distribution of the values are presented on July 23, 1998 in *Fig. 4.* As it was mentioned, the method could be applied only on cloudless days. A really cloudless day occurs only few times during the vegetation period. *Table 2* shows a comparison for the days which met the requirements in 1998. In few cases the table shows good coincidence, but in few cases not. The basic reasons of the not too good fitting is the use of universal constant. But taking into consideration the difficulties of the determination of coefficients, the permanent lack of the necessary ground truth, we could be satisfied with the results as a first guess.

Table 2. Comparison of measured (Pan A), calculated by the method of *Antal* (1968), and satellite born values for cloudless days. The given values are the simple arithmetic averages of the values of the available stations (as shown in *Fig. 4*)

Day of calculation	Pan A mm/day	Method Antal mm/day	Satellite born mm/day	A versus Antal %	A versus Satellite %	Satellite/ Antal %
June 03, 1998	5.7	5.7	5.7	100	140	139
June 10, 1998	6.1	6.1	7.9	100	128	130
July 01, 1998	4.1	3.8	4.9	92	120	129
July 23, 1998	8.3	8.2	7.9	98	96	97
July 25, 1998	13.2	12.9	12.6	98	96	97
July 29, 1998	1.2	1.2	1.8	102	141	137
July 31, 1998	6.4	6.5	8.1	101	124	123
Aug 01, 1998	6.3	6.5	7.8	102	123	120
Aug 02, 1998	7.6	7.7	8.6	99	111	111
Aug 04, 1998	15.0	15.0	16.3	100	108	108
Aug 07, 1998	5.9	5.9	8.6	101	147	145
Aug 09, 1998	8.1	7.1	8.5	88	106	119
Aug 10, 1998	9.2	8.1	9.0	88	98	112
Aug 12, 1998	6.8	6.9	8.5	101	124	122
Aug 13, 1998	8.1	7.8	8.2	96	101	105

6. Conclusion

Based on NOAA-AVHRR visible, near-infrared, and thermal infrared data in combination with meteorological data, it is possible to calculate daily sum of (actual) ET for days when the satellite born surface data are available. The calculated values of areal ET were compared with surface evaporation measurements values. There are no direct methods to "calibrate" either the satellite born surface temperature or the daily sum of ET satisfactorily. The results of our method were compared with the standard surface A-pan network, and in few cases with the measurements and calculated ET at agrometeorological research sites. The method could be used in case of cloudless summer days to estimate territorial distribution of ET values for large area, but its accuracy is about ± 1 mm day^{-1}. In our case, the main goal is not the precise determination of actual ET but to inform extension service about the possible drought situation or about area water stress status. To prepare the application of the method, air-plane born surface temperature measurements were carried out in some years. The goals of these measurements were double-folded. The first goal was to help the establishment of satellite calibration. The second one was to discover the surface temperature inequality. Cloudy weather could limit the application of the method. The longer cloudy period can mitigate the water stress status or completely stop it, when the soil moisture content is satisfactory. In this case, the areal evapotranspiration from the practical point of view is less important. The main parts of the investigation were the near-surface skin temperature measurements and the comparison of collected data with satellite born surface temperature. The determination of areal evapotranspiration for a large region was the main goal.

The results could be summarized that a system was introduced to determine the daily sum of evapotranspiration. The system is suitable for everyday operative application. Using the introduced method one day after the measurements, we can get the daily sum of evapotranspiration. The method is useful to calculate the areal evapotranspiration for a large region with the given error and limitation factors. Continuous application of the method can act as drought monitoring system as well.

Acknowledgements–The present work, mainly the field experiments needed many resources. The author would like to express his grateful acknowledgement to the leaders of the mentioned project (project leader in brackets) and colleagues without help of whom this work would not have been accomplished. The financial supporting projects were OTKA (Hungarian National Science Found) 2024 (Major, G.), UN-Hungarian Joint Found 923/B (Vorosmarty, Ch. J and Dunkel, Z.), COST 93024 study (Dunkel, Z.), COST-STY-97-4018 (Dunkel, Z.). The participating colleagues were *Prof. Dr. Gábor Szász* (not only as a scientific leader but pilot of the aeroplane during the field experiments), *Ms. Ildikó Grób-Szenyán* (calculation of satellite data), *Mr. Zoltán Nagy* (data logging during the field experiments), and *Ms. Ágnes Sáhó* (data processing, text and picture editor).

References

Antal, E., 1968: Irrigation schedule on the basis of meteorological data (in Hungarian). *CSc Thesis*, Magyar Tudományos Akadémia, Budapest.

Antal, E. and *Tóth, E.*, 1980: Climatological method for determination of areal evapotranspiration (in Hungarian). *Időjárás 84*, 83-92.

Becker, F. and *Li Zhao Liang*, 1990: Temperature-independent spectral indices in thermal infrared bands. *Remote Sensing of Environment 32*, 17-34.

Caselles, V., Delegido, J., Hurtado, E., and *Sobrino, J.A.*, 1992: Evaluation of the maximum evapotranspiration over La Mancha region, Spain using NOAA AVHRR data. *Int. J. Remote Sensing 13*, 939-945.

Dunkel, Z. and *Vadász, V.*, 1993: Estimation of regional evapotranspiration over Hungary combining standard and satellite data. *Adv. Space Res. 13*(5), 275-260.

Dunkel, Z., Bozó, P., Szabó, T., and *Vadász, V.*, 1989: Application of thermal infrared remote sensing to the estimation of regional evapotranspiration. *Adv. Space Res. 9*(7), 255-258.

Dunkel, Z., Pásztor, K., and *Tiringer, Cs.*, 1991: Calculation of diurnal variation of surface temperature using a simplified energy balance model. *Időjárás 95*, 170-179.

Hunkár, M., 1985: The sun radiation and plant stand, with special regards to penetration of PhAR into canopy and efficiency (in Hungarian). *PhD Thesis*, ELTE, Budapest.

Hurtado, E., Artigo, M.M., and *Caselles, V.*, 1994: Estimating maize (Zea mays) evapotranspiration from NOAA-AVHRR thermal data in the Albacete area, Spain. *Int. J. Remote Sensing 15*, 2023-2031.

Jackson, R.D., Reginato, R.J., and *Idso, S.B.*, 1977: Wheat canopy temperature: a practical tool for evaluating water requirements. *Water Resource Res. 13*, 651-672.

Jackson R.D., Idso, S.D., Reginato, R.J., and *Pinter, P.J. Jr.*, 1981: Canopy temperature as a crop water stress indicator. *Water Res. Res.* 17, 1133-1138.

Jackson, R.D., Kustas, W.P., and *Choudhury, B.J.*, 1988: A re-examination of the crop water stress index. *Irrig. Sci. 9*, 309-3.

Kerényi, J., 1993: Surface temperature derived from METEOSAT infrared data using atmospheric correction. *Időjárás 97*, 251-257.

Kerényi, J., 1994: Investigation of the surface temperature using METEOSAT satellite images. *Adv Space Res. 14*(3), 31-35.

Kerényi, J. and *Putsay, M.*, 2000: Investigation of land surface temperature algorithms using NOAA/AVHRR images. *Adv. Space Res. 22*(5), 637-640.

Kustas, W.P., Moran, M.S., Jackson, R.D., Gay, L.W., Dueli, L.F.W., Kunkel, K.E., and *Matthias, A.D.*, 1982: Instantaneous and daily values of the surface energy balance over agricultural fields using remote sensing and a reference field in an arid environment. *Remote Sens. Environ 32*, 125-134.

Lagouarde, J-P., 1991: Use of NOAA AVHRR data combined with an agrometeorological model for evaporation mapping. *Int. J. Remote Sensing 12*, 1853-1874.

Sandholt, I. and *Andersen, H.S.*, 1993: Derivation of actual evapotranspiration in Senegalese Sahel, using NOAA-AVHRR data during the 1987 growing season. *Remote Sens. Environ 46*, 164-182.

Seguin, B. and *Itier, B.*, 1983: Using midday surface temperature to estimate daily evaporation from satellite thermal IR data. *Int. J. Remote Sensing 4*, 371-383.

Sellers, P.J., Mintz, Y., Sud, Y.C., and *Dalcher, A.*, 1986: A simple model for use within general circulation models. *J. Atm. Sciences 43*, 505-532.

IDŐJÁRÁS

Quarterly Journal of the Hungarian Meteorological Service
Vol. 107, No. 3–4, July–December 2003, pp. 237–248

The impacts of the increasing drought frequency on the agricultural water management

Péter Köles[1], Emánuel Antal[2] and Judit Dimény[1]

[1]*Department of Water Management and Land Reclamation,*
Faculty of Agriculture and Environment Sciences, Szent István University,
Páter Károly u. 1, H-2103 Gödöllő, Hungary

[2]*Hungarian Meteorological Service, P.O. Box 39, H-1675 Budapest, Hungary*
E-mail: antal.e@met.hu

(Manuscript received October 28, 2003; in final form November 17, 2003)

Abstract—The high risk of drought in Hungary can be illustrated by the high crop failure in the year 2000 when compared to the average crop of the past years. The crop failure of grain and industrial plant species varied between 15–40%. About 1.3 million hectares of arable land were affected by drought.

Increase in the frequency, length, and intensity of drought is more likely during the warming periods. The series of droughts in the past decades may be explained as a sign of global warming. The studies have shown that a small degree (+0.5 and +1°C) of global warming can cause significant climate change in Hungary. There will be a marked increase in summer temperature and a decrease in annual precipitation of about 10% (60 mm). Increase in sunshine hours can also be expected, and the length of periods with low relative humidity will probably grow, too. The drier air is accompanied with increasing potential evapotranspiration, that results in increasing transpiration intensity. Therefore, it is to be expected that the water demand of crops will increase.

As a result of global warming, the more frequent occurrence of drought will be an important challenge of the Hungarian society and economy during the following decades. That is why it is urgent to make efforts towards the development of a national drought strategy, that will coordinate and maximize the effectiveness of the work of all Ministries involved.

In this paper the authors present a survey of the drought situation in Hungary, and outline the most urgent tasks for reducing its harmful effects for the country.

Key-words: drought, drought frequency, drought strategy, climate change, irrigation water requirement.

1. Introduction

In Hungary, mainly in the Great Plain, the climate and weather have significant roles in the agricultural sphere, first of all through the variability of precipitation. Although the average climate conditions are favorable for the agricultural production in the Great Plain, there are some years or periods or months of years when the crop is decimated by drought, flood, or surplus water (*Szlávik* and *Fejér*, 1999). Nowadays, when there are permanent extreme climate occurrences or they last for years, the whole national economy can be shaken by the caused harms, while in the previous past they were accompanied by starvation, epidemics, and other social and economic tragedies (*Vágás*, 1982). However, nowadays it is concluded that unfavorable alterations of weather and climatic conditions and the potential coincidences of events observed in the past could lead to extraordinary consequences in the Tisza watershed (and in this manner on the Great Plain), as it was unfortunately evidence by large floods in 1998–2000 (*Szlávik*, 2002).

Because of the great climate sensibility of our society and economy, when there are some extreme or permanent weather oscillations, people instantly suspect a climate change, and they try to proclaim it as a result of human activities. Through the past centuries, deforestation, flood protection, drainage and riverbed controls were thought to be driven to serial, long lasting, and intensive extremes of weather. In the last century, building of dams and water basins, irrigation and other water management activities, nuclear explosions, air pollution, and changes in agricultural cultivation have become the supposed or real causes of the proceedings of extreme weather conditions or supposed climate change.

In Hungary, the question of climate change and the components of water balance was brought up in connection with flood release in the Great Plain after a permanent droughty period in the 19th century. During the last two or three decades, when some extreme weather events occurred, the scientists and the society concentrated on a possible global warming. While earlier the question was that whether the drainage of marshlands, moors, and flood inundated area of the Great Plain and the important riverbed controls had changed the climate of the country and caused a start of turning into desert. From the last two decades, people and scientists wonder whether the beginning of a warming up period is statistically significant? If yes, what kind of climate and water balance changes can be expected in this area? Will there be a change in the climate? Will there be a warmer and drier climate type? What kind of climate scenarios will be expectable in the following decades? What about temperature increase and the amount of precipitation? How will our economy and society change as a result of the climate change? What changes can be

expected in the nature? Will there be an increasing drought frequency and intensity on the Great Plain?

In the last 150 years, some experts took up the question of climate change in the Great Plain, that was supposed to be the consequence of flood protection in particular after a series of droughty periods in the first half of the 1860s. In the 1930s, our acknowledged experts on climatology (*Róna*, 1936; *Réthly*, 1936) had to prove repeatedly, that the series of droughts in the first part of the '30s were not the consequence of flood protection, but concomitant characteristics of our climate. They could analyze a century-old time series of climate monitoring, because the systematic instrumental monitoring had been started in the first part of the 19th century. They both found out, that the control of the River Tisza and its creeks did not cause any turning into desert in the macroclimate of the Great Plain, however, the local microclimates became drier.

The weather of the last years can be characterized by the water balance of our climate with its long-lasting floods (*Szlávik* and *Fejér*, 1999), surplus waters besides unusual droughts and long-lasting heat waves. On the basis of climate records we can state that these climate extremities can be caused clearly neither by the flood protection or control of rivers in the 19th century, nor human activities in the 20th century (*Szlávik*, 2002).

It is founded on facts, that the frequent droughts and extreme weather events (floods, surplus waters, long-lasting periods of heat) from the last one or two decades are characteristics of our climate, but the increasing frequency and intensity of them can be the consequence of the global warming in the Carpathian Basin. However, we should consider the possibility of a warming up rising phase of a period of natural climate fluctuation, too.

2. Expectable climate changes increase the drought suspectibility in Hungary

Apart from the consequences of global warming, experts state that among the circumstances that cause drought in Hungary, we should emphasize the weather, hydrological, soil, and agronomical conditions equally. These factors can be particularly affected by the geographical position of a farm or the relief conditions. As mentioned above, the drought suspectibility is a typical characteristic of the climate in Hungary. The drought frequency shows significant regional variability, as it can be seen in *Fig. 1*. Drought affects the western part of the country which is richer in precipitation, as well as the much drier counties of the Great Plain. In summer, which is most important for cultivation, there is high drought frequency in the region of the Great Plain, and it causes significant damage to the fields with poor water management.

The high risk of drought in Hungary can be illustrated by the high crop failure in the year of 2000 compared to the average crop of the past years. The crop failure of grain and industrial plant species varied between 15–40%. About 1.3 million hectares of arable land were affected by drought that caused more or less crop failure.

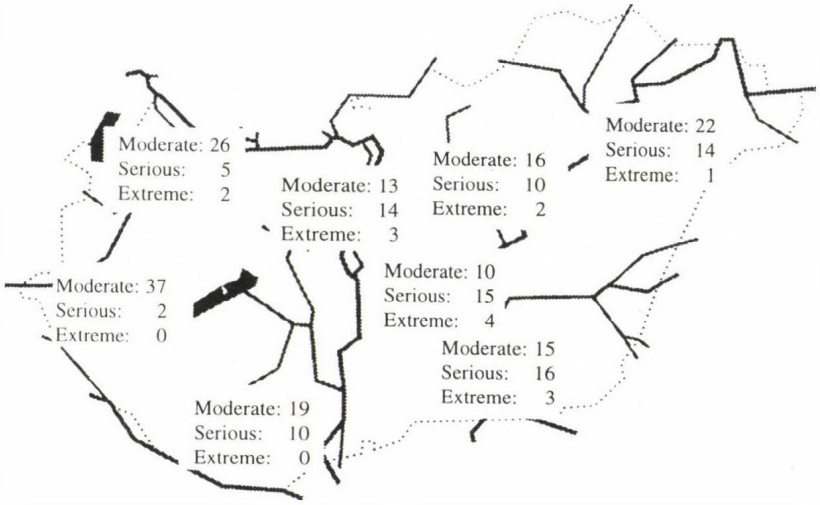

Fig. 1. Moderate, serious, and extreme drought occurrences in Hungary between 1951 and 1992 (after *Dunay* and *Tölgyesi*, 1993).

Table 1. Expectable changes in temperature and precipitation in Hungary till 2050 (after *Mika*)

Global change, °C	Change in temperature in Hungary, °C		Change of annual precipitation, mm/°C
	summer	winter	
0,5	1.5	0	−60 (±20)
1.0	0.8	1.0–2.5	−60 (±40)
2.0	0.8	1.5	about 0
4.0	0.6–0.9	1.5	+10 (±100)

According to the researches on climate in Hungary (*Antal*, 1988, 1991, 1992, 2002; *Mika*, 1988, 1991, 1993), an increase in frequency, length, and intensity of drought can be supposed during the warming period to come. On one hand, the series of droughts in the past few years and decades may probably be explained as a sign of global warming. The studies have shown

that a small degree (+0.5 and +1°C) of global warming can cause significant climate change in Hungary (see *Table 1*).

A marked increase in summer temperature and a significant decrease in annual precipitation of about 10% (60 mm) can be expected. Increase in sunshine hours can also be expected, while the length of periods with low relative humidity will probably grow. The drier air is accompanied with increasing potential evaporation, that results an increase in the intensity of transpiration. Therefore, it is to be expected, that the water demand of crops will increase, while the amount of precipitation and probably the number of rainy days will decrease during the warmer and drier growing season (*Antal*, 1988, 1998).

Table 1 shows that in summer, in case of little global warming (0.5°C), about one and a half times higher (that is 0.75°C) rising in temperature is expectable, while the annual precipitation can be reduced with 60 mm by each degree rise. In case of 1 or more degrees rise in temperature in the northern hemisphere, more moderate warming up is expectable in Hungary in summer, while in winter higher warming up can be expected (1.0–1.5°C). It is remarkable, that in case of higher global warming, the decrease of precipitation is not so significant, but its deviation in time increases (*Mika*, 1991, last line of *Table 1*).

3. Indirect and direct impacts of climate change on the agricultural water management

The indirect and direct impacts of climate change in Hungary is considerable by the following aspects (*Antal* and *Szesztay*, 1994):

- From the point of view of the agricultural sphere, the supposed climate change (first of all an increase in the frequency of drought) is one of those uncertain factors that have direct practical importance to the long-distance planning of agricultural water management.
- In the land ecological parts of a given area, the *water supply* for plant production that gathers precipitation, appears for farmers as the provider of complicated interactions between the climate, soil, and plants that in the end becomes the question of cultivation, pasture management, forestry and regional planning through water balance processes of the root zone.
- Finally, the examination of the possibility of feedback is essential. That is to find out the relationship between the role of climate regulation of atmospheric water cycle and the expectable climate change (climatic scenario).

When we try to analyze the effects of the increasing drought frequency on the agricultural water management, and to give a rough estimate of them, we have to emphasize that the changes in surface and subsurface water resources, caused by climate change or agricultural (or other anthropogen) activity in catchment areas, can be found out exactly only by the cognition and numerically definition of interactions between the water balance units and land ecological units divided into three parts of agricultural region.

The climate change can have a direct effect on the water supply of cultivated fields through the changes of hydrological cycle. In a qualified sense, besides the potential water supply, the whole water demand of the agricultural sphere may alter as a result of warming up, and because of it, an unfavorable change in the elements (first of all precipitation and evaporation) of climate may appear that will have an influence on the agricultural water management technologies (*Orlóci* and *Szesztay*, 2002).

In the future, the conditions of the agricultural water management can be modified by the change in climate, first of all the change in the elements of agricultural water balance. According to the latest examinations, the trends of the possible changes in the climate and water balance of our area are as follows:

- Global warming have a modifying influence on *water cycle and water supply* (surface and subsurface) that is commensurable with the effects of human activities on them, and sometimes it is more significant. As our climate is turning into drier, the damages caused by drought could be increased, because 1% decrease of precipitation (annual 6–7 mm) causes 1 m decrease of karst water level. A long-lasting period of decrease of ground water level could increase the sensitivity of plants in such areas, where it supplies more water to the stocks of plants nowadays.
- While *the soil moisture content* of the root zone follows the weather conditions (mainly precipitation) fast, the influence of climate change appears later as a change in the average humidity of soil supply of many years (turning into one direction).
- The change of *ground water content* during the time is influenced by precipitation and potential evaporation, and as these meteorological elements have a marked annual course, the ground water level also follows an annual rhythm. However, the long lasting warming up periods and the decrease of precipitation cause slow, but considerable decrease in the average of subsurface water resources of several years. The change can be dramatic in the areas having high ground water level, while in fields with lower ground water level it can be a bit more favorable.

4. Climatic water shortage and irrigation water requirement

As drought appears more often and more intensively, first of all, it has a marked influence on the development of need for irrigation water of plant stands in those fields, where there is a possibility for irrigation. However, the estimation of the expectable changes in the plant water requirements (numerical data) is one of the most complicated water management modeling tasks. The irrigation water requirement of plants changes in time and space, because it is controlled by the changing water demand of plants through the changeability of weather, water storage capacity of the root zone, depth of water table, physical properties of soil, and biological characteristics of plants (species, type, phase of development, population density, nutrient supply, etc.).

The available water supply for plants in cultivable lands can be well characterized by *climatic water demand* and its change in space and time. According to surveys in Hungary, as a consequence of worse precipitation supply, the climatic water demand is growing in the whole Carpathian Basin in the future. So the agricultural water management will ask for more and more water for irrigating purposes, while the neighbouring countries use more and more water from streams flowing through Hungary. As a consequence, our surface water supply decreases because of the decrease in precipitation and the decrease of water output of streams (*Antal*, 1988; *Nováky*, 1988; *Szesztay*, 1995). It is to be remarked that 10% decrease of precipitation causes more than 10% decrease of surface runoff. It is true for the climatic conditions in Hungary, that the modification effects of soil surface and cropcover (that causes a progressive change in crop rotation structure because of the increasing drought frequency) can cause a change of surface runoff in space and time, which can be equal with the change of precipitation, or it can be higher than that (*Nováky*, 1988; *Várallyay*, 1990).

According to the above, it is clear, that the supposed (predicted) climate change in Hungary has an unfavorable influence on almost all contaminants of plant water balance - supposing warming up in the Carpathian Basin and decreasing of precipitation as a consequence of it. Besides them longer, more intensive and more frequent droughts, as well as wider range of extremities in climate elements are expectable - so the availability of water supply will be less for the agricultural water management, while the quality of water will grow worse. This means that the costs of irrigation water and other water utilization will grow by the cost of purification of water. According to the water directives of EU, during the compulsory adaptation and implementation, additional cost growth is expectable.

5. The expectable impacts of the increasing drought frequency on biomass production

The effect of climate change on cultivation is significant from the point of view of the society, economy, and ecology, because the crop, the effectiveness and success of farming, and the annual fluctuation of it are caused by weather, and they have an effect on food industry, export market, the price structure of the domestic food market, and the employment. You should know that the agricultural sphere is almost the only stage utilizing the primer natural resources and converting its power (*Antal*, 1984; *Láng et al.*, 1983; *Szász*, 1985).

From the point of view of potential production, the temperature increasing is the smaller risk, although we can not neglect it. According to surveys in Hungary, in case of 2°C of temperature rise, the number of those days when the temperature reaches 30°C (that is they can be characterized by atmospheric drought) can be doubled (at present it is 15–30 days yearly). It will have a harmful influence on dry matter production (high breathing rate, turgor loss in the midday hours, intensive transpiration, disadvantageous water transport in plants etc.), mainly in the periods of droughts.

The expectable decrease of precipitation amount will cause more troubles for the agricultural water management with its worse water balance system. Supposing an annual 1 mm decrease of precipitation for 2020, the annual precipitation amount can fall under 470 mm in the middle of the Great Plain. Thus, producing of intensive plant species with more drought resistance is recommended, or we should calculate that the crop-time chart will be saturated, that is the crop will not grow in case of more intensive supplying of nutritive. It seems that in the next few decades of the 21st century, the agricultural water management (decrease of precipitation, irrigation) will be the most critical scientific problem of primer biomass production (*Varga-Haszonits* and *Harnos*, 1988).

On the basis of the above, it is evident that working out a well-adaptable ecological strategy and practical application of new technologies will be essential for our agriculture (*Szász*, 1993), because in case of high frequency of drought, the degree of supplying of precipitation will become one of the most important factors of ecological crisis. The indications of it have been shown since the beginning of the '80s and every Hungarian climate scenario has shown us the possible extrapolation of droughty tendency of the past one and half decades. They equally prognosticate rising in temperature and decreasing in precipitation. In *Fig. 2*, three categories of Palmer Drought Severity Index (PDSI; *Palmer*, 1965) are shown by way of illustration of increasing drought frequency since the beginning of the '80s (*Bussay et al.*,

1999). To the classification of droughts according to PDSI, they use three categories - *moderate* (PDSI<-2.0 and the drought extends to 50% of Hungary), *serious* (PDSI<-3.0 and the drought extends to 33% of the country) and *extreme* (PDSI<-4.0 and the drought extends to 20% of our country). These categories have been determined by *Bussay et al.* (1999). It can be seen that in the past two decades moderate and serious droughts have been ensued almost continuously in every year. On country-wide scale, drought occurred more frequently and more clustered at the end of the investigated period (1881-1995). The climatic stations exhibited a drying tendency verified by regression analysis. At most of the examined meteorological stations, the majority of the months show decreasing PDSI values (*Fig. 3*).

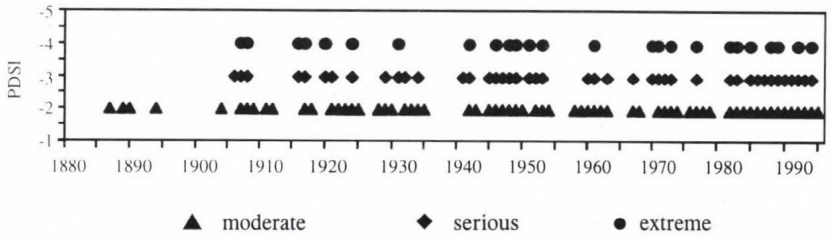

Fig. 2. Classifications of droughts according to the Palmer Drought Severity Index (PDSI) (after *Bussay et al.*, 1999)

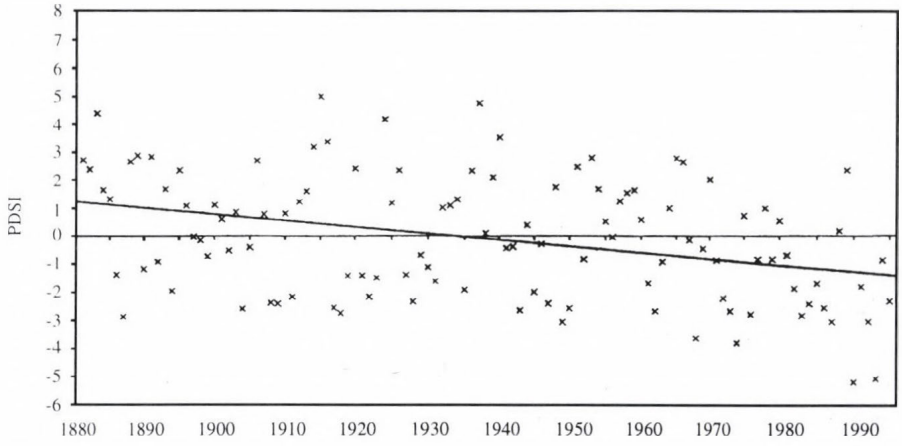

Fig. 3. The values and trend of PDSI in July (after *Bussay et al.*, 1999)

6. Increasing frequency of drought – national drought strategy

On the basis of experience of drought frequency in the last 1–2 decades, we can state as a summary that if we count on the decrease only of precipitation amount in the following decades, and a significant temperature rise will not occur in 20–30 years, we can not avoid working out a new ecological strategy to keep and even increase biomass production because of the expectable changes in the use of land.

The basis of the new ecological strategy is an up-to-date strategy of defending against drought (mainly passively), that is due to summarizing as a scientifically established national drought strategy (as a part strategy of the agricultural water management) and dealing with it as a government program (*Vermes*, 1998; *Vermes et al.*, 2000). On the other hand, it is necessary to increase the active agricultural water management interventions (irrigation, keeping precipitation in water basin, reducing evaporation and transpiration, reducing the surface runoff, managing the humidity of the soil more effectively, etc.).

Among the active processes of defence, we must review the technological and economical conditions of irrigation, and the practical and technical state of it. The present situation can not be preserved for a long time (preference, effectiveness, quality of crop, supply of liquid nutrients, soil-physical and chemical problems, etc.).

As in Hungary the agricultural sector remains a significant part of the economy for a long time (because of natural conditions of Hungary), it is essential to draw the political and economical decision makers' attention to all risk factors that can have influences on the agriculture of Hungary as the consequences of global environmental changes, which can endanger the use of land and primer plant production.

Among the natural factors we must emphasize the consequences of global warming in Hungary, but while working out the agricultural strategies (including national drought strategy), nowadays, and even in the future in connection with joining the EU, it is compulsory to considerate other anthropogenic effects, e.g., agricultural consequences of acid rains, acidification of soil as part of soil degradation, low ground water table and other environmental effects caused by global changes. The aim of a national drought strategy is to serve the expert and social cooperation, summarizing all the necessary concepts, methods, steps, and financial sources that are important in the fight against drought damages in a longer term (*Antal et al.*, 2002; *Vermes*, 1998). There will be a governmental body, which could maintain all those coordination tasks which are indispensably necessary in due time for the complex measures against drought damages and for an effective drought mitigation.

References

Antal, E., 1984:Atmospheric potential and agricultural relations (in Hungarian). *Országos Meteorológiai Szolgálat Hiv. Kiadv.* LVII. kötet, Budapest, 121-133.

Antal, E., 1988: Comparative analysis of the irrigation water requirement and aridity conditions. In *Identifying and Coping with Extreme Meteorological Events* (eds.: *E. Antal* and *M.H. Glantz*). Országos Meteorológiai Szolgálat, Budapest, 205-254.

Antal, E., 1991: Impacts of the climate change on the Hungarian droughts. (in Hungarian). *Acta Geographica Debrecina 1989-1990*, Debrecen. Tomus XXVIII-XXIX, 17-28.

Antal, E., 1992: Impacts of climate change on drought in Hungary (in Hungarian). *Beszámolók az 1988-ban végzett tud. kutatásokról.* Orsz. Meteorológiai Szolgálat, Budapest, 156-164.

Antal, E., 1998: Relation of the weather and climate with plant water circulation (in Hungarian). In *Meteorológiai Tudományos Napok '98.* Orsz. Meteorológiai Szolgálat, Budapest, 15-28.

Antal, E., 2002: Increasing drought susceptibility, plant water supply and consideration of expectable impacts (in Hungarian). In *Levegő, növény és talaj rendszer* (ed.: *A. Jávor*). Debrecen, 39-45.

Antal, E. and *Szesztay, K.*, 1994: Interactions between the presumed climate change and the environment (in Hungarian). In *Agro-21 Füzetek. Az agrárgazdaság jövőképe,* 1. Magyar Tudományos Akadémia, Budapest, 8-40.

Antal, E., Dimény, J., and *Köles, P.*, 2002: The influence of the increasing drought frequency on the agricultural water management - drought strategy (in Hungarian). In *JUTEKO-2002, Tessedik Sámuel Víz- és Környezetgazdálkodási Napok* (ed.: *I. Komlovszky*). Tessedik Sámuel Főiskola, Szarvas.

Bussay, A., Szinell, Cs., and *Szentimrey, T.*, 1999: Investigation and measurements of droughts in Hungary (in Hungarian). In *Éghajlati és Agrometeorológiai Tanulmányok*, 7. Orsz. Meteorológiai Szolgálat, Budapest, 9-66.

Dunay, S. and *Tölgyesi, L.*, 1993: Drought–with agrometeorological aspect (in Hungarian). In *Az 1992. évi aszály értékelése* (eds.: *I. Pálfai* and *L. Vermes*). FM, MAE, MHT, Budapest, 17-24.

Láng, I., Csete, L., and *Harnos, Zs.*, 1983: *Agroecological Potential in Hungary on the Thousandturning* (in Hungarian). Mezőgazdasági Kiadó, Budapest.

Mika, J., 1988: Regional characterics of the global warming up in the Carpathian Basin (in Hungarian). *Időjárás 92*, 178-189.

Mika, J., 1991: Regional features of a stronger global warming over Hungary (in Hungarian). *Időjárás 95*, 265-278.

Mika, J., 1993: Effects of the large-scale circulation on local climate anomalies in relation to GCM outputs. *Időjárás 97*, 21-34.

Nováky, B., 1988: : Methodological problems in the cartographic representation of engineering hydrologic information (in Hungarian). *Hidrológiai Közlöny 68*, 193-206.

Orlóci, I. and *Szesztay, K.*, 2002: Hydroecological risks of crop production in Hungary. *Időjárás 106*, 185-196.

Palmer, W.C., 1965: *Meteorological Drought.* US Weather Bureau, Res. Paper, No. 45. Washington, D.C., 58.

Réthly, A.., 1936:Did the free from floods change our climate? (in Hungarian). *Vízügyi Közlemények*, XVIII., 134-165.

Róna, Zs., 1936: A few remarks to Hungarian climate change (in Hungarian). *Időjárás XL* (3-4), 45-52.

Szász, G., 1985: The climatic potential and its use in the agricultural production. In *The use of climatic potential and agrometeorological information in the national economy*. Országos Meteorológiai Szolgálat, Budapest.

Szász, G., 1993: The role of climate change in the crop production (in Hungarian). In *Meteorológiai Tudományos Napok '91*. Országos Meteorológiai Szolgálat, Budapest, 9-23.

Szesztay, K., 1995: Climate change and irrigation water demands in Hungary (in Hungarian). VITUKI, OTKA-716, Budapest .

Szlávik, L., 1999: Conception and realization of the national information system for the water damage avert and protection works (in Hungarian). *Vízügyi Közlemények*, 99 (1).

Szlávik, L., 2002: Flood protection (in Hungarian). In *A hazi vízgazdálkodás stratégiai kérdései* (ed.: *L. Somlyódi*). Magyar Tudományos Akadémia, Budapest, 205-243.

Szlávik, L. and *Fejér, L.*, 1999: Surplus waters and floods in 1999 spring (in Hungarian). *Természettud. Közlöny 130*, (8).

Vágás, I., 1982: *Floods of Tisza* (in Hungarian). VIZDOK, Budapest.

Varga-Haszonits, Z. and *Harnos, Zs.*, 1988: Effect of climate variability and drought on wheat and maize production. In *Identifying and Coping with Extreme Meteorological Events* (eds.: *E. Antal* and *M.H. Glantz*). Országos Meteorológiai Szolgálat, Budapest, 138-166.

Várallyay, G., 1990: Influence of climatic change on soil moisture regime, texture, structure and erosion. *Soils on a warmer earth* (eds.: H.W. Schanserpeel, M. Schomaker and A. Ayoub), Developments in Soil Science, 20, Elsevier, Amsterdam, 39-49.

Vermes, L. (ed.), 1998: *How to work out a Drought Mitigation Strategy an ICID Guide*. DVWK Guidelines, 309. ICD-KWVGK mbH, Bonn.

Vermes, L., Fésűs, I., Nemes, Cs., Pálfai, I., and Szalai, S., 2000: Status and progress of the national drought mirigation strategy in Hungary. *Proc. of the Central and Eastern European Workshop on Drought Mitigation* (eds.: *L. Vermes* and *Á. Szemessy*), ICID.MTESz, Budapest, 55-63.

IDŐJÁRÁS

Quarterly Journal of the Hungarian Meteorological Service
Vol. 107, No. 3–4, July–December 2003, pp. 249–255

Estimate of the dry deposition of atmospheric nitrogen and sulfur species to spruce forest

László Horváth[1*], **Joseph Pinto**[2] and **Tamás Weidinger**[3]

[1]*Hungarian Meteorological Service,*
P.O. Box 39, H-1675 Budapest, Hungary; E-mail: horvath.l@met.hu

[2]*U.S. Environmental Protection Agency,*
Research Triangle Park, NC 27711, U.S.A.

[3]*Department of Meteorology, Eötvös Loránd University,*
P.O. Box 32, H-1518 Budapest, Hungary

(Manuscript received January 23, 2003; in final form March 11, 2003)

Abstract—A field campaign to determine the dry fluxes of nitrogen and sulfur compounds between the atmosphere and a Norway spruce forest was conducted during the spring of 1998. The field site was located in the Mátra mountains in north-eastern Hungary. Fluxes of particulate phase ammonium, nitrate, and sulfate were determined in addition to fluxes of gas phase ammonia, nitric acid, and sulfur dioxide. Dry deposition velocities determined by the gradient method are 1.9 and 1.3 cm s^{-1} for nitric acid, 3.7 and 1.1 cm s^{-1} for ammonia and 0.6 and 0.3 cm s^{-1} for sulfur dioxide in unstable and stable cases, respectively. For fine ammonium and sulfate particles there were no detectable concentration differences between the different measuring heights. For nitrate particles, existing mostly in the coarse fraction the gradient method is not applicable to determine the dry flux.

Key-words: dry deposition velocity, gradient method, sulfur dioxide/sulfate, nitric acid/nitrate, ammonia/ammonium.

1. Introduction

Knowledge of the dry deposition flux of different nitrogen and sulfur containing species is necessary for estimating the nitrogen and sulfur balance in forest ecosystems. However, there are substantial differences among the few

*Corresponding author

existing data sets caused in part by differences in climatic conditions during the collection of the data.

Field studies carried out mostly during the last decade over forests have derived dry deposition velocities for gaseous ammonia ranging typically between 0.8 and 4.5 cm sec^{-1} (*Andersen et al.*, 1993; *Erisman et al.*, 1995; *Duyzer et al.*, 1994; *Wyers et al.*, 1995). In some cases emission was reported (*Andersen et al.*, 1999). Dry deposition velocities for nitric acid determined in field studies are much higher (*Janson* and *Granat*, 1997) than had been estimated on the basis of theoretical and field studies (*Baldocchi et al.*, 1992) due to the low canopy resistance of these species.

In the case of sulfur dioxide the dry deposition velocity measured over forests ranges between 0.05–3 cm s^{-1} (*Mennen*, 1995). For aerosol particles, limited field studies (*Erisman*, 1995; *Wyers*, 1995) have obtained systematically higher deposition velocities than there were determined by theoretical calculations and wind tunnel experiments (*Ruijgork et al.*, 1993 and *Borrell et al.*, 1997).

The aim of this paper is to provide data set for dry deposition velocities of these compounds, to increase the available data based on experimental investigations.

2. Measurements and calculations

Gradient flux measurements were carried out in the Mátra mountains, Hungary (Nyírjes station) in a Norway spruce forest, during a field campaign in May 1998. Characteristics of the measuring site are:

latitude = 47° 54' N,
longitude = 19° 57' E,
altitude = 560 m a.s.l.,
type of vegetation: Norway spruce (8 ha),
surroundings: Pine, Beech,
average height: 16 m,
age 33–35 years,
leaf area index (LAI): 3.3.

Concentrations of gaseous and aerosol species were measured with parallel three stage filter packs, located at heights of 13 and 23 meters on an instrumented tower for 8 hour sampling periods, during day and night (corresponding to unstable and stable conditions). Since the average calculated displacement height was 12 m, the lower height (13 m) is also above the

canopy layer, therefore the turbulent motions are not disturbed by the canopy between the two measuring heights. A total of 18 measurements were carried out partly during daytime, partly in the night. A Teflon filter collected particles on the first stage of the filter packs, and on the second and third stages Whatman filters with basic and acid coatings collected acidic (nitric acid, sulfur dioxide) and alkaline (ammonia) gases, respectively. Concentrations of ammonium ions were determined by spectrophotometry using the indophenol-blue method, while nitrate and sulfate ions were determined by ion chromatography. The bulk precision of sampling and analysis was determined by parallel sampling at the same (23 m) level. The results of 10 measurements show that the mean relative error of sampling and measurements for all components is around $\pm$ 5 %.

The eddy-diffusivity of heat was calculated from the measured wind and temperature profiles on the basis of the *Monin-Obukhov* similarity theory (*Horváth et al.*, 1998; *Weidinger et al.*, 2000). The Monin-Obukhov length was calculated using the Richardson number derived from profile measurements and the universal functions for momentum and heat transfer (for details see *Horváth et al.*, 1998). It was assumed that the average bulk eddy-diffusivity for the trace materials is same as for the eddy-diffusivity of momentum and heat transfer. The values of the heat (K_T) were calculated on the basis of profile-flux relationship using the measured wind and temperature profiles. During the evaluation of the profile measurements the similarity theory provides the more appropriate estimations for the calculation of turbulent momentum and heat flux and hence for the calculation of the eddy-diffusivity (*Weidinger et al.*, 2000).

The eddy-diffusivity depends on the surface roughness as well as on meteorological conditions in the surface layer, especially the on stratification. During stable conditions (mostly during nighttime) the rate of exchange is generally lower, when the eddy-diffusivity is generally lower (0.3 $m^2 s^{-1}$) by a factor of three as compared to unstable conditions (0.9 $m^2 s^{-1}$ as an average, daytime). The eddy-diffusivity of the heat was considered as the measure of the turbulent exchange for all species. Stable and unstable cases were separated by the sign of the Richardson number.

3. Results and discussion

Dry deposition velocities of gases were calculated according to the gradient method. Concentration gradients of gases were multiplied by eddy-diffusivities. Eddy-diffusivities (K_T) and concentration gradients were determined separately for unstable (mainly daytime) and stable (nighttime)

conditions. Concentration differences between the two sampling heights ranged between 4 and 82 per cent as shown in *Table 1*. The precision of concentration measurements was determined to be about ± 5 per cent in field and laboratory tests. The mean eddy-diffusivities for unstable and stable stratifications were 0.89 and 0.17 $m^2 s^{-1}$, respectively.

Table 1. Deposition velocities, mean concentrations and mean concentration differences of gases and aerosols

Compound	Period	Mean deposition velocity (cm s^{-1})	Mean concentration (nmol m^{-3})		Mean concentration difference (%)
			23 m	13 m	
HNO_3	day	1.9±0.4	11	8.1	27
	night	1.3±0.1	2.7	0.5	82
NH_3	day	3.7±0.4	28	18	35
	night	1.1±0.1	16	8.2	47
SO_2	day	0.6±0.4	134	124	8
	night	0.3±0.1	59	49	18
NO_3^-	day		6.9	4.8	30
	night		12	7.6	37
NH_4^+	day	<0.4±0.4	68	72	6
	night		82	78	4
SO_4^{2-}	day	<0.4±0.4	54	51	6
	night		51	49	5

According to the *Table 1*, in the case of nitric acid the deposition velocities for both unstable and stable conditions are similar, indicating substantial cuticular uptake. These figures are in the range of the deposition velocities collected by *Baldocchi* (1992), 0.5–5.0 cm s^{-1} for deciduous forests on the basis of model calculations compared to experimental results. The deposition velocity provided by *Janson* and *Granat* (1997), 7 cm s^{-1} for coniferous forest, is substantially higher, suggesting that canopy resistance is higher than it was expected by these authors.

For ammonia, where the stomatal uptake is the dominant deposition process, the deposition velocity figure (*Table 1*) is about three times higher when stomata are open (daytime) than during nighttime. These figures are in a good agreement with other field measurements above forests: *Andersen et al.*, 1993: 2.6 cm s^{-1} or 4.5 cm s^{-1} in the intensive vegetation period; *Duyzer et al.*,

1994: 2–3 cm s^{-1}; *Erisman et al.*, 1995: 2.5 cm s^{-1}; *Wyers et al.*, 1995: 1.5–4.3 cm s^{-1} at night, 0.8–4.0 cm s^{-1} in daytime, however the last authors did not found any difference between the deposition velocities during day and night hours. *Andersen et al.* (1999) pointed out the importance of ammonia emission from the forest, demonstrating that deposition dominates in the net flux when the ammonia concentration exceeds the compensation point.

The deposition velocity of sulfur dioxide is lower than that of nitric acid and ammonia during both stable and unstable conditions (*Table 1*). The sulfur dioxide deposition rate determined for forests ranges two orders of magnitude (*Mennen et al.*, 1995: 0.05–3 cm s^{-1}; *Erisman et al.*, 1995: 1.5 cm s^{-1}; *Horváth et al.*, 1997: 0.6–1.6 and 0.2–0.34 cm s^{-1}, during unstable and stable conditions, respectively).

As to the nitrate particles, annular denuder system (ADS) (cyclone, denuder tubes, filter pack) measurements made in parallel with the filter pack measurements show that nitrate particles are found mainly in the coarse fraction (*Table 2*). Therefore, the gradient method for determining the dry deposition of nitrate flux needs correction for the effects of gravitational settling.

Table 2. Share of nitrogen compounds in different phases in nmol m^{-3}

Phase	Nitrate/nitric acid	Ammonium/ammonia
Coarse particles d > 2.5 m	18	< 2
Fine particles d < 2.5 m	< 2	188
Gas	12	26

In contrast, ammonium particles were found solely in the fine fraction (d < 2.5 m). The majority of the total nitrogen, consisting of ammonia gas, nitric acid, and particulate nitrate and ammonium, was contained in the form of ammonium fine particles. The molar ratio of ammonium to sulfate in the samples was between 1 and 2, i.e., sulfuric acid has been neutralized by ammonia to ammonium bisulfate or ammonium sulfate. Because ammonium (bi)sulfate was present mainly in the fine fraction, the gradient method is applicable provided gravitational settling can be neglected.

However, the average concentration difference between the upper and lower levels was between 4 and 6 per cent for ammonium and sulfate during both unstable and stable conditions. Considering the precision in sampling and

measuring the concentrations with the filter pack method (about 5 per cent), and the precision (bulk relative error) of (estimated as 5–10 per cent) deposition velocities for ammonium and sulfate could not be determined. In *Table 1* estimated limits for deposition velocities of ammonium and sulfate can be found. According to the measurements concerning forests the dry deposition velocity of these compounds are: 2.4 cm s^{-1} for sulfate (*Sánchez et al.*, 1993); 1.2–1.5 cm s^{-1} for ammonium particles over 0.8 m size (*Wyers et al.*, 1995); 1–2 cm s^{-1} for fine and 5 cm s^{-1} for coarse sulfate and ammonium particles (*Erisman et al.*, 1995). Different research groups agree with the high uncertainty of these figures (*Lopez,* 1994). *Borrell et al.* (1997) suggests over 1 cm s^{-1} deposition velocity of particles according to the re-evaluation of theoretical, wind tunnel and field estimations (*Ruijgork et al.*, 1993). Our results contrast with most of these studies where relatively high ammonium deposition velocities were found suggesting that generalization of particle dry deposition field measurements is limited.

Acknowledgements–Investigations were funded by the US-Hungarian Research Joint Fund, No. 503. The authors would like to acknowledge the valuable technical assistance provided by *Lilla Váradi* throughout the measurement program.

References

Andersen, H.V., Hovmand, M.F., Hummelshøj, P., and *Jensen, N.O.,* 1993: Measurements of ammonia flux to a spruce stand in Denmark. *Atmospheric Environment 27A,* 189-202.

Andersen, H.V., Hovmand, M.F., Hummelshøj, P., and *Jensen, N.O.,* 1999: Measurements of ammonia concentrations, fluxes and dry deposition velocities to a spruce forest 1991-1995. *Atmospheric Environment 33,* 1367-1384.

Baldocchi, D.B., 1992: On estimating HNO_3 deposition to a deciduous forest with a Lagrangian random-walk model. In *Precipitation Scavenging and Atmosphere-Surface Exchange* (2) (eds.: *S.E. Schwartz* and *W.G.N. Slinn*). Hemisphere Publishing Corporation, Washington, Philadelphia, London, p. 1081.

Borrell, P., Builtjes, J.H., Grennfelt, P., and *Høv, O.* (eds.), 1997: *Transport and chemical transformation of pollutants in the troposphere. Vol. 10.* Photo-oxidants, acidification and tools: policy applications of EUROTRAC results. Springer, p. 116.

Duyzer, J.H., Verhagen, H.L.M., and *Weststrate, J.H.,* 1994: The dry deposition of ammonia onto a Douglas fir forest in the Netherlands. *Atmospheric Environment 28,* 1241-1253.

Erisman, J.W., Draajers, G., Duyzer, J., Hofschreuder, P., van Leeuwen, N., Römer, F., Ruijgork, W., and *Wyers, P.,* 1995: Particle deposition to forests. In *Acid Rain Research: Do we have Enough Answers? Studies in Environmental Science 64* (eds.: *G.J. Heij* and *J.W. Erisman*). Elsevier, Amsterdam, Lausanne, New York, Oxford, Shannon, Tokyo, p. 115.

Horváth, L., Nagy, Z., Weidinger, T., and *Führer, E.,* 1997: Measurement of dry deposition velocity of ozone, sulfur dioxide and nitrogen oxides above pine forest and low vegetation in different seasons by the gradient method. *Proc. of EUROTRAC Symposium '96.* (eds.: *P.M. Borrell, T. Cvitas, K. Kelly,* and *W. Seiler*), Computational Mechanics Publications, Southampton, p. 315.

Horváth, L., Nagy, Z., and *Weidinger, T.*, 1998: Estimation of dry deposition velocities of nitric oxide, sulfur dioxide and ozone by the gradient method above short vegetation during the TRACT campaign. *Atmospheric Environment 32,* 1317-1322.

Janson, R. and *Granat, L.*, 1997: Dry deposition of HNO_3 to the coniferous forest. *Proc. of EUROTRAC Symposium '96.* (eds.: *P.M. Borrell, T. Cvitas, K. Kelly,* and *W. Seiler*), Computational Mechanics Publications, Southampton, p. 351.

Lopez, A., 1994: Biosphere atmosphere exchanges: ozone and aerosol dry deposition velocities over a pine forest. *EUROTRAC Annual Report* Part 4, BIATEX, EUROTRAC ISS, Garmisch-Partenkirchen, p. 80.

Mennen, M.G., Hogenkamp, J.E.M., Ywart, H.J.M.A., and *Erisman, J.W.*, 1995: Monitoring dry deposition fluxes of SO_2 and NO_2: analysis of errors. In *Acid Rain Research: Do we have Enough Answers? Studies in Environmental Science 64* (ed$.: *G.J. Heij* and *J.W. Erisman*). Elsevier, Amsterdam, Lausanne, New York, Oxford, Shannon, Tokyo, p. 41.

Ruijgork, W., Nicholson, K.W., and *Davidson, C.I.*, 1993: Dry deposition of particles. *Models and methods for the quantification of atmospheric input to ecosystems. Nordiske Seminar og Arbejdsrapporter 1993*: 573. Nordic Council of Ministers, Copenhagen, pp. 145-161.

Sánchez, M.L., Domíngues, J., Sanz, F., and *Rodrígues, R.*, 1993: Preliminary study of dry deposition. *Air Pollution Research Report 47* (eds.: *J. Slanina, G. Angeletti*, and *S. Beilke*). CEC, p. 65.

Wyers, G.P., Veltkamp, A.C., Geusebroek, M., Wayers, A., and *Möls, J.J.*, 1995: Deposition of aerosol to coniferous forest. In *Acid Rain Research: Do we have Enough Answers? Studies in Environmental Science 64* (eds.: *G.J. Heij* and *J.W. Erisman*). Elsevier, Amsterdam, Lausanne, New York, Oxford, Shannon, Tokyo, p. 127.

Weidinger, T., Pinto, J., and *Horváth, L.*, 2000: Effects of uncertainties in universal functions, roughness length, and displacement height on the calculation of surface layer fluxes. *Meteorologische Zeitschrift 9*, 139-154.

IDŐJÁRÁS

Quarterly Journal of the Hungarian Meteorological Service
Vol. 107, No. 3–4, July–December 2003, pp. 257–272

On the relationship between the spatial variability of soil properties and transpiration

Ferenc Ács

Department of Meteorology, Eötvös Loránd University,
P.O. Box 32, H-1518 Budapest, Hungary; E-mail: acs@cezar.elte.hu

(Manuscript received November 25, 2002; in final form August 6, 2003)

Abstract—The sensitivity of transpiration, E, characteristics to areal variations of soil properties is analyzed. The study is performed by a *deterministic* model and a *statistical-deterministic* model. The core of the models is based on the *Penman-Monteith* concept. The transpiration characteristics are investigated in terms of analyzing the change of E versus soil moisture content, θ, relative frequency distribution of $E(\theta)$, and the algorithms for relating E obtained for a homogeneous and an inhomogeneous areal distribution of θ. The heterogeneity of soil characteristics is considered in terms of soil texture, areal variation of θ, and areal variation of soil hydraulic parameters (field capacity and wilting point soil moisture contents). In the study sand and clay are used as soil textures. The soil hydraulic parameters are evaluated for both the North-American and Hungarian soils. In the simulations strong and weak atmospheric forcing conditions are used.

According to the results, transpiration characteristics seem to be most sensitive to the areal variation of θ. The E characteristics are sensitive to the changes of soil texture and areal variation of soil hydraulic parameters at about the same rate, though the characteristics of the sensitivity are different. The analysis is valid when there are no advective effects and mesoscale circulation patterns. The results obtained can be useful for estimating area-averaged transpiration.

Key-words: transpiration, sand, clay, soil hydraulic parameters, heterogeneity, parameterization.

1. Introduction

A number of factors contribute to generate surface heterogeneity: (1) variability associated with surface type (e.g., vegetated surface, bare soil, inland water, snow, ice, urban area), (2) variability associated with terrain morphology (e.g., elevation, slope, and orientation), (3) spatial variability of

climatic forcings (e.g., precipitation pattern on macro, -meso, and microscale, wind field), and (4) spatial variability of soil characteristics (e.g., soil color, soil texture, hydrophysical and thermal properties of the soil). Among the factors mentioned, we focus on the spatial variability of soil characteristics.

For evapotranspiration, among soil characteristics soil texture and soil hydrophysical properties are the most important (*Ek* and *Cuenca*, 1994). The spatial heterogeneity of these factors is pronounced. The spatial heterogeneity of soil texture is mostly represented by soil texture maps. The maps have different scales (for instance 1:100 000 or 1:500 000 scale) (*Várallyay et al.*, 1980), and they are based on different data sources (*Mika et al.*, 2002). These data refer to soil surface layer. Subsurface soil texture data are rarely available. This missing information can be important in some cases, because soil evaporation is sensitive to the changes of soil texture not only in the soil surface layer but also in the soil subsurface layer (*Ács* and *Lőke*, 2001a). Among soil hydrophysical properties, soil moisture content, θ, and the hydrophysical parameters (field capacity and wilting point soil moisture content, θ_f and θ_w, respectively) are the most important. Soil moisture content shows spatial variability on both the microscale and macroscale (*Robock et al.*, 1998). The macroscale variability of θ is determined by the macroscale precipitation pattern. The microscale variability of θ is observed on a few m^2 (*Rajkai*, 1991; *Seyfried*, 1998) and also on a few km^2 (*Nielsen et al.*, 1973; *Bell et al.*, 1980; *Hawley et al.*, 1983) of the soil surface. This inhomogeneous θ-field can be characterized by normal distribution (*Erdős* and *Morvay*, 1961; *Bell et al.*, 1980). In the point and close vicinity of it, the variability of θ can be neglected, therefore, the θ-field is homogeneous. The hydrophysical parameters depend not only on soil texture but also on soil type. Therefore, they also depend on geomorphological characteristics of the location (*Tomasella et al.*, 2000; *Ács*, 2002b; *Ács* and *Drucza*, 2003).

The impact of areal variations of these soil characteristics on evapotranspiration or transpiration is extensively investigated (*Ek* and *Cuenca*, 1994; *Boulet et el.*, 1999; *Braud et al.*, 1995; *Kim* and *Entekhabi*, 1998; *Giorgi*, 1997a, 1997b; *Mika et al.*, 2002; *Ács*, 2002a; *Ács* and *Lőke*, 2001b; *Ács* and *Szász*, 2002). In these studies, the impact of only one soil characteristic is analyzed. There is no study dealing with a comparative analysis between transpiration and all the three above mentioned soil properties: areal variation of θ, soil texture, and areal variation of soil hydraulic parameters. This comparative aspect is the novelty of this study. Such a comparative analysis would give an insight into the relative importance of the soil heterogeneity effects mentioned above.

In the study, we applied a diagnostic approach. The transpiration models for both the homogeneous and inhomogeneous areal distribution of θ are based

on the *Penman-Monteith* concept (*Monteith*, 1981; *Ács* and *Hantel*, 1999; *Ács et al.*, 2000a; *Ács* and *Szász*, 2002, *Ács*, 2002a). In the study, we assumed that there are no advective effects accompanied by occasionally observed internal boundary layers (*Garratt*, 1992; *Hupfer* and *Raabe*, 1994), and there are also no mesoscale circulation patterns induced by surface discontinuities. Then the atmosphere can be assumed to be horizontally homogeneous with constant meteorological boundary conditions above a certain level (*Shuttleworth*, 1988).

In this study I use terms *homogeneous* and *inhomogeneous* θ rather than θ at the *point* and *local scale* as in the former studies (*Ács et al.*, 2000b; *Ács*, 2002a; *Ács* and *Szász*, 2002). I think the expressions "homogeneous θ" and/or "inhomogeneous θ" are more accurate than the expressions θ at the "*point*" and/or "*local*" scale. Namely, there is no any specific length scale to separate the so called point and local scales.

2. Models

Two model types are used for diagnozing transpiration: *deterministic* (D) and *statistical-detrministic* (SD) models. In the D-model there is no areal variation of θ, that is θ is homogeneous over the surface area under consideration. In the SD-model, in contrast to the D-model, there is areal variation of θ, that is θ is inhomogeneous over the surface area under consideration.

2.1 Deterministic model

In the model, we suppose that the vegetation canopy is completely closed, and that there is no interception. So the water vapor flux above vegetation is formed only by transpiration. The core of the model is based on the *Penman-Monteith* concept (*Monteith*, 1981) by the following equations:

$$H = A_e - \lambda E, \tag{1}$$

$$\lambda E = \frac{\Delta \cdot Ae + \rho \cdot c_p \delta e / r_a}{\Delta + \gamma (1 + r_v / r_a)}, \tag{2}$$

$$r_a = \mathrm{f}_1(u_*, L, \text{constants}), \tag{3}$$

$$u_* = \mathrm{f}_2(u_r, L, \text{constants}), \quad \text{and} \tag{4}$$

$$L = \mathrm{f}_3(u_*, H, E, \text{constants}) = \frac{-\rho \cdot T_r \cdot u_*^3}{g \cdot k \cdot \left(\frac{H}{c_p} + 0.61 \cdot T_r \cdot E \right)} \tag{5}$$

The latent heat flux is determined by Penman-Monteith's equation, and the sensible heat flux is obtained as residual from the energy balance equation. The surface and aerodynamic transfers are parameterized using a resistance representation. The aerodynamic transport is parameterized using Monin-Obukhov's similarity theory taking into account the atmospheric stability (*Ács* and *Kovács*, 2001). The surface resistance of vegetation canopy is parameterized by *Jarvis* (1976) formula. The moisture availability function, F_{ma}, is expressed as simply as possible via soil moisture content θ (e.g., Eq. (6) in *Ács et al.* (2001) or Eq. (35) in *Ács* and *Hantel* (1998)), that is I used the *Theta*-parameterization. The model is described in details in work of *Ács* and *Szász* (2002). A somewhat shorter description of the model is given in work of *Czúcz* and *Ács* (1999), *Ács* and *Hantel* (1999), and *Ács* (2002a).

2.2 Statistical-deterministic model

The model consists of a *deterministic* submodel for estimating transpiration (see section 2.1), a *statistical* submodel for generating θ as a random variable (*Wetzel* and *Chang*, 1988), and a submodel for calculating the area-averaged $E(\theta)$. As input it uses atmospheric boundary conditions, soil/vegetation parameters (roughness length, zero plane displacement height, leaf area index, moisture content at field capacity, and wilting point), and the averaged value and standard deviation of the soil moisture content. It is described in details in works of *Ács et al.* (2000b), *Ács* (2002a), and *Ács* and *Szász* (2002), therefore, it will not be presented.

3. Numerical experiments

The numerical experiments are performed by both the *deterministic* and *statistical-deterministic* models for grass covered surface. The simulations are made for different atmospheric forcing conditions, soil textures, and soil hydraulic parameters. Concerning atmopheric forcing conditions, we distinguished strong and weak atmospheric forcings (*Table 1*).

Concerning soil textures, the simulations are performed for sand and clay. It has to be mentioned, that there are differences in the textural composition between the North-American and Hungarian soils. This is presented in *Table 2*. For sand, there are practically no differences. In spite of this, the differences between the North-American and Hungarian clay are somewhat greater. The silt and the clay fraction of the North-American clay is 20 and 58 percent. For Hungarian clay, the silt and clay fractions are 30 and 50 percent (*Ács* and *Drucza,* 2003). These differences are presumably caused not only by the

differences in the geomorphological characteristics but also by the differences in the soil texture classification systems. A more detailed analysis of this subject can be found in the paper of *Ács* and *Drucza* (2003).

Table 1. Atmospheric forcing conditions

Variables	Strong atmospheric forcing	Weak atmospheric forcing
Net radiation flux (W m^{-2})	700	300
Air temperature at reference level (°C)	25.8	25.8
Vapor pressure at reference level (hPa)	18.0	32.0
Wind velocity at reference level (m s^{-1})	6.0	2.0

Table 2. Average values of textural fractions in percentage for sand, loam, and clay of North-American and Hungarian soils

Soil texture	Country	Sand fraction	Silt fraction	Clay fraction
Sand	Hungary	92	5	3
	USA	92	5	3
Loam	Hungary	52	26	22
	USA	43	39	18
Clay	Hungary	22	30	50
	USA	22	20	58

The soil hydraulic parameters (field capacity and wilting point soil moisture contents) are chosen for parameterizations of *Clapp* and *Hornberger* (1978) (hereafter CH-parameterization) on one hand, and for parameterization of *Várallyay et al.* (1979) and *Rajkai* (1984, 1988) (hereafter VR-parameterization) on the other hand. The former parameterizations refer to North-American, while the latter parameterizations to Hungarian soils. The soil hydraulic parameter values for both the North-American and Hungarian soils are presented in *Table 3*. The values are presented for sand, loam, and clay assuming both the homogeneous and inhomogeneous areal distribution of θ. Note that the parameters for loam are also given in *Table 2* and *3*, although they are not used in the analysis. The $\theta_{hom,f}$-values, irrespectively of the parameterization used, are defined for $K(\theta) = 0.1$ mm/day. Similarly, the $\theta_{hom,w}$-values are defined for $\log \Psi(\theta) = 4.2$, when $\Psi(\theta)$ is given in cm water column height.

Table 3. Boundary values of soil moisture content obtained for North-American (parameterization of *Clapp* and *Hornberger* (1978); briefly CH) and Hungarian (parameterization of *Várallyay* (1979) and *Rajkai* (1984, 1988); briefly VR) soils for sand, loam, and clay as soil textures

Boundary values of soil moisture content ($m^3\ m^{-3}$)	Sand		Loam		Clay	
	CH	VR	CH	VR	CH	VR
$\theta_{inhom,w}$	0.03	0.02	0.08	0.08	0.15	0.14
$\theta_{hom,w}$	0.07	0.02	0.15	0.15	0.29	0.25
θ_c	0.09	0.06	0.18	0.20	0.31	0.30
$\theta_{hom,f}$	0.14	0.15	0.24	0.31	0.37	0.40
$\theta_{inhom,f}$	0.27	0.27	0.36	0.39	0.47	0.50
θ_S	0.40	0.42	0.45	0.48	0.48	0.51

Abbreviations: $\theta_{inhom,w}$ = the wilting point soil moisture content for inhomogeneous θ, $\theta_{hom,w}$ = the wilting point soil moisture content for homogeneous θ, θ_c = a soil moisture content value in the transition region for which $E_{hom}(\theta_c)=E_{inhom}(\theta_c)$, $\theta_{hom,f}$ = the field capacity soil moisture content for homogeneous θ, $\theta_{inhom,f}$ = the field capacity soil moisture content for inhomogeneous θ, and θ_S = saturated soil moisture content.

During numerical experiments, $2 \times 2 \times 2$ runs are performed using both the *deterministic* and *statistical-deterministic* models. Of course, the computation time of the latter model is much longer because of the generation of statistical variables.

4. Simulation results

Verification of $E(\theta)$ model based on *Theta* parameterization assuming homogeneous areal distribution of θ is performed on the well known Cabauw data set from 1987 (*Beljaars* and *Bosveld*, 1997) . These results are presented in *Ács* and *Szász* (2002) and *Ács et al.*, (2000a).

The transpiration characteristics are considered in terms of analyzing the change of E versus θ, relative frequency distribution of $E(\theta)$, and the algorithms for relating E obtained for homogeneous and inhomogeneous θ. These features are analyzed for both North-American and Hungarian soils using sand and clay as soil texture.

4.1 Analysis of transpiration curves

The $E_{hom}(\theta)$ and $E_{inhom}(\theta)$ curves for strong and weak atmospheric forcing conditions are presented in *Fig. 1* and *2*, respectively. From the point of view of the inhomogeneity of θ, the main characteristics are as follows:

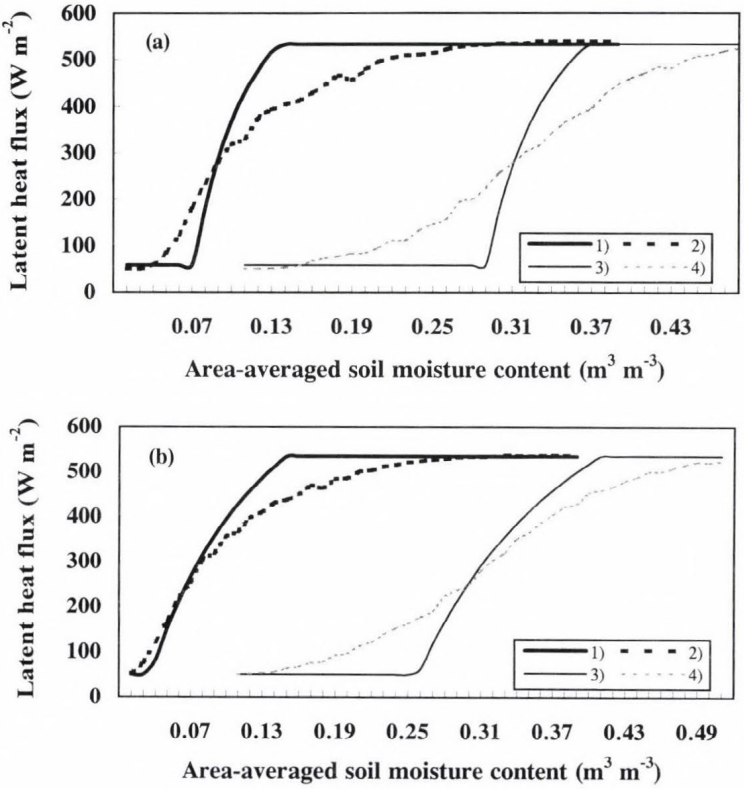

Fig. 1. Transpiration curve as obtained (*a*) by parameterization of *Clapp* and *Hornberger* (briefly CH-parameterization) (1) for sand and homogeneous θ (black continuous line), (2) for sand and inhomogeneous θ (black dashed line), (3) for clay and homogeneous θ (grey continuous line), and (4) for clay and inhomogeneous θ (grey dashed line); (*b*) by parameterization of *Várallyay* and *Rajkai* (briefly VR-parameterization) (1) for sand and homogeneous θ (black continuous line), (2) for sand and inhomogeneous θ (black dashed line), (3) for clay and homogeneous θ (grey continuous line), and (4) for clay and inhomogeneous θ (grey dashed line). The curves refer to strong atmospheric forcing conditions.

(1) the slope $S_{hom}=\partial E_{hom}(\theta)/\partial\theta$ is greater than the slope $S_{inhom}=\partial E_{inhom}(\theta)/\partial\theta$ in the transition region between the soil-controlled and atmospheric-controlled transpiration. This is caused because the transition region of $E_{inhom}(\theta)$ is much greater than the transition region of $E_{hom}(\theta)$. (2) The greatest $|E_{hom}(\theta) - E_{inhom}(\theta)|$ differences appear at θ_w and θ_f. At θ_w, $E_{inhom}(\theta) > E_{hom}(\theta)$, while at θ_f, $E_{inhom}(\theta) < E_{hom}(\theta)$. The course of $E(\theta)$ curves for North-American loam is also analyzed in details in the paper of *Ács* and *Szász* (2002).

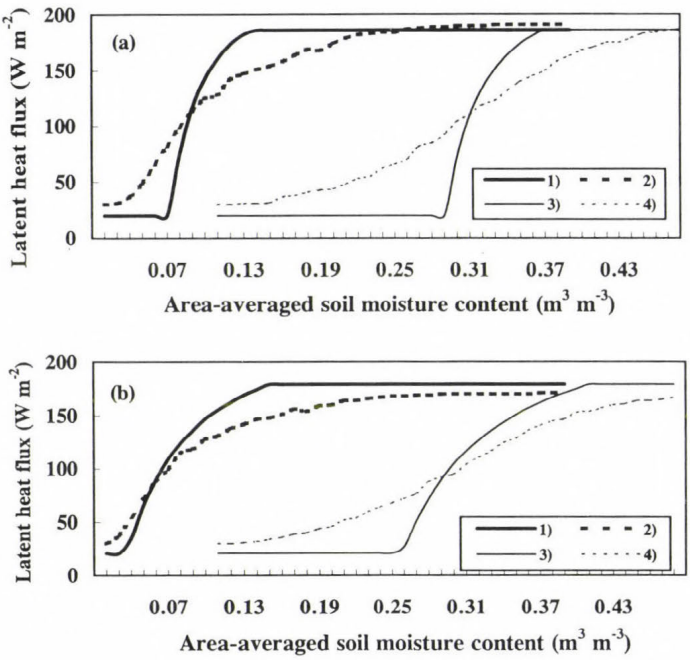

Fig. 2. As in Fig. 1 but for weak atmospheric forcing conditions.

From the point of view of the soil texture, the general characteristics of the course of $E(\theta)$ curves are as follows: (1) Potential (high θ-values ($\theta > \theta_f$) and atmospheric control) and water-stressed (low θ-values ($\theta < \theta_w$) and soil control) transpiration does not depend on the soil texture. (2) The slope $S_{hom} = \partial E_{hom}(\theta) / \partial \theta$ do not depend on soil texture, that is, $S_{hom}{}^{s} = S_{hom}{}^{c}$. In spite of this, $S_{inhom} = \partial E_{inhom}(\theta) / \partial \theta$ depends on soil texture, that is, $S_{inhom}{}^{s} \neq S_{inhom}{}^{c}$. The dependence of $E(\theta)$ curves on soil texture for North-American soils is also analyzed in details in the paper of *Ács* (2002a).

The course of $E(\theta)$ curves obtained for both the CH-parameterization (North-American soils) and VR-parameterization (Hungarian soils), separately for sand and clay is presented in *Figs. 3* and *4*, respectively. Inspecting the curves, the main characteristics are as follows: (1) The slope $S_{hom,CH} = \partial E_{hom,CH}(\theta)/\partial\theta$ is greater than the slope $S_{hom,VR} = \partial E_{hom,VR}(\theta)/\partial\theta$. (2) The potential and water-stressed transpiration are independent not only from the soil texture but also from the parameterization used. (3) The width of the transition region between the soil-controlled and atmospheric-controlled transpiration is different for North-American and Hungarian soils (see *Table 3*).

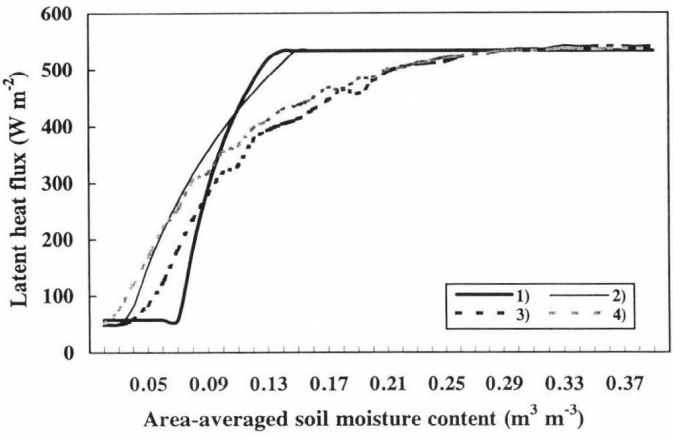

Fig. 3. Transpiration curve as obtained (1) for homogeneous θ using sand as soil texture and CH-parameterization (black continuous line), (2) for homogeneous θ using sand as soil texture and VR-parameterization (grey continuous line), (3) for inhomogeneous θ using sand as soil texture and CH-parameterization (black dashed line) and (4) for inhomogeneous θ using sand as soil texture and VR-parameterization (grey dashed line). The curves refer to strong atmospheric forcing conditions.

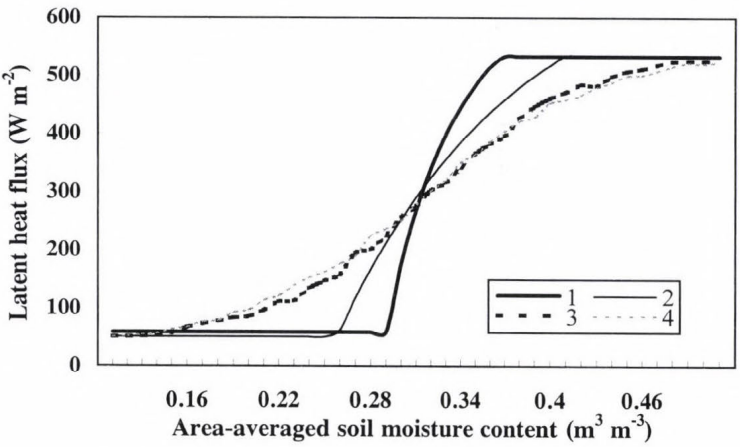

Fig. 4. As in Fig. 3 but for clay as soil texture.

The average width for all three textures is about 0.08 $m^3\ m^{-3}$ for CH-parameterization, while the same parameter for VR-parameterization is about 0.15 $m^3\ m^{-3}$. The greatest differences between CH-parameterization and VR-parameterization appear for sand at $\theta_{hom,w}$. In this case, the $\theta_{hom,w,CH} - \theta_{hom,w,VR} \approx$

0.05 m^3 m^{-3}. (4) The course of $E_{inhom,CH}(\theta)$ and $E_{inhom,VR}(\theta)$ curves are very similar; the differences between them are very small. The greatest differences (about 80–90 W m^{-2}) appear for sand and strong atmospheric forcing in dry conditions ($\theta_{hom,w}$–$\theta_{inhom,w}$ region).

4.2 Areal variations of transpiration

Areal variation of $E(\theta)$ is analyzed inspecting its relative frequency distribution RF. The estimates are performed for strong atmospheric forcing conditions and two different θ_m-values. The characteristic θ_m-values are $\theta_{hom,w}$ (0.07 and 0.02 m^3 m^{-3} for sand and 0.29 and 0.25 m^3 m^{-3} for clay) and $\theta_{hom,f}$ (0.14 and 0.15 m^3 m^{-3} for sand and 0.37 and 0.40 m^3 m^{-3} for clay). The histograms of $RF_{CH}{}^s$ and $RF_{CH}{}^c$ for $\theta_{hom,f}$ and $\theta_{hom,w}$-values are presented in *Fig. 5a* and *Fig. 5b*, respectively. The histograms for VR-parameterization are shown in *Figs. 6a* and *6b*.

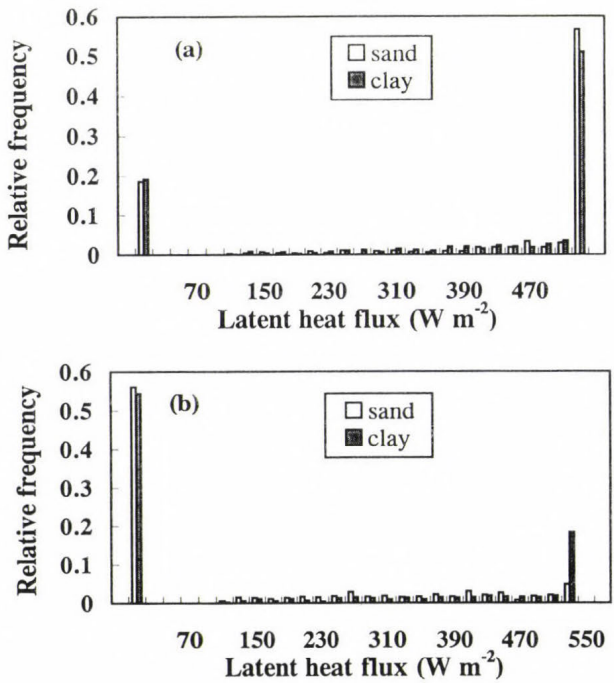

Fig. 5. Relative frequency distribution of latent heat flux from vegetation as obtained by CH-parameterization using sand (light columns) and clay (dark columns) as soil texture for (*a*) $\theta_{hom,f}$ and (*b*) $\theta_{hom,w}$. The results are obtained for strong atmospheric forcing conditions.

The RF^s and RF^c are very similar. In dry regime ($\theta_m = \theta_{hom,w}$), the RF maximum is on the left hand side of the spectrum. In wet regime ($\theta_m = \theta_{hom,f}$), the RF maximum is on the right hand side of the spectrum. For both parameterizations, the greatest deviation between the peaks referrig to sand and clay appear at $\theta_{hom,w}$ (see *Figs. 5b* and *6b*). For CH-parameterization, RF^s shows unimodal, while RF^c shows bimodal distribution. For VR-parameterization, both RF^s and RF^c show unimodal distribution.

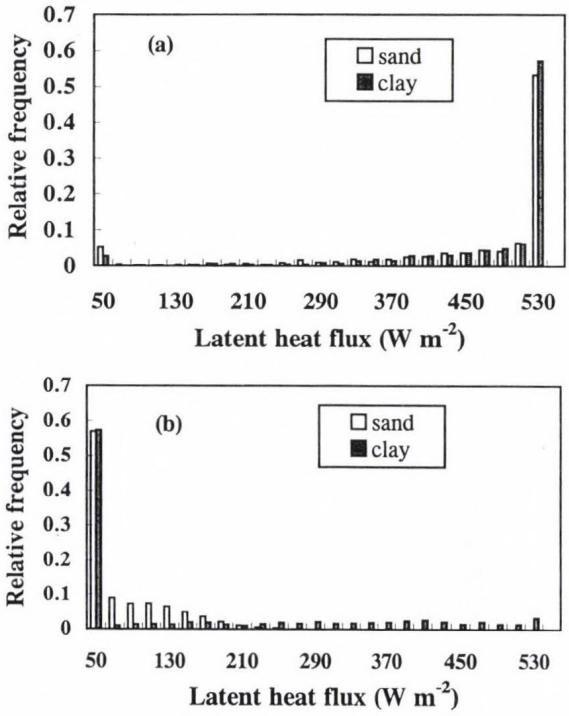

Fig. 6. As in Fig. 5 but for VR-parameterization.

Inspecting $RF_{CH}{}^s$ versus $RF_{VR}{}^s$ and $RF_{CH}{}^c$ versus $RF_{VR}{}^c$, the main characteristic is as follows: RF_{CH} (excepting sand at $\theta_{hom,w}$) possesses a bimodal, while RF_{VR} rather an unimodal distribution. Note that there is a difference between $RF_{CH}{}^s$ and $RF_{VR}{}^s$, though both relative frequency distributions are unimodal. It is hard to explain these RF-differences; they can presumably be related to the differences in soil moisture potentials obtained by CH- and VR-parameterizations (see *Ács* and *Drucza,* 2003).

4.3 Aggregated soil moisture content

The aggregated soil moisture content θ_{ag} is defined by

$$E(\theta_{ag}) = \langle E(\theta_m, \sigma_\theta) \rangle , \tag{6}$$

where $E(\theta_{ag})$ is the area-averaged transpiration calculated by the *deterministic* model using θ_{ag}, and $<E(\theta_m, \sigma_\theta)>$ is the area-averaged transpiration calculated by the statistical-deterministic model using θ_m and σ_θ. The relationship between θ_{ag} and θ_m can be obtained comparing $E_{hom}(\theta)$ and $E_{inhom}(\theta)$ curves (*Figs. 1* and *2*). The relationships obtained by such comparison refer to the transition zone of $E(\theta)$-curves. The change of $\theta_{ag,CH}{}^{s}$, $\theta_{ag,CH}{}^{c}$, $\theta_{ag,VR}{}^{s}$, and $\theta_{ag,VR}{}^{c}$ versus θ_m for strong and weak atmospheric forcing conditions is presented in *Fig. 7*.

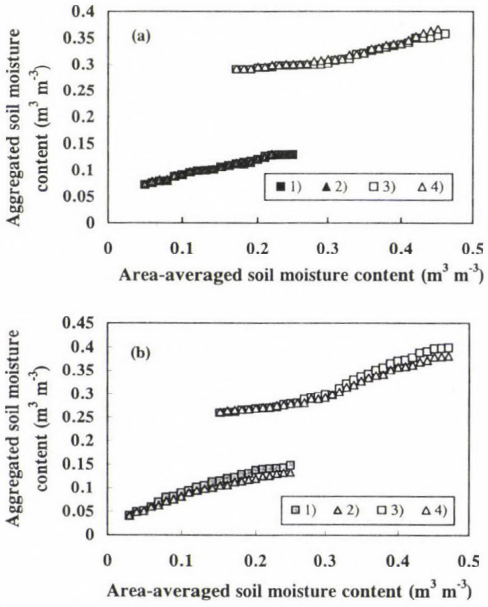

Fig. 7. Aggregated versus area-averaged soil moisture content as obtained (*a*) by CH-parameterization for (1) sand, using strong atmospheric forcing conditions (dark squares), (2) sand, using weak atmospheric forcing conditions (dark triangles), (3) clay, using strong atmospheric forcing conditions (light squares), and (4) clay, using weak atmospheric forcing conditions (light triangles); (*b*) by VR-parameterization for (1) sand, using strong atmospheric forcing conditions (grey squares), (2) sand, using weak atmospheric forcing conditions (grey triangles), (3) clay, using strong atmospheric forcing conditions (light squares), and (4) clay, using weak atmospheric forcing conditions (light triangles).

The relationship between θ_{ag}^{s} and θ_m is linear, while the relationship between θ_{ag}^{c} and θ_m is slightly non-linear. In all cases there is a dependence on the atmospheric forcing conditions. This dependence is weak in dry regime ($\theta_m < \theta_c$), but it is more stronger in the wet regime ($\theta_m > \theta_c$). This is in accordance with simulation results of *Shao et al.* (2001) made by a mesoscale atmospheric model.

The impact of atmospheric forcing conditions can be analyzed comparing $\theta_{ag}(\theta_m)$ courses for strong and weak atmospheric forcing conditions. The differences between $\theta_{ag,\,VR}(\theta_m)$ courses for strong and weak atmospheric forcings are greater than the differences between $\theta_{ag,\,CH}(\theta_m)$ courses for strong and weak atmospheric forcings. Therefore, the dependence on the atmospheric forcing conditions is stronger for VR-parameterization than for CH-parameterization. In spite of this fact, it has to be mentioned, that the course of $\theta_{ag,\,CH}(\theta_m)$ is quite similar to the course of $\theta_{ag,\,VR}(\theta_m)$.

5. Conclusions

The relationship between transpiration characteristics and areal variation of soil properties is analyzed. The transpiration characteristics are analyzed in terms of analyzing the change of E versus θ, relative frequency distribution of $E(\theta)$ and the algorithms for relating E obtained for homogeneous and inhomogeneous θ. The heterogeneity of soil characteristics is considered in terms of areal variation of soil moisture content, soil texture, and areal variation of soil hydraulic parameters (field capacity and wilting point soil moisture contents). In the analysis, sand and clay are used as soil textures. The soil hydraulic parameters are evaluated for both the North-American and Hungarian soils. The North-American soils are represented by parameterization of *Clapp* and *Hornberger* (1978), while the Hungarian soils by parameterization of *Várallyay et al.* (1979) and *Rajkai* (1984, 1988).

The transpiration for homogeneous θ is evaluated by a *deterministic* model. The transpiration for inhomogeneous θ is estimated by a *statistical-deterministic* model. The simulations are performed for strong and weak atmospheric forcing conditions. The results obtained can be summarized as follows:

- The slope of $E_{hom}(\theta)$ curves in the transition zone is much greater than the slope of $E_{inhom}(\theta)$ curves, irrespectively of the parameterization and soil texture used. In spite of this, the course of $E_{inhom,\,CH}(\theta)$ curves and $E_{inhom,\,VR}(\theta)$ curves are very similar. Further, the slope of $E_{hom}(\theta)$ curves in the transition zone, potential and water-stressed transpiration is independent from the soil texture used.

- The histograms of RF^s and RF^c for $\theta_{hom,f}$ and $\theta_{hom,w}$ are very similar. The greatest deviations between them appear for sand in dry conditions. In most cases the RF_{CH} possesses a bimodal distribution. In spite of this, the RF_{VR} shows an unimodal distribution.
- The $\theta_{ag}{}^s(\theta_m)$ relationship is linear, while the $\theta_{ag}{}^c$ (θ_m) relationship is slightly non-linear. In all cases there is a dependence on the atmospheric forcing conditions. This dependence is stronger for VR-parameterization than for CH-parameterization.

The results obtained are valid when there are no advective effects and mesoscale circulation patterns. In the latter cases the transpiration characteristics are more complex.

Acknowledgements—This study is partly financially supported by the OTKA Foundation, project number T-043695.

List of symbols

H – sensible heat flux,
λE – latent heat flux,
λ – latent heat of vaporization of water,
A_e – available energy of vegetation surface,
Δ – slope of saturated vapor pressure curve,
ρ – air density,
δ_e – vapor pressure deficit,
r_a – aerodynamic resistance,
γ – psychrometric constant,
r_v – surface resistance of vegetation canopy,
u_* – friction velocity,
L – *Monin-Obukhov* length,
u_r – wind speed at reference height,
T_r – air temperature at reference height,
c_p – specific heat of air at constant pressure,
g – gravitational acceleration,
k – von Karman constant,
f_1, f_2 – functions which depend on the stratification and choice of the universal functions,
θ – soil moisture content,
θ_m – area-averaged soil moisture content,
σ_θ – standard deviation of soil moisture content,
θ_{ag} – aggregated soil moisture content,
$\theta_{ag,CH/VR}$ – aggregated soil moisture content obtained by CH- or VR-parameterization,
$\theta_{ag,CH}{}^{s/c}$ – aggregated soil moisture content obtained by CH-parameterization for sand or clay,
$\theta_{ag,VR}{}^{s/c}$ – aggregated soil moisture content obtained by VR-parameterization for sand and clay,
$\theta_{hom,w}$ – homogeneous θ at wilting point,
$\theta_{hom,f}$ – homogeneous θ at field capacity,
$\theta_{inhom,w}$ – inhomogeneous θ at wilting point,
$\theta_{inom,f}$ – inhomogeneous θ at field capacity,
$\theta_{hom,w,CH/VR}$ – homogeneous θ at wilting point obtained by CH- or VR-parameterization,
$\theta_{inhom,w,CH/VR}$ – inhomogeneous θ at wilting point obtained by CH- or VR-parameterization,

$\theta_{inom,f,CH/VR}$ – inhomogeneous θ at field capacity obtained by CH- or VR-parameterization,
$E_{hom}(\theta)$ – area-averaged transpiration flux in W m^{-2} for homogeneously distributed θ,
$E_{inhom}(\theta)$ – area-averaged transpiration flux in W m^{-2} for inhomogeneously distributed θ,
$E_{hom,CH/VR}$ – area-averaged transpiration obtained by CH- or VR-parameterization for homogeneously distributed θ,
$E_{inhom,,CH/VR}$ – area-averaged transpiration obtained by CH- or VR-parameterization for inhomogeneously distributed θ,
$S_{hom}(\theta)$ – slope of $E_{hom}(\theta)$ transpiration curve in the transition zone between the soil-controlled and atmospheric-controlled regime,
$S_{inhom}(\theta)$ – slope of $E_{inhom}(\theta)$ transpiration curve in the transition zone between the soil-controlled and atmospheric-controlled regime,
$S_{hom,CH/VR}$ – slope of $E_{hom}(\theta)$ transpiration curve obtained by CH- or VR-parameterization,
$S_{inhom,CH/VR}$ – slope of $E_{inhom}(\theta)$ transpiration curve obtained by CH- or VR-parameterization,
RF – relative frequency distribution of $E(\theta)$,
$RF_{CH/VR}$ – relative frequency distribution of $E(\theta)$ obtained by CH- or VR-parameterization,
$RF^{s/c}$ – relative frequency distribution of $E(\theta)$ obtained for sand or clay
$RF_{CH}^{s/c}$ – relative frequency distribution of $E(\theta)$ obtained by CH-parameterization for sand or clay.

References

Ács, F., and *Hantel, M.*, 1998: Land-surface hydrology parameterization in PROGSURF: Formulation and test with Cabauw data. *Időjárás 102*, 109-127.

Ács, F., and *Hantel, M.*, 1999: The Penman-Monteith concept based land-surface model PMSURF. *Időjárás 103*, 19-36.

Ács, F., Hantel, M., and *Unegg, J.W.*, 2000a: Climate Diagnostics with the Budapest-Vienna Land-Surface Model SURFMOD. *Austrian Contribution to the IGBP. Vol. 3, National Committee for the IGBP, Austrian Academy of Sciences*, 116 pp.

Ács, F., Molnár, I., and *Sász, G.*, 2000b: Microscale bare soil evaporation characteristics: A numerical study. *Időjárás 104*, 143-159.

Ács, F., and *Kovács, M.*, 2001: The surface aerodynamic transfer parameterization method SAPA: description and performance analyses. *Időjárás 105*, 165-182.

Ács, F., and *Lőke, Zs.*, 2001a: Simulation of impact of soil texture upon surface soil moisture changes (in Hungarian). *Agrokémia és Talajtan 50*, 457-468.

Ács, F., and *Lőke, Zs.*, 2001b: Biophysical modelling in agrometeorology (in Hungarian). *Légkör* XLVI, No. 3, 2-8.

Ács, F., Tőkei, L., Hrotkó, K., Gergete F., Bulátkó, F., Márfy, J., Vajda, M., and *Tuba, Z.*, 2001: Relationship between microclimate, transpiration and sap-flow: measurements in a cherry plantation in the summer of 2000 (in Hungarian). *Légkör XLVI, No* 2, 20-25.

Ács, F., 2002a: On the relationship between transpiration and soil texture. *Időjárás, 106,* 277-290 .

Ács, F., 2002b: Soil hydrophysical functions and parameters: A comparative numerical study (in Hungarian). In Levegő-növény-talaj rendszer (ed.: *A. Jávor*). Debreceni Egyetem, Debrecen, 79-83

Ács, F., and *Szász, G.*, 2002: Characteristics of microscale evapotranspiration: a comparative analysis. *Theor. Appl. Climatol. 73,* 189-205.

Ács, F., and *Drucza, M.*: Comparative numerical analysis of the soil moisture potential of North-American and Hungarian soils (in Hungarian). *Agrokémia és Talajtan 52,* 245-262.

Bell, K.R., Blanchard, B.J., Schmugge, T.J., and *Witzak, M.W.*, 1980: Analysis of the surface moisture variations within large field sites. *Water Resour. Res. 16*, 796-810.

Beljaars, A.C.M., and *Bosveld, F.C.*, 1997: Cabauw data for the validation of land surface parameterization schemes. *J. Climate 10*, 1172-1193.

Boulet, G., Kalma, J.D., Braud, I., and *Vauclin, M.*, 1999: An assessment of effective land surface parameterization in regional-scale water balance studies. *J. Hydrol. 217*, 225-238.

Braud, I., Dantas-Antonino, A.C., and *Vauclin, M.*, 1995: A stochastic approach to styding the influence of soil hydraulic properties on surface fluxes, temperature and humidity. *J. Hydrol. 165*, 283-310.

Clapp R.B. and *Hornbeerger G.M.*, 1978: Empirical equations for some soil hydraulic properties. *Water Resour. Res. 14*, 601-604.

Czúcz, B. and *Ács, F.*, 1999: Parameterization of unstable stratification in land-surface model PMSURF: An examination of the convergence by empirical methods (in Hungarian). *Légkör XLIV* , No. 2, 2-6.

Ek, M., and *Cuenca, R.H.*, 1994: Variations in soil parameters: Implications for modeling surface fluxes and atmopheric boundary-layer developement. *Bound.-Layer Meteor. 70*, 369-383.

Erdős, L., and *Morvay, A.*, 1961: Soil moisture course of some soil types (in Hungarian). *Időjárás 65*, 47-55.

Garratt, J. R., 1992: The internal boundary layer-A review. *Bound.-Layer Meteor. 50*, 171-203.

Giorgi, F., 1997a: An approach for the representation of surface heterogeneity in land surface models. Part I: Theoretical Framework. *Mon. Weath. Rev. 125*, 1885-1899.

Giorgi, F., 1997b: An approach for the representation of surface heterogeneity in land surface models. Part II: Validation and sensitivity experiments. *Mon. Weath. Rev. 125*, 1900-1919.

Hawley, M.E., Jackson, T.J., and *McCuen, R.H.*, 1983: Surface soil moisture variation on small agricultural watersheds. *J. Hydrol. 62*, 170-200.

Hupfer, P. and *Raabe, A.*, 1994: Meteorogical transition between land and see in the microscale. *Meteor. Z. 3*, 100-103.

Jarvis, P.G., 1976: The interpretation of the variations in the leaf water potential and stomatal conductance found in canopies in the field. *Philos. Trans. Roy. Soc., Ser. B. 273*, 593-610.

Kim, C.P. and *Entekhabi, D.*, 1998: Impact of soil heterogeneity in a mixed-layer model of the planetary boundary layer. *Hydrological Sciences-Journal-des Sciences Hydrologiques 43*(4), 633-658.

Mika, Á., Ács, F., Radnóti, G., and *Horányi, A.*, 2002: Sensitivity of the ALADIN weather prediction model to the changes of soil texture. *Időjárás 106*, 39-58.

Monteith, J., 1981: Evaporation and surface temperature. *Quart. J. Roy. Meteorol. Soc. 107*, 1-27.

Nielsen, D.R., Biggar, J.W., and *Erh, K.T.*, 1973: Spatial variability of field measured soil-water properties. *Hilgardia 42*(7), 215-259.

Rajkai, K., 1984: Calculation of soil hydraulic conductivity using pF curve (in Hungarian). *Agrokémia és Talajtan 33* (1-2), 50-59.

Rajkai, K., 1988: The Relationship Between Water Retention and Different Soil Properties (in Hungarian). *Agrokémia és Talajtan 36-37*, 15-30.

Rajkai, K., 1991: Measuring surface soil moisture content distribution by TDR method (in Hungarian). *Hidrológiai Közlöny 71*, 37-43.

Robock, A., Schlosser, C.A., Vinnikov, K.Y., Speranskaya, N.A., Entin, J.K., and *Qiu, S.*, 1998: Evaluation of the AMIP soil moisture simulations. *Global Planet. Change 19*, 181-208.

Shao, Y., Sogalla, M., Kerschgens, M. and *Brüher, W.*, 2001: Effects of subgrid land-surface heterogeneity in a meso-scale atmospheric model. *Meteorol. Atmos. Phys. 78*, 157-181.

Seyfried, M., 1998: Spatial variability constraints to modeling soil water at different scales. *Geoderma 85*, 213-254.

Shuttleworth, J.W., 1988: Macrohydrology-the new challenge for process hydrology. *J. Hydrol. 100*, 31-56.

Tomasella, J., Hodnett, M.G., and *Rossato, L.*, 2000: Pedotransfer functions for the estimation of soil water retention in Brazilian soils. *Soil. Sci. Soc. Am. J. 64*, 327-338.

Várallyay, Gy., Rajkai, K., Pacsepszkij, J.A., and *Mironenko, E.V.*, 1979: Mathematical description od pF-curves (in Hungarian). *Agrokémia és Talajtan 28*, 3-14.

Várallyay, Gy., Szűcs, L., Murányi, K., Rajkai, K., and *Zilahy, P.*, 1980: Map of Soil Factors Determining the Agro-Ecological Potential of Hungary (1:100 000) II. (in Hungarian), *Agrokémia és Talajtan 29*, 35-69.

Wetzel, P.J. and *Chang, Y.T.*, 1988: Evapotranspiration from nonuniform surfaces: A first approach for short-term numerical weather prediction. *Mon. Wea. Rev. 116*, 600-621.

IDŐJÁRÁS

Quarterly Journal of the Hungarian Meteorological Service
Vol. 107, No. 3–4, July–December 2003, pp. 273–281

Reliability of estimated global radiation for crop model input

Nándor Fodor, Géza Kovács and **Klára Pokovai**

Research Institute for Soil Science and Agricultural Chemistry
of the Hungarian Academy of Sciences
P.O. Box 35, H-1525 Budapest, Hungary; E-mail: fodornandor@rissac.hu

(Manuscript received November 29, 2002; in final form July 1, 2003)

Abstract—There are several estimation methods to calculate daily global radiation using different input data. The Szász method uses the daily sum of sunshine hours, the Ritchie-Fodor method uses the daily thermal oscillation. It was investigated whether global radiation estimated by the Szász method or Ritchie-Fodor method can substitute the measured global radiation for biomass and yield predictions in the 4M crop simulation model. The reliability of estimated global radiation is much greater if the data is used for yield prediction than for biomass prediction. The global radiation estimated by the Szász method can substitute measured data in 4M and other CERES based crop models with 89–96% of reliability, when yield prediction is the goal. The Ritchie-Fodor method made less reliable radiation estimations. This method needs further development.

Key-words: radiation estimation, 4M crop model, yield predictions.

1. Introduction

The primary purpose of crop models is to describe the processes of the very complex atmosphere-soil-plant system using mathematical tools and to simulate them with the help of computers. The ultimate aim of using crop models, however, is to answer questions that otherwise could only be answered by carrying out expensive and time-consuming experiments.

In the year 2000 a workshop, called 4M, was set up within the new System Modelling Section of the Hungarian Soil Science Society, with the specific purpose of creating an easy-to-use package for modeling cropping systems. The 4M package was developed at RISSAC using predominantly the

results of Hungarian scientists from various institutes in the country. The CERES model was chosen to be a starting point for this project, since it has an open source code, and several studies have proved its competence in describing the soil-plant-atmosphere system (*Kovács et al.*, 1995; *Németh*, 1996; *Jamieson et al.*, 1998).

The accuracy of a crop model is judged mostly by how precise it is in estimating the production. The preciseness of a crop model is determined, on one hand, by the authenticity of the algorithms describing the processes of the real world, and on the other hand, by the quality of its input data. Even the "perfect" model would not be able to simulate the real processes precisely if inaccurate input data were fed into it.

Air temperature, global radiation, and precipitation are the key inputs for most crop models. In 4M, a number of calculations are based on the global radiation, such as soil evaporation, plant transpiration, and daily amount of photosynthesis. Despite of this, a considerable source of error is made while making direct measurements of solar radiation, all over the world. Accurate measured data is rarely available even in the United States. What adds to the difficulties of inaccuracy in Hungary is the limited number of the places where observations are made. This hinders the modelers in extending the spatial validity of crop simulation, which explains why modelers are interested in using estimated data instead of measured ones, that being the case when a good model is at hand for estimation, and easily accessible data are available. There are estimation methods to calculate daily global radiation using different input data: *Ångström*, 1924; *Szász*, 1968; *Bristow* and *Campbell*, 1984; *Fodor et al.*, 2000; *Donatelli* and *Bellocchi*, 2001. The first two methods use the daily sum of sunshine hours, the other three use the daily thermal oscillation. In our present study it was investigated whether the global radiation estimated by the Szász method or Ritchie-Fodor method can substitute the measured global radiation in 4M (*Fodor et al.*, 2003) crop simulation model.

2. Materials and methods

The 4M crop model was used for the test. Since the basis of 4M is the well-known CERES model, that was used as a starting point for several other crop models in the world, the result of this test gives relevant information for a wide range of scientists.

A daily global radiation estimation method was elaborated by *Szász* (1968). It calculates the daily global radiation from the daily sum of sunshine hours, depending on which month the observed day belongs to.

$$R = 0.024347 \cdot VI \cdot C \cdot \Omega \cdot G_{max}\,, \tag{1}$$

where R is the daily global radiation (MJ m^{-2}),
VI is the correction of Albrecht's loss factor,
C is the ratio of sunshine and sunlit hours,
Ω is the length of sunlit period of a day (h),
G_{max} potential value of daily global radiation (MJ m^{-2}).

For a given day of the year, knowing the sum of sunshine hours, the values of VI, C, Ω, and G_{max} can be read from a table given by Prof. Szász.

The Ritchie-Fodor method (*Fodor et al.*, 2000) uses the difference between the daily maximum and minimum temperatures for predicting the global radiation.

$$R = ETR \cdot FCD \cdot CDT^{OM}, \tag{2}$$

where R is the daily global radiation (MJ m^{-2}),
ETR is the extraterrestrial radiation (MJ m^{-2}),
FCD is the fraction of clear day (varies between 0 and 1),
CDT is the clear day transmissivity (varies between 0 and 1),
OM is the optical airmass (varies between 1.58 and 3.89 in Hungary).

Since ETR and OM are the functions of the latitude and day of the year solely, and CDT can be expressed as a function of the daily maximum temperature, and FCD can be expressed as a function of the daily thermal oscillation, with the help of Eq. (2) the daily global radiation can be estimated for a given location and day of the year – knowing the daily maximum and minimum temperature.

The algorithms of the two procedures were incorporated into the 4M cropping model package, therefore, there is an option to select the measured or estimated data directly for model runs. The Szász method was tested using a twenty-year long (1968–1987) independent dataset coming from the meteorological station of Pestlőrinc, Hungary (*Fig. 1*).

Since the Ritchie-Fodor method was developed using the dataset from Pestlőrinc, it was tested on a different, independent, ten-year long (1970–1979) dataset from Debrecen (*Fig. 2*), that was offered by Prof. Szász.

We were not only interested in the direct comparison of the observed and estimated values, since it had already been done from a meteorological point of view. Rather, the focus of this study was to figure out the effect of errors of radiation estimations on the crop model outputs. The obvious aim of this is to see the expected reliability of the generated radiation data for those locations,

where there was no observation of global radiation, but there was observation of sunshine hours or temperature, respectively.

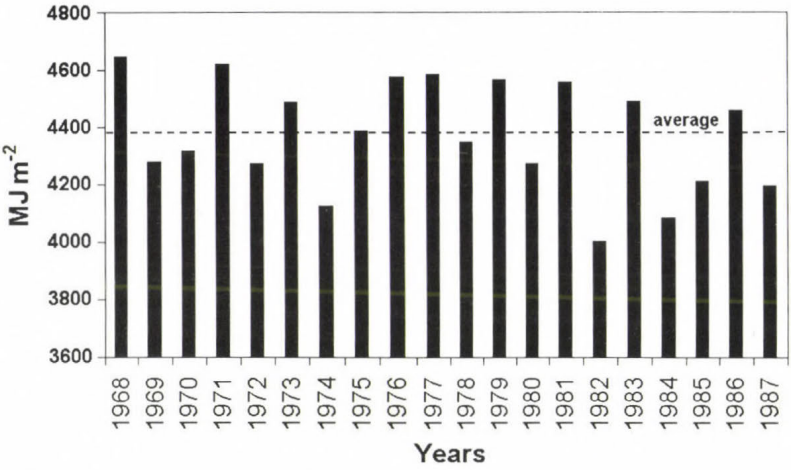

Fig. 1. The yearly sum of observed global radiation at Pestlőrinc, Hungary, during the studied period.

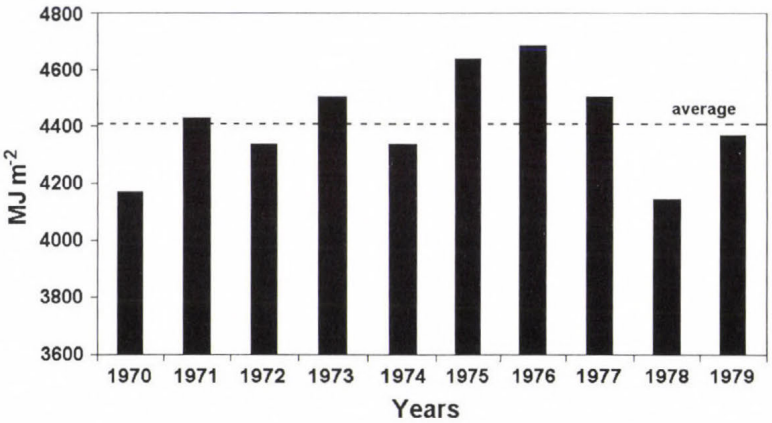

Fig. 2. The yearly sum of observed global radiation at Debrecen, Hungary, during the studied period.

A recent study on the sensitivity of crop models to the inaccuracy of meteorological observations (*Fodor* and *Kovács*, 2003) showed that the uncertainty caused by the errors of the measured global radiation can be up to 6% and 11% for the calculated biomass and yield, respectively. These

thresholds (acceptance limits) were used for deciding whether the radiation estimation is acceptable for the crop model or not. If the difference between the model results obtained by using estimated and measured radiation is less than the above mentioned limits, the radiation estimation is said to be acceptable.

Since global radiation indirectly affects the water balance of the soil, two soil profiles, having different water regimes, were selected for the model runs: a calcaric chernozem soil on loam (*Table 1*) and a meadow soil on clay (*Table 2*). Soil data were provided by the Research Institute of Soil Sciences and Agricultural Chemistry (*Rajkai et al.*, 1981; *Várallyay*, 1987).

Table 1. Some characteristics of the loamy chernozem soil profile. Ks stands for hydraulic conductivity

Horizon	Bulk density ($g\ cm^{-3}$)	Humus (%)	Ks ($cm\ d^{-1}$)	Sand (%)	Silt (%)	Clay (%)
A_p	1.49	4.23	8.82	17.7	60.1	22.2
A	1.45	3.69	4.63	19.4	58.1	22.5
B	1.32	2.49	6.33	18.1	57.5	24.4
BC	1.32	0.00	6.35	16.9	60.1	23.0
C	1.43	0.00	3.50	21.8	56.4	21.8

Table 2. Some characteristics of the clayey meadow soil profile. Ks stands for hydraulic conductivity

Horizon	Bulk density ($g\ cm^{-3}$)	Humus (%)	Ks ($cm\ d^{-1}$)	Sand (%)	Silt (%)	Clay (%)
A_p	1.22	4.48	5.96	6.9	32.4	60.7
B1	1.28	2.01	2.38	8.9	31.6	59.5
C	1.48	0.00	0.28	7.3	47.0	45.7

The genetic parameters of the Pi3978 cultivar (maize) were used as crop specific inputs. Each run started on the 1st of April, the initial water content of the soil profiles was set to 90% of the field capacity.

To test the Szász method, 80 model runs (one year – one run) were made using the measured and estimated global radiation input of the selected 20 years (Pestlőrinc: 1968–1987), on two soil types. Similarly, to test the Ritchie-Fodor method, 40 additional model runs were made (Debrecen: 1970–1979). For the simulated biomass and yield, the difference between the runs with measured and estimated radiation was calculated.

3. Results

First, the measured and estimated global radiation values were compared for the two methods (*Figs. 3–4*). As one can see, the correlation coefficient is very high for the Szász method, even though it slightly underestimates the global radiation (*Fig. 3*). The correlation coefficient is much worse for the Ritchie-Fodor method, the dots on the graph are much more scattered. This method slightly overestimates the global radiation (*Fig. 4*). This does not come as a surprise since the connection between the global radiation and daily sunshine hours is much stronger than between the radiation and daily thermal oscillation.

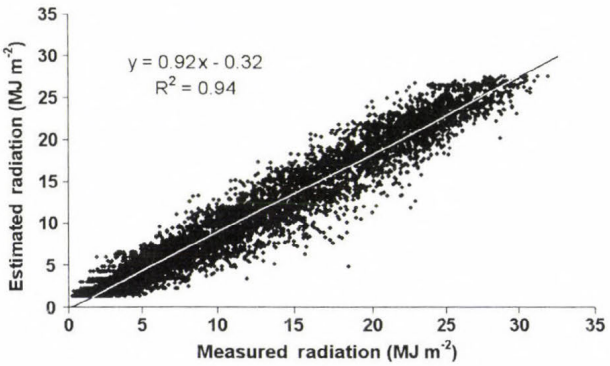

Fig. 3. Measured and estimated (with the Szász method) global radiation values at Pestlőrinc, Hungary, 1968–1987.

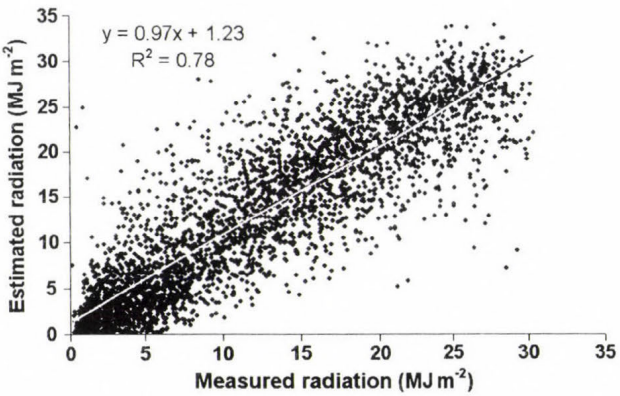

Fig. 4. Measured and estimated (with the Ritchie-Fodor method) global radiation values at Debrecen, Hungary, 1970–1979.

The 4M model was run for biomass and yield predictions using measured and estimated radiation. For the two soil types the same results were obtained (*Table 3*).

Table 3. Average difference between the run results with measured and estimated radiation as a percentage of the results obtained by using measured radiation. The ± values stand for the confidence interval having $\alpha = 0.05$

Method	Soil type	Biomass (%)	Yield (%)
Szász	Loamy	5.7 ± 2.1	8.9 ± 3.2
Ritchie-Fodor	Loamy	10.3 ± 3.6	15.7 ± 5.3
Szász	Clayey	5.4 ± 2.1	8.4 ± 2.9
Ritchie-Fodor	Clayey	8.7 ± 3.9	11.8 ± 5.2

Taking the average difference for the two soil types, the Ritchie-Fodor method made unacceptable radiation estimations causing 9.5% and 13.8% "errors" in average in the calculated biomass and yield, respectively. That means that even the average differences (for the biomass and yield) are greater than the acceptance limits. There were only two years (20% of the cases), where the radiation estimations were acceptable for the loamy soil, and five years (50% of the cases), where the radiation estimations were acceptable for the clayey soil.

If we take the average difference for the two soil types, we can conclude that the Szász method made acceptably good radiation estimations causing 5.6% and 8.7% "errors" in average in the simulated biomass and yield, respectively. Since these values are within the acceptance limits, this result is somewhat misleading. We calculated the level of confidences at which the whole confidence intervals are within the acceptance limits (*Table 4*).

Table 4. Level of confidences for the Szász method at which the whole confidence intervals are within the acceptance limits, and the corresponding percentages of the acceptable cases (years)

Soil type	Biomass	Yield
Loamy	$\alpha = 0.76 \rightarrow 62\%$	$\alpha = 0.22 \rightarrow 89\%$
Clayey	$\alpha = 0.60 \rightarrow 70\%$	$\alpha = 0.08 \rightarrow 96\%$

Only 62–70% of the radiation estimations were acceptable for biomass predictions and 89–96% for yield predictions depending on the soil type. The reason for this is that the Szász method slightly underestimated the global

radiation at Pestlőrinc. Perhaps the method is not valid for this site, or the "radiating circumstances" have been changed since 1968.

We modified Eq. (1) by simply multiplying it with 1.08, so that the slope of the graph in *Fig. 1* would be 1. The modified Szász method gave 100% acceptable radiation estimations for crop model input for Pestlőrinc.

5. Conclusions

Daily global radiation is one of the key inputs for most crop models. Since radiation is measured only in a few places, and the measurements are often loaded with errors, there is a great need for radiation estimators for crop models.

The reliability of estimated global radiation is much greater if the data is used for yield prediction than for biomass prediction.

Based on this study, the global radiation estimated by the Szász method can substitute measured data in 4M and other CERES based crop models with 89-96% of reliability, when yield prediction is the goal. The Ritchie-Fodor method is not reliable for radiation estimations for crop models yet, it needs further development. Since temperature is measured at many more locations than sunshine hours, our group continues to work on the method.

The Szász method should be revisited, so that it would be a 100% reliable method both for yield and biomass predictions for the whole country. It should be recalibrated by using the latest databases of more meteorological stations from the country.

Acknowledgements–This work was carried out by the projects T029217 and T032768 supported by OTKA. Special acknowledgements to *Prof. emeritus Gábor Szász* for his contribution to agricultural ecology and process modeling. Congratulations to Him on his 75th birthday.

References

Ångström, A., 1924: Solar and terrestrial radiation. *Quart. J. Roy. Meteorol. Soc. 50*, 121-125.

Bristow, R.L. and *Campbell, G.S.*, 1984: On the relationship between incoming solar radiation and daily maximum and minimum temperature. *Agriculture and Forestry Meteorology 31*, 159-166.

Donatelli, M. and *Bellocchi, G.*, 2001: Estimate of daily global solar radiation: new developments in the software RADEST 3.00. *Proc. of the 2nd International Symposium Modelling Cropping Systems*, Florence, 16-18 July, 2001, Italy, 213-214.

Fodor, N. and *Kovács, G.J.*, 2003: Sensitivity of crop models to the inaccuracy of meteorological observations. In *Physics and Chemistry of the Earth*. Elsevier Science, Amsterdam, The Netherlands (in press).

Fodor, N., Kovács, G.J., and *Ritchie, J.T.*, 2000: A new solar radiation generator for Hungary. Poster. ASA-CSA-SSSA, Annual Meetings. November 5–9, 2000, Minneapolis, MN, Abstract pp. 23.

Fodor, N., Máthéné-G., G., Pokovai, K., and *Kovács, G.J.*, 2003: 4M - software package for modelling cropping systems. *European J. of Agr. 18*, 389-393.

Jamieson, P.D., Porter, J.R., Goudriaan, J., Ritchie, J.T., van Keulen, H., and *Stol, W.*, 1998: A comparison of the models AFRCWHEAT2, CERES-Wheat, Sirius, SUCROS2, and SWHEAT with measurements from wheat grown under drought. *Field Crop Research 55*, 23-44.

Kovács, G.J., Németh, T., and *Ritchie, J.T.*, 1995: Testing simulation models for the assessment of crop production and nitrate leaching in Hungary. *Agricultural Systems 49*, 385-397.

Németh, T., 1996. *Organic Matter and Nitrogen Content of Soil* (in Hungarian). MTA TAKI, Budapest.

Rajkai, K., Várallyay, Gy., Pacsepszkij, J.A., and *Cserbakov, R.A.*, 1981: Calculation of water retention data from the texture and the bulk density of soils (in Hungarian). *Agrokémia és Talajtan 30*, 409-438.

Szász, G., 1968: *Determining the Global Radiation by Means of Calculation* (in Hungarian). Debreceni Agrártudományi Főiskola Tudományos Közleményei XIV, 239-253.

Várallyay, Gy., 1987: *Water regime of soil* (in Hungarian). Vol.2. Appendix 1. *DSc. Thesis*, Budapest.

IDŐJÁRÁS

VOLUME 107 * 2003

BUDAPEST, HUNGARY

AUTHOR INDEX

TABLE OF CONTENTS
I. Papers

II. Book review

SUBJECT INDEX

GUIDE FOR AUTHORS OF *IDŐJÁRÁS*

The purpose of the journal is to publish papers in any field of meteorology and atmosphere related scientific areas. These may be

- research papers on new results of scientific investigations,
- critical review articles summarizing the current state of art of a certain topic,
- short contributions dealing with a particular question.

Some issues contain "News" and "Book review", therefore, such contributions are also welcome. The papers must be in American English and should be checked by a native speaker if necessary.

Authors are requested to send their manuscripts to

Editor-in Chief of IDŐJÁRÁS

P.O. Box 39, H-1675 Budapest, Hungary

in three identical printed copies including all illustrations. Papers will then be reviewed normally by two independent referees, who remain unidentified for the author(s). The Editor-in-Chief will inform the author(s) whether or not the paper is acceptable for publication, and what modifications, if any, are necessary.

Please, follow the order given below when typing manuscripts.

Title part: should consist of the title, the name(s) of the author(s), their affiliation(s) including full postal and E-mail address(es). In case of more than one author, the corresponding author must be identified.

Abstract: should contain the purpose, the applied data and methods as well as the basic conclusion(s) of the paper.

Key-words: must be included (from 5 to 10) to help to classify the topic.

Text: has to be typed in double spacing with wide margins on one side of an A4 size white paper. Use of S.I. units are expected, and the use of negative exponent is preferred to fractional sign. Mathematical formulae are expected to be as simple as possible and numbered in parentheses at the right margin.

All publications cited in the text should be presented in a *list of references*, arranged in alphabetical order. For an article: name(s) of author(s) in Italics, year, title of article, name of journal, volume, number (the latter two in Italics) and pages. E.g., *Nathan, K.K.*, 1986: A note on the relationship between photo-synthetically active radiation and cloud amount. *Időjárás 90,* 10-13. For a book: name(s) of author(s), year, title of the book (all in Italics except the year), publisher and place of publication. E.g., *Junge, C. E.*, 1963: *Air Chemistry and Radioactivity*. Academic Press, New York and London. Reference in the text should contain the name(s) of the author(s) in Italics and year of publication. E.g., in the case of one author: *Miller* (1989); in the case of two authors: *Gamov* and *Cleveland* (1973); and if there are more than two authors: *Smith et al.* (1990). If the name of the author cannot be fitted into the text: *(Miller,* 1989); etc. When referring papers published in the same year by the same author, letters a, b, c, etc. should follow the year of publication.

Tables should be marked by Arabic numbers and printed in separate sheets with their numbers and legends given below them. Avoid too lengthy or complicated tables, or tables duplicating results given in other form in the manuscript (e.g., graphs)

Figures should also be marked with Arabic numbers and printed in black and white in camera-ready form in separate sheets with their numbers and captions given below them. Good quality laser printings are preferred.

The text should be submitted both in manuscript and in electronic form, the latter on diskette or in E-mail. Use standard 3.5" MS-DOS formatted diskette or CD for this purpose. MS Word format is preferred.

Reprints: authors receive 30 reprints free of charge. Additional reprints may be ordered at the authors' expense when sending back the proofs to the Editorial Office.

More information for authors is available: antal.e@met.hu

Information on the last issues: http://omsz.met.hu/irodalom/firat_ido/ido_hu.html

Published by the Hungarian Meteorological Service

Budapest, Hungary

INDEX: 26 361

HU ISSN 0324-6329